FLASHLAMP PUMPED DYE AMPLIFIERS

By

THOMAS EFTHIMIOPOULOS, B.Sc., B.A.Sc., M.Eng.

A Thesis

Submitted to the School of Graduate Studies

In Partial Fulfilment of the Requirements

for the Degree

Doctor of Philosophy

McMaster University

October 1978

FLASHLAMP PUMPED DYE AMPLIFIERS

TO

MY PARENTS

HELLEN and PERIKLES

DOCTOR OF PHILOSOPHY (1978) McMASTER UNIVERSITY
(Physics) Hamilton, Ontario
Canada.

TITLE: Flashlamp Pumped Dye Amplifiers

AUTHOR: Thomas Efthimiopoulos, B.Sc. (University of Athens), B.A.Sc.
(University of Toronto), M.Eng. (McMaster
University).

SUPERVISOR: Professor B.K. Garside

NUMBER OF PAGES: xv , 272

ABSTRACT

The major purpose of the work described in this thesis is the
experimental and theoretical study of the amplification of the spontaneous
emission in dye amplifiers. This work falls into three distinct sections:
(a) the study of high-current short-pulse flashtubes operating in (or near)
the ablation regime; (b) the study of the amplification process of the
spontaneous emission in a homogeneously broadened medium, such as a dye
material, in the thin cell case, where there is no variation of the pumping
across the cell; and, (c) the study of the amplification of the spontaneous
emission in the thick cell case, where gain and index of refraction in-
homogeneities exist across the cell thickness.

In each case, we have developed theoretical models and compared
their predictions with the experimental results. In particular, for the
ablation-type flashlamps, it is shown that their behaviour is well repre-
sented by an analysis in which the discharge plasma is supposed to radiate
as a blackbody at the temperature of the plasma. This model accounts for
the fact that the light output from a flashlamp saturates whereas the
current does not, provides a more accurate value for the plasma resisti-
vity as a function of temperature and gives a useful design criterion

for determining the physical dimensions of an ablation-type flashlamp.

With respect to the amplification of the spontaneous emission in a thin cell, it is mainly shown that (i) the spontaneous emission propagating along the gain medium is subject to narrowing along with shifting of its peak wavelength; (ii) even at moderate pumping the population of the excited singlet state, which determines the gain of the system, is non-uniform along the cell; (iii) it is possible to calculate the unsaturated gain by calculating the intensity of a particular wavelength and its spectral narrowing both as a function of the excitation and compare them with the same quantities measured experimentally; (iv) it is also possible to develop a semianalytic system-independent method to measure the gain approximately.

The theory developed to account for the propagation of the amplified spontaneous emission (ASE) has been partly extended to cover the case of the propagation and spectral narrowing of the ASE in a thick cell, where non-uniformities of the index of refraction and the gain are important along with the diffraction losses. In this particular case, it is shown that a model, which assumes an index step variation across the cell, and solves the Maxwell's equation for the field propagating along the cell, can account for the spatial distribution of the field across the cell and its manifestation at the far field. Most of the predictions of the model are verified experimentally. In particular, it is shown that (i) in a thick cell, part of the ASE propagates outside the gain medium, because of the lensing effect caused by heating of the lasing material; (ii) the field across the cell can exhibit stable spatial modes,

which can produce a far field far from the amplifying cell axis; (iii) it is possible to improve the spectral narrowing of the ASE since saturation can be delayed to higher pumping than before and most of the narrowing occurs below saturation of the gain; (iv) it is also possible to measure the temperature and the index of refraction change due to heating by measuring the far field angle, and estimate the diffraction losses involved in the propagation of the ASE in a thick cell.

Finally, a number of suggestions on further research are proposed.

ACKNOWLEDGEMENTS

TABLE OF CONTENTS

LIST OF FIGURES

CHAPTER 1

INTRODUCTION

1.1 General Review

Today, dye lasers cover a broad spectral region, which includes the visible and near ultra violet and infrared regions, and have been used extensively in a variety of applications, such as spectroscopy, isotope separation, pumping sources for other laser systems, etc. Although a lot of research has been done, this field is still far from maturity and many more very interesting discoveries and applications can be certainly anticipated. In the following sections, we will present background information related to the characteristics and principles of operation of dye laser oscillators and amplifiers. In this thesis, we will mainly deal with the interaction of light with the dye medium as the light propagates inside the excited medium and details on the contents of this thesis will be presented in a later section of this chapter.

1.1.1 General characteristics of dye lasers

Dye lasers were discovered around 1966,[1] well after the discovery of several other laser active materials. The dye laser oscillator consists of a dye cell, which holds a solution of the gain medium, enclosed in an optical cavity to provide the necessary feedback. The excitation of the gain medium can be carried out by the use of other laser sources, high intensity flashlamps or even an ordinary discharge for a gas phase gain medium. The optical cavity basically consists of two

specially coated mirrors. The coupling to the world outside the cavity is done through a partially transmitting mirror, while wavelength dependent loss elements can be used inside the cavity to affect the spectral narrowing of the emitted light and the peak wavelength. Dye lasers are attractive in several aspects: the lasing material can be used in solid, liquid or gas phase. The concentration of the dye can be easily changed, in the liquid case, which affects the characteristics of the emitted light. Also, a liquid dye material is a self-repairing system in contrast to some solid state media, where damage from high intensities is permanent. Additionally, the cost of the dye laser material is small compared to solid state material and reasonably high power can be achieved with the dye laser oscillators. As far as the time evolution is concerned, several laser pumped continuous wave (cw) systems have been developed and short pulses in the picosecond region have been demonstrated. Today, enough laser dyes have been found to cover the near UV, visible and IR regions of the spectrum and non-linear mixing techniques are used to extend the UV region down to 1000 Å. Still, the major advantage of the dye lasers is their tunability (the ability to control the wavelength of the emitted light) which can extend to several hundreds of angstroms. Certainly, dye lasers are very important coherent sources with a wide range of applications.

1.1.2 General characteristics of dye amplifiers

Because of the relatively high gain exhibited by the dye material, it is possible to use the dye material in the amplifier configuration without any feedback from the cavity mirrors. For relatively high dye

laser concentrations, of the order of 10^{-2} mole/litre, and strong excitation, using laser sources, gains of up to 300 db/cm are predicted. Dye amplifiers can be used in two distinct ways; either to amplify an incoming coherent or incoherent signal or as narrow-band light source by themselves without any incoming signal. In the first case, the incoming signal stimulates the emission of photons from the available excited molecules at the same wavelength region and phase as the incoming signal. Thus, the signal gets amplified as it propagates through the medium. In the second case, the spontaneously emitted photons from the excited dye molecules (which happen to travel along the axis of the medium) get amplified in number by interacting with the excited atoms and inducing transitions which emit light in the same direction. This amplification of the spontaneous emission (ASE) can result in a very narrow wavelength range, very intense light beam ($\gtrsim 1$ MW/cm^2), which has a small angular divergence and does not exhibit any cavity imposed mode structure. This last effect is particularly attractive in applications where the presence of modes or the hopping between the modes could be detrimental. In real situations, where we want to amplify a particular signal, we always have to take into account the effect of ASE. This competition between the signal under amplification and ASE restricts the maximum intensity/cm^2 out of the amplifier to levels well below the saturation intensity (which is the intensity required to drop the gain to 1/2 its value when there are no photons present). Typical saturation intensities are of the order of 100 KW/cm^2 to 1 MW/cm^2. Because the excited state of the dye material has a relatively short life time (of the order of a

few nanoseconds), pumping energy cannot be stored for a long time in this excited state and consequently extremely high pulse powers cannot be generated as in the case of the solid state lasers. The dye amplifiers are satisfactory for amplifying weak signals to moderately high intensities. A detailed study of the amplification of the spontenaous emission is undertaken in a following chapter. Next, we will deal with some basic properties of the dye molecule which are related to the experimentally observed characteristics of the dye amplifiers.

1.1.3 Principles of dye amplifier operation

In what follows, we will give a short description of some basic ideas on structure and bonding of the laser material, the broadening and shifting of the spectrum, the triplet state, the energy diagram of a dye molecule, and the non-radiative deactivation processes. This is done in order to facilitate understanding of material covered in subsequent chapters. There is an excellent book edited by Schäfer[2] which gives a detailed account on the principles of operation and the problems involved, and also includes an extensive reference list for more detailed investigation.

I. Structure and Bonding

A survey of the molecular structure of the dyes, which are known to lase, provides few clues as to what structural elements are most important for lasing. Most dyes have in common a chain of carbon atoms with alternating single and double bonds, the so-called conjugated chain. A single bond in this case is a hybrid bond, which we

get by combining one s-type orbital bond with p-type orbitals or even d-type (e.g., sp^1, sp^2, sp^3 and sp^3d^2). An s-type orbital has a spherical distribution of the electronic charge while a p-type orbital has a dumbbell-shaped distribution. The single bonds sp, sp^2, sp^3 or sp^3d^2 give an electron cloud which is symmetrical about the axis joining the two combined atoms. Such single bonds are called sigma (σ) bonds. On the other hand, it is possible to form a bond between unhybridized p orbitals of adjacent atoms to give another kind of bond called pi (π) bonds. The pi bond can form only when the two p orbitals of the atoms are parallel so that the two p orbitals overlap to form the pi-molecular orbital which has a charge distribution not symmetrical along the line joining the bonded atoms. In short, a single bond is a sigma type bond and a double bond is one sigma type bond and one pi type bond. All dyes, with high absorption in the visible part of the spectrum possess several conjugated double bonds. Also, the fluorescence wavelength of a dye molecule is related primarily to the length of the chain of the conjugated double bonds and the number of π bond electrons.

This relation can be shown assuming a free-electron gas model for the dye molecule.[3] According to this model, all the atoms lie on a plane and are linked with σ bonds, while the π bonds are above and below this plane. These π type electrons are thus moving in a periodic potential, with nodes at the chain atoms, extending as far as the chain goes. Then, the energy E_n of the nth eigenstate of a π electron is given by $E_n = h^2n^2/8mL^2$ where h is Planck's constant, m the mass of

the electron, and n is the number of antinodes of the eigenfunction along the chain, and L is the chain length. Thus, for N electrons, we have 1/2 N empty states (since according to Pauli's principle, we can have a maximum of two electrons per state) and the wavelength of a photon absorbed by an electron, moving from the top of the filled states to the bottom of the unfilled, gives the smallest energy change possible and consequently the maximum absorption wavelength. Accordingly, we have, for the energy and the wavelength:[2]

$$\Delta E_{min} = \frac{h^2}{8mL^2} (N + 1); \quad \lambda_{max} = \frac{8mC}{h} \frac{L^2}{N + 1} \quad (1-1)$$

where C is the light velocity in vacuum.

In conclusion, we see that all dyes possess several conjugated double bonds to form a chain, and the wavelength of the emitted light is primarily dependent on the length of the chain and the number of π bond electrons.

II. Broadening of the Absorption Spectrum

Dye molecules, as opposed to atoms or ions, possess a spectrum which is very broad covering a few hundreds of angstroms. This is immediately understood if we take into account the fact that dye molecules consist of many atoms, each one giving rise to numerous possible vibrational levels coupled to each electronic level. Furthermore, collisional and electrostatic perturbations, caused by the surrounding solvent molecules broaden the individual lines of such vibrational series. Additionally, for each vibrational level, we have a

ladder of rotationally excited sublevels. These rotational sublevels
are strongly broadened because of the frequent collisions with the
solvent molecules. The net result is that each electronic state can
be described by a quasicontinuum of states. The population of these
states, in contact with thermalized solvent molecules, is determined
by a Boltzman distribution. Taking into account that at room tempera-
ture a large dye molecule is experiencing at least 10^{12} collisions/sec
with the solvent molecules, this equilibrium is reached approximately
within one picosecond. The broadening mechanism is the same for all
electronic levels and transitions can take place between any two sub-
levels of different electronic bands. Consequently, dye molecules have
a broad absorption spectrum and also a broad emission spectrum. Typi-
cal full width half maximum of the emission spectrum is of the order of
400 Å. This broad spectrum permits the use of wavelength dependent
loss elements in the optical cavity in order to tune the wavelength
of the emitted light over a considerable range of the order of 300 Å.

III. Shifting of the Emission Spectrum

Lasing in dye materials is greatly facilitated by the fact
that the emission spectrum is shifted with respect to the absorption
spectrum; because now the emitted fluorescence is subjected to much
less absorption losses. It was mentioned before that because of
the very many collisions from the solvent molecule, dye molecules have
quasicontinuous electronic bands which thermalize within a few pico-
seconds. Consequently, this fast thermalization process ensures that

8

electronic transitions from the lower part of the excited electronic
band will have a larger probability to terminate on the empty excited
levels of the ground state band, thereby shifting the fluorescence
spectrum to longer wavelengths. This fact has been exploited to
achieve better pumping efficiency in the flashlamp pumped dye lasers
by employing two different dyes in the same solution. In this case,
the emission spectrum of the first dye coincides with the absorption
of the second and thus a broader spectrum of the flashlamp spectrum
is used to pump the dye laser.[2]

IV. Triplet State

Another very important characteristic property of the dye laser
material is the existence of the triplet state. This state has an
absorption spectrum which overlaps the singlet fluorescence spectrum
and consequently, introduces wavelength dependent losses in the ampli-
fication process. The lifetime of the triplet state ($\sim$ 300 nsec) is
much longer than the singlet state lifetime ($\sim$ 5 nsec), because direct
transitions are spin-forbidden between the triplet and ground state.
This introduces time dependent losses and it is of major importance
for pulses of the order of (or longer than) the triplet lifetime. The
free-electron model mentioned before, can also provide a simple explana-
tion of the position of the triplet state with respect to the excited
singlet state in the energy spectrum. According to this model, the
ground state of a dye molecule has the 1/2 N lowest levels filled with
N electrons; two at each level with their spin antiparallel to give a

total spin of zero. When we excite one of the electrons, it is possible for this electron to retain the direction of its spin or reverse it. In the first case, the total spin is zero and in the second, the spin is one. This means that for the same energy we can have either a singlet state (S = 0) with total symmetric spatial wave function and antisymmetric spin function or a triplet state (S_z = +1, 0, -1, and S = 1), with total antisymmetric spatial wave function and symmetric spin function. This ensures that the Dirac formulation of the Pauli exclusion principle, (which states that the total wave function for electrons including spatial and spin parts has to be antisymmetric with respect to the exchange of any two electrons) will be obeyed. According to this model, we can think of the generalized coordinates of the spatial wave function with respect to two exchanged electrons as actual positional coordinates. In that case, the repulsion energy of the two electrons will be larger when the electrons are as close as possible, each within the π type lobes of the chain of the carbon atoms. In other words, when one of the exchange electrons is on the top lobe and one on the bottom lobe of the same π bond, in exactly symmetrical positions, the potential energy is high and the corresponding wave function is the symmetric singlet total spatial wave function. Exactly the opposite is true for the triplet state which has an antisymmetric spatial wave function because of a symmetric spin function. This antisymmetry places the interchangeable electrons farther apart and consequently, at a lower potential energy. In conclusion, we end up with a triplet state which lies somewhat lower in energy than that of

the singlet state.

V. The Energy Diagram of a Dye Molecule

It was mentioned before that dye molecules have broad bands associated with their electronic excitation levels. In order to have a more complete picture of the dye molecule, we will present a typical energy diagram. Figure 1-1 shows such a diagram. Radiative transitions are shown will full lines and the non-radiative ones with broken-lines. Only the first and second excited states are shown because the rest have much less significant effect on the lasing process, because of their extremely short lifetimes relative to those of the first excited singlet and triplet states.

VI. Non-radiative Transitions

Non-radiative transitions are very important because they strongly influence the efficiency of the dye. In a dye molecule, the important non-radiative transitions for its amplifier performance are between the first excited state and the ground state $(S_1 \rightarrow G)$, the first excited state and the triplet state $(S_1 \rightarrow T_1)$, (the so-called intersystem crossing) and between the triplet state and the ground state $(T_1 \rightarrow G)$. According to Pauli's exclusion principle for elec- trons, only wave functions which are totally antisymmetric with respect to exchange in coordinates and spin are allowed. When there is no interaction between spin and orbit, the total spin S is a good quantum number and it can be shown that, because the electric dipole

Figure 1-1 Typical energy level diagram of a dye molecule. G, S_1, S_2 are the ground state, the first excited singlet electronic state and the second excited singlet correspondingly. T_1 is the triplet state and T_2 is the first excited triplet. P is the pumping rate, σ_e is the emission crossection from $S_1 \to G$, σ_{01}^a is the absorption crossection $G \to S_1$, σ_{12}^a is the excited singlet state absorption crossection and σ_t^a is the triplet state absorption crossection. Solid lines indicate radiative processes and broken lines non-radiative ones. τ_{th} is the thermolization time within the electronic states and τ_{nr} is the non-radiative relaxation lifetime between electronic bands. τ_{th} and τ_{nr} are of the order of a few picoseconds for most of the known dye material in solutions. Higher order excited states are not included in these graphs because of their insignificant role in the lasing process.
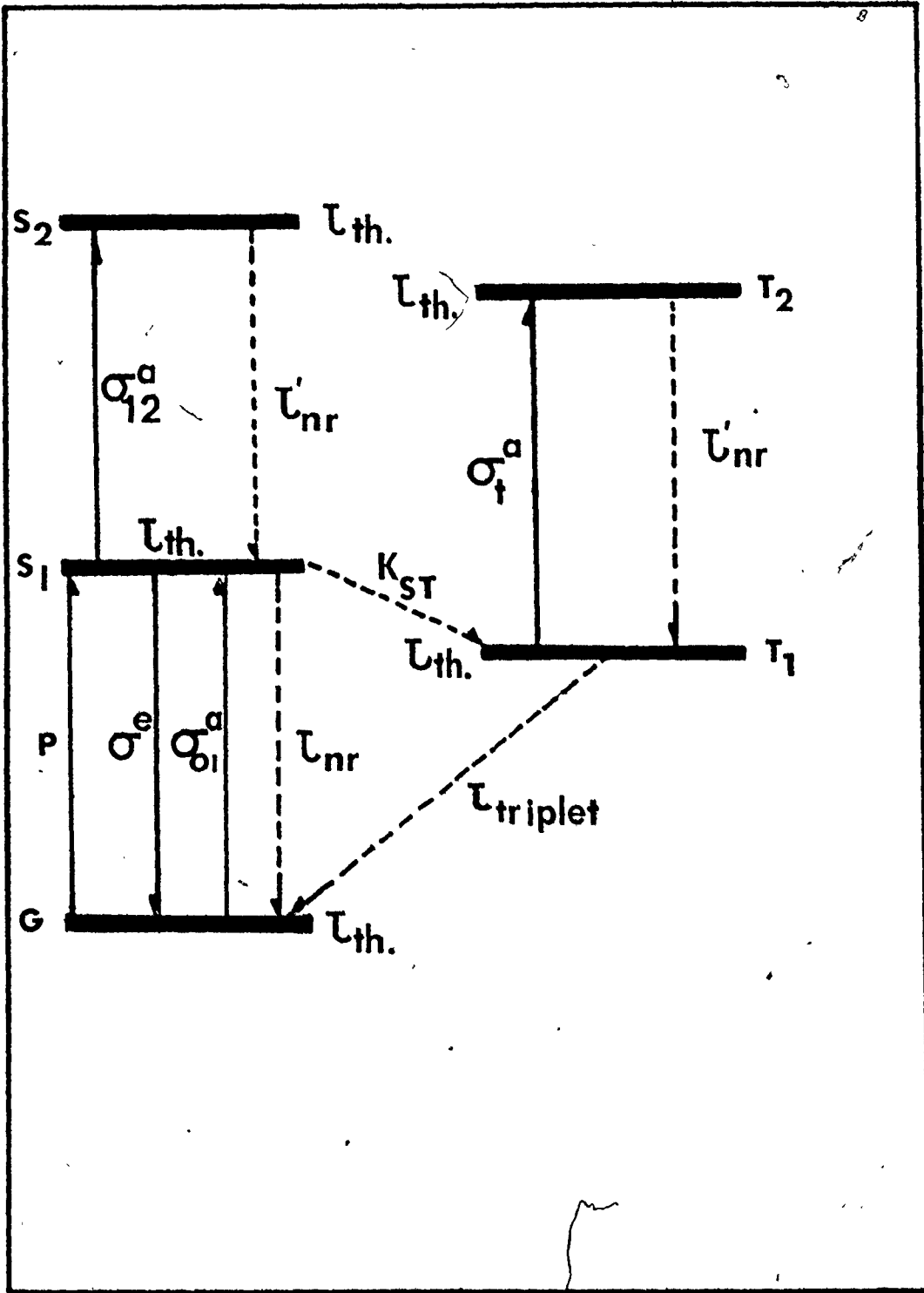
FIG. 1-1

moments do not operate on the spin functions, matrix elements of electric dipole moments taken between spin functions of different total spin S will vanish, because the symmetric and antisymmetric spin wave functions are orthogonal. In conclusion, the selection rule for the total spin S is given by $\Delta S = 0$. According to this rule, transitions between the S_1 state (S = 0) and T_1 (S = 1) with the emission of a photon are forbidden. The same is true between T_1 and G states. It is possible though to have radiationless transitions between S_1 and T_1, either by spin orbit coupling or by external collisions.

Spin orbit coupling exists when the orbital angular momentum created by π electrons of the ground state oscillating between the end groups of the molecular chain, interact with the total spin. Intersystem crossing can also be achieved by collisions with a paramagnetic molecule (which has a spin different from zero) in the dye solution. These spin orbit and spin-spin coupling effects can also cause transitions from the triplet state to the ground state. Such internal conversion processes depend on the rigidity of the molecular structure of the dye and the properties of the solvent.[4],[5] In general, a rigid molecular structure does not favour internal conversion because it does not provide additional degrees of freedom to accomodate for stepwise energy transfer. The consequence of this is that for mobile structures, the fluorescence will be strongly temperature dependent.[6] On the other hand, rigid structures do not

necessarily have high fluorescence efficiency, because there are other quenching processes, such as the one due to hydrogen vibrations,[7] which can be of importance. Because of the small mass of hydrogen atoms, the quanta of hydrogen stretching vibrations have the highest energies in organic dyes and thus are most likely to be involved in the conversion of the lower vibrational level of S_1 to the higher vibrational level of G.[7] This important aspect of internal conversion in dye molecules is far from being clearly understood and more details can be found in the article of Drexhage in reference 2.

In conclusion, the radiationless decays of $S_1 \rightarrow G$ and $T_1 \rightarrow G$ along with the intersystem crossing $S_1 \rightarrow T_1$ are very important in determining the efficiency of the dye amplifier. The dye molecules are very complex, with behaviour governed by many parameters which have not been measured for most dyes. Consequently, it is extremely difficult to develop a general theory which can predict all the phenomena which have been observed experimentally. One of the best known and characterized dyes is rhodamine 6G which we therefore used in our experiments to facilitate comparison with the theoretical predictions of our model.

1.1.4 Principles of flashlamp operation

Flashlamps have been used for many years to convert electrical energy into radiation and they are of major importance for photochemical studies and laser pumping. Basically, we can distinguish two kinds of flashtubes. First, there are flashtubes whose emission

spectrum depends on the particular gas filling and second, there exist flashtubes which have an emission spectrum which approximates a blackbody radiation spectrum. We will call them spectral flashlamps and ablation flashlamps, respectively. The name ablation flashlamps is used because, to reach the blackbody radiation stage, a lot of energy/cc/sec is used and ablation of the wall of the flashtube takes place. In spectral flashlamps, we use low input power densities and relatively high rare gas pressures and depend on the specific gas emission spectrum for efficient conversion. A number of different commercial and laboratory flashlamps of this kind exist today. Their electric and spectral characteristics are described in a number of papers.[8]-[30] It has been shown[26] that continuous emission spectra are the result of the transitions of electrons from a bound state to a free one and from a free state to another free state. The resultant continuous spectra are superpositions of several continua due to individual transitions. In the case of high power densities, the spectrum approximates a blackbody spectrum. Several papers have been published on ablation flashtubes and their characteristics.[31]-[37]

The choice between the two basic types of flashtubes depends on the particular application. In the case of the spectral flashlamp a relatively moderate temperature ($\sim 10,000°K$) slow discharge will deliver the available stored energy in the region of interest. It is the particular spectral distribution which makes this process ef-

ficient in the appropriate wavelength range. As soon as we want, though, to increase the intensity of the flashlamp by pumping more energy in the tube, the continuum part of the emitted radiation (which extends beyond the region of interest) predominates over the characteristic spectral part and the efficiency will drop. It is then possible for high enough energies and fast discharge time to get much higher temperatures of the order of 40,000°K. In such high temperatures, the plasma radiates like a blackbody from its surface and the available intensity within the region of interest will be more than before. Of course, the efficiency will keep on droping as we increase the temperature, because this moves the peak of the intensity to shorter wavelengths. Notice, though, that to get high temperatures, we have to use shorter discharge times, because the temperature reached by the plasma is determined by the energy per unit time. In conclusion, a high efficiency requirement is associated with spectral flashlamps and ablation flashlamps will provide higher peak intensities in short pulses. The ablation flashtubes are very important in pumping dyes which have low quantum efficiencies and time-dependent losses.

1.1.5 Gain measurement techniques in pulsed amplifiers

Radiative de-excitation of an excited singlet state in a dye molecule can be produced in the following two ways. First, through spontaneous emission which is independent of the presence of radiation. Second, by way of stimulated emission which is caused

by the interaction of the excited molecules with the radiation field. This process depends on the intensity of the light present during the interaction. The de-excited molecule emits a photon, which, in the spontaneous case, is of random phase and direction; while in the stimulated emission case, has the same phase and direction as the interacting field. The light intensity $I(\lambda,z)$, propagating along a gain medium which extends in the direction of the z-axis, for a particular wavelength λ, will be given by the equation

$$\frac{dI(\lambda,z)}{dz} = g(\lambda,z)I(\lambda,z) + \eta g(\lambda,z) \tag{1-2}$$

where $g(\lambda,z)$ is the gain coefficient and η is a coupling constant for the spontaneously emitted radiation. The gain is proportional to the number of the excited state molecules. High intensity will de-populate the excited state by stimulated emission and thus decrease the gain. In other words, the gain is an intensity-dependent function. Because the intensity is not the same throughout the cell, and because the intensity is wave length dependent, the gain will also exhibit spatial and wavelength dependance. Accurate knowledge of the gain is very important in characterizing any amplifier and providing specific information about the dye molecule. Therefore, different ways have been developed to determine the gain.

There are several direct or indirect ways to find the gain. We are obviously interested in the value of the gain in the absence of radiation (unsaturated gain) because this parameter does not de-

pend on the intensity but only on the pumping and the absorption and emission cross-sections. In the direct way of measuring gain, a probe signal of known intensity and spectrum is passed through the amplifier and its intensity at different wavelengths is recorded with the amplifier pumped and unpumped.[38] The ratio of the two recorded intensities is related to the gain through the equation

$$I(\lambda)/I_0(\lambda) = \exp(g(\lambda) \cdot L) \tag{1-3}$$

where L is the length of the active medium. This method assumes no spatial variation of the gain and neglects the presence of the amplified spontaneous emission. Consequently, it is restricted to intensity values well below the saturation intensity where the spontaneous emission is small and the intensity does not cause any saturation of the gain. Also, it requires an extra tunable laser to supply the probe signal.

An indirect way to measure the gain is to use the amplified spontaneous emission (ASE) itself.[39] Again, we have to restrict the measurement to the low pumping region where the intensity does not saturate the gain. Then, if we assume that the contribution of the spontaneous emission is negligible, we can integrate equation (1-2) to get for the intensity at distance $p \gg L$

$$I_L(\lambda) = (\exp(g(\lambda)L) - 1)C$$

$$I_{L/2}(\lambda) = (\exp(g(\lambda)L/2) - 1)C$$

(C is a proportionality constant)

where L is the length of the cell. Combining these two equations we have for the gain

$$g(\lambda) = \frac{2}{L} \ln \left[\frac{I_L(\lambda) + 1}{I_{L/2}(\lambda) + 1} \right] \tag{1-4}$$

In the case, we have $g(\lambda)L/2 \gg 1$, we can approximate equation (1-4) to get

$$g(\lambda) \doteq \frac{2}{L} \ln \frac{I_L(\lambda)}{I_{L/2}(\lambda)} \tag{1-5}$$

Then, we can measure the intensities at the end of the cell for the full length cell and the half-length cell and use equation (1-5) to determine the gain. This blocking of the half-cell length is not always possible, particularly in flashlamp pumped dye amplifiers where the cell and the lamps are enclosed in a water cooled housing. Again, this method provides only approximate values for the gain, because it assumes no spatial variation of the gain and neglects the presence of the amplified spontaneous emission, which could be considerable in high gain media.

Another, more sophisticated way for the gain measurement is to measure the narrowing of the spectrum of the amplified spontaneous emission (ASE) and relate it to the non-saturated gain.[40] This seems particularly attractive, because it does not require a probe source, it can easily be done, takes into account the presence of the ASE and puts no restriction on the level of pumping. The ASE gets

narrower as it propagates through a gain medium, because of the non-
uniformity of the gain profile as a function of wavelength.[40] The
full spectral width of the output ASE intensity at half-maximum (FWHM)
$\Delta\lambda$, is given for a homogeneously broadened gain medium by the rela-
tion[41,42]

$$\Delta\lambda/\Delta\lambda_h = [\log_e 2/(g_0 l_{eff})]^{1/2} \tag{1-6}$$

where $\Delta\lambda_h$ is the FWHM of the line shape function, which for rhodamine
6G in ethanol is about 420 Å, and l_{eff} is an effective length, which
can be computed and to a crude approximation, is equal to the length
of the amplifier for very low intensity of the ASE. For inhomogeneously
broadened gain systems (such as amplifiers in the gas phase, where the
Maxwell-Boltzmann distribution of the thermal velocities will make
the molecules see the radiation field frequency shifted and consequently
interact preferentially with particular wavelength regions of the field),
the spectral line first narrows with increasing gain and subsequently
rebroadens.[43,44]

    It is possible, as we will see in a later chapter, to develop a
model which will deal with the propagation of the ASE in a gain me-
dium with uniform absorption across the cell and relate the output
intensity spectrum to the unsaturated gain. This method, which actually
solves the rate equations for the propagation of the ASE, gives very
accurate results and can be used to test all the above-mentioned ap-
proximate methods, because it is exact and it does not include any

assumptions regarding gain saturation. This model has been tested experimentally and was found to give very accurate predictions. The only disadvantage is that a computer is required to solve the appropriate non-linear coupled equations. It is possible, though, under certain assumptions (Lorentzian gain profile and enough narrowing before saturation starts) to develop an approximate method which takes into account the saturation. This approximate semi analytical method can be very useful in several systems where the other methods are either difficult to apply or forbidden because of their assumptions.

1.1.6 Spatial modes in a dye amplifier

In many experimental situations, the pumping light from either a flashlamp or a laser is absorbed in depth generally much less than the thickness of the pumped cell. This will create a non-uniform gain profile across the cell. Additionally, there is heating of the dye solution, resulting from the thermalization processes within the electronic bands of the dye molecules and from the existence of non-radiative de-activation processes between the electronic bands. Furthermore, there can be heating of the solvent directly in the case where it too absorbs in the spectral region of the pumping source. This heating can be non-uniform across the cell when the absorption length (defined as the depth of material to absorb $1/e$ of the incident light intensity) is of the same order as the cell thickness. These various heating effects will cause a non-uniform change of the index of refraction across the cell, because the refraction index is a function

of temperature. An additional change of the index of refraction comes
from the presence of the gain itself. As we will see in Chapter Four
in more detail, the gain is related to the imaginary part of the di-
electric constant by the equation

$$q = \frac{\epsilon''}{n_0} \epsilon'' \tag{1-7}$$

where q is the gain, n is the real index of refraction far from the
resonance and ϵ'' is the imaginary part of the dielectric constant,
which is related to the real part of the dielectric constant ($\epsilon =
\epsilon' + i\epsilon''$) by the Kronig-Kramers relations. The index of refraction
is related to ϵ' and, consequently, to the gain. As we will see in
Appendix B, the change in the index of refraction, Δn, is related to
the gain by the equation

$$\Delta n = \frac{-1}{4\pi^2} \int_{-\infty}^{+\infty} \frac{q(v')}{v-v'} \, dv' \tag{1-8}$$

In conclusion, in many experimental situations, the dye amplifier
exhibits a non-uniform gain profile across the cell and also a non-
uniform index of refraction profile. The spatial gain and index of
refraction variation raises the possibility that the ASE will pro-
pagate along the cell in a distinct pattern exhibiting spatial modes
across the cell. In an actual case, the smaller index near the
walls of the cell will push the field to partly propagate outside the
gain region. This investigation of the light propagation in a thick

cell comes as a natural extension of the research on thin cells and gain measurement techniques, because we want to investigate the amplicability of these gain measurement techniques to thick cells, which are used in many experimental situations. The study of light propagating in a thick cell leads to consideration of existence of propagating modes, which affect both the spectral narrowing and the near and far field distribution patterns.

The spatial modes will exhibit themselves in the near field which will consist of approximately sinosoidal intensity distributions (which diminish toward the centre of the cell for high enough concentrations) and produce two diverging beams of ASE separated by an angle of a few degrees. Some experimental evidence along with a theoretical model based on the geometrical ray approximation of the propagation of the ASE have been published.[45-49] Similar far field observations have been made on electron beam pumped semiconductor lasers and calculation based on spatial variations of gain and index of refraction (in the simple case of an index step) have been carried out to explain the far field angular change as a function of the index step change.[50]

Understanding the way the ASE propagates is of importance, because it is, in principle, possible to relate the far and near field intensity distributions to the gain of the amplifier. From a practical point of view, such an understanding could lead to useful optimization of the parameters involved to increase the narrowing of the ASE spectrum. This could be possible, because of the wave-

length dependent diffraction losses and the decrease of the ASE intensity in the gain region (since some light will propagate outside the gain region) which permits higher pumping without saturation. Higher pumping results in higher unsaturated gain, which, according to the relation (1-6), gives narrower spectrum.

1.2 Outline of the Contents of the Thesis

This thesis consists of the following chapters:

(i)   Introduction

(ii)   Operating characteristics of high-energy, short-pulse flash-
        lamps

(iii)   Amplification of the spontaneous emission

(iv)   Spatial modes in the ASE

(v)   Discussion and Conclusions.

In Chapter two, we present a detailed study of the ablation type flashlamps. This work was done primarily for two reasons: first, in order to obtain a better understanding of the flashlamp operation itself, since flashlamps are of prime importance in pumping lasers; second, in order to use the information gained to build a high-energy short-pulse flashlamp to be used subsequently in experiments concerning the propagation of the amplified spontaneous emission. Such flashlamps are not available commercially. In this study, we demonstrate that a simple blackbody radiation model can account for the

behaviour of these flashlamps at high enough input energies per unit time. We will also see that a simple relation can be used to relate the current passing through a particular flashtube, to the resistivity of the plasma in the flashtube. Under certain conditions, it will be shown that the energy stored in the storage capacitor per unit volume of the tube plasma can be used as a very useful parameter to predict the flashtube behaviour. Another major feature of the model mentioned above is the functional dependence of the resistivity on temperature, namely, $n = BT^{-3/2}$. The constant B is determined by fitting the variation of the discharge current vs the input energy per unit volume of the plasma. This model also makes possible the comparison of performance between flashtubes of different lengths and radii, and provides a very useful design criterion for determining the physical dimension of ablation flashlamps. We present extensive experimental data to support the claims of the model, supply information on optimization of several parameters, such as pressure, and suggest ways to improve performance on lifetime of the flashlamp.

Chapter Three deals with the amplification of the spontaneous emission in a dye medium. This study is very important because:

(1)   it provides an especially simple case for understanding the interaction of a non-coherent source with a homogeneous medium;

(2)   dye amplifiers have the potential of producing high intensity,

highly directional, narrow bandwidth light pulses without
mode structure and with a smooth temporal profile;

(3)   it provides an accurate way to measure the gain of a system
.from the narrowing of the amplified spontaneous emission
(ASE), which is especially useful in the case where other
even approximate methods cannot be used.

In this chapter, we study experimentally, the ASE in a dye
material enclosed in a very narrow flat cell, which is pumped on both
sides by two flashlamps. Our aim is to exploit the spectral nar-
rowing of the output radiation to measure the unsaturated gain as a
function of pumping. A theory is developed, which allows for excited
state absorption (which proved to be very important), capable of pre-
dicting the variation in intensity, spectral width and peak wavelength
as a function of the flashlamp pumping intensity. It will be shown
that this theoretical model can be fitted accurately to experimental
observations and very good values for the unsaturated gain are ob-
tained. Such gain measurements only require that the intensity and
the spectral variation of the intensity be measured as a function of
pumping. This model requires very accurate knowledge of the values
of the different cross-sections of the dye employed. It will be
shown that the excited single state absorption (ESSA) is of major
importance and this model can actually be used to predict the ESSA
for other dye materials.

The general model we will develop is appealing as far as the

accuracy of the predictions are concerned.   However, to exploit

our approach in more general situations, we require a simpler non-

system specific model which can be applied approximately to many

different gain media.   Accordingly, we develop a relatively simple

theory for the ASE, in which the gain line is assumed to be homo-

geneously broadened, and attempt to fit to experiment in the al-

ready characterized dye system (by using the general exact theory).

This represents a very severe test because the approximate theory

does not take into account that the peak of the ASE shifts with pumping

and also that the excited state absorption is very important.   We will

show that even in this case we can use appropriate techniques to match

theory and experiment and get reasonably good values for the gain.

We will also compare our approximate simple theory to another approxi-

mate one, which was published recently and which makes basically the

same assumption as far as gain profile, ESSA and considerable nar-

rowing before saturation are concerned.

Chapter Four deals with the propagation of the ASE in cells

thick with respect to the absorption length of the dye. This is very

important in practice, because in most experimental situations, thick

cells are used.   It is then natural to look for ways to measure gain

and relate it to spectral narrowing in thick cells. This leads to

consideration of the existence of propagating modes in a thick cell.

Chapter Four also deals with the spatial modes in a dye amplifier.

While in Chapter Three, we restrict ourselves in studying the ASE in cells with no spatial variations of the gain or the index of refraction across the cell, in Chapter Four we try to deal with the more complex problem of the thick cells which have gain and index non-uniformity across them. We present a model which is based on solving the Maxwell equations for the field in the cell under the assumption that both the gain and the index of refraction have a similar stepwise profile across the cell. It turns out that the index change due to the change in temperature is much larger than the change due to the presence of gain itself and this is equivalent to a converging lens along the cell. We will demonstrate that for relatively medium thickness cell with respect to the dye absorption length, the field will propagate filling up the whole cell cross-section. On the contrary, for very thick cells with respect to the absorption length of the dye, the field will propagate filling up only the gain region and a small part of the rest of the cross-section of the cell (confinement of the field). This different behaviour of the modes will manifest itself in the divergence of the beam from the axis of the cell and also in the shape of the far field itself. We will also present some experimental data, which show qualitatively this behaviour of the field. Because the stepwise approximation of the index of refraction is only a first degree approximation to the real exponential change, it is not expected that complete agreement with the experimental data will be obtained. However, it does present useful approxi-

mation to get to understand the physics of the processes involved.

In Chapter Five, we will present a summary of the different topics covered in the previous chapters. Because the topics covered in Chapters Two, Three and Four are self-contained, most of the discussion is presented at the end of each chapter and only the main features will be considered in Chapter Five. The important section covering suggestions for future fruitful research will also be included in this chapter.

CHAPTER 2

OPERATING CHARACTERISTICS OF HIGH-ENERGY SHORT PULSE FLASHLAMPS

2.1 INTRODUCTION

The study of the flashlamps was undertaken in order to get a
better understanding of the operation of the flashlamps themselves, to
be able to design a fast high power flashlamp system needed to pump our
dye amplifier whose characteristics we wanted to study and to be in a
position in the future to make our own special designs of the flashlamp
without cost, or characteristic restrictions imposed by the available
commercial flashlamps. Also, flashlamps have been used to pump other
lasers besides dye laser such as Neodymium in the infrared region and
dyes of the UV region and it seemed natural that the study of the flash-
lamp pumping sources could lead in more efficient laser systems in an
extended spectral region. Our particular study was restricted to the
ablation-type flashlamps only, because of their great potential to pro-
vide short intense pulses of radiation needed in our intended research
area.

There are several parameters which can be varied to effect con-
trol over the output of the flashlamp, namely, flashlamp dimensions, gas
fill and pressure and discharge energy. The trade-off between the various
parameters is far from obvious, because it depends on the projected appli-
cation, and the impact of the various parameters on the overall perfor-
mance of the system cannot always be separated. The investigations re-

ported here were aimed, as far as possible, at studying only the dependence of the characteristic flashlamp discharge behaviour on the various parameters. Accordingly, a particular value of the flashtube length was selected since, over the operating range investigated, the flashlamp plasma resistance is directly proportional to the discharge length. It is then a straightforward matter to calculate the impact of changes in discharge length using a simple circuit element approach[8,12,14] once the relevant discharge characteristics are known. Similar considerations apply to the importance of the discharge circuit elements. We can simply select fixed circuit components and vary only the voltage supplied to the storage capacitor. The discharge current delivery, risetime, etc., can be optimized[8] once the parametric dependence of the flashlamp plasma resistance per unit length is known.

Taking into account the above considerations, the investigations described in this chapter are mainly addressed towards supplying answers to the following questions with respect to ablation flashlamp operation:

i. How do the risetime and the falltime of the output light pulse (in a chosen wavelength range) depend on the flashlamp characteristics and the supplied energy density?

ii. Over what range of lamp, gas fill and discharge energy characteristics does the flashtube operate in the ablation (and the black-body emission) regime?

iii. For a given flashtube length and input energy, how can the tube bore be chosen to give maximum peak output, and what other considerations are important?

iv. Can the onset of excessive tube ablation be characterised. in terms
of input energy and tube parameters and how does the fall time of
the output depend on these parameters?,

v.   Can a simple model be constructed to adequately describe the be-
haviour of the flashtube?

In what follows, we investigate the above and related questions
after we.present a literature review, and a description of the experi-
mental apparatus. This experimental investigation is afterwards comple-
mented by the development of a theoretical model which can adequately
describe the behaviour of the flashlamp. The whole investigation is
then ended by presenting the main conclusions along with suggestions con-
cerning the design of ablation flashlamps for optimum performance.

2.2 LITERATURE REVIEW

.2.2.1 Rare-Gas Flashlamp Characteristics

For years, rare-gas flashlamps have been used to pump lasers.
The primary objective is to convert electrical energy to radiation ef-
ficiently and to generate high fluxes of radiation within a specified
spectral band. To do this, we have to know the behaviour of the gas
plasma. There are two basic parameters which determine the performance
of the lamp, namely, the gas pressure and the current density. Also,
practical considerations such as the lamp envelope material, the elec-
trode material and the type of rare gas used have an effect on tube life
expectancy, reliability and cost. In the following paragraphs, we will
deal briefly with the performance of the rare-gas flashlamps and we will
devote some attention to the radiative processes involved, the spectra,
and the electrical characteristics of these flashlamps.

(1) Radiative processes

The continuous spectra of rare gas atoms, which are of interest in pumping lasers, are due to radiative transitions of electrons from free to bound states and from one free state to another free state. Bound electrons can be situated in an atom, a positive ion or a negative ion; a free electron can travel through the field of an atom or ion. So we can distinguish the following processes:

for free-bound transitions:

$$A + e \rightarrow A^- + h\nu$$
$$A^+ + e \rightarrow A + h\nu \qquad (2\text{-}1)$$
$$A^{++} + e \rightarrow A^+ + h\nu, \text{ etc.}$$
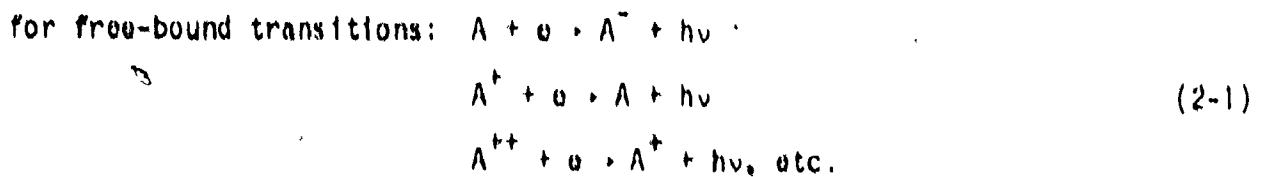
and free-free transition in the presence of an atomic or ionic field (Bremsstrahlung):

$$A + e(v_1) \rightarrow A + e(v_2)$$
$$A^+ + e(v_1) \rightarrow A^+ + e(v_2) \qquad (2\text{-}2)$$
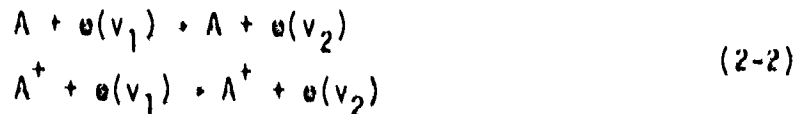
where

$$\frac{1}{2} M_e v_1^2 - \frac{1}{2} M_e v_2^2 = h\nu$$

and $h\nu$ is the energy of the emitted photon. The resultant continuous spectra are superpositions of several spectra produced by individual transitions.[26,27] The ions needed for some of the above processes are the result of inelastic collisions such as

$$A + e^- \rightarrow A^+ + 2e^-$$
$$A^* + B \rightarrow A + B^+ + e^- \qquad (2\text{-}3)$$

which occur when electrons get accelerated by the applied field along the tube.

(11) Spectra

A description of some rare gas spectra is given by Oliver et al.[11,13] According to these data, the spectra of the rare gases show strong peak regions in the near IR, for input energies of a few Joules ($1/cm^3/\mu sec$). In the visible region, the spectra appear to be varying smoothly with wavelength. There is a considerable increase (more pronounced in the near UV and blue region) of the absolute irradiance with the current density, and slight increase of the irradiance with the increase of pressure over the region 200 to 500 Torr.[11,13] It is important to note that above 400 Torr and high current densities above 3000 A/cm^2, the continuous spectrum dominates over the resonant peaks.[13] Also, the irradiance of Xenon is slightly higher than the rest of the rare gases, and this is related to the smaller ionization potential of the xenon gas, which results in higher electron densities of the plasma. Also, for a given input energy density, there is an optimum pressure for maximum irradiance. Above certain pressure, the plasma becomes self-absorbing and in that case, the radiation we get comes only from a thin layer at the surface of the plasma.[12,38] For low pressures, though, an increase of pressure will result in higher resistance and thus more energy dissipation within the flashlamp.[11] In other words, pressure is a parameter which has to be optimized for best results under fixed current density and flashtube diameter and length. It has been found that the addition of certain dopants (such as Zn) in the tube will enhance the brightness of the flashlamp in the near UV region,[51,52] because those dopants provide additional bound-bound transitions whose energy corresponds to the UV region. Consequently, we get radiation from the new broadened

lines of the dopant in this near UV region   Additional enhancement
in the near UV region can be achieved by applying the double-discharge
technique.[51,53] This method utilizes a relatively long duration low
current discharge, which is followed by a short high current main dis
charge. It is not clear yet how this mechanism works and the enhance
ment may be due to several effects such as metastable atoms, UV photons
or diffuse plasma production by the slow discharge.

(iii) Electrical characteristics

In order to design an efficient driving circuit for rare gas
flashlamps, it is important to know the resistivity of the plasma during
the discharge. Here we will deal only with the Xenon plasma resistivity,
because Xenon is the most efficient of all rare gases. By simultaneous
monitoring on a dual beam oscilloscope of the current through a flash-
lamp and the voltage across the tube, Gonz[23] found (after experimenting
on several bore and length tubes)   that the xenon plasma resistivity
can be represented by the equation

$$\rho = 1.13/J^{1/2} \ \Omega\text{-cm}$$ (24)

where J is in Amps/cm^2. This relation was found to be true for current
densities between 3000 A/cm^2 to 10,000 A/cm^2, bore diameters between 1.3 mm
to 28.0 mm and length 0.25 inches to 12.0 inches. In this range of cur
rent density, the resistivity of the xenon ranges from 0.011 to 0.021 Ω-cm,
after the time the discharge has been fully developed. Similar results on
the xenon resistivity have been also reported by Bakeev et al.,[25] (ρ =
1.13/J$^{1/2}$ Ω-cm). Additionally, Bakeev[25] reported a weak dependence of

the resistivity on the cold pressure of the xenon which fills the flash
lamp. As the pressure increases from 100 Torr to 400 Torr, the con-
ductivity drops by a factor of approximately 1.5.[25] Above 400 Torr,
there is no significant change in the xenon conductivity. Bekeev[25]
also measured the conductivity as a function of the plasma temperature
for pressures between 100 and 600 Torr and temperatures between 8,000°K
and 14000°K. It was found that the xenon conductivity dependence is
quite different from the one predicted theoretically by Spitzer[27]
for a Lorentzian gas (fully ionized with no electron-electron inter
action and all positive ions at rest). This indicates the importance
of electron-electron interactions in this range of high pressure where
the degree of ionization can be as high at 10%. It was shown by Rovinskii[55]
that at these high pressures, even at a low degree of ionization (frac-
tion of a percent) but with relatively high values of concentration of
charged particles ($\sim 10^{16}$ cm^{-1}), the main contribution to resistivity
comes from collision between electrons and ions. Therefore, such plasma
could be considered as fully ionized but electron-electron interaction
should be taken into account to get the right results theoretically.
This is so, because though mutual electronic interactions do not change
the conductivity directly, since the total change of momentum in such
interactions is zero, nevertheless, they alter the velocity distribu-
tion of the travelling electrons between collisions with the ions. This
effect produced by electrons beyond the interionic distance may be attri-
buted to statistical fluctuations of the electron density, which pro-

duces a local field of random direction.

After we have established the resistivity of the xenon gas for a particular current density and pressure, we can establish a transfer efficiency of the electrical energy to the lamp. Thus, knowing that

$$\rho = KJ^{-1/2}; \quad E = \rho J$$

we get for the voltage across the discharge

$$V = K_0 I^{1/2} \tag{2-5}$$

and the efficiency

$$\eta_{eff} = \frac{K_0 I^{1/2}}{K_0 I^{1/2} + R_c I} = \frac{K_0}{K_0 + R_c |I|^{1/2}} \tag{2-6}$$

with

$$K_0 = \frac{2KL}{d\pi^{1/2}}$$

where E is the electric field, L the lamp length, d the diameter and R_c the lamp discharge circuit resistance. To get high efficiency, we thus have to minimize the circuit resistance. Depending on the application, different driving circuits have to be devised. There are several papers published on the design of driving circuits[14,56-61] and the triggering of the flashlamps.[59,61-66] Markiewicz et al.[8] provided a computer solution to single mesh circuit for driving the flashlamp for pulses longer than 30 μs. According to his analysis for a given lamp type, energy input probe duration and pulse shape factor, the inductance, the capacitance and the operating voltage can be determined uniquely for the case of a fully developed discharge. During the period of arc formation, either

or both of the arc inductance $L_{arc}(t)$ and its time derivative $L'_{arc}(t)$ become very important, because the arc starts as a thin filament and expands rapidly. This very important case is treated by Dishington et al.[60] According to these authors, the experimentally observed voltage drop along the flashlamp does not resemble the $V = K_0 \sqrt{I}$ relation at the start of the pulse. There is a voltage spike along the lamp at the start of the pulse, which is attributed to the arc growth. It was also found that the diameter of the arc is dependent non-linearly on the amount of energy fed into it, and the arc diameter changes faster during the wall free expansion period than during the wall-dependent expansion. The changeover in these distinctive periods of growth is dependent on the input energy for given diameter tubes of fixed length. Taking this wall effect into account, a general set of equations is derived which can be used to calculate the parameters of the mesh circuit for given input energy and pulse duration. To avoid the wall effects and also restrict the expansion of the discharge, a new method has been developed, namely the vortex stabilization technique[67] which positionally stabilizes the arc at the centre of the tube by vortex induced pressure gradient across the tube.

In conclusion, rare-gas flashtubes have been extensively investigated and a good deal is known about the mechanisms responsible for the different spectra, the spectral dependence on pressure, current density dopants and pre-ionization. Their resistivity has also been known very accurately and methods have been developed to find the appropriate circuit parameters and take into account the transverse expansion of the discharge. Rare-gas

flashlamps have been used to pump efficiently different systems in the
IR and visible spectrum in cases where relatively slow (above a few micro-
sec) pulses are adequate. Fast pulse operation (in the fraction of a mi-
crosec region) can not be achieved with these types of flashlamps with-
out altering the mode of operation because of the high gas pressure,
the discharge expansion and the tube wall presence. These flashtubes
operate in a relatively low temperature of the plasma and the spectrally
selective radiated emission comes from all the plasma volume available.
On the contrary, the ablation flashlamps with which we deal next, operate
at a much higher temperature, emit as a black body for high enough current
density, and are capable of producing much faster pulses, but are not as
efficient as the rare-gas ones in transforming electrical energy into a
specific spectral interval.

2.2.2 Ablation flashlamp characteristics

Ablation flashlamps, are so called because the discharge in these
lamps occurs primarily in vapours ablated from the quartz envelope. These
lamps produce intense light pulses of lengths varying from a fraction of
a microsecond up to 30 μsec with submicrosecond risetimes. They are made
of thick wall, small annulus quartz with flexible connections at the end
to withstand the current-induced shock waves and can be tailored in shape
to satisfy the particular applications. The peak emission of the ablation
flashlamp has been found to approximate that of a high temperature black-
body (20,000 to 30,000°K range) from the near ultraviolet into the infra-
red.[31,35,66] In order to increase the strength of the tube to shock
waves, most designs include ballast chambers at the tube ends, to damp the

pressure build-up during the discharge. Details on the construction of these lamps can be found in a number of references, which also include some operating characteristics.[36,37,68,69] We will give a more detailed discussion of these characteristics later.

It should be noted here, though, that a flashlamp designed to deliver the maximum possible fraction of the total available discharged energy to a particular emission band (which is the case with rare-gas lamps discussed before) will almost certainly not have the same characteristics as a system designed to deliver maximum peak output within a given wavelength range (ablation flashlamps). This inevitably leads to a consideration of the instantaneous energy delivery per unit volume to the flashtube plasma to make it a blackbody radiator with as high temperature as possible. It is true that for a blackbody radiator, the temperature increase will move the peak of radiation to shorter wavelengths but at the same time, the radiation delivered within a certain wavelength region will keep on increasing. In that respect, a blackbody radiating ablation flashtube is the best we can achieve as far as peak radiation intensity is concerned. Certainly, in this way we do not optimize the total intensity with respect to the electrically stored energy, but we are after high peak intensities in a specific region in the form of very fast risetime pulses.

2.3 EXPERIMENTAL APPROACH

Figure 2-1 is a schematic diagram of the flashtube assembly which was used in the experiments described later. The flashtube is of the linear type, it is demountable and consists of a fixed length (8 cm) of

Figure 2-1. Schematic diagram of the flashtube assembly: (1) quartz thick wall capillary tube; (2) ballast chamber; (3) stainless steel electrodes; (4) rubber tube; (5) water inlet; (6) gas inlet; (7) glass tube to keep the water around the flashtube only; (8) aluminum support part of the elliptical cavity; (9) perspex end housing of the flashtube; (10) O-ring seal for the low pressure flashtube.
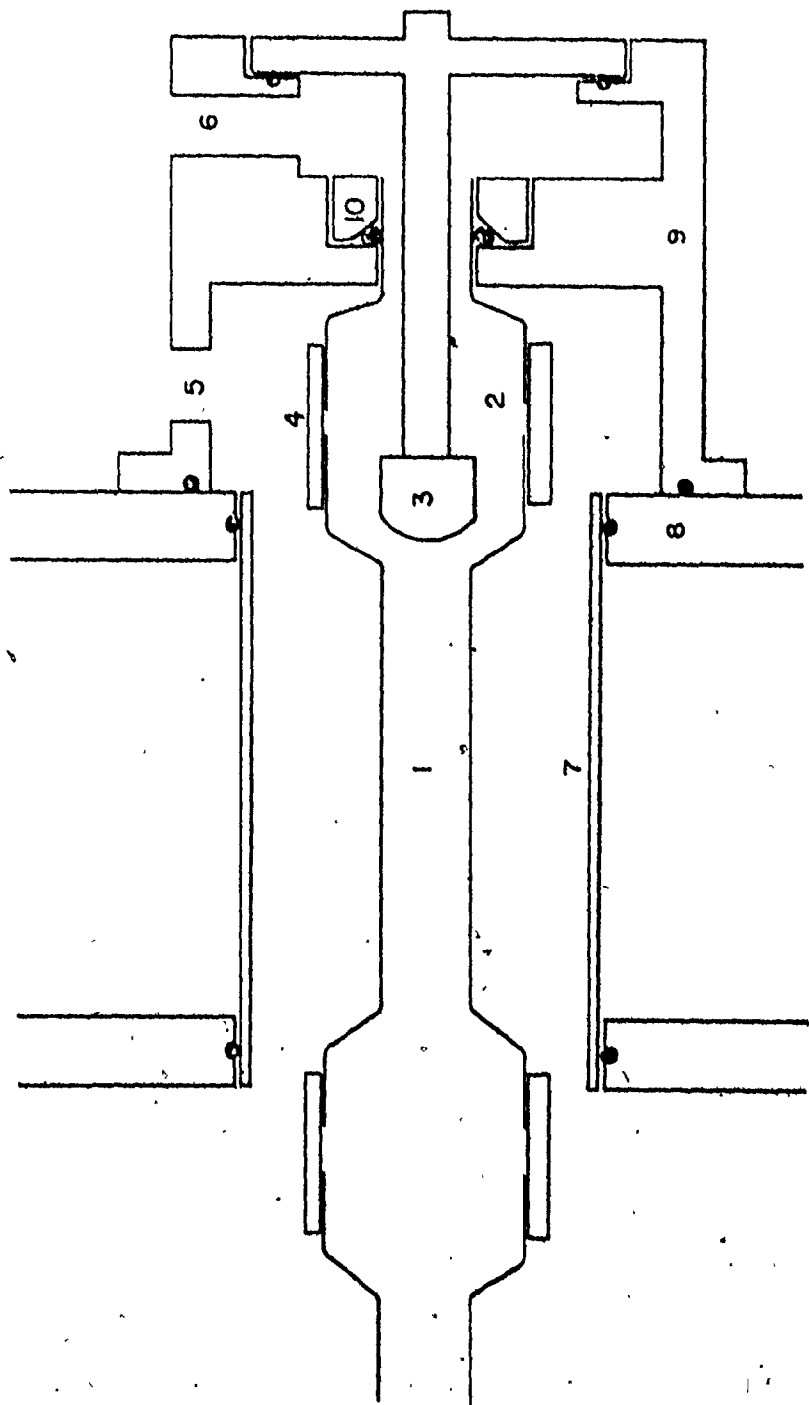
FIG. 2—1

thick walled (3 mm) quartz capillary tube. At each end of the capillary tube, we provide a ballast chamber which has more than fifty times the volume of the flashtube. This serves to dampen the impact of high pressure waves which are created during the discharge. Two electrodes made of stainless steel are used and a section of rubber tubing is employed to help support the tube, damp any axially transmitted pressure shock and seal the tube from the surroundings to provide for the vacuum which is needed. Distilled water circulates continuously around the flashtube, serving to cool the tube, absorb some UV radiation and provide an additional dampening mean for the shock waves across the tube, because the shock wave will find a smaller density discontinuity in the interface. The rest of the UV radiation is absorbed by the pyrex tube which contains the water stream. It has been found that UV radiation can dissociate some of the dyes,[2] so care is taken to contain the UV radiation. A vacuum pump is used to lower the pressure within the discharge region and the flow of the filling gas is regulated by two needle valves at each end of the tube in order to control the pressure variation along the tube to within a few percent of the average pressure desired.

The quartz ablated during a discharge solidifies at the walls of the ballast chambers where the sputtered part of the electrodes is also collected, leaving the main flashtube clean. The electrodes were cleaned each time a set of measurements was taken. It was found that after a long time of operation some ablated quartz will also cover the electrodes and thus increase the resistance of the tube at the start of the pulse and during the triggering time. The loss of the quartz due to ablation also finally alters the diameter of the tube and consequently, the energy

density delivered to the tube causing a decrease of the produced radiation.

Although we have not done any explosion tests, we found that our thick wall tubes (ID ≈ 1.7 mm, L ≈ 8 cm) could easily sustain more than 10000 μsec pulses with energy densities in excess of 350 J/cm^3 and repetition rates of one pulse every few seconds. This explosion limit is a factor of three higher than the one predicted for similar tubes[13] and this is attributed to the thick walls of the tube and the shock absorbing construction. The electrical storage device consists of a low-inductance (a few nH) high voltage capacitor (0.14 μF) selected to give the smallest reverse current within the desired voltage range of operation and current risetimes. This capacitor is connected to the lamp with very short and flat connectors to minimize the circuit resistance and inductance. The circuit is fired by a very fast spark gap (EG&G 14B), triggered by a triggering module (EG&G TM11A) which in turn is driven by a pulse generator for push button or automatic operation at the desired repetition rate. The capacitor charging voltage was varied between 10 and 30 KV, and the time varying discharge current was routinely monitored by employing a current transformer (Pearson Electronics, model 411). The flashtube was placed on one of the two axes of an elliptical cylindrical reflector which was made out of a stainless steel tube by compressing it appropriately. The inside of the reflector was, to a very good approximation, a perfect elliptical reflector and high reflectivity could be maintained by using highly reflecting mylar paper. The other axis of the elliptical cylindrical reflector was occupied by a cylindrical dye cell where the dye solution could circulate using a micropump. The light emitted by the flashlamp was sampled through a small hole in the elliptical lamp housing. A broad-band filter was used

to select the band of radiation of interest to us around 5300 Å, charac-
teristic of the absorption band of Rhodamine 6G, the dye mostly used in
subsequent experiments. The detection of the light was done using either
a fast p-i-n photodiode or a photomultiplier. It was found that the
photodiode was affected less by the electrical noise produced by the
storage capacitor discharge but eventually to reduce the noise we had
to construct a Faraday box and include both the detector and the scope
in it. Both light pulses and current pulses were simultaneously dis-
played on the screen of a dual beam 556 Tektronix scope triggered from
the pulse generator used to trigger the high voltage spark gap. The
traces of the two pulses on the screen were photographed using a scope
camera and a fast polaroid film (No. 410 with 10,000 ASA).

2.4 RESULTS

In this section, we will include both experimental results obtained
and theoretical predictions based on the blackbody radiation model which
we have adapted for the flashlamp. In this way, a better understanding
of the ablation flashlamp is achieved, which can be used to gain specific
information related to the design of the flashlamp.

2.4.1 A Measure for the Peak Power

As indicated in the previous section, for flashlamp operation in
or near the ablation region, it is the instantaneous rate at which energy
is fed into unit volume of the plasma which counts. It is more convenient
experimentally to monitor the energy delivered to the discharge from the
storage capacitor. This serves, together with the variation of the cur-
rent as a function of time to establish the time dependence of the power

delivered to the discharge under the reasonable assumption of approximate constant voltage drop between the electrodes for given pressure. Consequently, if the time length of the current pulse varies little over the investigated range of experimental parameters, the energy delivered to the unit volume of the discharge acts as a measure of the power delivered to the plasma per unit volume. Accordingly, we will seek first to establish the current pulse length variation with flashlamp and discharge circuit parameters.

In general, fully developed discharges (which are the ones with no more expansion of the plasma column) operate with an approximately constant voltage drop between the electrodes for a given pressure. We have found that, in the region of 5 to 40 Torr, the DC breakdown voltage for the rare gases exhibits a minimum which does not change very much with pressure. This is in accordance with the familiar Paschen's Law for the breakdown voltage, which states that the breakdown voltage depends on the product of gas pressure and electrode separation. Then, for a fixed electrode separation at low pressure, the collision frequency of electrons with gas atoms is low and to have a breakdown we have to increase the probability of ionization by supplying more kinetic energy to the colliding electrons which is done by increasing the applied voltage. At high pressures, the collision frequency is high because there are plenty of gas atoms available for ionization. However, the mean free path is small and the kinetic energy, which can be gained by an electron, is small. Therefore, to get enough ionization to sustain the discharge, we must once again raise the voltage.

Figure 2-2 gives the pressure dependence of the breakdown voltage of Argon for a tube of 1.7 mm diameter and a length of 8 cm. We also observed that the shape of the current pulse could be approximated by a damped sinosoid. The ratio of the second cycle maximum current to the one of the first is obviously a measure of the efficiency with which we can couple power into the system. The dependence of this ratio on pressure is shown in Figure 2-3, for three different voltages between the electrodes. Clearly, we see that in order to have most of the available stored energy into the flashtube as rapidly as possible, pressures in the region of 5 to 40 Torr should be chosen for our given external discharge circuit. In our experiments, we have used voltages well above the breakdown voltage along with a triggering circuit which enhances the starting of the discharge. The consequence of this is that we have a discharge occupying the whole tube, which is under constant voltage, and whose power consumption change is governed by the current pulse shape flowing into the discharge. In conclusion, we can select the current pulse as a parameter to investigate the effect of the delivered energy into the discharge.

Figure 2-4 shows the behaviour of the current pulse length as a function of the stored energy in the capacitor for two different radii of the discharge tube. The argon cold gas pressure was 10 Torr. There is a small tendency for the current pulse to shorten somewhat with increasing input energy. This is entirely consistent with the reduction in discharge resistance provided that the storage capacitor voltage is much larger than the breakdown voltage of the filling gas, which is certainly the case here. As we will see later, the current pulse length does not change very much with the pressure either over the region of

Figure 2-2. D.C. breakdown voltage of Argon for a 1.7 mm diameter,

8.0 cm long quartz tube.

BREAKDOWN VOLTAGE (KV)

PRESSURE (TORR)

FIG. 2—2

200

100

4.0

2.0

46
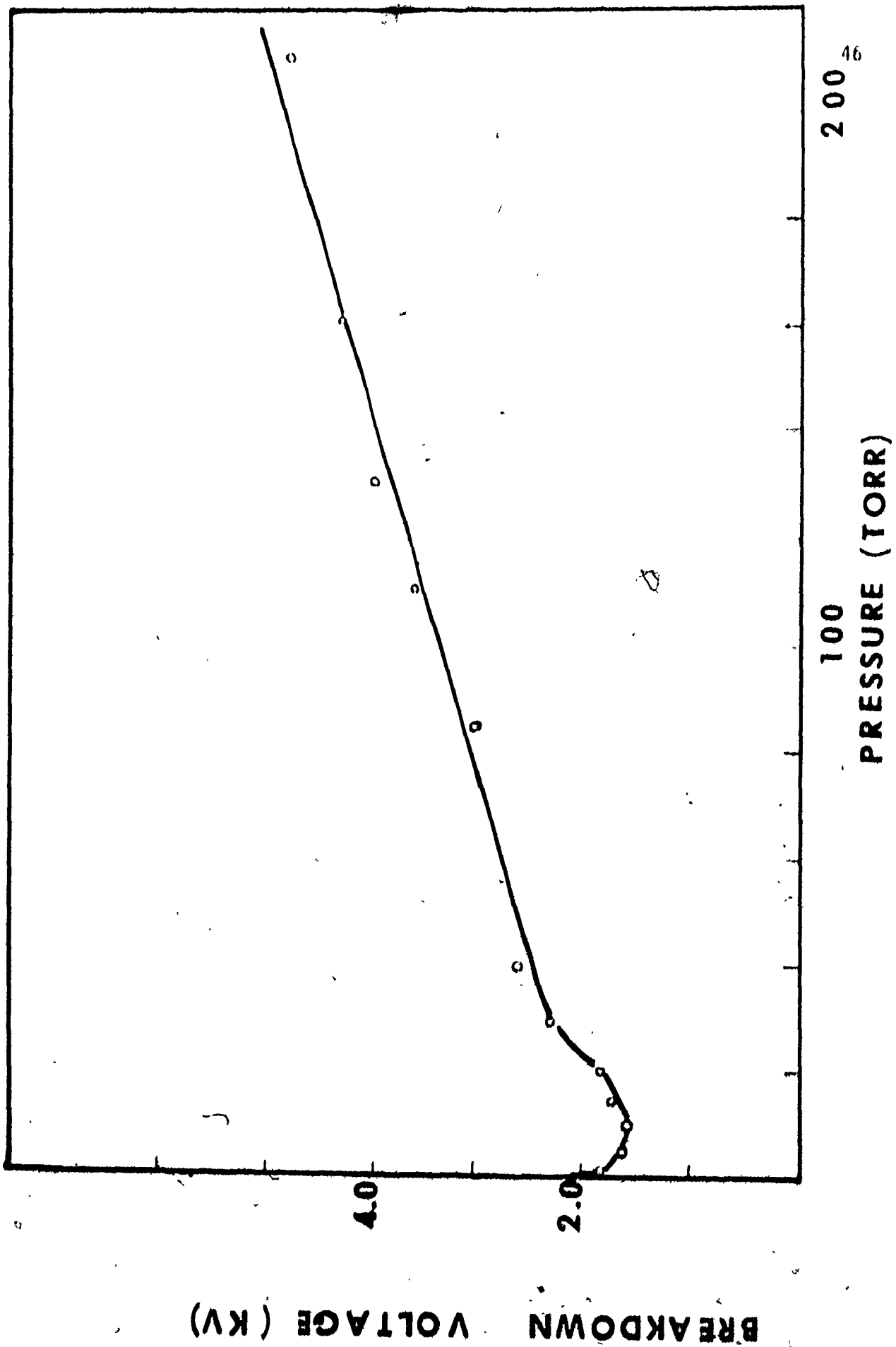
Figure 2-3. Current overshoot versus pressure for three different
voltages. The overshooting is defined as the ration of
the maximum reverse going current to the maximum forward
going current. The tube has an 1.7 mm diameter and is 8.0
cm long. The capacitance is 0.143 μF.

FIG. 2—3

PRESSURE (TORR)

SHOOT (%)

26 KV

24 KV

20 KV

20.0 30.0 40.0

5.0 10.0 15.0

47
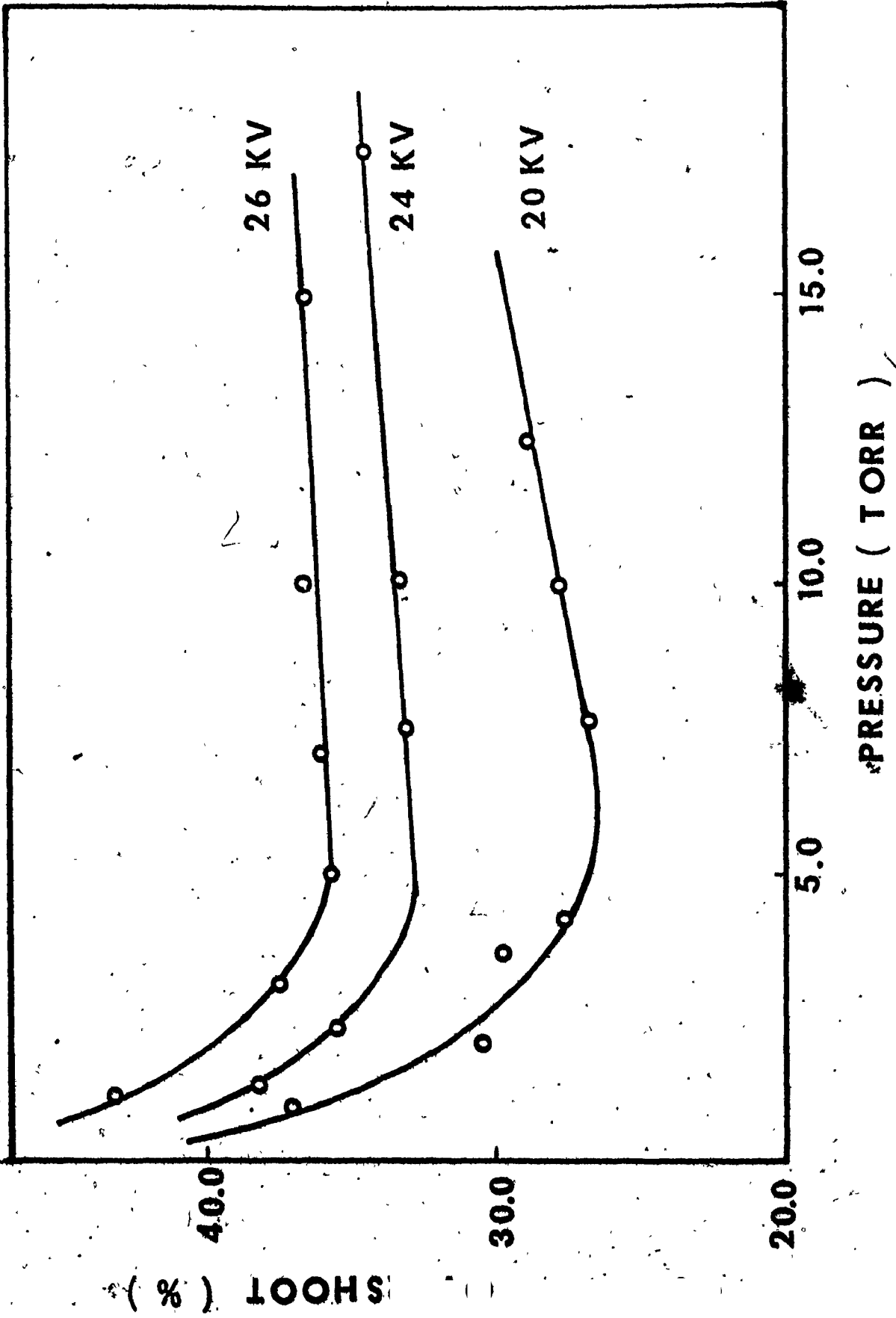
Figure 2-4. Current pulse length as a function of the capacitor stored energy for flashtubes with diameters of 1.7 mm (O) and 2.5 mm (Δ). The gas fill is 10 Torr of argon, and the tube length is 8 cm. The capacitance is 0.143 μF.
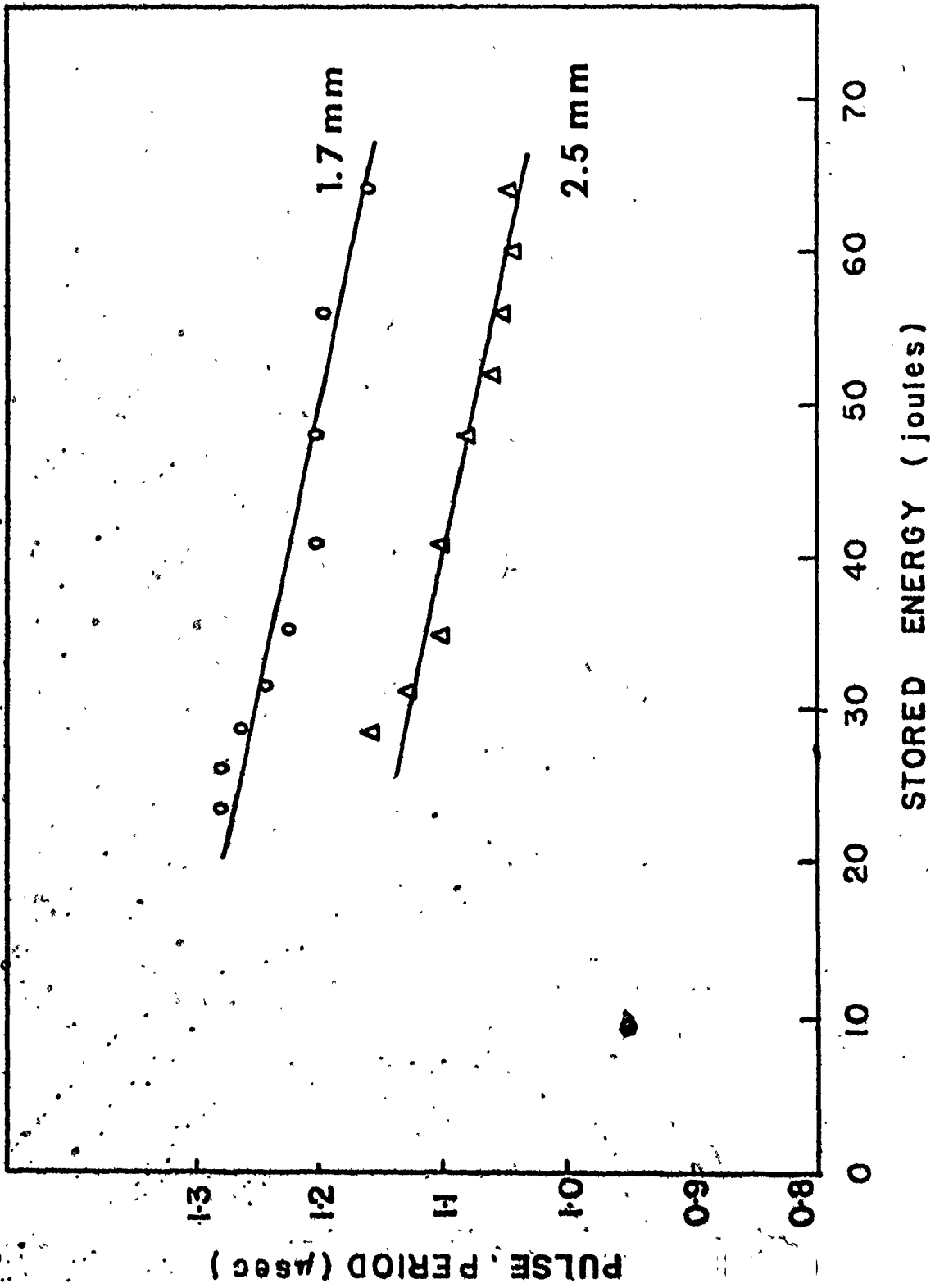
FIG. 2—4

operation. As a consequence, we can employ the energy input per unit volume of the discharge as a measure of the peak power delivered to the unit volume of the discharge for the measurements reported in subsequent paragraphs.

2.4.2 The Blackbody Radiation Model

High current, short pulse flashlamps have been previously considered to radiate as blackbodies at the temperature of the plasma,[12,66] with temperatures of the order of 20,000°K,[66] and more.[32] Evidently, the maximum intensity available from the plasma, in the ablation case, is when the medium radiates as a blackbody at the plasma temperature. Accordingly, provided that we deal with a highly ionised plasma, the radiation at the plasma temperature will be maximal within any spectral region, regardless of the physical make-up of the plasma. In this case, the radiation comes only from the surface of the plasma and can be related to the plasma temperature by the well-known Steffan-Boltzman's Law

$$S = 2\pi r L a T^4 \qquad (2-7)$$

where r is the radius of the plasma column, L is the tube's length, T the plasma temperature, S is the total radiation emitted and $a = 5.6 \times 10^{-12}$ w cm^{-2}(°K).^{4}

Gusinow[32] has presented a model which relates the discharge current density to the temperature of the plasma under the following assumptions:

(1)   The resistivity of the flashlamp is that of a fully ionized plasma. The plasma is assumed to be a Lorentzian one (the ions are assumed to be infinitively massive, at rest, and the

electrons do not interact with each other).

(ii)   Electrode and wall effects are ignored and so, the total elec-
        trical input power goes into producing radiant energy.

(iii)   The plasma surface radiates as a blackbody and the plasma com-
        pletely fills the container.

(iv)   An Ohm's Law-type relation holds between voltage and current
        with the constant of proportionality being the resistance.

According to this model, the resistivity of the plasma is given
by (reference 27, page 138):

$$\eta = 2.28 \times 10^4 \, T^{-3/2} \text{ ohm-cm} \tag{2-8}$$

for the region of temperatures and electron densities of interest in our
case, (temperatures above 20,000°K and electron densities of the order
of 10^{16}/cc or more). Then, the relation between temperature and current
density is found by assuming that the total blackbody radiation is equal
to the total ohmic heating. Accordingly, for a tube with radius r,
length L, resistivity η, the resistance is given by

$$R = \frac{\eta L}{\pi r^2} \tag{2-9}$$

and the energy balancing relation will be

$$(2\pi r L)aT^4 = \frac{\eta L}{\pi r^2} I^2 \tag{2-10}$$

where I is the discharge current. The temperature can then be deduced
using equations (2-8), (2-9) and (2-10), resulting in:

$$T = 603(J\sqrt{r})^{4/11} \tag{2-11}$$

This empirical relation is in agreement to within 50% with some experimental data presented in Figure 1 of reference 32. The reasons for disagreement lies in the assumptions made. First of all, the wall effects cannot be ignored totally for such small diameter tubes (mm size) and such high energy inputs and second, the Lorentzian plasma assumption is not really true in this case; because when particles interact according to inverse square forces, the velocity distribution function, which will affect the resistivity, is affected by the many small deflections produced by relatively distant encounters. There are many simultaneous encounters during the time a particle travels over its mean free path, which will affect its velocity for electron densities in excess of 10^{16} cm^{-3}. Next, we will determine a more accurate value for the resistivity, relevant to our experimental conditions.

To improve the model, we assume that the resistivity of the plasma has the same form as (2-8), and compare predictions with appropriate experimental data to obtain a more accurate value for the constant in the resistivity equation. Accordingly, for the present, we take

$$\eta = BT^{-3/2} \text{ ohm-cm} \tag{2-12}$$

Then, using equations (2-10) and (2-12), we get for the temperature

$$T = (B/2\pi^2 a)^{2/11} (I^2/r^3)^{2/11} \tag{2-13}$$

This, in turn, permits the total radiation, S, to be expressed in terms of plasma tube diameter and discharge current ($S = 2\pi r L a T^4$):

$$S = (\frac{L B}{\pi})(\frac{B}{2\pi^2 a})^{-3/11} (\frac{1}{r})^{13/11} (I)^{16/11} \tag{2-14}$$

The blackbody radiation in a given spectral interval $\Delta\lambda$ can be expressed as

$$S_E \cdot S(\Delta\lambda) = S \cdot F(\Delta\lambda, T) \tag{2-15}$$

where $F(\Delta\lambda, T)$ is the fraction of the total blackbody radiation which occurs in the spectral interval $\Delta\lambda$ at temperature T.[70] According to the tables of blackbody radiation function,[70] the spectral radiance of a blackbody N_λ is given by

$$N_\lambda = \frac{C_1}{\lambda^5 (\exp(\frac{C_2}{\lambda T}) - 1)} \frac{Watt}{cm^3 \, ster \, ad} \tag{2-16}$$

where $C_1 = \frac{2hC^2}{\Omega_0}$, $C_2 = [\frac{2\pi^5 hC^2}{15\alpha}]^{1/4}$, h is Planck's constant, α is the Steffan-Boltzman constant, Ω_0 is the solid angle, and C is the velocity of light. The relative spectral radiance D, which is the total radiance emitted in a certain region of the spectrum divided by the total radiance emitted in the whole spectrum is given by

$$D = \int_0^\lambda N_\lambda d_\lambda / \int_0^\infty N_\lambda d_\lambda$$

We are interested in the interval 5000 Å to 5500 Å, which is where the Rhodamine 6G dye absorbs (absorption peaks at 5300 Å). In that case,

$$F(\Delta\lambda, T) = D_{5500 \, Å} - D_{5000 \, Å} \tag{2-17}$$

and we can easily calculate it from the tables of reference 70 and plot the total radiation $S_E(5500 \, Å - 5000 \, Å)$ vs the maximum current (where equation (2-8) has been used for the resistivity). Figure 2-5 supplies this plot for a flashlamp of 1.7 mm diameter and 8.0 cm length.

Figure 2-5.   Variation of the total emitted radiation, $S(\Delta\lambda)$, in a given spectral interval (5000-5500 Å) with the discharge current. Tube diameter is 1.7 mm. Tube length is 8.0 cm. The storage capacitance is 0.143 µF.

FIG 2

S(Δλ) × 10⁴ (WATTS) vs _MAX. CURRENT (KA)_
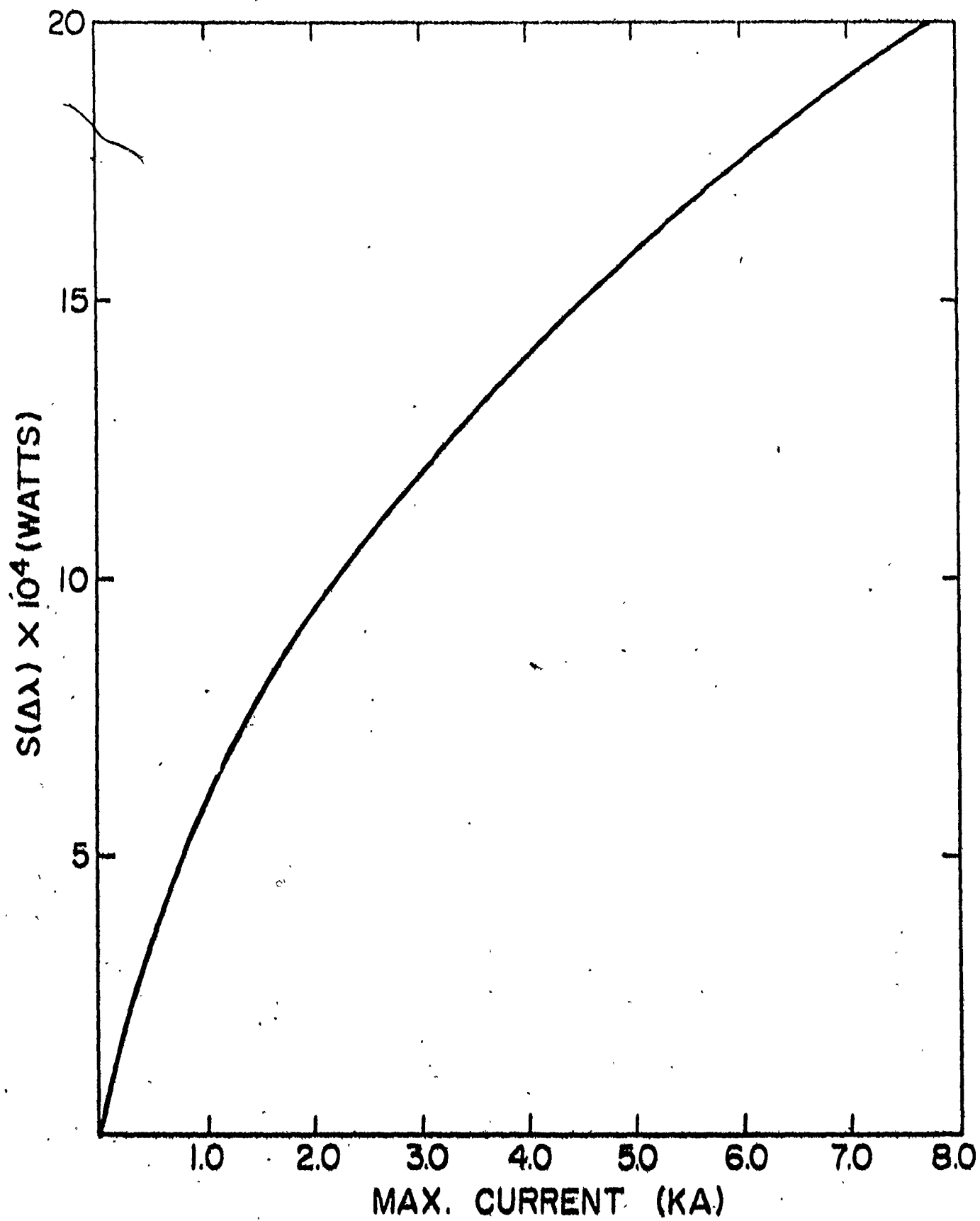
Experimentally, it is more convenient to treat the energy input to the plasma than the discharge current; it is also more revealing theoretically to treat the flashtube behaviour in terms of the energy input to unit volume of the plasma. This can be done in the following way; the energy supplied to the plasma is assumed to be proportional to $I^2 R$ then the specific input energy E_N is

$$E_N = (I^2 R / \pi r^2 L) \Delta t \qquad (2\text{-}18)$$

and the light emitted in the interval $\Delta \lambda$ is

$$S_E = (\pi r^2 L) \cdot E_N \cdot F(\Delta \lambda, T) \qquad (2\text{-}19)$$

because all the energy (E_N · VOLUME) goes to give the total radiation S ($S = \pi r^2 L \cdot E_N$).

The input energy is given by

$$E_{IN} = I^2 R \Delta t \qquad (2\text{-}20)$$

assuming a roughly constant rate of energy input. Using (2-9) and (2-12) we get:

$$R = \frac{\beta L}{\pi r^2} = \frac{\beta T^{-3/2} L}{\pi r^2} = \frac{\beta L}{\pi r^2} \frac{1}{(\frac{\theta}{2\pi^2 a})^{3/11} (\frac{I^2}{r^3})^{3/11}}$$

which can be written:

$$R = \frac{\beta L}{\pi} (\frac{\theta}{2\pi^2 a})^{-3/11} \cdot (\frac{1}{r})^{6/11} (\frac{1}{r})^{13/11} \qquad (2\text{-}21)$$

Then, (2-20) becomes

$$E_{IN} = I^2 R \Delta t = \frac{L \beta}{\pi} (\frac{\theta}{2\pi^2 a})^{-3/11} (\frac{1}{r})^{13/11} I^{16/11} \Delta t \qquad (2\text{-}22)$$

But

$$l_{IN}/\pi r^2 L \sim l_N$$

and (2-22) can be written as

$$E_N = (B\Delta t/\pi^2)(B/2\pi^2 a)^{-3/11}(1/r)^{36/11}(1)^{16/11} \qquad (2\text{-}23)$$

where Δt is the length of the current pulse. The predicted functional form of the relationship between E_N and I in equation (2-23) can be tested by direct experiment. Furthermore, for a known pulse and discharge tube radius, the numerical constant B in equation (2-23) can be found. Figure 2-6 shows a plot of E_N against $I^{3/2}$ (which is sufficiently close to $I^{16/11}$ for this purpose) for a 1.7 mm tube and an initial gas fill of 10 Torr of argon. The results are typical of those observed for other gas fills and tube diameters. Evidently, excellent agreement is obtained between theory and experiment. The value of the parameter B was determined from a series of measurements of this type, resulting in the following expression for the resistivity of the plasma

$$\eta = BT^{-3/2} \text{ ohm-cm} \qquad (2\text{-}24)$$

where

$$B = 0.96 \times 10^4 \text{ ohm-cm}(^\circ K)^{3/2}$$

which is less than the predicted value of 2.28×10^4 (equation (2-8)).

The variation of light intensity which is obtained experimentally as a function of the input energy per unit volume of the discharged plasma is displayed in Figure 2-7. These data were obtained using two different diameter tubes, 1.7 mm and 2.4 mm, and an initial gas pressure of 10 Torr of argon. On the same graph, the expected radiation in the interval 5000-5500 Å from the theory (using equations (2-14) and (2-23)) is plotted.

Figure 2-6. Plot of the maximum current to the 1/2 power against the
specific input energy. The flashtube diameter is 1.7 mm,
the length is 8.0 cm and the capacitance is 0.143 uf.

E_n (J CC)   300

FIG. 2-6

100

30

10

$I^{3/2}$ ($kA^{3/2}$)
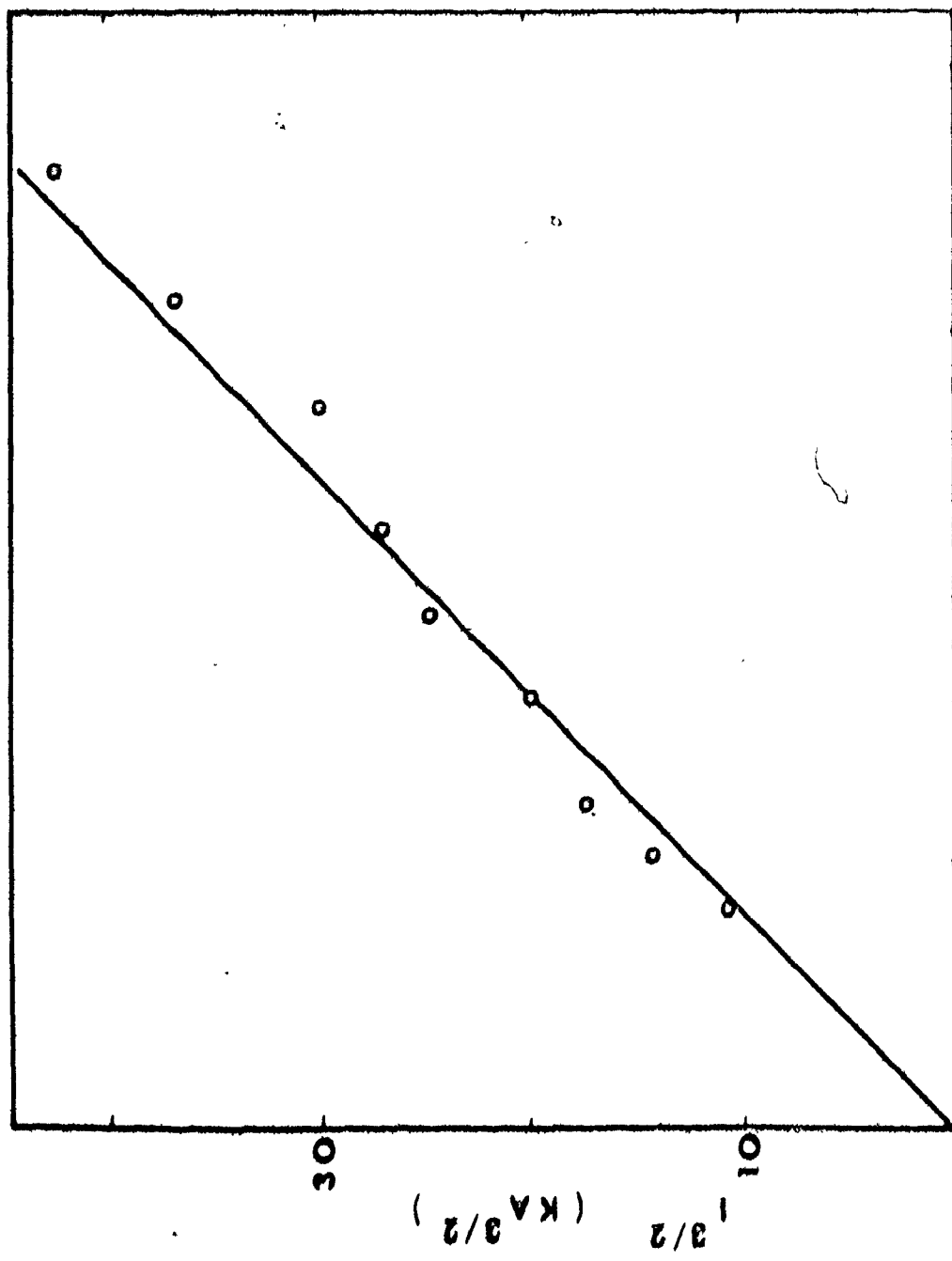
Figure 27. Maximum light intensity within the 5000 5500 Å region (I_1) as a function of the energy input per unit volume of the plasma. $\bigcirc$, 1.7 mm diameter; $\blacksquare$, 2.4 mm diameter. The initial cold gas fill is 10 Torr Argon. The tube length is 8.0 cm and the storage capacitance is 0.141 µf.
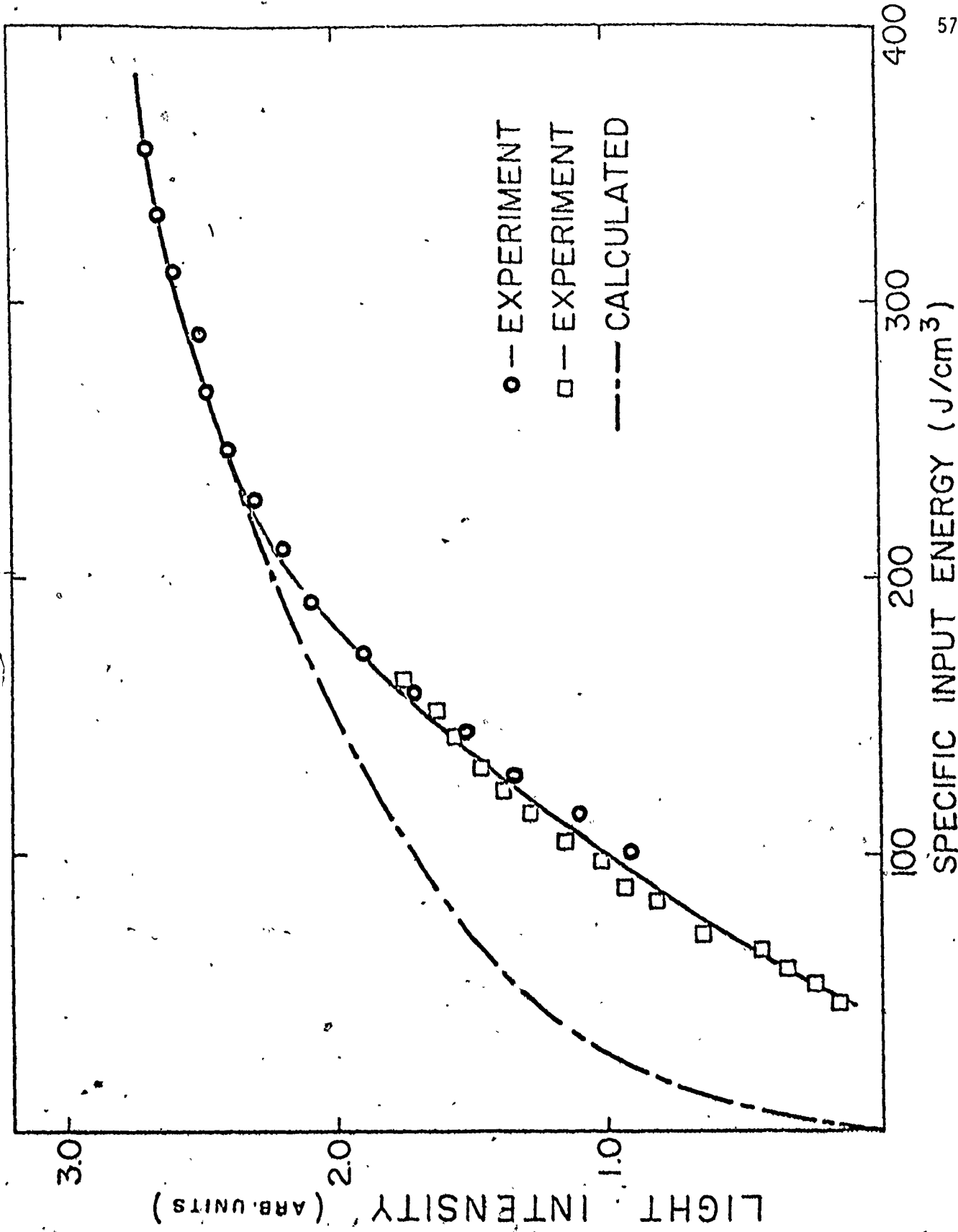
FIG. 2—7

Observe that the variation of light output against E_N has two characteristic regions:

I.   For lower excitation energies (< 150 J/cm^3), the emission is somewhat dependent on the gas fill employed and it is less than that expected if the output followed the predicted relationship by the blackbody radiation theory.

II.   For specific input energies greater than approximately 150 J/cm^3, the light output intensity follows the behaviour of a blackbody radiation emitter as predicted by the theory.

It can be seen that using input energy densities in excess of 250 J/cm^3 would produce very little change in the emitted radiation within our region of interest. As we will see later, the excess energy will cause additional ablation of the quartz tube and it will lengthen the light pulse.

Next, we show that the behaviour of the flashlamp output illustrated in Figure 2-7, particularly the tendency to saturate as a function of specific input energy, does not simply reflect the behaviour of the peak discharge current variation with specific input energy. Figure 2-8 is a plot of the peak discharge current, obtained in the same discharge tube employed for some of the data illustrated in Figure 2-7, against specific input energy. We see that there is no saturation occurring here above 200 J/cm^3 and that the behaviour is insensitive to the pressure of the gas initially in the flashtube at pressures less than approximately 100 Torr. As we will calculate later, the evaporated quartz produces pressures of the order of 200 Torr. So, to see any initial filling gas pressure effects, this pressure will have to approach 200 Torr. It can,

Figure 2-8. Peak discharge current against the specific input energy for two different filling gas pressures. The diameter of the tube is 1.7 mm, the length is 8.0 cm and the storage capacitance is 0.143 μF.
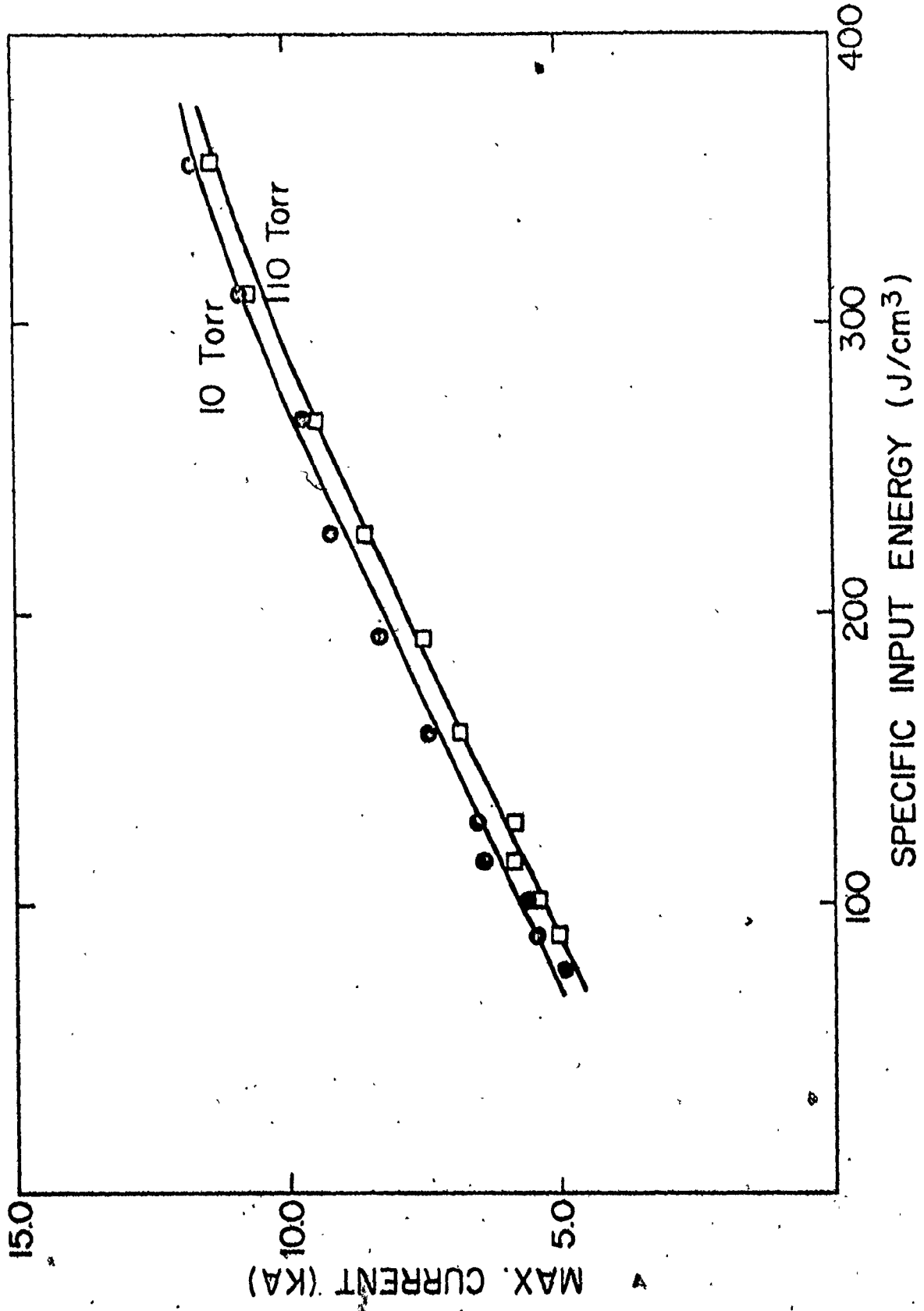
FIG. 2—8

then, be concluded that the measured saturation of the output light with increasing discharge specific input energy does not merely reflect a saturation of the discharge current with the specific input energy.

It could be argued that the rapid increase of tube wall ablation with increasing input energy could be sufficient to absorb a large fraction of the total input energy for high enough specific energies. Accordingly, we measured the material ablated from the discharge tube walls as a function of the specific input energy (E_N). The results are plotted in Figure 2-9 where the average mass of quartz lost per flash is shown as a function of E_N. It can be seen that above 200 J/cm^3, the mass lost is considerable, but still the energy needed to evaporate this mass is much less than one Joule/cm^3, and can be ignored with respect to specific input energies of 200 J/cm^3. On the contrary, though, the pressure created by this evaporation mass is of the order of 200 Torrs ($SiO_2 \rightarrow SiO + O$). This value is probably higher than the actual one because the flashtube is open-ended and expansion into the ballast chambers will reduce the pressure considerably. Nevertheless, the available quartz mass is much more than the initial cold gas mass and it is expected to dominate in the behaviour of the flashlamp. This is illustrated in Figure 2-10, which shows the maximum light intensity against the initial cold gas filling pressure for a tube of 1.7 mm diameter and 8 cm length, a storage capacitor of 0.143 μF and three different charging voltages, 23 KV, 26 KV and 28 KV. The specific input energy is such that the flashtube operates well within the ablation region. We see that the initial cold gas filling pressure has no effect on the intensity below 50 Torr. Its effect is seen only when the initial pressure increases to levels comparable to the ablation-created pressure.

Figure 2-9. Average mass of quartz lost per flash per unit of plasma volume as a function of the specific input energy. The tube diameter at the start is 1.7 mm, the length is 8.0 cm, the filling gas is argon at a pressure of 10 Torr and the storage capacitor is 0.143 μF.

FIG. 2—9

SPECIFIC INPUT ENERGY (J/cm³)

MASS LOST/FLASH/UNIT VOLUME (μgr.)
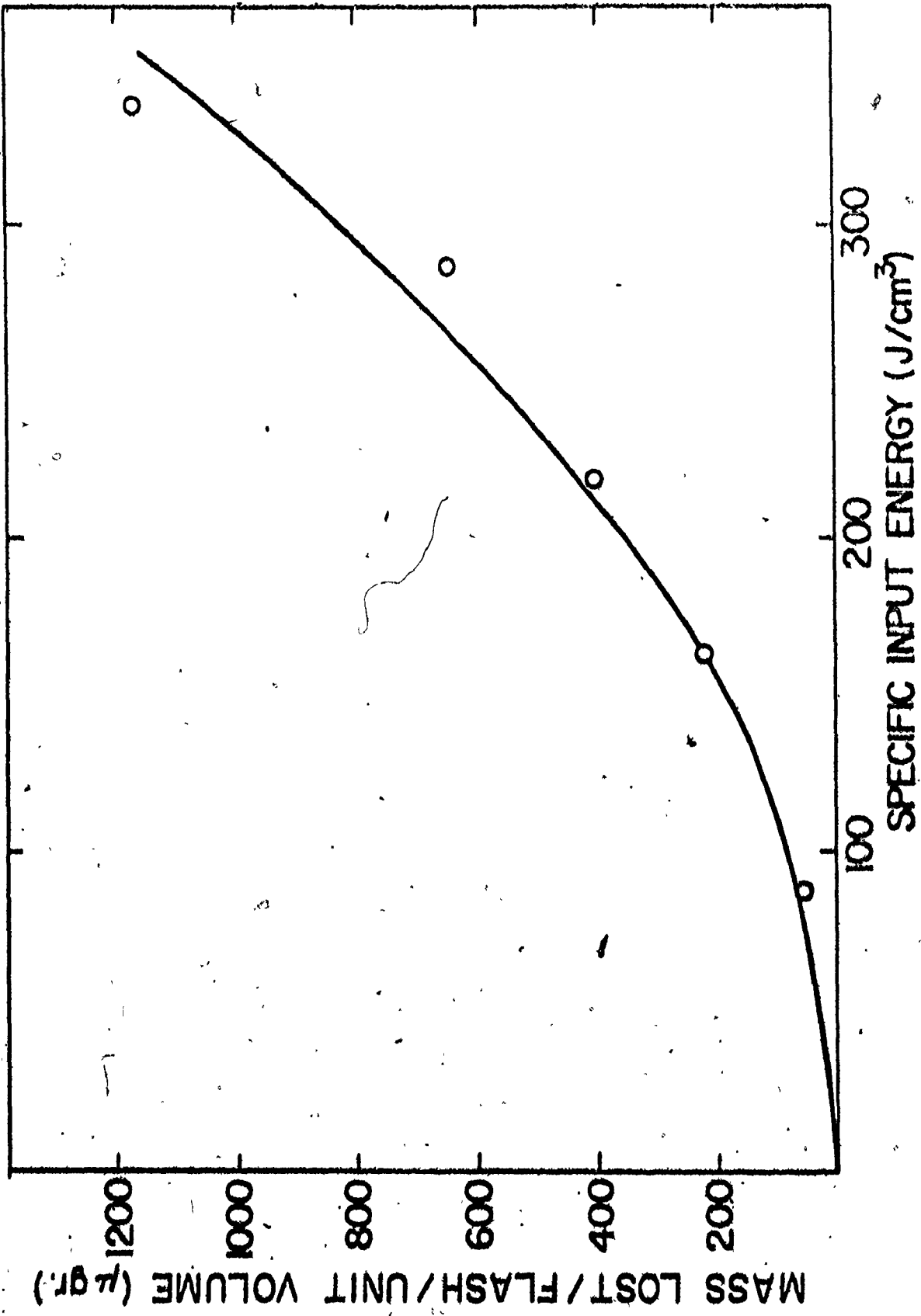
Figure 2-10. Maximum light intensity within the spectral region of interest (5000-5500 Å) as a function of the initial cold gas pressure in the flashtube. The tube diameter is 1.7 mm and its length is 8.0 cm. The storage capacitor is 0.143 µF and the intensity variation is shown for three voltages near and in the saturation region.

FIG. 2—10

MAX. LIGHT INTENSITY (arb. units)

PRESSURE (Torr)

28 KV

26 KV

23 KV

62
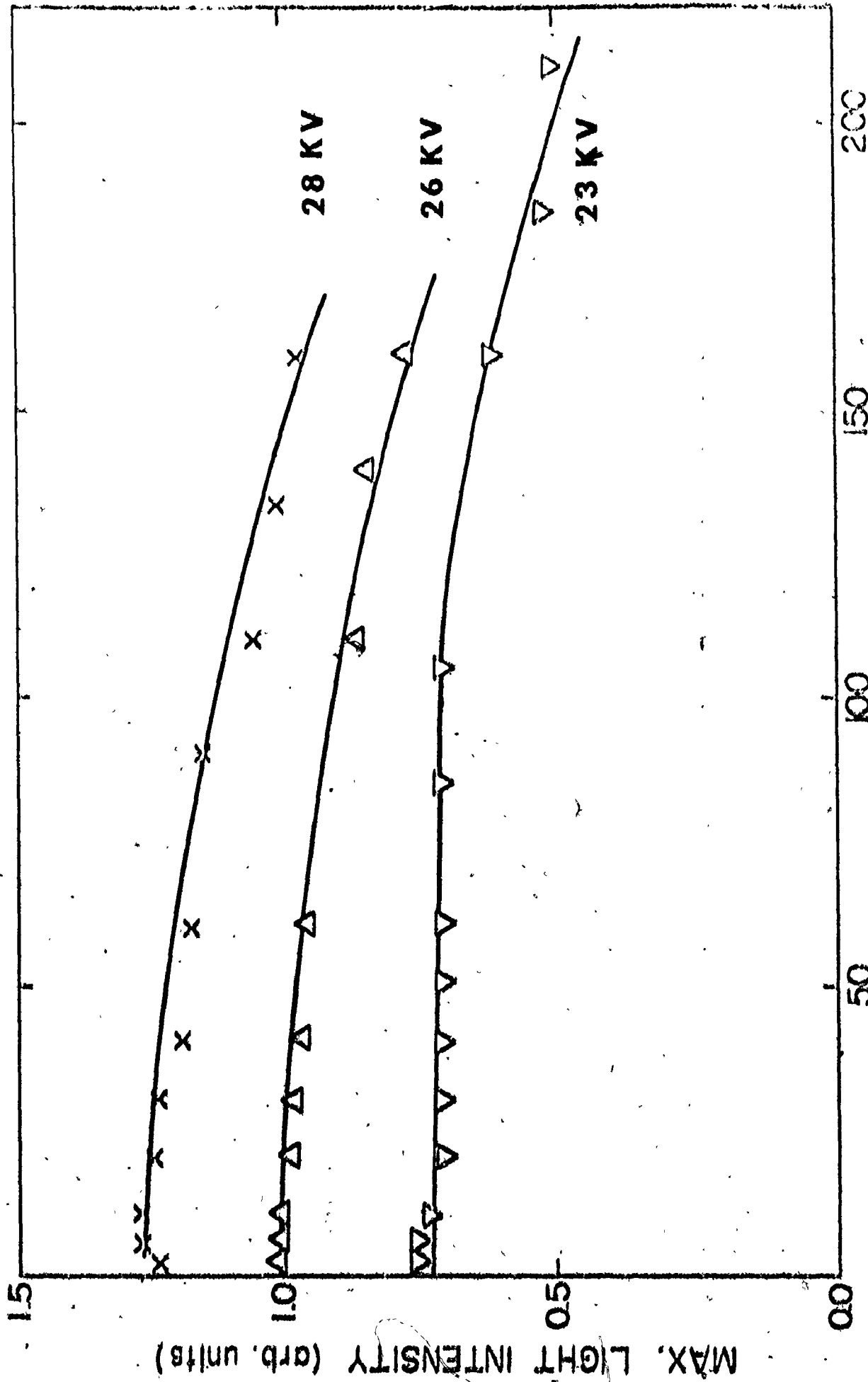
We mentioned before that calculations show that the energy required to ablate the mass of the quartz in the ablation region is a very small fraction of the available input energy and has little impact on the plasma energy balance. Consequently, this mechanism has an insignificant impact on the theoretical description presented earlier of the discharge tube operation. However, the presence of large amounts of hot ablation products in the discharge tube at the end of the current pulse does have a major consequence. The fall-time of the light output pulse depends on the rate at which heat can be lost from the discharge tube, and also on the energy stored within the tube. This stored energy depends on the density of the radiating plasma, which for high input energies is such that the plasma reabsorbs the emitted radiation and the only radiation which emerges is the one which comes from regions near the surface of the plasma, which is actually the blackbody radiation case. The falling of the light pulse can be approximated by an exponential time function. Figure 2-11 shows how the light pulse exponential decay constant, t_p, varies with the specific input energy E_N for different tube diameters and filling gas pressures. It is clear that for short pulses, we will have to stay in the small ablation region and there is a trade-off between the intensity of the pulse and its length.

At this point, the major features of the operation of high current, short pulse flashlamps operating near or in the ablation region are clear. Next, we turn to the variation of the maximum light output, in the chosen wavelength region (around 6300 Å), with specific input energy density, E_N, for different initial gas pressures. Figure 2-12 presents these results along with the variation expected from the simple blackbody radiation theory we presented earlier. It can be seen that the

Figure 2-11. The exponential decay constant of the light pulse as a function of the specific input energy for two different tube diameters and three different initial cold gas pressures of argon: O, 2-mm tube and 3-torr pressure; |, 1.7 mm tube and 3-torr pressure; A, 1.7-mm tube and 6.5-torr pressure; +, 1.7-mm tube and 140-torr pressure.

FIG. 2—11

SPECIFIC INPUT ENERGY (J/cm³)

T_2 (μ sec)
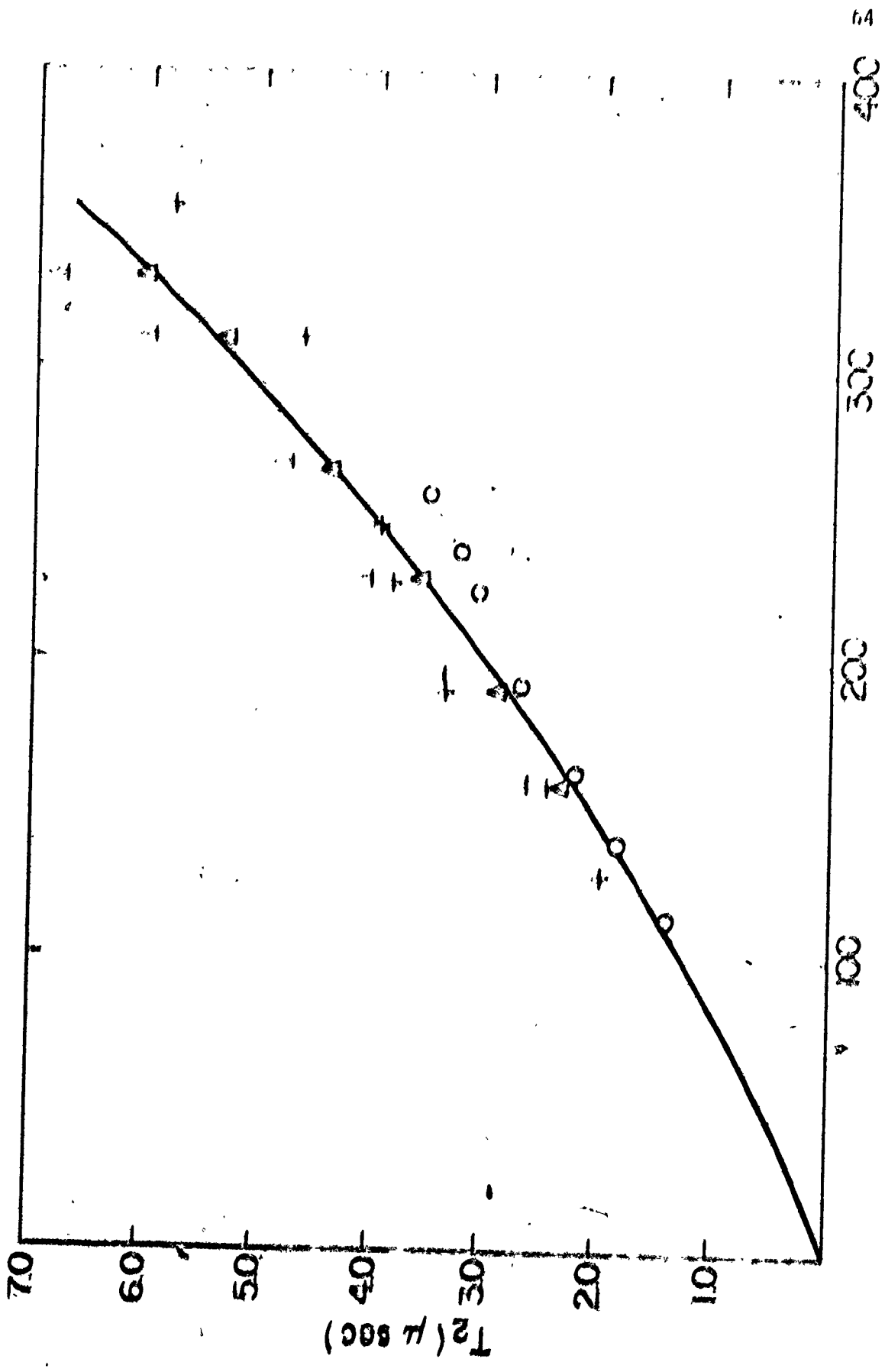
Figure 2.12. (A) Maximum light intensity as a function of the specific energy input for a variety of initial gas fill pressures and for a tube diameter of 1.7 mm

(B) Light intensity variation as a function of the specific energy input expected from the theory

FIG. 2—12

SPECIFIC INPUT ENERGY (J/cm³)

ε_{g}, I_{MAX} (arb. units)

□—10 Torr
o—110 Torr
△—185 Torr
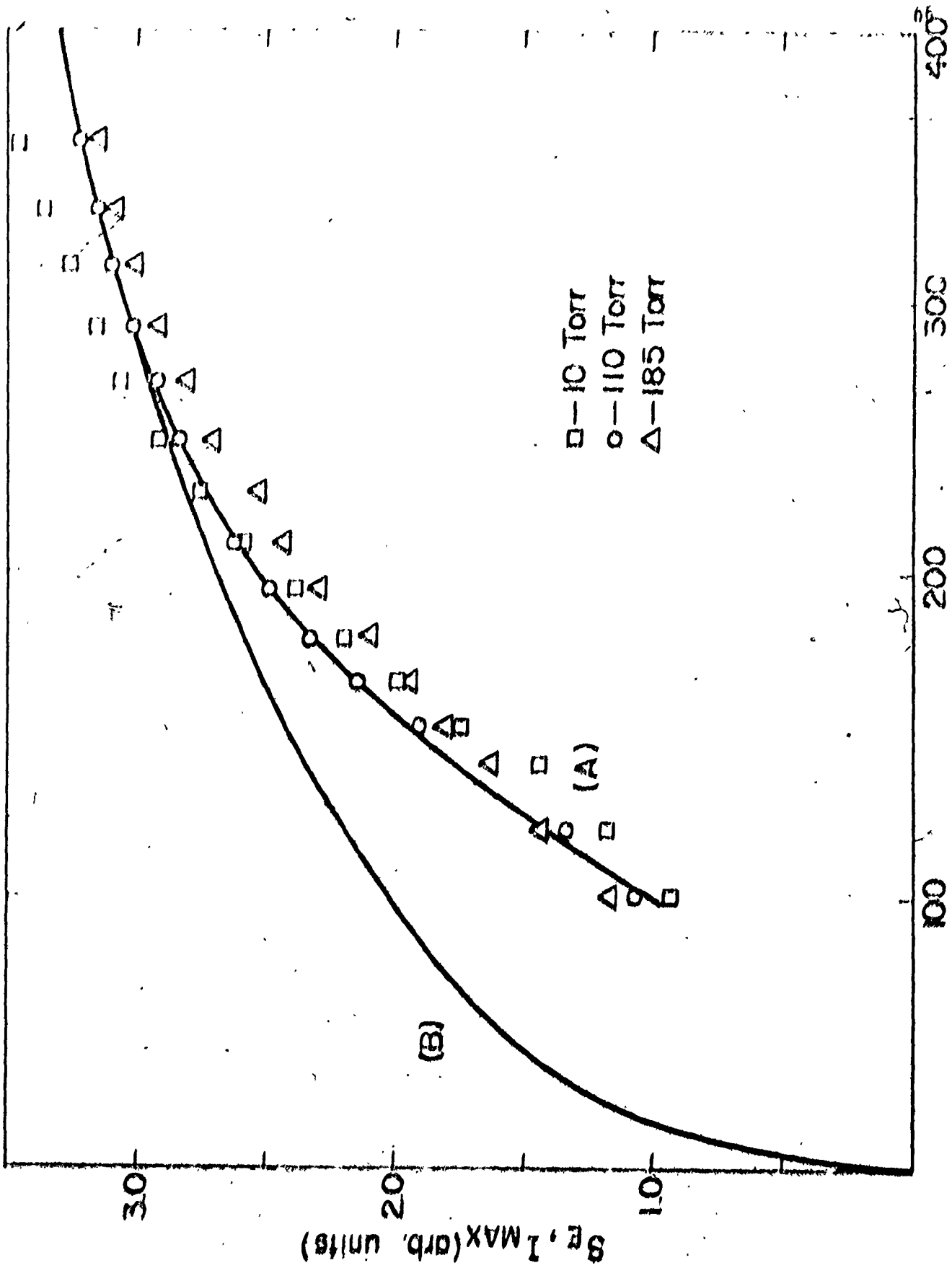
effects of the pressure are not very significant and that all the curves
exhibit the same behaviour, within the accuracy of the experiment (a few
percent).

There is one feature of the light output for which we have pre-
sented no experimental data yet. That is, the risetime of the output
light pulse. In a general way, to produce shorter pulses one must simply
design a pulsing circuit with the lowest possible inductance for given
capacitance. It should be kept in mind, though, that the circuit resis-
tance is equally important because during the fully developed discharge,
the tube resistance comes down to a few ohms. Because of their associated
inductance and resistance, the flashtube characteristics do have some
influence on the risetime of the pulse for a given discharge circuit.
Next, we present some typical results showing the size of the variations
which can be produced by varying the flashtube parameters. Figure 2-13
shows the variation of light output pulse risetime (10% - 90%) and cur-
rent pulse risetime as a function of initial gas pressure at specific
input energies near the ablation region. The light pulse risetime fol-
lows the current pulse risetime except in the pressure region below 20 Torr
where it gets closer to the current pulse, probably due to smaller reverse
current which thus will raise the temperature faster for the same avail-
able energy to the discharge. Figure 2-14 illustrates the reduction in
the output pulse risetime obtained for increasing the specific input energy
by changing the voltage, for two different gas pressures of 10 and 110 Torr.
Also illustrated are the corresponding current pulse risetimes. Observe
that the light output pulse, in both cases, has a risetime longer than
the current pulse, but shortens towards the risetime of the current pulse

Figure 2-13. Current pulse (lower curve) and output light pulse risetime (10-90%) variation with the initial gas pressure (1.7-mm x 80-mm tube, 23-kV voltage, 0.143 μF).

RISETIME (nsec)

PRESSURE (Torr)

FIG. 2—13

67
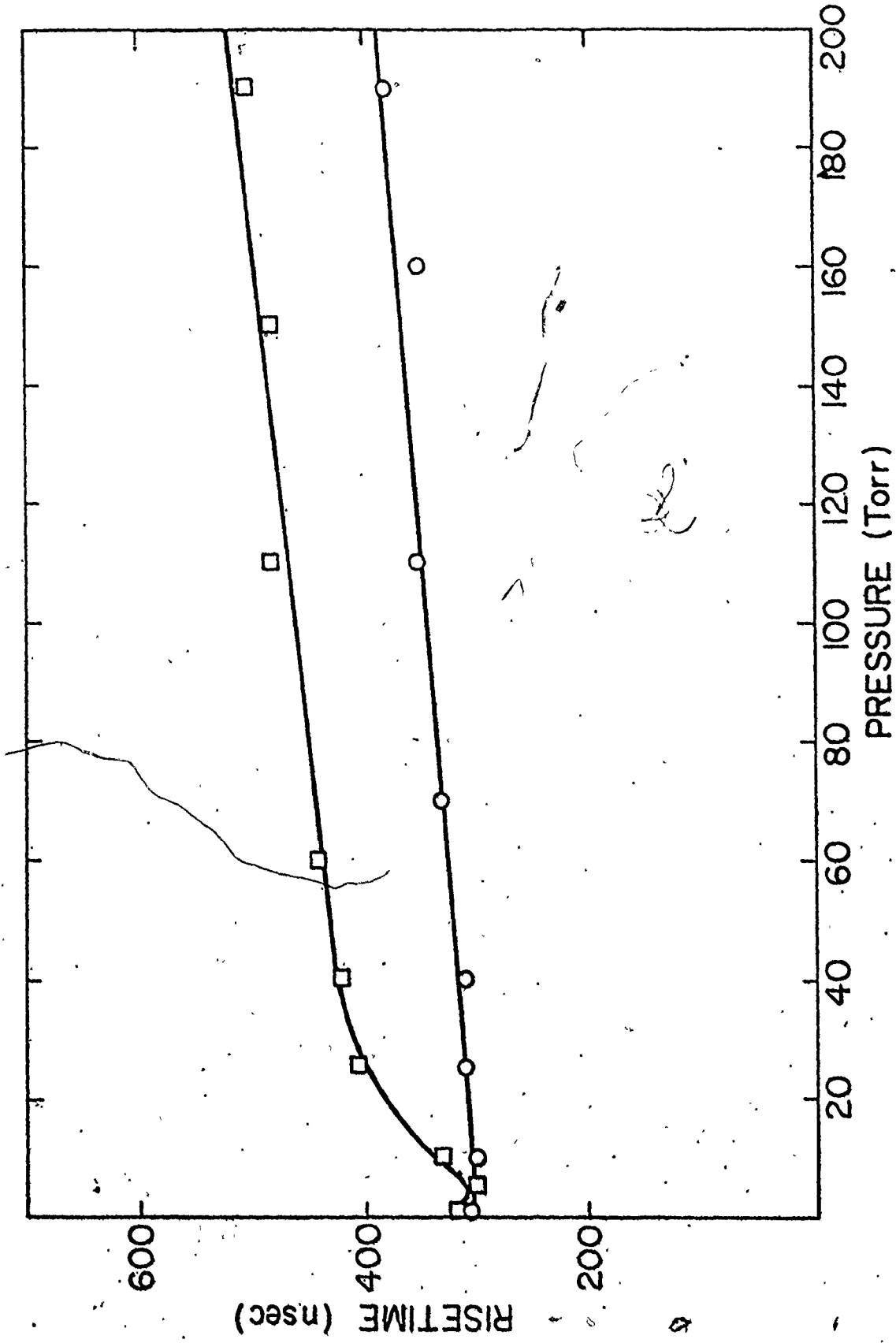
Figure 2-14. Current pulse and light pulse risetime variation with
the specific energy density for initial gas pressures
of 10 Torr and 110 Torr; Δ, 10-Torr current pulse rise-
time; X, 10-Torr light pulse risetime; O, 110-Torr cur-
rent pulse risetime; ▣, 110-Torr light pulse risetime.
The tube has a 1.7-mm diameter, and a broadband green
filter is used to select the spectral region of interest.
The current and light pulses were simultaneously displayed
and photographed.

SPECIFIC INPUT ENERGY (J/cm³)

RISETIME (n sec)

FIG.2—14

68
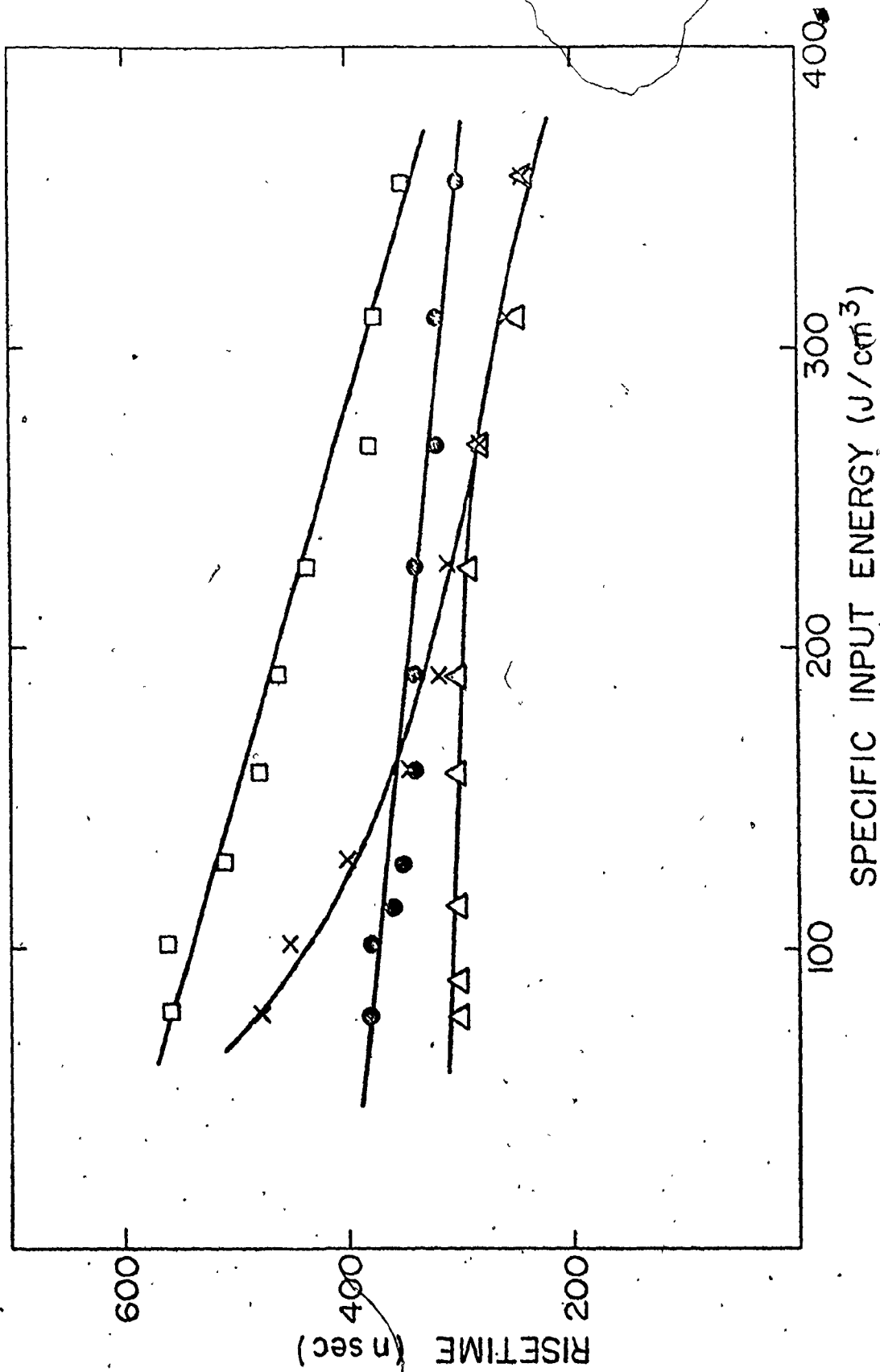
as E_N increases. The reason for this is that the more energy we try to push through the tube, the faster we reach the high temperature point from where on the remaining energy is stored in the heated ablation products to contribute in the increase of the fall time of the pulse, and for low pressures this point can be reached faster because the amount of mass available for heating is less.

2.5 DISCUSSION AND CONCLUSION

2.5.1 Discussion

It has been shown that high-current, short-pulse flashtubes can be characterised in a very useful fashion by studying their behaviour as a function of the specific input energy to the flashtube plasma. Over a considerable range of operation, the light output behaviour is consistent with a model assuming that the plasma radiates as a blackbody. For low specific input energies, the emitted radiation is lower than the one predicted by the blackbody radiation model. This is the region where the emission spectrum distribution of the particular gas used will determine the efficiency of the pumping system. Accordingly, we can employ the blackbody radiation model for the flashlamp to give a design criterion for high current flashtubes with current pulse lengths in the microsecond region. To obtain optimum output intensity along with moderate levels of ablation, we select the tube characteristics so that

$$E/\pi r^2 L = 150 \text{ J/cm}^3 \qquad\qquad (2\text{-}25)$$

where E is the stored energy in the pulse capacitor scaled by the pulse length (we require the specific energy delivered per microsecond). This

ensures that the flashlamp operates in the blackbody radiation regime. Also, the fall time of the light pulse is relatively close to that of the current pulse. Operation at much higher specific energies will produce higher peak discharge current, but little more peak intensity in the emitted radiation. It will, though, cause an extended fall time of the light output, and rapid ablation of the flashtube bore leading to early failure of the tube. On the other hand, operation at much lower specific input energies per microsecond will cause the flashtube to operate below the blackbody emission regime and therefore produce less peak emission for the particular wavelength region of interest.

Use of the above design criterion determines the important flashtube characteristics. There are still several variables to be determined besides the dimensions. The gas pressure should be selected in the range of 5 to 50 Torr. The value chosen should be such that the breakdown voltage of the gas employed is considerably below the available voltage which charges the storage pulsed capacitor. This may dictate the use of rare gases for the case of higher pressures or longer tubes. Unless other system requirements demand it, the low end of the pressure range should be selected, particularly if it is important to produce the shortest possible risetime pulse for the circuit employed. Furthermore, there is some advantage to be gained in terms of light pulse risetime by delivering energy to the flashtube plasma at as high an overvoltage as possible.

2.5.2 Conclusions

A study has been presented of high output, short pulse flash-

lamps operating in, or near, the ablation regime. The discharge of
this type of flashtube is expected to radiate as a blackbody at the tem-
perature of the plasma. A model of the plasma originally discussed by
Gusinow has been employed to model the discharge current variation with
input energy. A major feature of the model is the functional dependence
of the plasma resistivity on temperature, namely $\eta = BT^{-3/2}$. The con-
stant B has been determined by fitting the variation of the discharge
current with input energy to unit volume of the plasma. The blackbody
radiation model of the tube has allowed the development of a useful model
of the tube behaviour in terms of E_N, the specific input energy to the
plasma. Employing this, we are able to calculate the output from a
given flashtube in any particular wavelength range once the rate at which
energy is supplied to the unit volume of the plasma is known. The model
makes it possible to compare tubes of different lengths and radii. In
particular, we have developed a useful design criterion for determining
the physical dimensions of ablation-type flashtubes, namely that

$$\frac{E_N}{\Delta t} \approx 150 \text{ joules/}\mu\text{sec}$$

On the one hand, this ensures operation in the blackbody regime (which
necessarily gives the optimum output in any wavelength range at the
relevant blackbody temperature) at a plasma temperature giving relatively
good efficiency for conversion of energy to optical pumping of absorption
bands in the visible. On the other hand, the specific input energy to
the plasma is not so high as to cause a very high rate of ablation of
the walls of the plasma tube, causing premature failure. Similar con-
siderations will apply to the design of these tubes for pumping absorp-

tion bands in other spectral regions.

The criteria mentioned above were subsequently used to design a
double flashlamp system in order to pump a dye amplifier, which was used
to study the amplification of the spontaneous emission discussed in the
next chapter. As it was mentioned before, the available commercial
flashlamps are of the rare-gas-type and besides being expensive, cannot
give fast risetime pulses and higher light intensities. In this aspect,
our ablation flashlamps are superior to the commercial ones. Additionally,
because our flashlamps are of the open-type, they can withstand more
current-induced shock and their electrodes and tube can be kept clean
which produces better pulse repeatability and lifetime.

CHAPTER 3

AMPLIFICATION OF SPONTANEOUS EMISSION

3.1 INTRODUCTION

In this chapter, we study the interaction of the spontaneously emitted radiation with the dye molecule in the particular case of the flashlamp pumped dye amplifier. This study is particularly important, because it provides an especially simple case in understanding the interaction of a non-coherent source with a homogeneous medium and has great practical consequences. This is so because dye amplifiers have the potential of producing high intensity, highly directional, narrow bandwidth, variable wavelength light pulses without mode structure and with a smooth temporal profile. Additionally, this study shows that it is possible to measure the unsaturated gain of a dye amplifier system by recording the spectral narrowing of the emitted intensity for different excitation levels. Since the early days of successful operation of dye lasers, it has become clear that flashlamp pumped dye systems can exhibit gains of the order of 1 cm^{-1} and laser pumped systems can have still higher gains.[71] Under these conditions, the presence of the amplified spontaneous emission (ASE) cannot be ignored. The existence of the spontaneous emission is a quantum mechanical effect which requires full quantization of the atomic variables and the E-M field to be properly treated.[72,73] In this study, we have accepted the presence of the spontaneous emission and tried to investigate its interaction with the

dye molecules as it propagates along the cell. We have investigated the ASE both experimentally and theoretically. Our aim has been to exploit the spectral narrowing of the radiation emitted from the end of the cell to measure the unsaturated gain. Our theory, which allows for the presence of the excited singlet state absorption (ESSA) and the triplet loses, is capable of predicting the variation of the intensity, the spectral width, the peak wavelength and the gain as a function of the flashlamp pumping intensity, very accurately. Our theoretical model used for the ASE in the dye system requires very accurate values for the absorption and emission crossection of the particular dye molecule used. This is particularly true for the behaviour of the spectral output at low pumping and the shift in the wavelength at which the output intensity is maximal. It is satisfying to have been able to develop a theoretical model which can predict the ASE output characteristics to a high degree of accuracy. However, considerable numerical computations are involved along with a requirement for exact values of the crossections. In order to exploit our approach of measuring gain from the narrowing of the intensity profile in a more general way, a simpler model was developed. This approximate semi-analytical model can be applied in many different gain media. The assumptions in this simple theory are that the gain line is homogeneously broadened and that the intensity spectral width becomes narrower than the natural linewidth before saturation sets in.

   In order to evaluate the applicability of this relatively simple theory, we have attempted to fit the experimental results to the already characterized dye system (by using the exact theoretical model).

In this way, the degree to which the simpler theory can be used to measure gain values can be determined. This, of course, represents a severe test since we know that the spectral peak of the ASE shifts with pumping and excited singlet state absorption is important; neither of which is allowed for in the simpler theory. It will be shown that even in this case, using an appropriate technique to match theory to experiment, reasonably good values can be obtained for the gain. Another simple theory, developed with basically the same assumptions as our own has appeared recently,[40] and it will be shown that we can match this theory to the experiment with similar results.

In what follows, we will first review the literature on the subject and then present the theoretical model, with its solution, the experimental results, the fitting of the theory to the experiment, the approximate theories along with their fitting to the experimental results and finally the discussion and the conclusion.

3.2   LITERATURE REVIEW OF THE ASE

The importance of the ASE, either as an interference phenomenon in the amplification of signal or as a means of producing modeless, high intensity sources of radiation, has received considerable attention and has been observed in many other systems besides dye amplifiers. Operation of the dye solutions in the ASE mode has been reported by many authors,[74-80] using both laser or flashlamp pumping and a variety of dye cell configurations. In these experimental investigations, attention was focused on the general characteristics of the ASE produced with different pumping mechanisms and cell configurations. Several typical examples are the qualitative results

concerning the angular divergence of the ASE beam from the axis of the cell
in several polymethine dyes pumped with a mode locked ruby laser,[74] the
high efficiency (< 40%) of the ASE from a rhodamine 6G dye pumped by a second
harmonic of a Q-switched Nd glass laser,[75] the effect of the concentration
on the peak wavelength of the ASE and the effect of the pumping power also
on the peak wavelength.[75] It was shown that the higher the concentration,
the more the peak wavelength will be shifted toward longer wavelengths for
the same pumping power. This is so because, for high concentrations, there
are more molecules per unit length of the cell and, consequently, there is in-
creased absorption losses due to the ground state absorption and the re-
sult is a shift of λ_0 toward longer wavelength. The effect of the increasing
pump is shown to decrease λ_0, because with more gain available, the light
can sustain more losses which increase towards shorter wavelengths. Con-
sequently, the higher pumping will lead to shorter wavelengths. We have
observed similar results in our experiments and we will present them in
a later section.

One particularly interesting experimental result, from a practical
point of view, is the spectral narrowing of the ASE reported by Marowsky.[77]
Using a non-resonant feedback technique, he produced a spectrum of ASE of
6 Å FWHM which shows the potential of the ASE to produce spectrally narrow
pulses. Effects related to the ASE in the near or farfield were reported
by Burlamacchi et al.,[79] for the case of 4 mm cell diameter and concentra-
tions between 10^{-5} - 5×10^{-4} M/L of rhodamine 6G. The output beam has been
shown to diverge from the axis of the cell because of the lensing effect
caused by the non-uniform heating. Similar results were observed by us in

a more quantitative manner and we will present them in the fourth chapter, where we deal with the propagation phenomena in thick cells.

The first attempt to use the ASE to measure gain was made by Shank et al.[80] According to this technique, the ratio of the ASE intensity at a particular wavelength, for two different cell lengths, is directly related to the gain. The limitation of this method is that it does not take into account saturation effects on the gain, which can be very important unless we keep the ASE intensity well below the saturation point. Also, it does not provide any information related to the physical processes involved in the determination of the gain and it can be difficult to apply this method experimentally.

Some important theoretical work has also been done on the ASE with emphasis on the gain measurement. Casperson and Yariv[42] derived expressions for the narrowing of the spectrum of the ASE as a function of the gain for both homogeneously and inhomogeneously broadened systems. Their treatment, though, was limited to the one way propagation of the ASE within the cell and the case where the intensity spectrum of the ASE is much narrower than the gain line shape well before the saturation occurs.

Nevertheless, they predicted the approximate variation of the wavelength integrated ASE intensity within the cell which varies either exponentially with distance (unsaturated region) or linearly (saturated region). They also found an approximate relation between the spectral width ($\Delta\lambda$) of the ASE and the gain at the centre line $g(o)$ for the homogeneously broadened system:

$$\Delta\lambda/\Delta\lambda_h = \left[\frac{\log_e 2}{g(o)L}\right]^{1/2} \qquad \text{unsaturated regime} \qquad (3\text{-}1)$$

$$\Delta\lambda/\Delta\lambda_h = [\frac{\log_e 2}{\log_e (g(o)L)}]^{1/2} \qquad \text{saturated regime} \qquad (3.2)$$

Here, $\Delta\lambda_h$ is the FWHM of the homogeneous lineshape function and L is the cell length. We note that the narrowing of the spectrum of ASE continues even in the saturated regime. This behaviour is quite different for in-homogeneously broadened systems where rebroadening can take place.[42,81]

An extension of this work was carried out by Casperson,[40] who included the propagation of the ASE in both ways in the cell to find a more accurate expression for the narrowing $\Delta\lambda$ with respect to the unsaturated gain at line centre $g(o)$ for a cell length L and a coupling parameter x_0. Accordingly, Casperson's expressions are:

$$\Delta\lambda/\Delta\lambda_h = \{\frac{\log_e(g(o)L/2x_0 + 1)}{\log_e(g(o)L/4x_0 + 1)} - 1\}^{1/2} \qquad \text{unsaturated regime} \qquad (3-2)$$

$$\Delta\lambda/\Delta\lambda_h = [\frac{g(o)L}{\log_e(\exp(g(o)L + 1)/2)} - 1]^{1/2} \qquad \text{saturated regime} \qquad (3-3)$$

We should note though that the assumptions of a homogeneous gain line profile and considerable narrowing of the ASE before saturation are still present and this theory does not take into account the shift of the peak wavelength with the increase of gain or the absorption of the excited singlet state, which we will see is very important.

A departure from this analytical approach is the treatment by Ganiel et al.[82] of the ASE based on solving numerically the rate equations for the dye molecule and the radiation. They have shown that the predicted behaviour of the intensity and spectrum narrowing of the ASE is in general agreement with observation, but no detailed quantitative comparisons were

undertaken. Furthermore, the model did not take into account either the triplet losses or the ESSA and no explicit gain predictions were made for comparison with experiment. ASE has also been studied theoretically by Menegozzi and Lamb[83] who used a more complex density matrix approach. The rate equation approximation, which is a special case of the optical Block equations obtained in the limit of very rapid electric dipole phase interruptions (no phase correlations) can introduce errors in treating the ASE in the case of extreme nonlinearities introduced by the gain saturation at very high pumping, when $\Delta\phi/\phi$ is not much less than unity (ϕ is the photon flux). There is also the expectation that the statistical nature of the incoherent spontaneous emission over the integration step used in solving the equations, which is Gaussian at the start of the amplification, will evolve towards a different kind of statistics in the case of extreme non-linearities in the gain.[83] Nevertheless, the rate equation approximation, which we are going to use, is quite adequate for the case of flashlamp-pumping which cannot introduce extreme nonlinearities with pumping rates up to 10^7 sec^{-1}. The development of a model for the ASE based on the rate equation approximation is taken up in the next section.

3.3 A MODEL FOR THE AMPLIFICATION OF THE SPONTANEOUS EMISSION

3.3.1 Rate Equations

Figure 3-1 shows a typical energy diagram for a dye molecule along with the diagram of a plane dye cell used in our calculations. The different electronic bands are represented by lines but actually they have semicontinuous structure which includes all the vibrational and rotational levels. Because of fast thermalization processes, of the order of a pico-

Figure 3-1.   (a) Energy level diagram of rhodamine 6G. $S_{0,1,2}$ are

the singlet ground state, first excited and second excited

electronic bands. T_1, T_2 are the triplet state and the

first excited triplet state correspondingly. Solid lines

indicate radiative transitions and broken lines the

non-radiative transitions. PUMP is the pumping rate and

σ_i or σ_{ij} are the crossections of the processes involved.

K_{st} is the crossover rate and τ_t is the triplet state

lifetime.

(b) Dye cell configuration. The length of the cell is

L and the crossection is indicated by the letter A.
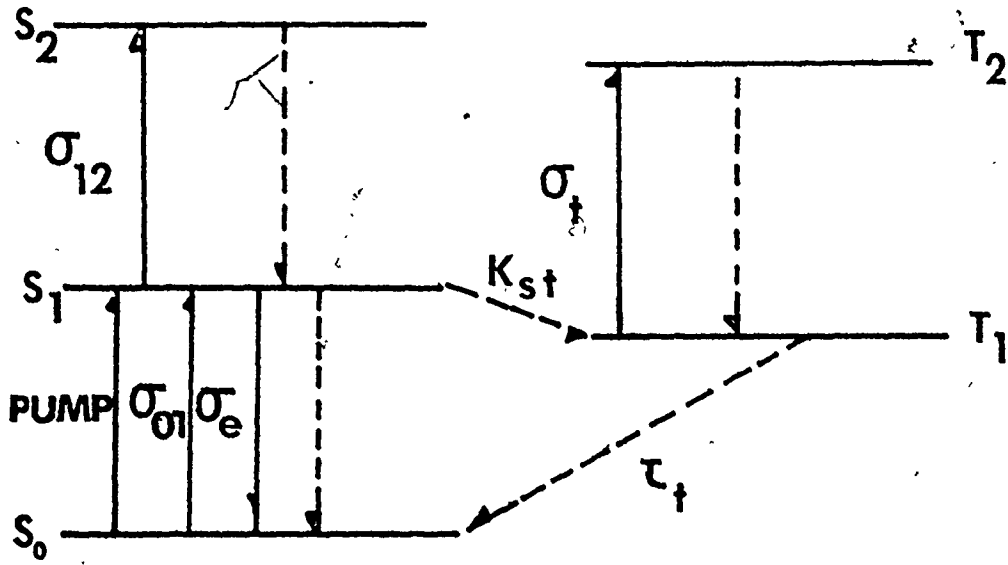
(a)
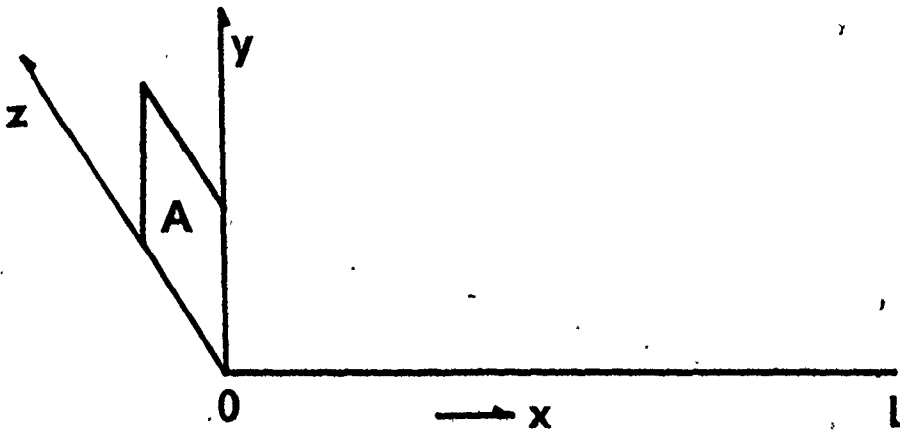
(b)

FIG. 3-1

second,[84,85,86] the excited atoms will fill the lowest available states within the band. Also, the non-radiative transitions between higher excited states and the first excited state are very fast, of the order of 1 to 10 picoseconds.[85] For pumping rates of the order of 10^7 sec^{-1}, which is the case for the flashlamp pumping with microsecond pulses, this deactivation time is far too fast to allow any important interaction of the radiation with molecules in higher excited states. Consequently, we will assign to them a zero population. Then, from conservation of the number of molecules in the system, we will have

$$N_0(x,t) + N_1(x,t) + N_t(x,t) = N \tag{3-4}$$

where N_0, N_1, N_t are the population densities of the levels S_0, S_1, T_1 and N is the concentration of the dye material in the solution. This concentration should be kept below the point where the dye material starts forming dimers, which introduce additional wavelength dependent losses and remove the monomers from the amplification process. The population of the S_1 and T_1 levels is governed by the following rate equations:

$$\frac{dN_1(x,t)}{d_t} = w(t)N_0(x,t) - \frac{N_1(x,t)}{\tau} - N_1(x,t)\int_\lambda \sigma_e(\lambda)I(x,t,\lambda)d\lambda$$

$$+ N_0(x,t)\int_\lambda \sigma_{01}(x)I(x,t,\lambda)d\lambda - K_{ST}N_1(x,t)$$

$$- N_1(x,t)\int_\lambda \sigma_{12}(\lambda)I(x,t,\lambda)d\lambda - w'(t)N_1(x,t) \tag{3-5}$$

$$\frac{dN_t(x,t)}{d_t} = K_{ST}N_1(x,t) - \frac{N_t(x,t)}{\tau_t} - N_t(x,t)\int_\lambda \sigma_t(\lambda)I(x,t,\lambda)d\lambda \tag{3-6}$$

where W(t) is the pumping from S_0 to S_1, $\sigma_e(\lambda)$ is the emission crossection

of S_1, $\sigma_{01}(\lambda)$ is the absorption crossection of S_0, K_{ST} is the $S_1 \rightarrow T_1$ crossover rate, $\sigma_{12}(\lambda)$ is the S_1 absorption crossection, $W'(t)$ is the pumping from S_1 to S_2, τ_t is the triplet state lifetime, $\sigma_t(\lambda)$ is the triplet state absorption crossection and $I(x,t,\lambda)$ is the total photon flux per unit of wavelength (photons/sec/cm^2/cm) at position x and and wavelength λ with

$$I(x,t,\lambda) = I^+(x,t,\lambda) + I^-(x,t,\lambda) \qquad (3-7)$$

Here I^+ is the $+x$ and I^- is the $-x$ propagating intensity of the ASE. Note that we do not include any variation of the parameters along the y or z direction. We assume that our cell thickness is much smaller than the absorption length for the particular concentration used. In particular, for the rhodamine 6G in ethanol, the absorption length required to decrease the pumping radiation by 1/e, is roughly given in cm by 1/12/M, where M is concentration in units of 10^{-4} mole/litre. The very important case of the thick cells, where the absorption length is less than the thickness of the cell and where we expect to have quite different field distribution across the cell, we treat in Chapter Four.

The rate equation for the photon flux is given by:

$$\frac{d}{dx} I^\pm(x,t,\lambda) = N_1(x,t)\sigma_e(\lambda)I^\pm(x,t,\lambda) + \frac{N_1(x,t)}{\tau} E(\lambda)g(x)$$

$$- \sigma_{01}(\lambda)N_0(x,t)I^\pm(x,t,\lambda) - \sigma_t(\lambda)N_t(x,t)I^\pm(x,t,\lambda)$$

$$- \sigma_{12}(\lambda)N_1(x,t)I^\pm(x,t,\lambda) \qquad (3-8)$$

where $\sigma_{12}(\lambda)$ is the first excited singlet state absorption crossection and $E(\lambda)$ is the $S_1 \rightarrow S_0$ fluorescence spectrum normalized so that

$$\int_\lambda E(\lambda)d\lambda = \phi$$

ϕ being the quantum efficiency of the dye. The emission crossection is related to the fluorescence spectrum via the equation

$$\sigma_e(\lambda) = \frac{\lambda^4 E(\lambda)}{8\pi\tau n^2 c} \qquad (3-9)$$

where c is the vacuum velocity of light, n is the index of refraction of the solution and τ the S_1 lifetime.

The function $g(x)$ in equation (3-8) is a coupling function for the spontaneous emission. In flashlamp pumped amplifiers with cell length of the order of a few cm and gain in the cm^{-1} region, the amount of the spontaneous emission which couples into the cell is important only in the start of the amplification near the end of the cell, because afterwards the contribution of the ASE is much larger than the contribution of the spontaneous emission.

The coupling function can be approximated by a constant which is approximately equal to the solid angle which is defined by an area equal to the cell crossection at a distance from the origin equal to the cell length. In any case, $g(x)$ will be treated as a parameter and its exact value will be specified by direct comparison of the theoretical results with the experimental results.

It is appropriate to mention the physical processes corresponding to each term in equations (3-5) to (3-8). In equation (3-5), the first term is the contribution of the pumping to the increase of N_1, the second is the loss of N_1 due to spontaneous emission, which is independent of the field present, the third term is the stimulated emission contribution, the fourth is the increase of N_1 because of the ground state absorption of the total

laser light absorption, the fifth is the loss of N_1 due to the intersystem crossing, and the sixth is loss of N_1 due to the excited singlet state absorption. It should be noted that the last pumping term is small with respect to $W(t)N_0(x,t)$ and can be omitted for the case of transversely flashtube pumped dye lasers. It is important, though, in a laser pumped dye laser where N_1 can be a considerable fraction of N_0. The pumping term $W(t)$ in equation (3-5) can be represented by

$$W(t) = p(t)/A \int_\lambda \sigma_{01}(\lambda)f(\lambda)\lambda/c\eta d \qquad (3-10)$$

where $p(t)$ is the time profile of the pumping pulse, A is the area of pumping, $\sigma_{01}(\lambda)$ is the ground state absorption of the dye used and $f(\lambda)$ is the normalized spectral distribution of the pump radiation ($\int f(\lambda)d\lambda = 1$). Here we will be interested more in steady state solutions and since the flashlamps we used are operating in the blackbody region and the emission of blackbody radiation does not vary much over the narrow absorption region of the dye ($\sim 400 \overset{\circ}{A}$), we will take the pump as a parameter which is constant in time and wavelength.

In equation (3-6), the first term is the contribution of the crossover mechanism, the second is due to the non-radiative depopulation of the triplet state and the third is due to the absorption of the triplet state of the radiation present. Because of the long lifetime of the triplet state (for R 6G it is 2.5×10^{-7} sec)[87] its effect, especially for high pumping, is extremely important, because it not only absorbs the photons present but also because it removes molecules from the lasing route ($S_0 \to S_1 \to S_0$), which is equivalent to decreasing the concentration. There are certain chemical additives which

can depopulate T_1 by collisional de-excitation to a great degree.[88] The most efficient of these chemicals for the case of rhodamine dyes is the cyclo-octatetraene (COT).[88] Taking into account that the triplet state lifetime is of the order of 10^{-7} sec and that the absorption cross-section is of the order of 10^{-17} cm^2, we see that the last term of the equation (3-6) is much smaller than the term N_t/τ_t unless the photon flux exceeds 10^{24} photons/cm^3/sec which is not the case of the flashlamp pumped dye amplifiers. Consequently, we can omit this term for the present analysis. Using a triplet state quencher is equivalent to decreasing the triplet lifetime, which will strengthen the above argument. In the case of laser pumped dye amplifiers, it is possible to reach high intensities and then the last term of (3-6) must be included in the case the pumping pulse length is of the same order as the triplet lifetime and no triplet state quencher is used.

In the combined equation (3-8) for the intensities I^+ and I^- the first term is due to stimulated and the second to spontaneous emission. The third represents the loss due to the ground state absorption; the fourth is the loss due to the triplet state absorption and the fifth is the loss due to the excited singlet state absorption (ESSA). The ESSA cross-section $\sigma_{12}(\lambda)$ in the region of interest is of the same order of magnitude as the emission cross-section $\sigma_e(\lambda)$,[89] and consequently the last term of equation (3-8) is very important in determining accurate gain values and predicting other characteristics of the ASE. We will see in a later section that the proper allowance for the ESSA is absolutely necessary in order to match the theory with the experiment.

Equations (3-4) to (3-8) constitute a system of coupled non-linear differential equations which cannot be solved analytically and must be treated numerically. In the next section, we will present a way of solving the steady state case of the rate equation using parameters corresponding to the dye rhodamine 6G in ethanol solution. The steady state solution is not only applicable in the continuous pumping case, but it can be also used for pulsed systems, when the lifetimes in the system are much faster than the changes of the pumping. In this case, the dye system can follow the changes in the pumping and it will behave like a system under a constant excitation as far as the maximum of the pumping pulse is concerned. In our case, the flashlamp pulse had a risetime of approximately one μsec and the singlet state lifetime for rhodamine 6G is 5.5 nsec.

3.3.2 Numerical Solution of the Rate Equations and Results

According to the discussion presented in the previous section, for our experimental case, we can assume that our slowly varying pumping pulses allow us to treat the system as if it was under steady state condition, where the maximum of the pumping pulse is taken as the actual pumping. Because we have used the triplet state quencher (COT), it is reasonable to assume that the triplet state will play a very small role in determining the gain. In the usual case, without a triplet state quencher the ASE pulse peaks ahead of the pumping pulse because the triplet state losses increase with increasing N_1 population. Therefore, we can test the effect of the quencher by observing the peak position

of the ASE pulse with respect to the pumping pulse peak. The coincidence of the two peaks suggests effectively complete quenching of the triplet state. Nevertheless, we have introduced a quenching factor Q_f in our computation to take account of the possibility that no complete quenching has occurred. $Q_f = 1$ will mean no effect of the quencher on T_1.

Then, the steady state solution for equation (3-6) is given by,

$$K_{ST}N_1(x) - N_t(x)[\frac{1}{Q_f\tau_t} + \int_\lambda \sigma_t(\lambda)I(x,\lambda)d\lambda] = 0 \qquad (3-11)$$

As we have seen in the previous section, for very small Q_f values and pumping intensities within the reach of flashlamps the integral term of this equation is much smaller than the $1/Q_f\tau_t$ term. Consequently, we write equation (3-11) as,

$$N_t(x) = K_{ST}Q_f\tau_t N_1(x) \qquad (3-12)$$

In a similar manner, the steady state solution of equation (3-5) will give for $N_1(x)$ the result shown below where we have substituted $W(t) \equiv P$ and omitted the last term of (3-5) $(W^*(t)N(x,t))$ which is very small for the case of transverse flashlamp pumping:

$$N_1(x)[\frac{1}{\tau} + \int_\lambda \sigma_e(\lambda)I(x,\lambda)d\lambda + K_{ST} + \int_\lambda \sigma_{12}(\lambda)I(x,\lambda)d\lambda]$$

$$= N_0(x)[P + \int_\lambda \sigma_{01}(\lambda)I(x,\lambda)d\lambda] \qquad (3-13)$$

From equation (3-4) we get

$$N_0(x) = N(x) - N_1(x) - N_t(x) \qquad (3-14)$$

Using equation (3-12) in to (3-14) we have

$$N_0(x) = N(x) - N_1(x)[1 + K_{ST}Q_f\tau_t] \qquad (3-15)$$

Replacing the $N_0(x)$ in equation (3-13) with its equivalent from equation (3-15) we get for $N_1(x)$ the following:

$$N_1(x) = N(x)[P + \int_\lambda \sigma_{01}(\lambda)I(x,\lambda)d\lambda]/[P + \frac{1}{\tau} + K_{ST} + \int_\lambda \sigma_e(\lambda)I(\lambda)d\lambda$$

$$+ \int_\lambda \sigma_{12}(\lambda)I(\lambda)d\lambda + (1 + K_{ST}\tau_t Q_f)\int_\lambda \sigma_{01}(\lambda)I(\lambda)d\lambda] \tag{3-16}$$

Equations (3-8), (3-15) and (3-16) are the basic equations, which we have to solve numerically. The values of the parameters and the appropriate cross-sections for the Rhodamine 6G dye (which was used because its parameters are relatively better known than for other dyes), appear in Appendix A. Because the values of the corresponding $\sigma_{01}(\lambda)$ and $\sigma_e(\lambda)$ in the literature[90,91] were just not sufficiently accurate to permit the matching of theory with experiment to the desired degree of precision, we had to measure for ourselves the ground state absorption cross-section using a Cary-14 spectrophotometer and the fluorescence spectrum using a PERKIN-ELMER MPF-44 fluorescence spectrophotometer. In particular, published cross-sections gave erroneous values for the peak wavelength of the emitted ASE and the narrowing with ASE. Evidence for the inaccuracy of the published ground state absorption cross-section were also reported by Sahar and Treves.[89] These authors have also measured the excited single state absorption (ESSA) and found that the ESSA cross-section is of the same order as the ground state absorption cross-section. As a first approximation, we employed the approximate ($\pm$ 10%) cross-section values they obtained. Their data cover only a restricted wavelength range. We compared intensities at low pumping between theory and experiment to refine the cross-section values and to extend the wavelength range. It

should be noted that not only the magnitude of the cross-sections is
of importance to get accurate matching between theory and experiment but
also are the relative slopes of the cross-sections over the range of
interest.

Figure 3-2 is a flow chart which indicates the main steps of
the computer program written to solve the two-way propagation of the
ASE based on equations (3-8), (3-15) and (3-16). The program listing
appears in Appendix A. The cell is divided up in a large number of
sections Δx. We solve the equations for each Δx, and calculate the self-
consistent values for I^+ and N_1, N_0, N_t. Then we assign $I^-(0 \rightarrow L)$ =
$I^+(L \rightarrow 0)$ and repeat the process of self-consistent calculation of I^+,
N_1, N_0, N_t for each Δx, with $I = I^+ + I^-$ this time. At the end of each
propagation, we check for symmetry in the $N_1(x)$ function which is the
condition to have $I^+(x) = I^-(L - x)$. After this symmetry has been ob-
tained, we calculate the gain as a function of wavelength λ and position
within the cell, the emitted intensity of the ASE vs λ, the unsaturated
gain constant vs λ, the intensity at fixed λ vs the coordinate x, and
the total intensity, integrated over λ, vs x. From the plot of $I^+(\lambda, x=L)$,
we determine the full width half maximum $\Delta\lambda$ for the pulse. The inten-
sity of the ASE, integrated over the wavelength at $x = L$, the intensity
of the ASE at fixed wavelength λ, the wavelength where $I^+(x = L)$ peaks
and the narrowing $\Delta\lambda$ for different pumping are employed for comparison
with corresponding experimental data. Figures 3-3 to 3-6 show some
typical results of the computation for fixed pumping, concentration,
cell dimensions and coupling constant of the spontaneous emission. The
particular dye material is rhodamine 6G with lifetimes and triplet state

start

read in parameters, cross-sections

compute I^+ at $o-\Delta x$

convergence ?

$I^+_{\Delta x,i} - I^+_{\Delta x,i+1} \ll 1$

yes | no

compute I^+

compute N_1, N_t, N_o for $I_{\Delta x,i+1}$

$I = I^+ + I^-$

advance to next Δx

no

$x = L$?

yes

set $I^-_x = I^+_{L-x}$

A

A

$N_{1,x} \doteq N'_{1,L-x}$?

no

calculate, print

gain vs λ
     vs x

I^+ vs λ
     vs x

N_1 / N vs x

end
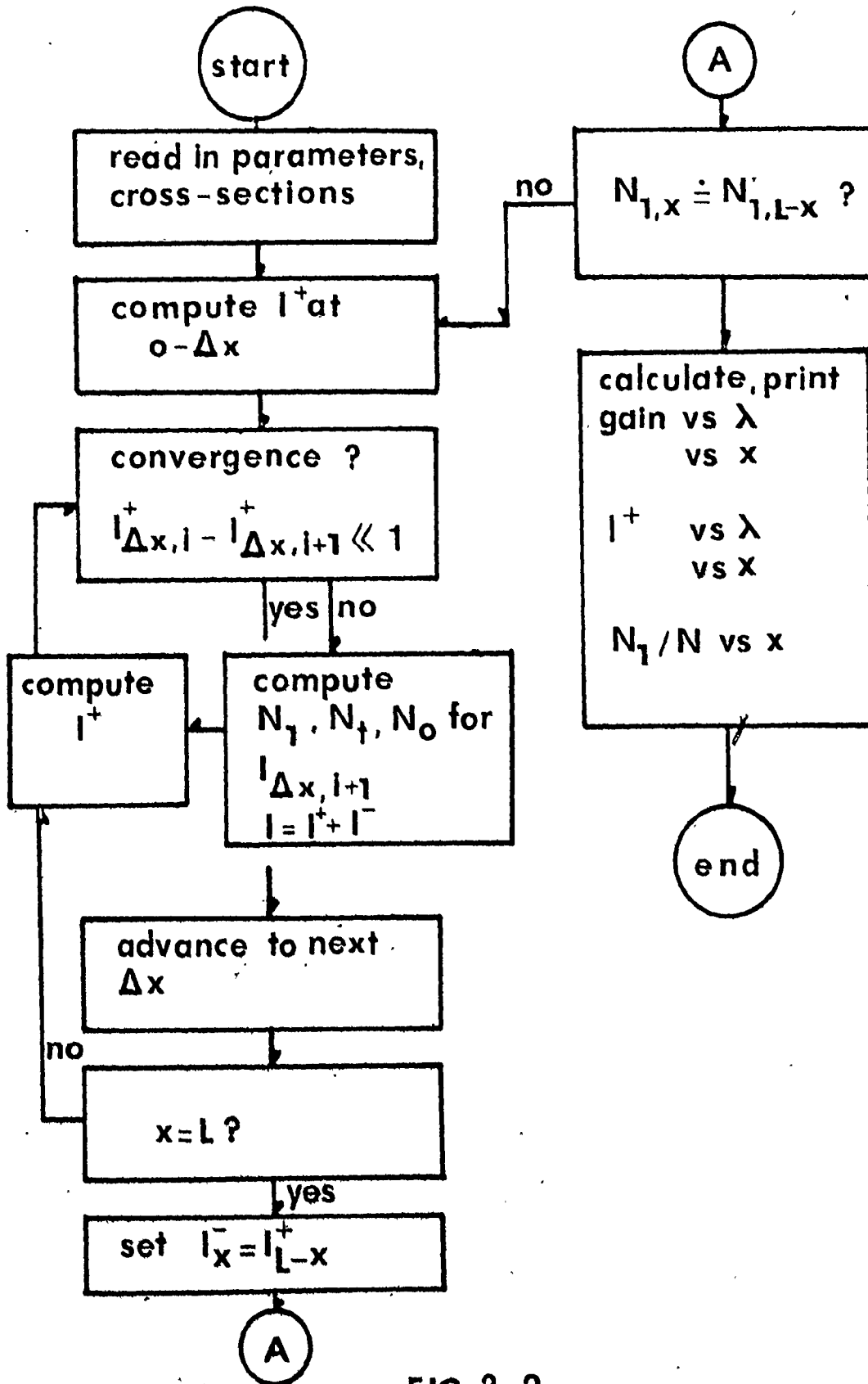
FIG. 3-2

Figure 3-3. Intensity spectrum of the ASE in four different positions
along the cell. (L/100, L/4, L/2, L). The concentration
is 1.5×10^{-3} M rhodamine 6G/ethanol, the pumping rate
is 2.0×10^6 sec^{-1} and the cell dimensions are 70 μ x 1 mm
x 18.2 cm.

$P = 2.0 \times 10^6$

L/100

L/4

L/2

L

WAVELENGTH (Å)

FIG. 2-2

5700   5940   6180

91

.8   .6   .4   .2   O
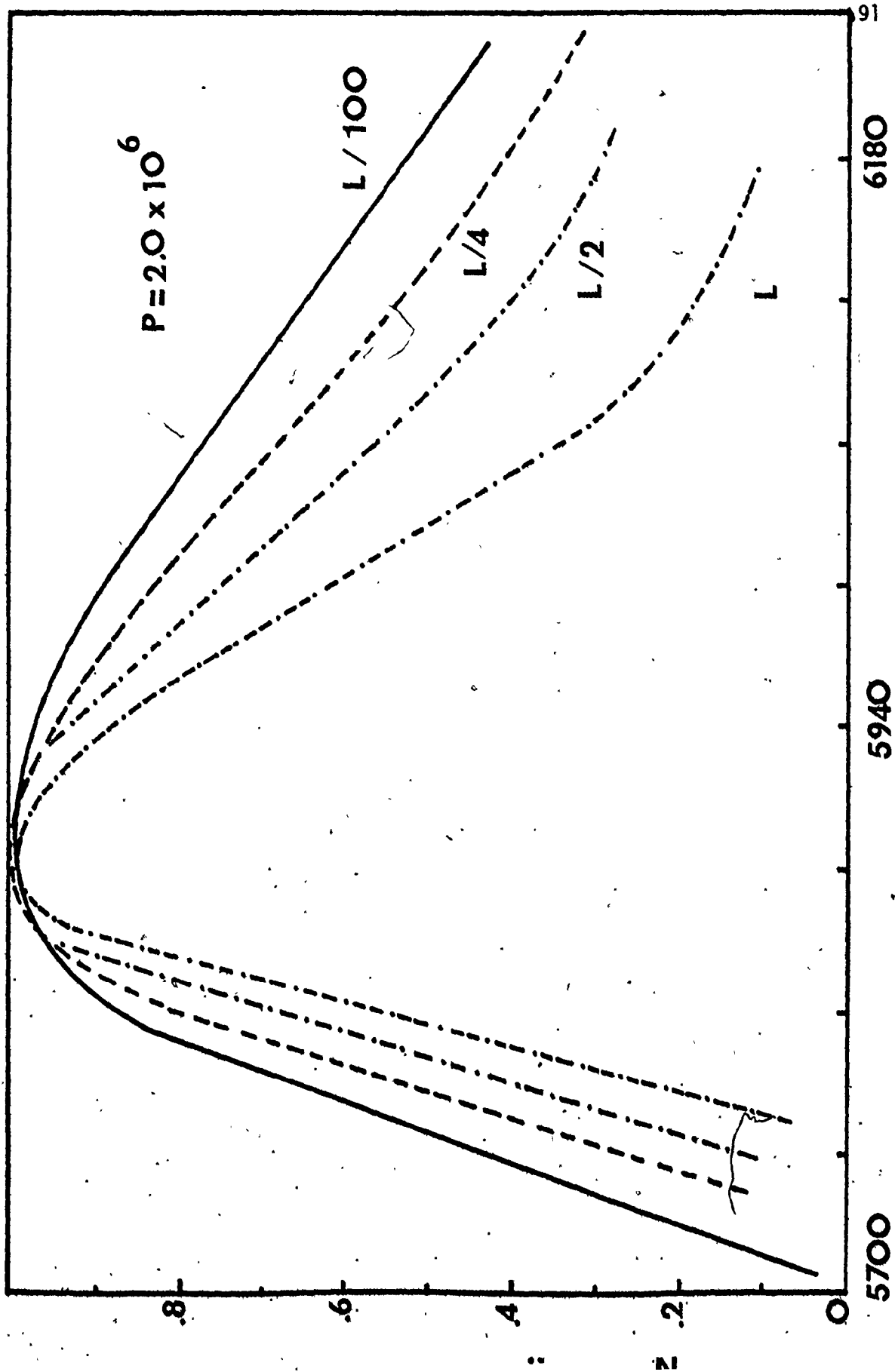
Figure 3-4.   Total intensity, integrated over wavelength and propagating
             in the +x direction as a function of position. The con-
             centration is 1.5×10^{-3} M   rhodamine 6G/ethanol, the
             pumping rate is 0.8×10^6 sec^{-1} and the cell dimensions
             are 70 μ x 1 mm x 18.2 cm.

FIG. 3-4

$P = 0.8 \ 10^{6}$

TOTAL INTENSITY

LOG_{10}

X (cm)

16.0

17.5

L/2

0.

10.

18.

L

92
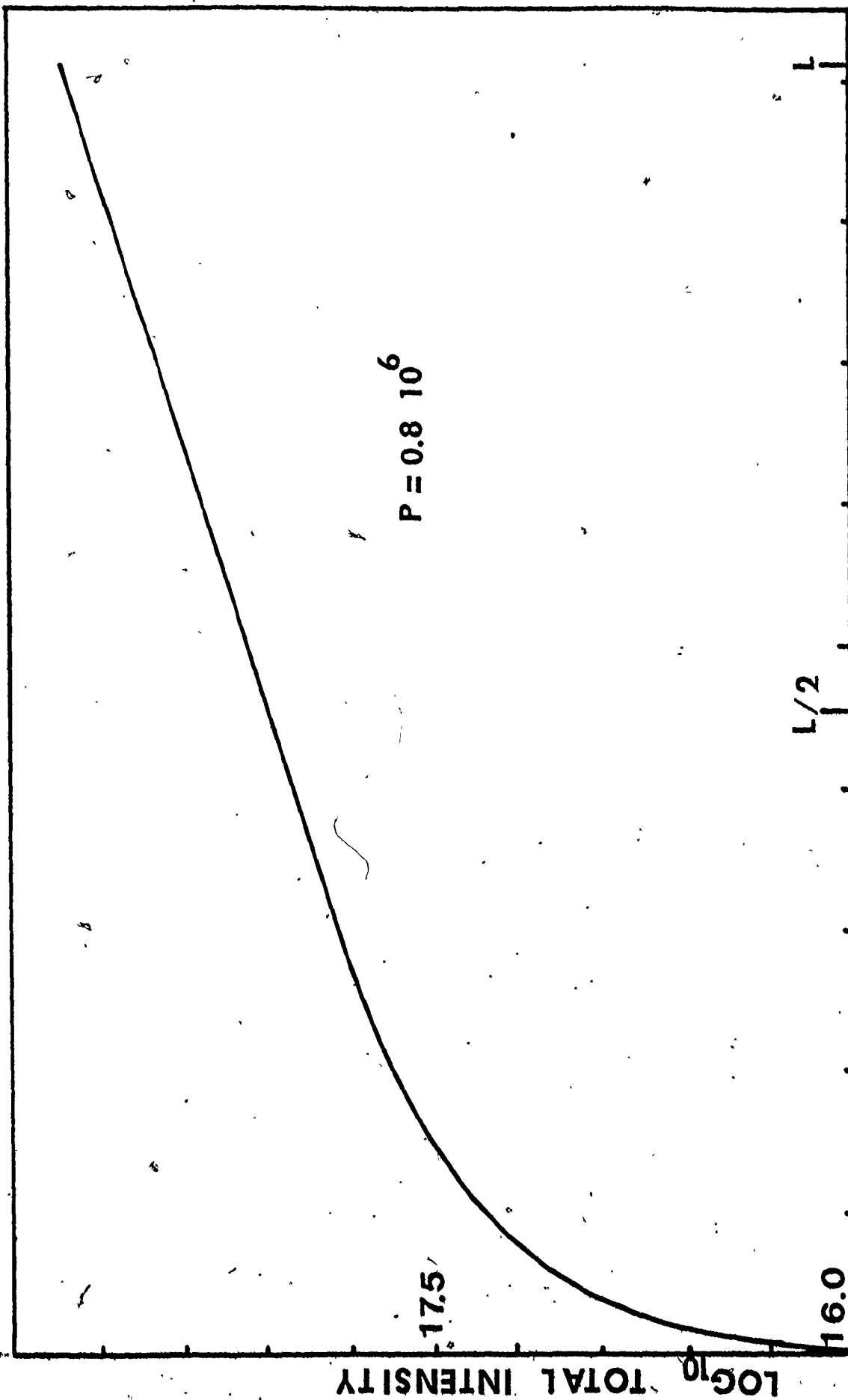
data from reference 82 and references cited, S_1 absorption and emission cross-section measured by us and appearing in Appendix A and ESSA cross-section from reference 89 corrected and extended appropriately as we will see in the next section and also appearing in Appendix A. Figure 3-3 shows how the spectrum of the intensity $I^+(\lambda)$ varies as a function of position within the cell. It can be seen that because of positional and wavelength dependence of the intensity, the intensity dependent gain can change drastically within the cell. We also observe that the peak of the intensity shifts and any approximate theory which does not take this into account is bound to introduce errors. It is the peak of the ASE at $x = L$ which we will use to compare with experiment.

Figure 3-4 shows how the I^+, integrated over the wavelength, will vary with position. It can be seen that for small x,.for this particular concentration and pumping, the intensity varies very fast but it slows down when the intensity begins to saturate the available gain. The significance of this is that above saturation, we have only small increase of the intensity of the ASE and as far as the narrowing of the ASE is concerned, it will mostly take place in the unsaturated region where the gain is much larger than the saturated region. It should be noted that the integration step in the wavelength space is usually 10 Å. For high pumping, especially for laser pumped dye amplifiers, a finer net of points in the position - wavelength space (x,λ) is needed for smoother parameter variation and consequently more accurate results. In our case, we usually used a position step of 0.092 cm (200 steps for the 18.2 cm cell length) in order to restrict the computing costs to

reasonable amounts and still have accurate enough results. These step values of position and wavelength were chosen after we had performed a series of computations studying the effect of the steps on the accuracy of the results. For a wavelength step of 10 $\overset{\circ}{A}$, we found that, even in the narrowest pulses relevant to the experimental situation, each pulse could be represented by more than 30 points in the wavelength grid which was sufficient to determine the pulse shape, peak wavelength and the full width half maximum spectral width.

Figure 3-5 shows the gain coefficient G(x) at the last section of the cell, (x = L). The expression used to calculate G(λ) is the following:

$$G(\lambda,x) = N_1(x)\sigma_e(\lambda) - N_0(x)\sigma_{01}(\lambda) - N_t(x)\sigma_t(\lambda) - N_1(x)\sigma_{12}(\lambda) \qquad (3\text{-}17)$$

where N_1, N_0, N_t are the population densities of the levels S_1, S_0, T_1 $\sigma_e(\lambda)$ is the emission cross-section of S_1 and $\sigma_{01}(\lambda)$, $\sigma_t(\lambda)$, $\sigma_{12}(\lambda)$ are the absorption cross-sections of S_0, T_1 and S_1, correspondingly. The un-saturated gain coefficient for a given pumping is calculated from the same expression assuming zero intensity.

Figure 3-6 shows the variation of the population density of the excited state S_1 divided by the total density of the dye molecules in the solution. For low pumping, $N_1(x)/N$ varies little over the length of the cell. Since $N_1(x)/N$ is directly related to the gain, this nearly constant value of $N_1(x)/N$ implies a constant unsaturated gain throughout the cell. For high pumping, $N_1(x)/N$ varies drastically and consequently the gain changes accordingly along the cell. This gain change can result in considerable computational error unless the step size in the calculation is adjusted accordingly. The change of gain with position also

Figure 3-5. (a) Gain coefficient near the end of the cell as a function
of wavelength for a particular pumping $P = 3.4 \times 10^6 \text{ sec}^{-1}$.
(b) Unsaturated gain coefficient vs wavelength (no photon
flux present). The concentration is $1.5 \ 10^{-3} \text{ M}$ and the
cell dimensions are 70 μ x 1 mm x 18.2 cm. .

UNSATURATED GAIN

SATURATED GAIN
AT X=L
$P=3.4 \times 10^6$

GAIN (cm^{-1})

WAVELENGTH (Å)

FIG.3-5

5680   5840   6000   6160   6320

.2   .4   .6   .8
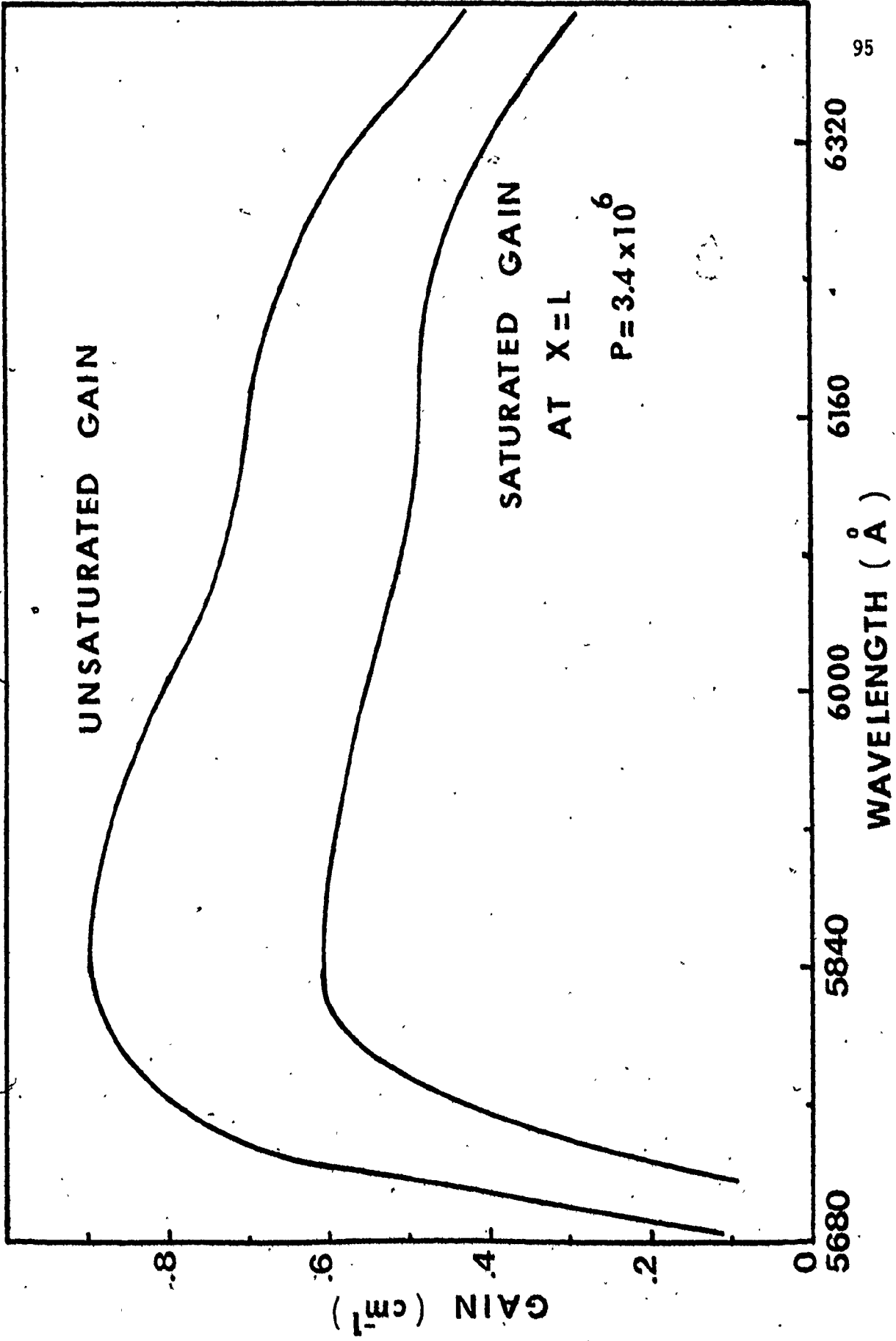
95

Figure 3-6.   Percentage ratio of the excited molecules over the total number of molecules in the solution as a function of position within the cell for three different pumping strengths $P_1 = 2.0 \times 10^6$, $P_2 = 3.0 \times 10^6$ and $P_3 = 3.4 \times 10^6$. The concentration is $1.5 \ 10^{-3}$ M rhodamine 6G/ethanol and the cell dimensions are 70 μ x 1 mm x 18.2 cm.
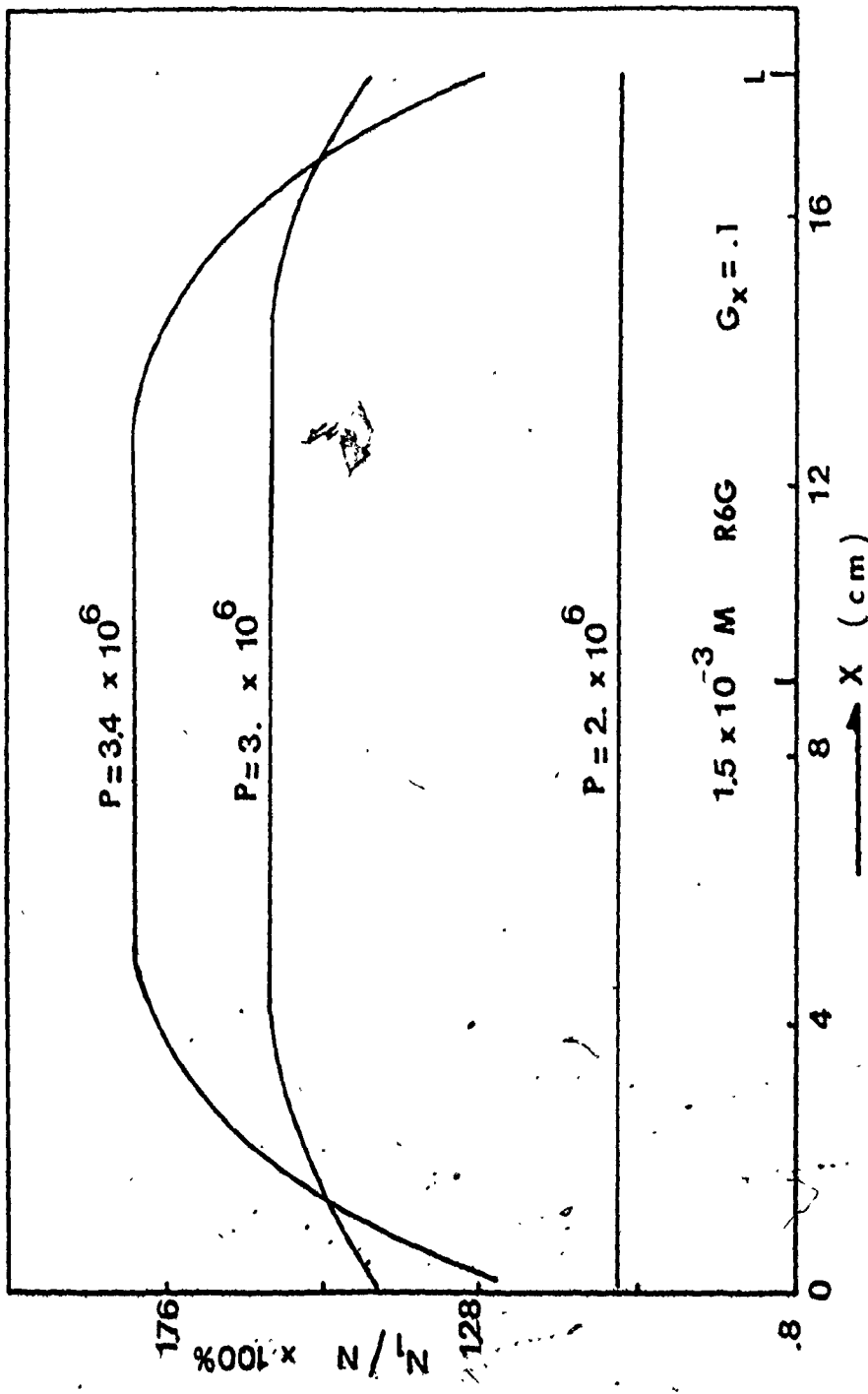
FIG.3-6

gives an indication of the error, which can occur in the approximate theories mentioned in the introduction, unless care is taken to ensure operation of the amplifier well below the saturation region. Some similar results concerning the $N_1(x)/N$ behaviour and the intensity of the ASE within the cell have been published recently by Ganiel et al.[82]

Up to this point, we have mainly presented results for a fixed pumping value, which aids the understanding of the way the ASE develops within the dye cell. In what follows, we will present results for different pumping values. This is useful in helping us to develop an even better comprehension of the mechanisms involves in the ASE and, from the practical point of view, to find the most appropriate ways to compare theory with the experiment, and thereby to determine the gain of real systems in the laboratory. Figure 3-7 shows the variation of the ASE at the end of the cell and at a fixed wavelength λ (which is chosen close to the wavelength where the intensity peaks in the high pumping region, which is also the high unsaturated gain region). Clearly, there are three distinct regions. First is the below threshold region where there is no significant stimulated emission contribution. In this region only the spontaneous emission contributes. Second is the exponential region where the stimulated emission dominates over the spontaneous one. Third is the saturation region where the intensity is so high that it saturates the available gain.

Figure 3-8 is a similar plot of the total intensity integrated over wavelength vs pumping. It exhibits similar behaviour to the single wavelength intensity of Figure 3-7, with a slightly smaller slope in exponential region because of the wavelength dependence of the gain

Figure 3-7.   ASE flux at a wavelength of 5900 $\overset{\circ}{A}$ vs pumping. A Jarell-
Ash 0.25 m spectrometer with 150 μ slits was used. The
concentration of the rhodamine 6G/ethanol solution is
1.0 10^{-3} M   and the cell dimensions are 70 μ x 1 mm x
18.2 cm. The spontaneous emission coupling constant G_x
is 0.1.
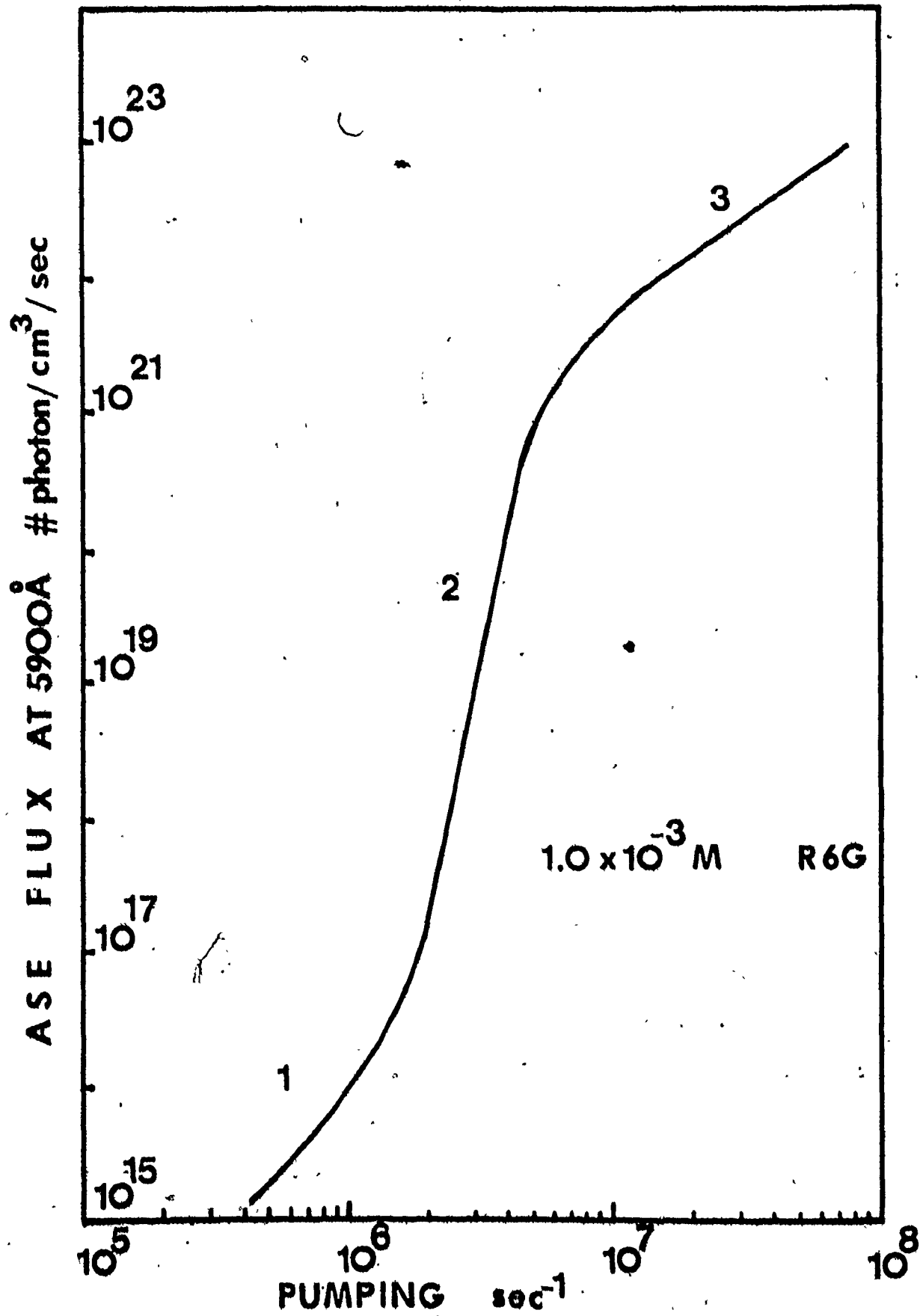
FIG. 3-7

Figure 3-8.   Total flux of the ASE, integrated over wavelength, against

pumping.   The concentration of the rhodamine 6G/ethanol

solution is $1.0 \ 10^{-3}$ M   the cell dimensions are 70 μ x

1 mm x 18.2 cm and the coupling constant G_x is 0.1.
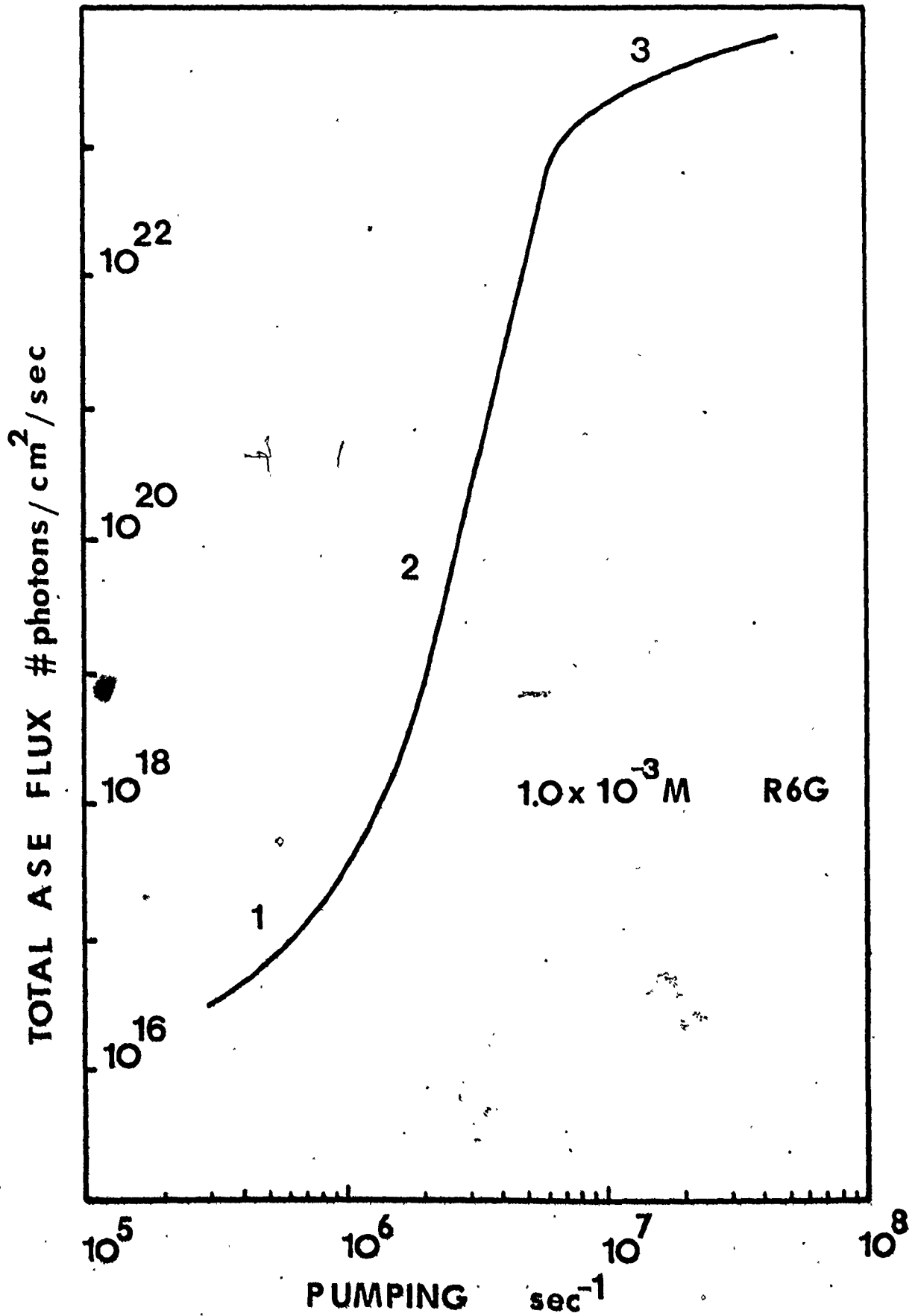
FIG. 3-8

(Figure 3-7 corresponds to the maximum of the gain profile while Figure 3-8 corresponds to an average gain which is obviously smaller than the maximum). Note that we consider both the intensity at fixed wavelength (near the peak wavelength at the highest pumping available) and the intensity integrated over wavelength. The reason is that because the gain spectrum is not symmetric, the peak of the intensity will change with pumping. Consequently, it is more accurate to consider the intensity at a fixed wavelength and compare it with the corresponding experimental plots. Additionally, we want to have a way to evaluate the approximate theories, mentioned in the introduction, which do not take into account this peak wavelength shift and deal only with intensities integrated over wavelength. Therefore, we calculate the intensity integrated over wavelength for different pumping intensities for use in the evaluation of approximate theories.

Figure 3-9 shows the variation of the wavelength λ_0 (which corresponds to the peak intensity $I_L^+(\lambda)$) as a function of pumping with and without the presence of ESSA. For low pumping the intensity of the ASE peaks at longer wavelengths where the absorption losses are smaller, but as the pumping increases the gain increases and consequently, the peak can move towards regions of higher loss. This peak wavelength λ_0 is a very sensitive function of the cross-section values and their slopes in the region of interest. Consequently, it can be used as a monitor to test the accuracy of the measured cross-sections. The effect of the ESSA on the peak wavelength is clearly shown on this graph. It should be mentioned again that all the graphs in this section have been produced

Figure 3-9.   Peak wavelength of the emitted ASE vs pumping. The con-
              centration of the rhodamine 6G/ethanol solution is $1.5 \ 10^{-3}$
              M   and the cell dimensions are 70 μ x 1 mm x 18.2 cm.
              The absorption of the excited singlet state is not included
              in this particular plot.
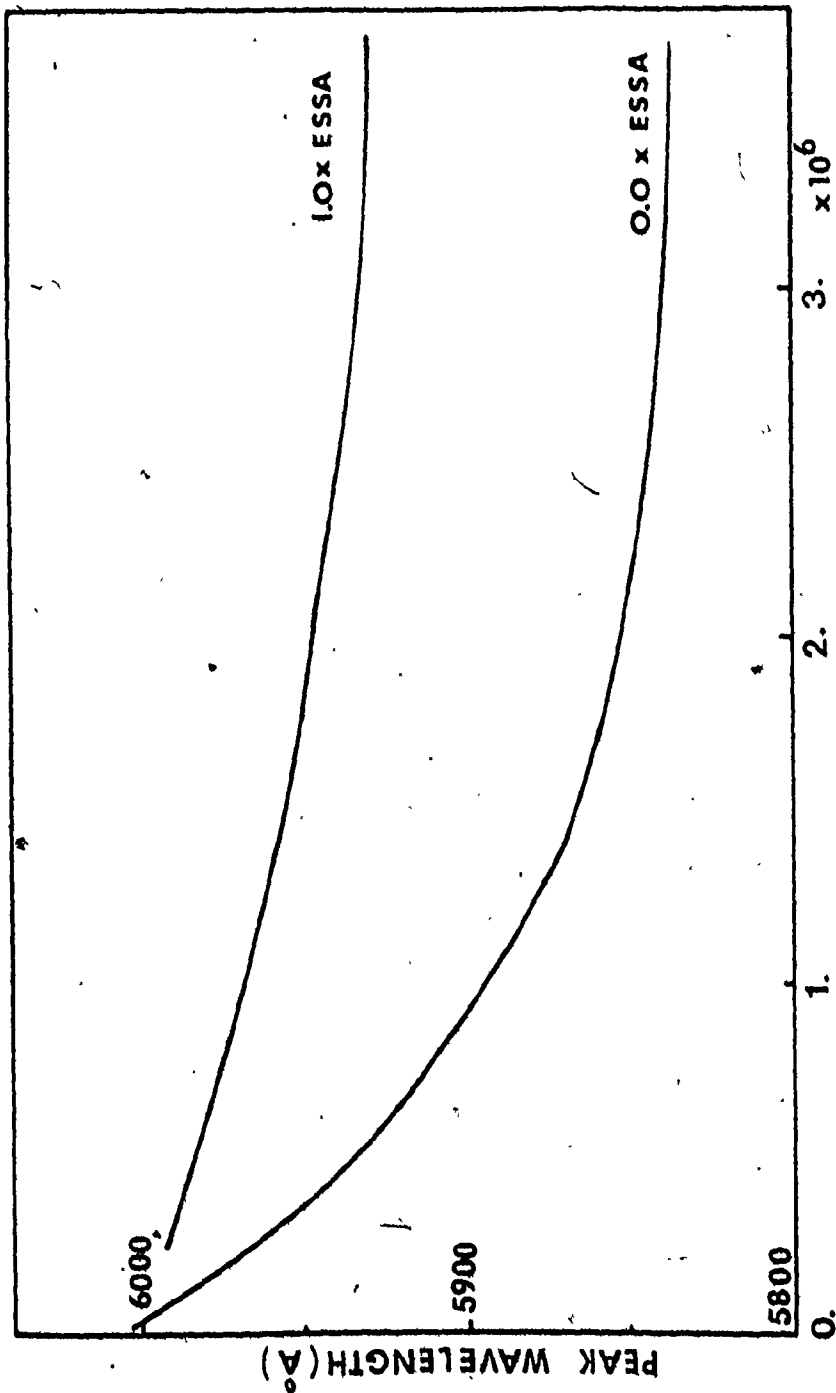
FIG. 3-9

for the particular case of rhodamine 6G dye medium in ethanol.

Finally, Figure 3-10 shows the calculated narrowing of the ASE vs pumping, where the value of $\Delta\lambda$ at very low pumping has been assigned the value of 420 Å, which is very close to that observed experimentally, as we will show later. Notice that as the pumping is increased, the output spectral width narrows rapidly at first but later on, for pumping into the saturation region, the narrowing slows down considerably, but still continues to narrow with increasing pumping.

In this section, we have presented some solutions of the rate equation approach of the modelling of ASE. We have also demonstrated the characteristics of the ASE as it propagates in the dye material. In the next section, we will compare the predictions of the theory with experiment and calculate the unsaturated gain of the particular dye system used, namely rhodamine 6G in ethanol.

3.4 EXPERIMENTAL RESULTS AND COMPARISON WITH THEORY

3.4.1 The Experimental Setup

Before going into the presentation of the experimental results, which are compared with our theory, a brief description is given of the experimental system used to obtain these results. The system is a flashlamp pumped amplifier. Figure 3-11 is a photograph of the assembled dye amplifier along with the 0.5 µF capacitor, which stores the energy, the spark gap and the triggering unit, which initiates the discharge of the stored energy into two ablation flashlamps. These flashlamps operate at a low pressure (~ 30 Torr) which is achieved by the use of a vacuum pump. The initial cold gas is argon and a set of needle valves

Figure 3-10. Spectrum width of the emitted ASE (FWHM) vs pumping. The concentration of the rhodamine 6G/ethanol solution is $1.5 \ 10^{-3}$ M and the cell dimensions are 70 µ x 1 mm x 18.2 cm.
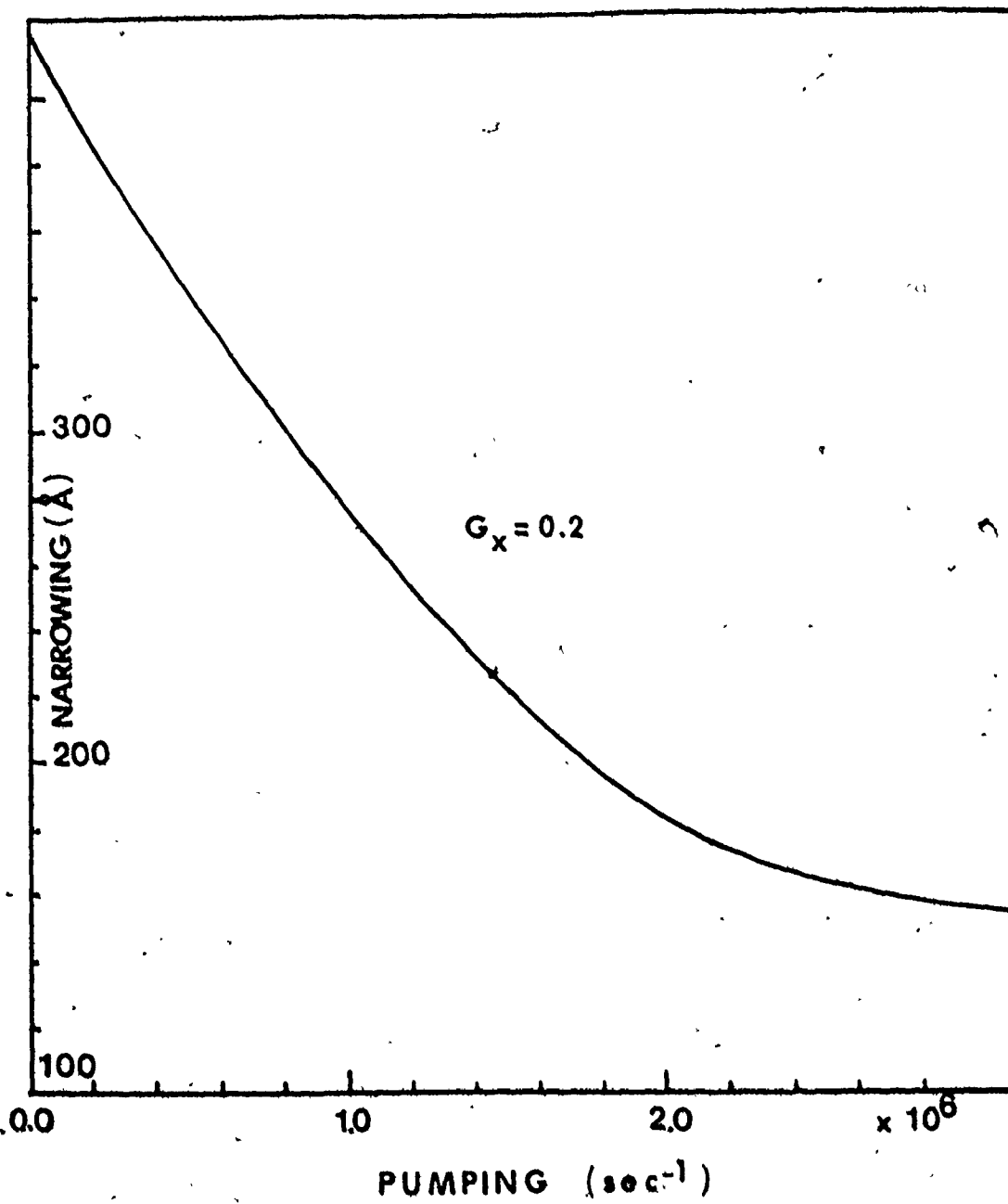
FIG. 3-10

Figure 3-11. Picture of the assembled dye amplifier with the spark gap, the trigger module, the vacuum line, the storage capacitor, the dye circulation line, the DC pre-ionization power supply and part of the flashlamp light detector unit.
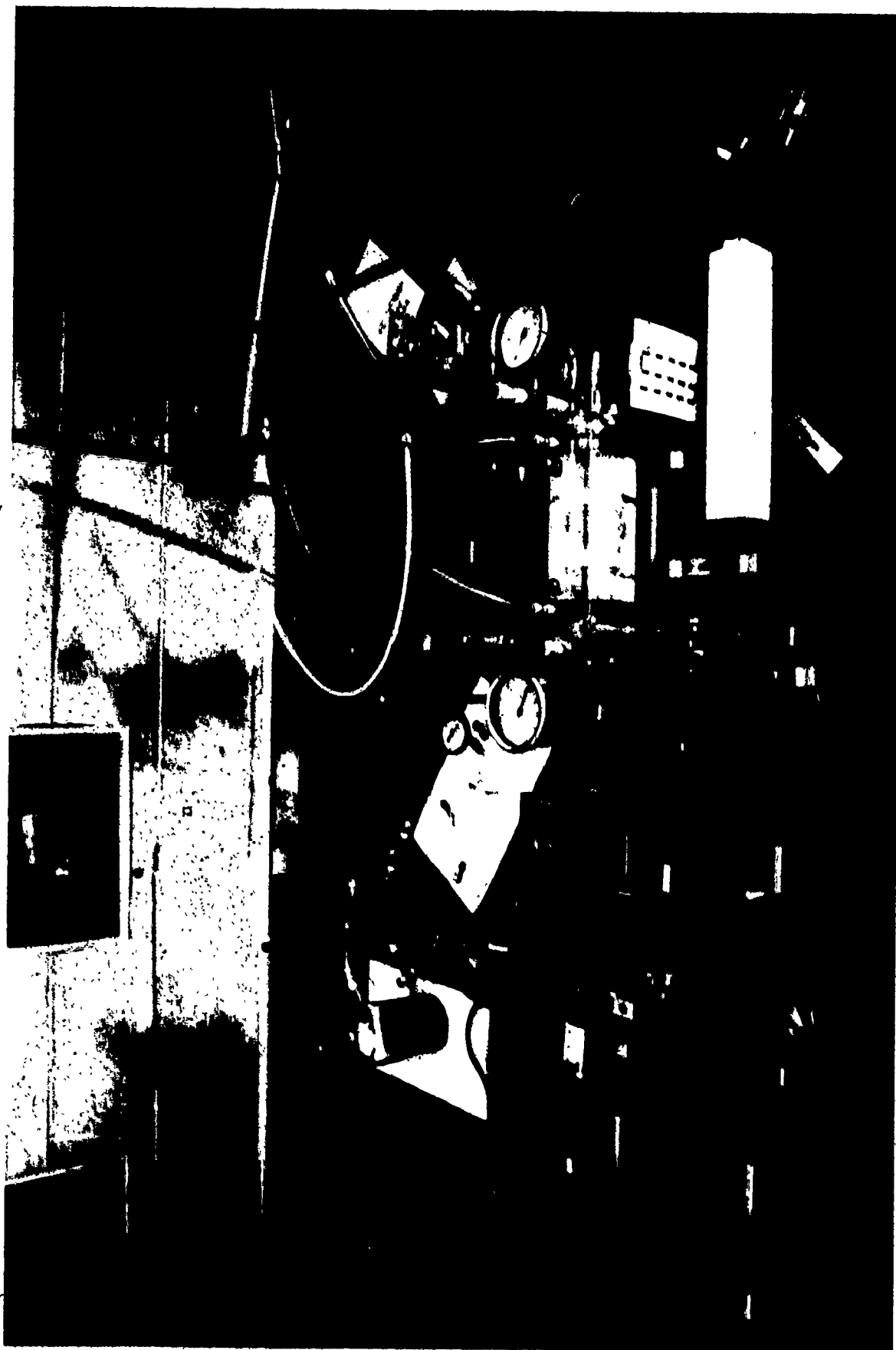
at each end of the flashtubes control the flow and the differential
pressure along the flashlamps. Details of flashtube operation have
been mentioned in Chapter 2. The two flashlamps occupy the two focal
axes of a double cylindrical reflector with elliptical cross-section·
which concentrates the light on a thin dye cell. The dye solution is
circulated through the dye cell with a variable speed micropump. The
dye solution is constantly passed through a 2 micron pore diameter filter
to remove any aggregated dye molecules and a heat exchanger is used to
control the temperature of the solution. The cooling of the flashlamp
inside the amplifier housing is done either with circulating distilled
de-ionized water or with a clean air stream. Water cooling is preferred
because it provides damping for the shock waves produced during the
discharge, which travel perpendicular to the axis of the flashlamp.
Furthermore, it provides better heat conduction and also helps to eliminate
the UV radiation produced by the flashlamps, which can dissociate some
dye materials. The discharge is fired by a pulse generator, which trig-
gers a TM-11A, EG & G sparkgap trigger module, thereby producing a 30 KV
pulse to fire the spark gap. It was found that forced·air cooling was
as efficient for our experimental situation. A continuous pre-ionization
of the flashlamps is provided by a low current discharge driven by a
He-Ne laser power supply with a current controlling resistance followed
by a special high voltage diode to protect the power supply. This con-
siderably improved the flashlamp shot-to-shot repeatability especially
for operation at voltages close to the DC breakdown voltage of the
argon gas of the flashlamp. A planar, variable-width dye cell was used

throughout the measurement and aluminized high reflecting mylar sheet was used to cover the inside of the cylindrical brass reflectors. To avoid deterioration of the reflectivity of the mylar sheet by the presence of water, we used forced air cooling. Appropriate plastic Wratten filters were used to block the UV radiation from reaching the cell, to prevent UV photodegradation of the dye molecule.[92] Photodegradation can occur when molecules in the triplet state T_1 are transferred to the state T_2 and these excited molecules can then cause a C-H bond rupture of the solvent molecule by energy transfer, creating a free ethanol radical and a leuco-compound out of the dye molecule. This process is not reversible and thus affects the concentration of the dye. However, since it is dependent on the number of molecules in the triplet state, the effect can be greatly reduced by the use of triplet state quenchers such as cycloactatraene.[88,93] It should be mentioned here also that the dye molecule rhodamine 6G can photodegrade through absorption of visible light by molecules in the triplet state (T_1) which then produce another radical which depends on the structure of the dye.[92] This process is partially reversible and is diminished by the use of triplet state quencher. Additionally, a study by Borisevich et al.[94] of the spectral-time characteristics of the emission spectrum of flashlamp pumped rhodamine 6G solutions, revealed that the rate of creation of the photoproducts, $K_{ph}(\lambda,t)$, had a different wavelength and time dependence from the rate of the triplet loses $K_t(\lambda,t)$ and their competition for molecules of the T_2 state resulted in non-regular time evolving pulses

and maximum wavelength. It was found that the removal of UV radiation resulted in a smooth time variation of the emission from the rhodamine 6G.

It is obvious then from the above that the use of COT is needed. The negative effect of the excess amount of COT used was recently reported by Wang et al.[95] They claimed that COT at high enough concentration, beside quenching the triplet state, will compete with the dye molecules for the available UV photons of the pump. Because of the great importance of the presence of the triplet state, we have investigated ourselves the effect of the concentration of COT on the emitted ASE. The results are shown in Figure 3-12a, where the maximum intensity for fixed pumping is plotted against the concentration of COT (cm^3 of COT in 100 cm^3 of solution 1.0 10^{-3} M rhodamine 6G/ethanol). It should be noted that no special effort has been made to remove the oxygen present in the solution which acts as a quencher, too,[88] but we observed that oxygen of the air present alone was not enough to quench the triplet state. We observe that a maximum ASE in Figure 3-12 occurs at 0.57 cm^3 COT/100 cm^3 solution of rhodamine 6G 1.0 10^{-3} M. This amount of COT scaled properly for other concentrations was used in all our experiments in this chapter. The rise of the ASE at the beginning of the graph is attributed to the fact that in our pulses system, the maximum of the ASE occurred ahead of the maximum of the pumping pulse before the use of COT. With the addition of COT, the ASE peak moves towards the peak of the pumping pulse which results to the highest ASE possible for this particular pumping. This effect is shown in Figure 3-12b for a concentration of 1.0 x 10^{-3} M and two different pumping rates corresponding to

Figure 3-12a. Intensity of the ASE at $\lambda = 5860$ Å (near the intensity peak at saturation pumping) vs the concentration of the triplet state quencher COT (cyclooctatetraene). The concentration of the rhodamine 6G/ethanol is 1.0×10^{-3} M and the dimensions of the cell are 70 μ x 1 mm x 18.2 cm.

FIG. 3-12a

COT CONCENTRATION (cc / 100cc solvent)

ASE INTENSITY AT 5860 Å (arb.units)

1.0×10^{-3} M   R6G
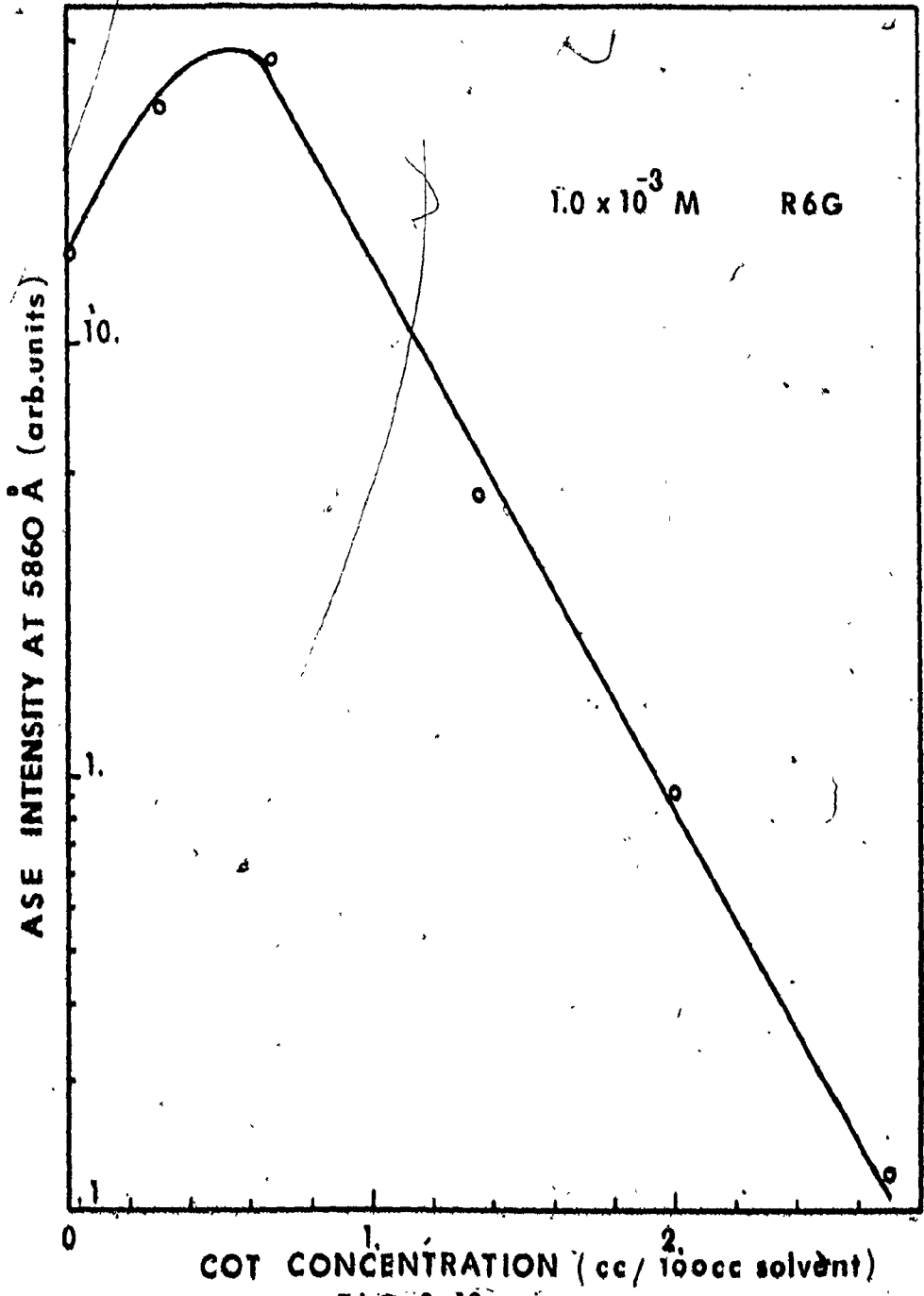
Fig. 3-12b. Flashlamp light (top) and ASE pulses without (a) and with the addition of triplet state quencher (COT). The time scale is 0.2 μs per division and the vertical scales are not comparable.
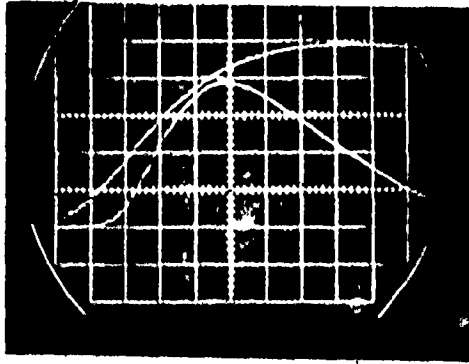
a
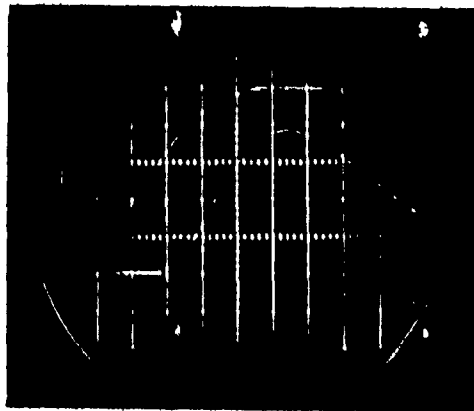
b

FIG. 3-12 b

charging voltages of 21 KV and 25 KV.

It has also been reported that the ASE can terminate earlier. than expected from the available pumping pulse, because of the formation of shock waves due to the absorption of infra red radiation by the solvent.[96] We have found that in our case, the absence of an IR filter (plexiglass) did not contribute to the early termination of the ASE pulse, probably because our cell thickness of 70 microns is much smaller than the absorption length of the ethanol in the IR. Consequently, we do not have any index of refraction inhomogeneity either from the shock or from the local heating of the solvent.

Figure 3-13 presents a number of pictures of pump pulses and their corresponding ASE pulses for different pumping intensities in order to illustrate the kind of pumping and ASE we dealt with in the experiments. We see that increasing the discharge voltage will cause the pump rise time to decrease slightly but this has no effect on our measurements, because we always refer to the peak intensities both of the pump and ASE pulses. The light pulses are detected through a broad-band green filter, by a P-I-N (HP 5220) fast photodiode assembly. The ASE is detected using an EG & G, DT-40 photodiode which collects the spectrally resolved light at the exit slit of a Jarrell-Ash 0.25 m spectrometer. Both pulses can be displayed simultaneously on a dual beam oscilloscope (Tektronix) and be photographed using an appropriate oscilloscope camera and a fast polaroid film (Type 410, 10,000 ASA).

Another important aspect from the experimental point of view is the construction of the dye cell. Because of the relatively high gains available, it is important that we restrict the feedback into the

Figure 3-13. Flashlamp light pulses and ASE pulses for different dis-
charge voltages. (a) 10 KV, (b) 13 KV, (c) 16 KV, (d) 20 KV,
(e) 24 KV and (f) 27 KV. The storage capacitor is 0.5 μF,
the flashtube's diameter is 1.7 mm, their length is 20 cm
and the initial gas pressure is 30-Torr argon. The con-
centration of the rhodamine 6G/ethanol solution is 1.5
10^{-3} M and the cell dimensions are 70 μ x 1 mm x 18.2 cm.
The time scale is 0.5 μsec per division. The vertical
scales are not comparable.
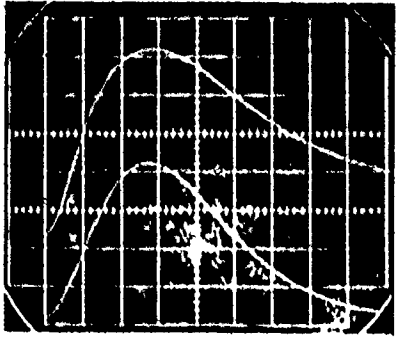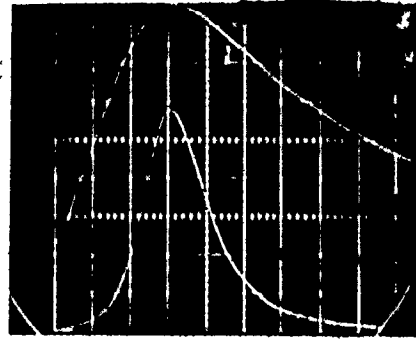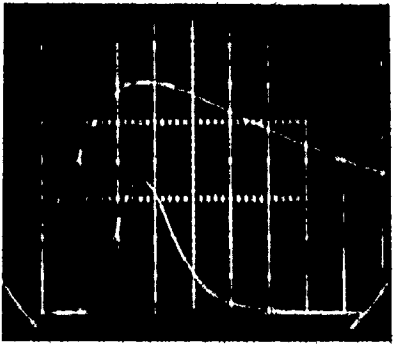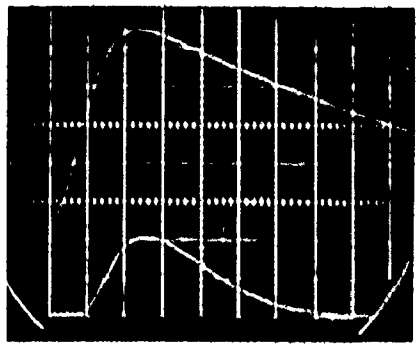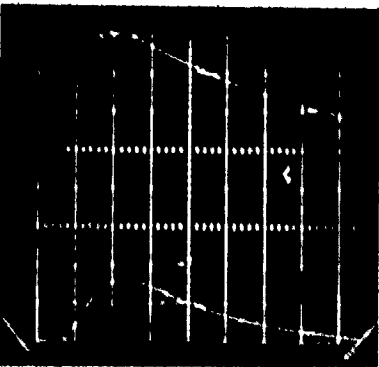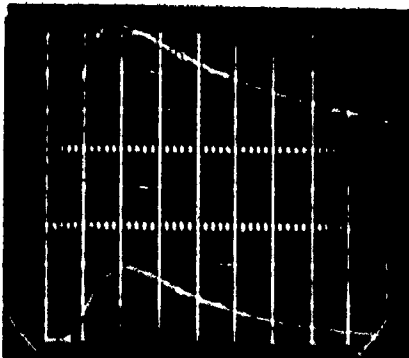
FIG. 3-13

cell to values well below the amount of spontaneous emission, which
originates near the end of the cell and feeds into the cell. Otherwise,
the scattering will compete with the spontaneous emission produced
locally within the cell. Our dye cell consisted of a black anodized
aluminum body supporting two pyrex plates flat to within $\lambda/4$ (1.5 cm x
19.8 cm x 1/8") separated with appropriate plastic spacers. The whole
assembly is made waterproof by using rubber o-rings. Two antireflection
coated pyrex glass output windows are used, inclined, on purpose, to avoid
any residual reflections and cavity resonance effects. The thickness
of the cell can be adjusted so that, for a particular concentration used,
the absorption across the cell is uniform. The dye solution can be cir-
culated, but even slow circulation creates turbulence, which can affect
the intensity of the ASE by as much as 30%. Therefore, all the measure-
ments have been taken with stationary dye solution, which is renewed
before each shot. Additionally, we used a heat exchanger to keep the
temperature of the dye constant and independent of the temperature fluc-
tuations in the lab. This precaution was taken because it has been re-
ported by Huth et al.[6] that the quantum efficiency of some dyes is
strongly dependent on temperature. They reported changes of the quantum
efficiency of the order of 0.8% per degree Celcius for the rhodamine B
and 0.2% for the rhodamine 6G in ethanol.

The major portion of the experimental data has been taken by
recording, in polaroid pictures, both the pumping pulse and the ASE pulse.
This was done to ensure accuracy, because even small variation of the
pumping, which is proportional to the unsaturated gain, will cause large
changes in the ASE in the unsaturated gain region where the ASE intensity

depends exponentially on the pump. This retroactive technique is not always necessary and a careful design of the flashlamp along with the pre-ionization[96] of the flashlamp greatly improves the repeatability of the pumping light pulse. Figure 3-14 shows results of such DC pre-ionization where improvement by a factor of 1.8 can be seen. Five successive pulses, 20 sec apart, are superimposed in each picture. It seems that the presence of ions, electrons and metastable atoms (created by applying a few KV along the tube, with a current limited to a few ma to avoid heating the amplifier housing) in advance of the main discharge creates a more reproducible pumping pulse. This is so, because high current densities required by the main discharge can be obtained more easily if a stable low current discharge preceeds the main discharge.[53,96] In conclusion, pre-ionization should be used to increase the repeatability of the flashlamp pulses.

In the next section, we present the experimental results obtained and compare them with the theoretical prediction of the previous section. A major purpose is to find a way to accurately determine the unsaturated gain of the system. On the way to achieving this goal, we have determined more accurate values of the absorption and emission cross-sections for rhodamine 6G. Most notably, we have generated the excited single state absorption cross-section values over the wavelength region of interest. All these cross-section values are listed in Appendix A.

Figure 3-14. Flashlamp light pulses and their corresponding ASE pulses
without pre-ionization (a) and with pre-ionization (b).
·Four successive pulses are superimposed. The flashlamp
diameter is 1.7 mm, their length is 20 cm and the initial
gas pressure is 30-Torr argon. The storage capacitor is·
0.5 µF and the concentration of the rhodamine 6G/ethanol
solution is $1.5 \ 10^{-3}$ M . The cell dimensions are 70 µ x
1 mm x 18.2 cm.
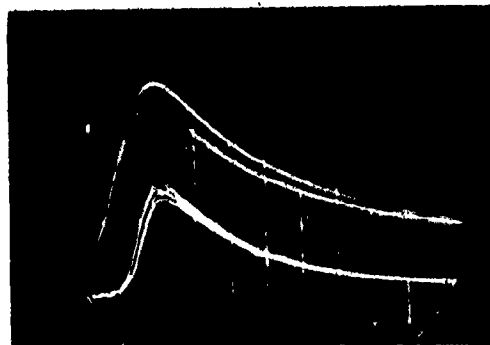
a
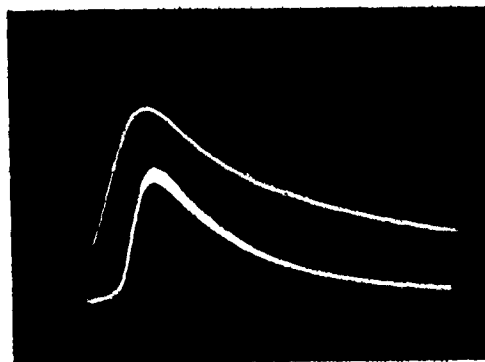
b

FIG. 3-14

3.4.2 The Experimental Results

In this section, we will present the experimental results, which we used to compare theory with experiment. It was mentioned in a previous section that it is very important to use accurate cross-section values in the calculations and that the ASE narrowing along with the peak wavelength of the ASE are very sensitive functions of these cross-sections. It is natural then to test the accuracy, of the cross-sections used by comparing the ASE we get from the theoretical model with the experimental values of ASE at very low pumping where no saturation exists and the gain is close to zero. Any failure to match theory and experiment at very low pumping is a strong indication that the cross-section values are incorrect.

Figure 3-15 shows the ASE intensity as a function of wavelength measured experimentally for very low pumping as well as that calculated from the theoretical model using published data[90] for the cross-section, or improved cross-section data measured by ourselves. It can be seen that, when we used the published values [90] for the ground state absorption and fluorescence, the calculated ASE differs from the measured one in both the low and high wavelength regions of the spectrum. The calculated spectrum width (FWHM) is only 350 Å. This is considerably smaller than the 420 Å, which we get by extrapolating to zero pumping the measured narrowing at low pumping as we will see later. The use of our measured cross-section values improves the fit to the ASE spectrum but there is still some small descrepancy at the short wavelengths and the spectral width (400 Å) is still too small. With the addition of the

Figure 3-15. Intensity of the ASE vs wavelength.

--- Calculated ASE using published values of crossections[71.]

for the singlet state absorption $\sigma_{01}(\lambda)$ and the fluorescence

$E(\lambda)$ (FWHM $\Delta\lambda = 350$ Å)

-.- Calculated ASE using $\sigma_{01}(\lambda)$ and $E(\lambda)$ values measured

by ourselves, but without any excited singlet state absorp-

tion (ESSA) involved (FWHM $\Delta\lambda = 400$ Å).

— Calculated ASE using $\sigma_{01}(\lambda)$ and $E(\lambda)$ values we measured

with an 80% contribution of the ESSA (FWHM $\Delta\lambda = 420$ Å)

o   Experimentally observed intensity of ASE vs wavelength

for very low pumping. All calculated intensities corres-

pond to low pumping (P = .01 10^6). The concentration of

rhodamine 6G/ethanol solution is $1.5 \, 10^{-3}$ M   and the cell

dimensions are 70 μ x 1 mm x 18.2 cm.

FIG. 3 – 15

EXPER. 1.5 x 10⁻³ M   R6G
from
PUBLISHED σ_{o1}, $E(\lambda)$

MEASURED σ_{o1}, $E(\lambda)$, 0.8 ESSA

0.0 ESSA

420 Å

WAVELENGTH (Å)

IN I (arb. units)
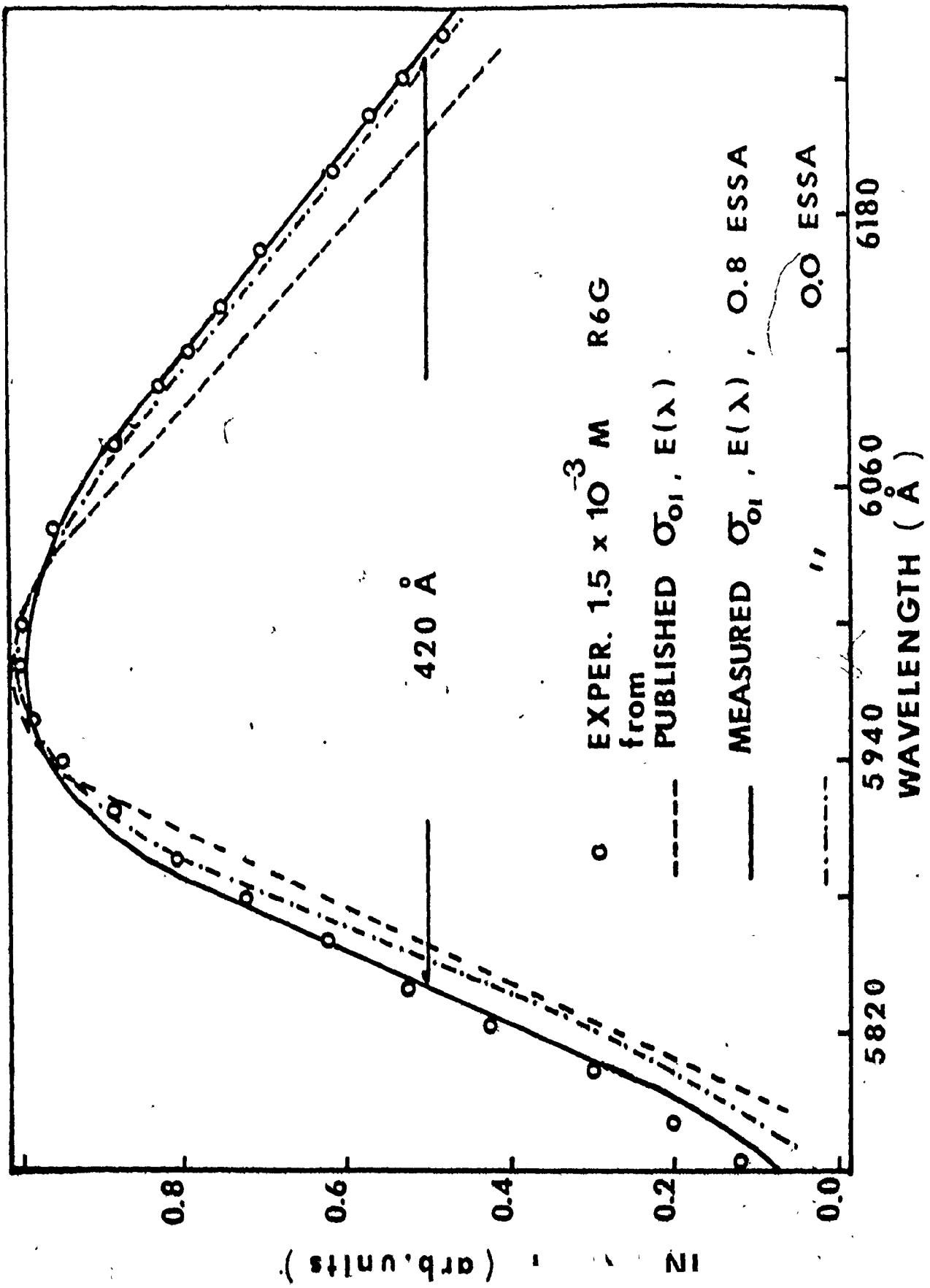
ESSA cross-section (the amount of ESSA to use is determined by the study of the peak wavelength shift with pumping as we will see later on) a very good fit is achieved between the calculated and measured ASE spectra.

Next, we consider the effect of the ESSA on the peak wavelength shift with pumping. Sahar et al.[89] have reported ESSA values for rhodamine 6G in ethanol for wavelengths up to 6100 Å, but, at low pumping, our ASE spectrum extends beyond this wavelength. Values for the ESSA cross-section for wavelengths above 6100 Å were obtained from the best fit of the intensity profile at low pumping (Figure 3-16) in the long wavelength range. Sahar et al.[89] put the accuracy of their ESSA data at $\pm$ 10%, however, our measurements give the values which are 20% lower than those indicated by Sahar for wavelengths up to 6100 Å. Figure 3-16a shows the change of the wavelength (λ_0) at which the ASE is maximal as a function of pumping both for theory and experiment, and for several contributions of the ESSA cross-section (such as no ESSA at all, 60%, 80% and 100% of its calculated value). It can be seen that for high pumping, the value of λ_0 does not change and any scaling (which is going to be discussed later) between the experimental and theoretical pumping values will not affect λ_0. Again, the best fit to the λ_0 data is obtained when we assign a value to the ESSA cross-section which is 20% smaller than the one reported by Sahar et al.[89] This method of testing the ESSA cross-section is very important, first because it can be used to test other already calculated or measured values of ESSA and second it can be directly used to estimate the ESSA cross-section with a high degree of accuracy because λ_0 is a very sensitive function of the ESSA

Figure 3-16a.   Peak wavelength λ_0 of the ASE vs pumping for several
excited single state absorption (ESSA) contributions along
with the experimentally observed values of λ_0. The con-
centration of the rhodamine 6G/ethanol solution is 1.5×10^{-3}
M   and the cell dimensions are 70 μ x 1 mm x 18.2 cm.

Figure 3-16b.   Excited single state absorption (ESSA) cross-section
vs wavelength, (a) according to Shahar et al.,[89]
(b) according to our calculations. The concentration of
the rhodamine 6G/ethanol solution is 1.5×10^{-3} M   and the
cell dimensions are 70 μ x 1 mm x 18.2 cm.
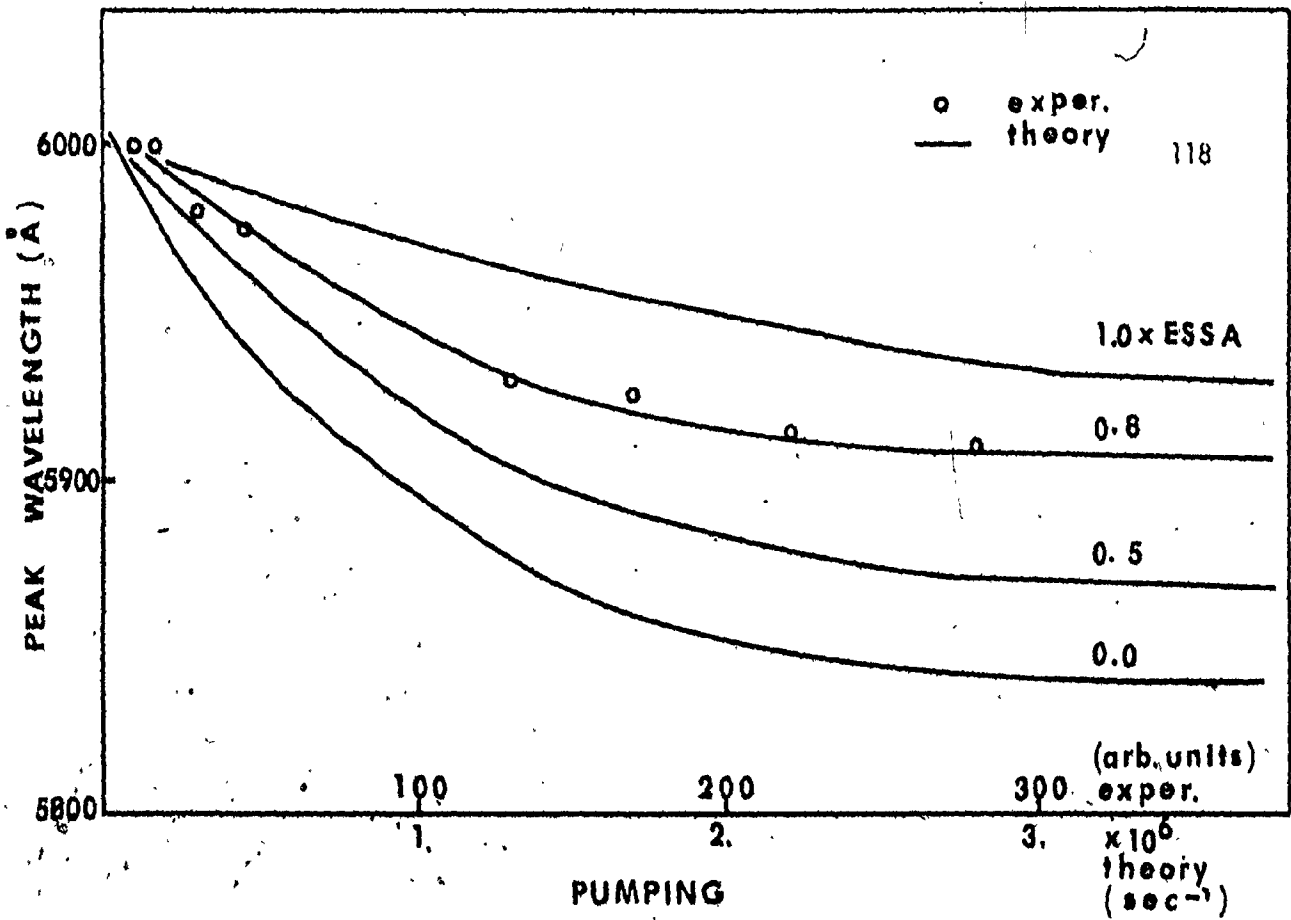
FIG. 3-16a
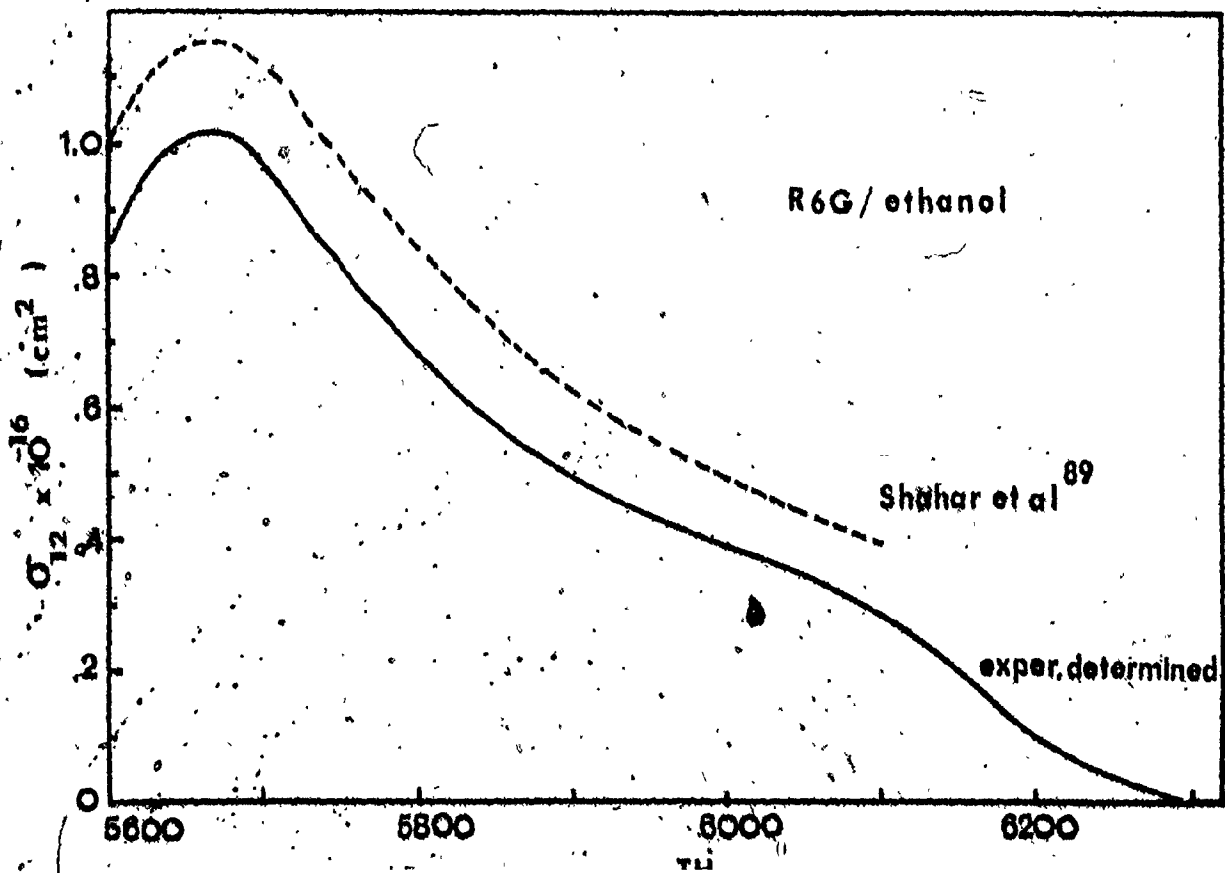
amount involved. Figure 3-16b shows the ESSA cross-section vs wavelength reported by Sahar et al.[89] and the ESSA cross-section we have obtained, extended over the entire spectrum of interest, which was used in our subsequent calculations. From the discussion presented above, the importance of the ESSA has been demonstrated clearly. Next, we deal with ASE intensity profile change with pumping both theoretically and experimentally. This is important because in principle we could calculate the gain for every pumping by matching the calculated intensity profiles of the ASE with experiment. For reasonably smooth spectra though, we can approximate the corresponding profiles, if we know the peak wavelength λ_0 and the spectral width $\Delta\lambda$. Another equivalent way is to match the intensities of the ASE at fixed wavelength and the spectral widths $\Delta\lambda$. This last way is the one we are going to use. We will also record the total intensity integrated over wavelength, because it can be related to the approximate theories for measuring gain as we will see in a later section.

Figures 3-17 and 3-18 show intensity spectra, for the experimentally measured ASE and the calculated ASE, respectively, for several values of pumping, from very low level of excitation to excitations well within the saturation region. In Figure 3-17, the pumping is given in relative units as it is measured by a photodiode and corresponds to the peak of the pumping pulse. In Figure 3-18, the pumping is given by the rate at which molecules are excited from the ground state and is given in sec^{-1}. Comparing the ASE spectra in Figures 3-17 and 3-18 we observe that for increased pumping the long wavelength part of the spectrum changes much more than the short wavelength side. This is a reflection of the cross-section change of the

Figure 3-17. Intensity of the ASE vs wavelength measured experimentally for several pumping values. The concentration of the rhodamine 6G/ethanol solution is 1.5 10^{-3} M and the cell dimensions are 70 μ x 1 mm x 18.2 cm (70 μ is the thickness). A Jarell-Ash 0.25 m spectrometer with 150 μ slits was used.

FIG. 3—17

120
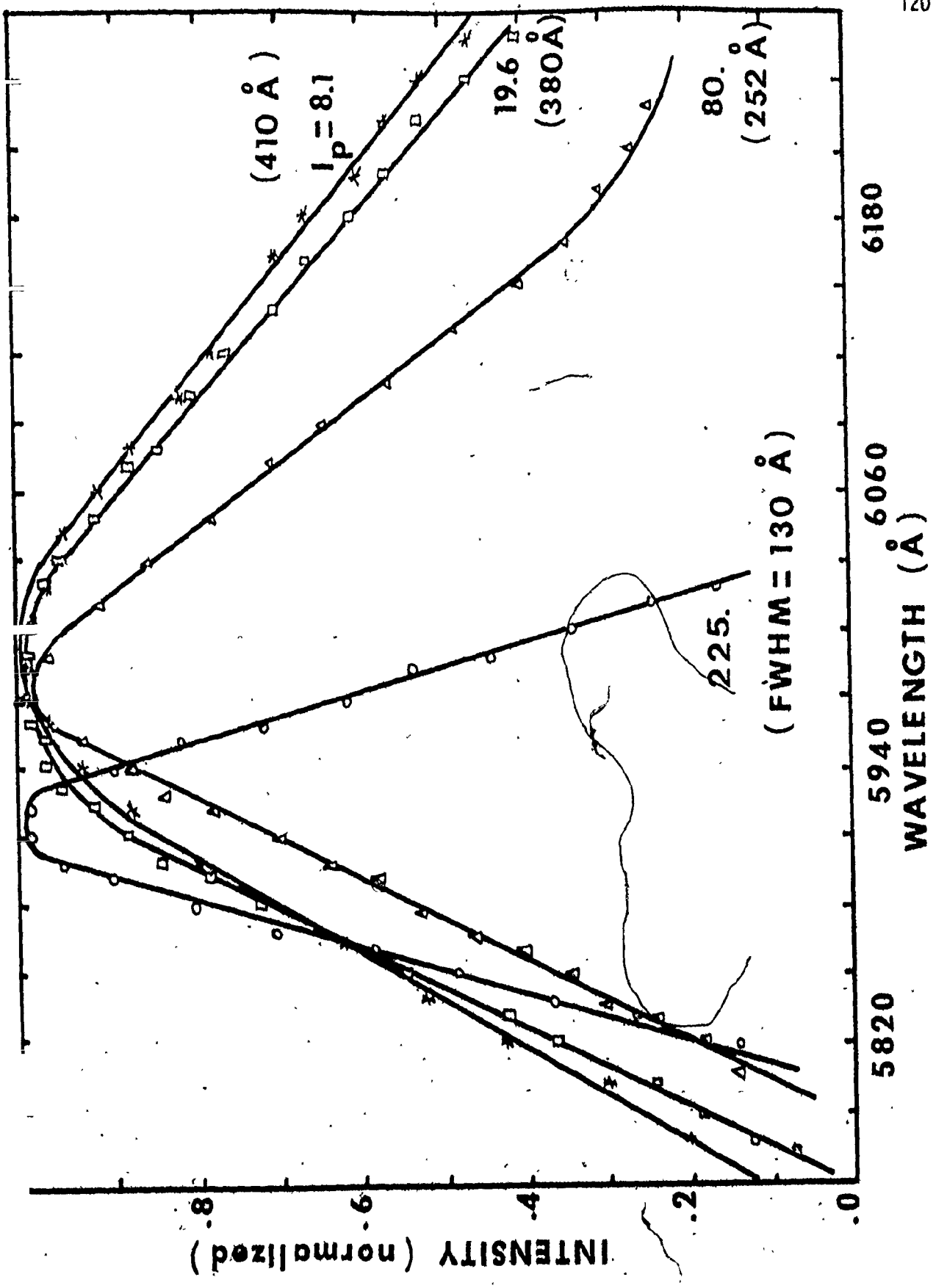
Figure 3-18. Calculated intensity spectrum of the ASE for several pumping levels. The concentration of the dye rhodamine 6G/ethanol is $1.5 \cdot 10^{-3}$ M

INTENSITY (normalized)
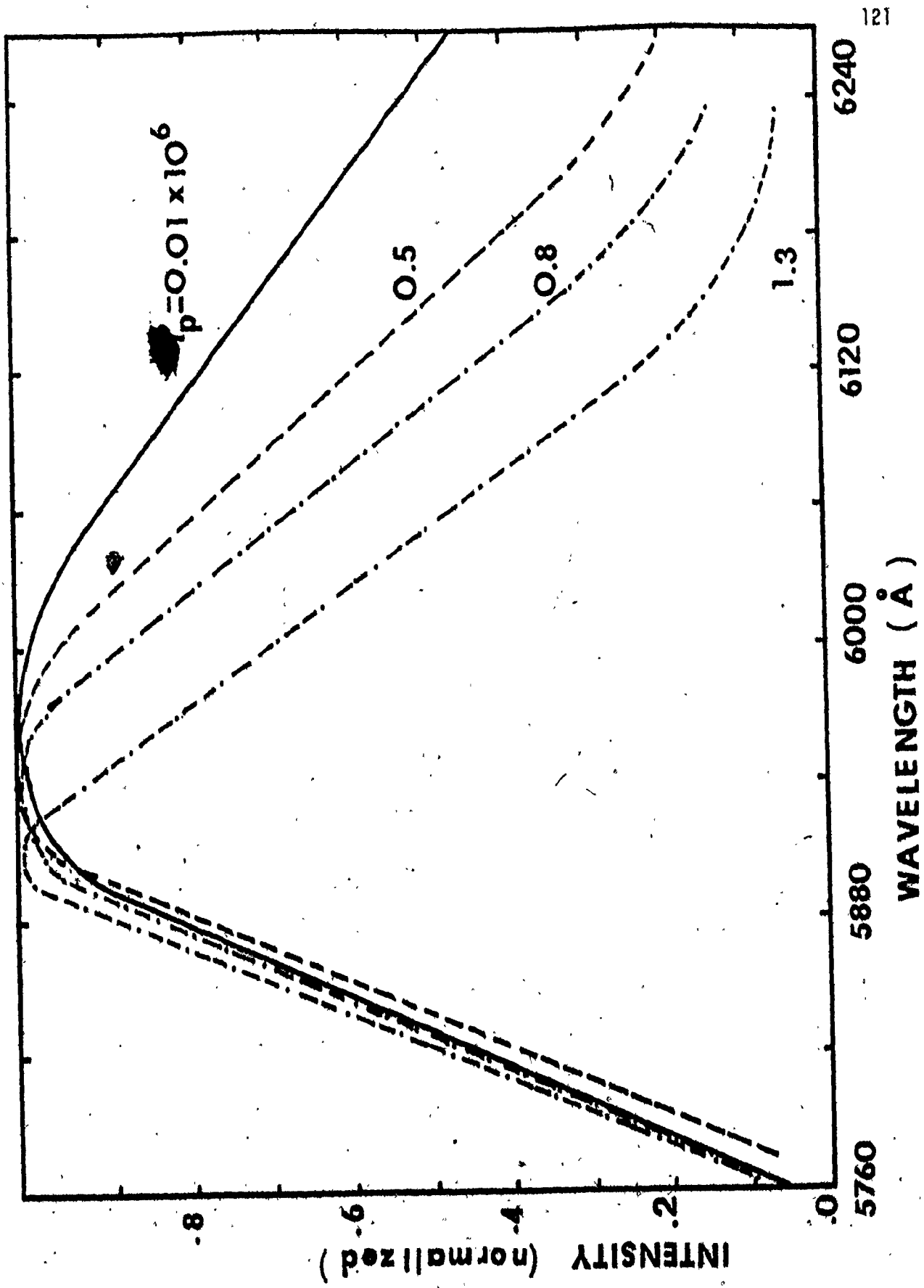
WAVELENGTH (Å)

FIG. 3—18

$I_p = 0.01 \times 10^6$

0.5

0.8

1.3

121

ground state absorption which gets steeper for shorter wavelengths. Additionally, we observe that the wavelength of maximum ASE λ_0 moves to shorter wavelengths from 6000 Å down to 5910 Å, approximately, for both theory and experiment. The change is not linear, again reflecting the ground state absorption dominance at short wavelengths. Nevertheless, the ASE spectra become progressively more symmetric as the pumping increases and, consequently, these spectra can be accurately represented by λ_0 and $\Delta\lambda$, the peak wavelength and the spectral width, respectively, or equivalently, in the case we want to compare intensities of ASE, by the intensity at a fixed wavelength near λ_0 and the spectral width $\Delta\lambda$. Then, the basic procedure to match theory and experiment is as follows:

(i)   find experimentally or theoretically the peak wavelength λ_0 of the ASE with pumping in the saturation region

(ii)   measure the ASE intensity at λ_0 vs pumping

(iii)   calculate from theory the ASE intensity at λ_0 of the ASE vs pumping

(iv)   measure and plot the spectral width $\Delta\lambda$ of the ASE vs pumping

(v)   calculate and plot the spectral width $\Delta\lambda$ of the ASE vs pumping

(vi)   scale the relative pumping scales of the spectral width against pumping to match the narrowing against pumping plots

(vii)   use the scaling factor obtained in (vi) to compare the slopes of the intensities at λ_0 vs pumping plots. Good matching will give the same slopes in both graphs

(viii)   adjust the spontaneous emission coupling constant ($g(x)$) in order to get proper matching of the intensities at the saturation region also. With this new value of $g(x)$, check the matching in (vi)

(ix)   use the theory to calculate the unsaturated gain for any parti-
        cular scaled pumping

(x)   use the theory to calculate any other relevant quantity such as
        ASE distribution within the cell, gain as a function of position,
        etc.

Following this basic procedure, we matched theory with experiment
in the particular case of $1.5 \; 10^{-3}$ M   rhodamine 6G in ethanol. The
dye cell had a width of 70 μ, a length of 18.2 cm and a height of 1.0 mm.
Figure 3-19 shows the intensity of the ASE at $\lambda_0 = 5920$ Å vs the pumping
from the flashlamp. A set of pinholes helped to sample only the ASE,
which was emitted within an angle of 2° with respect to the axis to ensure
the gain measurement at the centre line of the cell. Figure 3-20 shows the
experimentally measured spectral width vs pumping provided by the flash-
lamp and also the calsulated spectral width vs the pumping. On the same
graph, we show the scaled theoretical plot. It can be seen that in order
to scale the theoretical pumping to the experimental, we have to multiply
the theoretical pumping values by $6.0 \; 10^{-5}$.   Next, we turn to match the
intensity vs pumping plots.

It was mentioned before (equation (3-8)) that a parameter g(x) is
used which determines the exact amount of the spontaneous emission which
couples into the cell and is subsequently amplified. This coupling para-
meter is approximately equal to the solid angle subtended by one end of
the cell at the other. Consequently, we can write

$$g(x) = Q_x \; \frac{RH}{2(L - x)^2}$$

(3-18)

Figure 3-19. Intensity of the ASE at $\lambda = 5920$ Å vs pumping measured experimentally for $1.5 \ 10^{-3}$ M rhodamine 6G solution and 70 μ x 1 mm x 18.2 cm cell dimensions. A Jarell-Ash 0.25 m, 150 μ slit spectrometer was used.

FIG. 3-19

The figure shows a plot of ASE INTENSITY AT 5920 Å (arb.units) versus PUMPING INTENSITY (arb.units), labeled 1.5 10⁻³ mole/litre R6G.
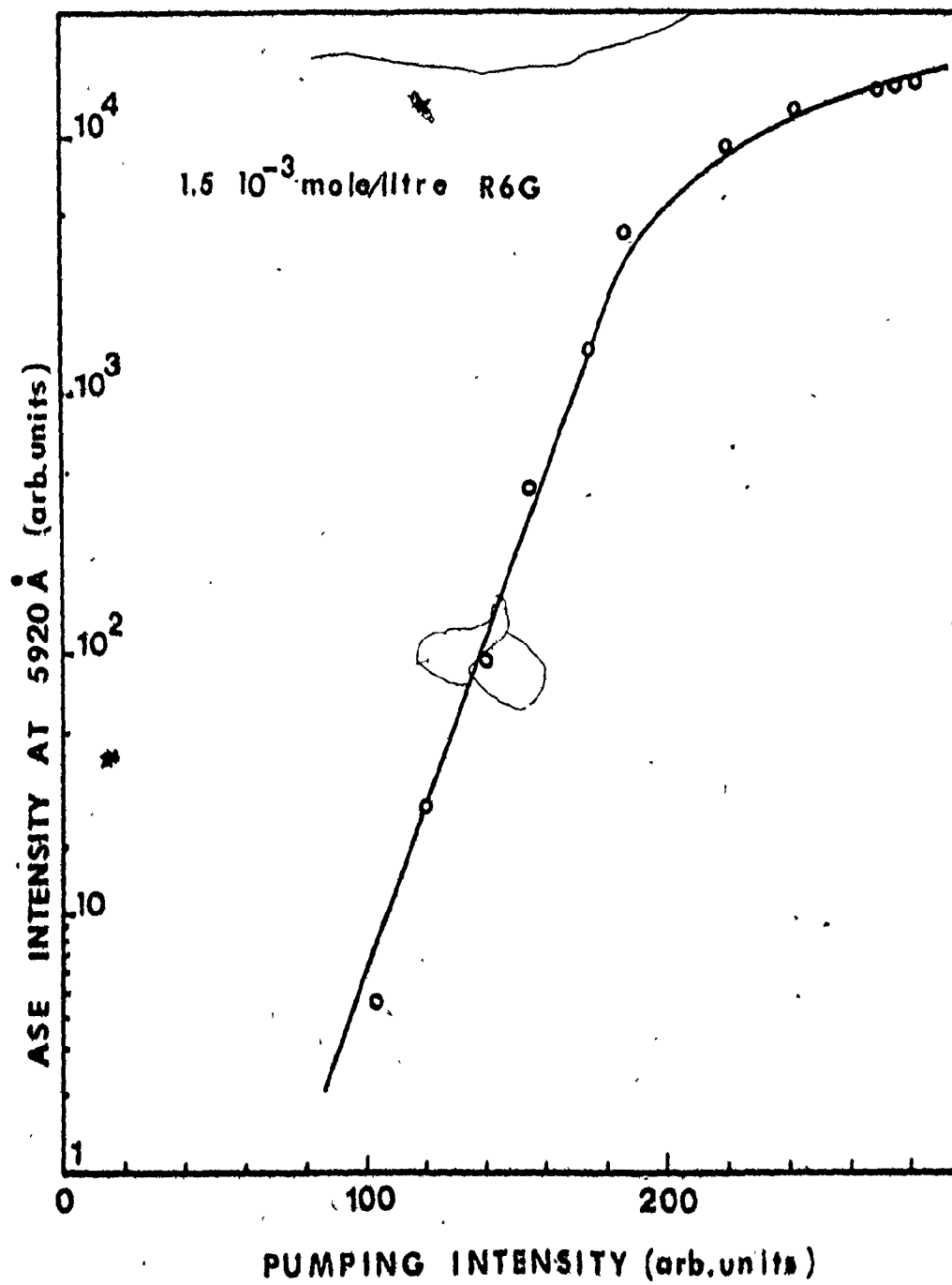
Figure 3-20. Calculated and measured spectral width (FWHM) of the ASE
vs pumping before and after scaling has been applied to
the calculated plot. The concentration of the rhodamine
6G/ethanol solution is 1.5×10^{-3} M   and the cell dimensions
are 70 μ x 1 mm x 18.2 cm.
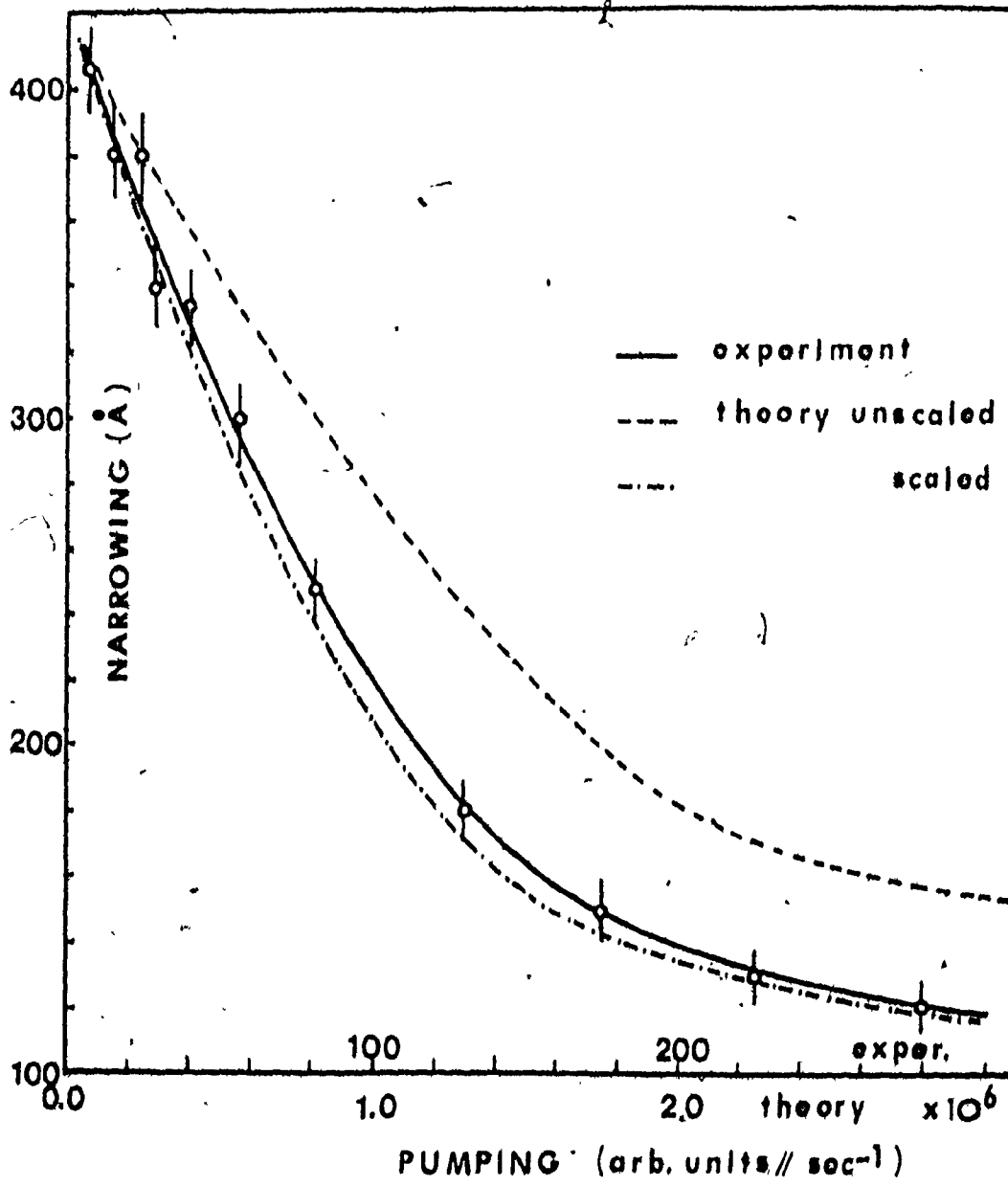
FIG. 3-20

where R, H, L are the cell thickness, height and length, respectively, and G_x is an adjustable parameter. For R ~ 1, g(x) can be taken as a constant equal to g(o), because, for the pumping available from a flashlamp, the spontaneous emission contribution is comparable to the ASE only in the first cm or so of the cell. From that point on, the ASE completely dominates the amplification process. In conclusion, we treated G_x as an adjustable parameter in the calculation of ASE vs pumping. For increased values of G_x the ASE intensity will saturate at smaller pumping, but the narrowing is hardly affected by small changes of the G_x parameter. Figure 3-19 shows the experimentally measured intensity vs pumping which is going to be used for the scaling process. Figure 3-21 shows the intensity of the calculated ASE vs the scaled pumping (obtained from the narrowing vs pumping plots) for three different G_x values. On the same graph we also plotted the experimentally measured intensity of the ASE at $\lambda_0 = 5920$ Å vs pumping from Figure 3-19. We note that the slope of both theoretical and experimental plots is the same after scaling and that the appropriate value of G_x is 0.2. Next, from the unsaturated gain calculated for any point of the pumping on the theoretical curve (intensity of ASE at 5920 Å vs pumping) we can find the gain which corresponds to any experimental pumping and narrowing. In other words, as long as we have established the correspondence between gain and narrowing, we only need to measure the narrowing to determine the unsaturated gain. For example, in this particular case for a theoretical pumping of $P_{th} = 3.0 \ 10^{+6}$, which is equivalent to $P_{exper} = 180$ after the scaling, we have calculated an unsaturated gain of $g_0 = 0.76 \ cm^{-1}$ and a spectral width (FWHM) of $\Delta\lambda = 155$ Å. Experimentally, we have measured a spectral width of $\Delta\lambda = 150 \pm 5$ Å.

Figure 3-21. Calculated and measured intensity of the ASE at $\lambda_0 =$ 5920 $\overset{o}{A}$ vs pumping after scaling has been applied to the calculated plots (a 1.0×10^6 pumping of the theory corresponds to a pumping of 60 in the experiment). Three different plots of the calculated intensity vs pumping are shown for values of the coupling parameter of 0.1, 0.2 and 0.5. The concentration is 1.5×10^{-3} M rhodamine 6G/ethanol. The cell dimensions are 70 μ x 1 mm x 18.2 cm.
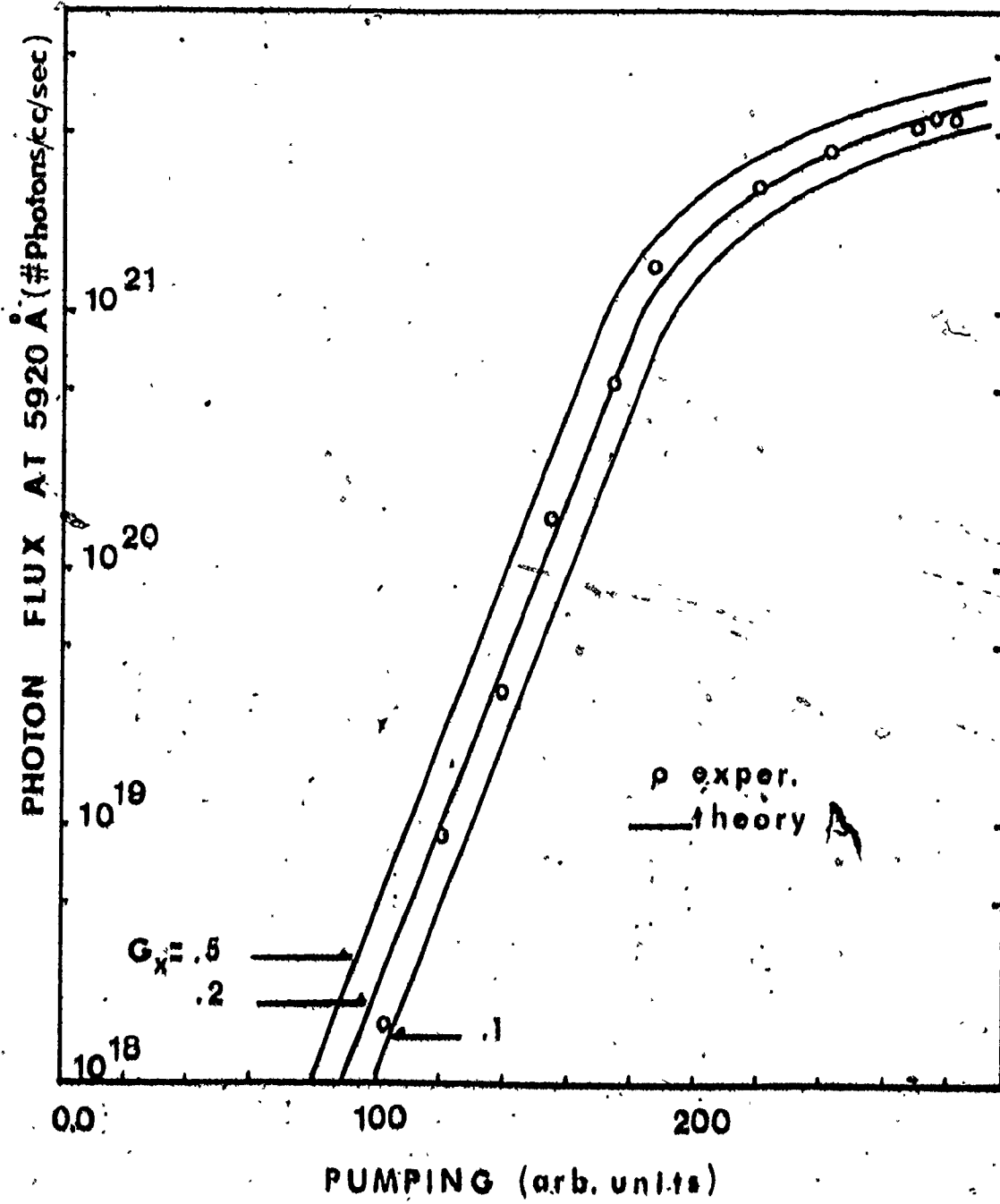
FIG. 3 – 21

for $P_{exper} = 180$. The ± 5 Å is the error of the experimentally measured spectral width caused by the spread of the intensity readings at fixed wavelength on successive shots. The replacement of the conventional spectrometer with an optical multichannel analyzer would eliminate this error, because the whole spectrum can be recorded simultaneously.

Furthermore, we did an additional experiment to see the agreement of our method of gain calculation with the approximate method of Shank et al, [39] According to this method, the ratio of the intensity for two different lengths of the dye cell, for the unsaturated region, is related to the gain by the relation,

$$I_1/I_2 = (\exp(gL_1) - 1)/(\exp(gL_2) - 1) \tag{3-19}$$

The underlying assumption is that the gain has not been saturated and, consequently, for a homogeneously broadened dye material

$$g = \frac{g_0}{1 + I/I_s} = g_0 \tag{3-20}$$

where g_0 is the unsaturated gain, g the actual gain and I_s is the saturation intensity given in our case by

$$I_s = (4\pi n^2 \Delta v h v)/t_{spont}\lambda^2) \tag{3-21}$$

where n is the index of refraction, $\Delta v = \frac{c}{\lambda^2}\Delta\lambda$, $\Delta\lambda = 420$ Å, t_{spont} is the spontaneous lifetime for the rhodamine 6G in ethanol and is equal to 4.5 nsec[82] and λ is the wavelength. According to this method of measuring the gain at a particular wavelength, we measure the intensity at $\lambda_0 = 5920$ Å as a function of pumping first for the entire cell pumped

and second with part of the cell blocked. The results are shown in
Figure 3-22, where two cell lengths of 18.2 and 10.0 cm have been chosen.
Using equation (3-19) and the two intensities of the ASE corresponding
to the pumping of P_{exp} = 180, we get a gain g = 0.66 cm^{-1} ± 0.03. This
approximate gain is within 15% to the more accurate value of 0.76 cm^{-1}
calculated by our method. The gain measured by this approximate method
is expected to be slightly smaller because even at a pumping of P_{exp} = 180
some saturation starts to take place as we can readily check by calcula-
ting the gain as a function of position from the theory.

In the preceding sections, we have clearly demonstrated that our
model for the ASE in rhodamine 6G cannot only display all the major fea-
tures of the ASE observed in the experiment, but it can also be used to
calculate the gain in an accurate way since it takes into account the
shift of the ASE spectrum with pumping, the saturation and the ESSA effect.
In order to extend the confidence in our model, we carried out extensive
measurements for various cell thickness and concentrations with similar
success. We shall not attempt to present all this data here, but we
will restrict ourselves to displaying the quality of the fit obtained
between theory and experiment for one other case. In particular, we dis-
play the matching between theory and experiment for a concentration of
2.5 x 10^{-3} M   rhodamine 6G in ethanol.

Figure 3-23 shows the ASE intensity for a wavelength of 5940 Å
vs the pump intensity, which we get from the experiment with a concentra-
tion of 2.5 x 10^{-3} M. R 6G/ethanol and a cell width of 50 microns.
Figure 3-24 shows the experimental spectral narrowing vs pumping and the

Figure 3-22. Measured intensity of the ASE at 5920 $\overset{\circ}{A}$ vs pumping for
two cell lengths $L_1 = 18.2$ cm and $L_2 = 10.0$ cm. The
cell thickness is 70 μ and the rhodamine 6G/ethanol con-
centration is 1.5×10^{-3} M .
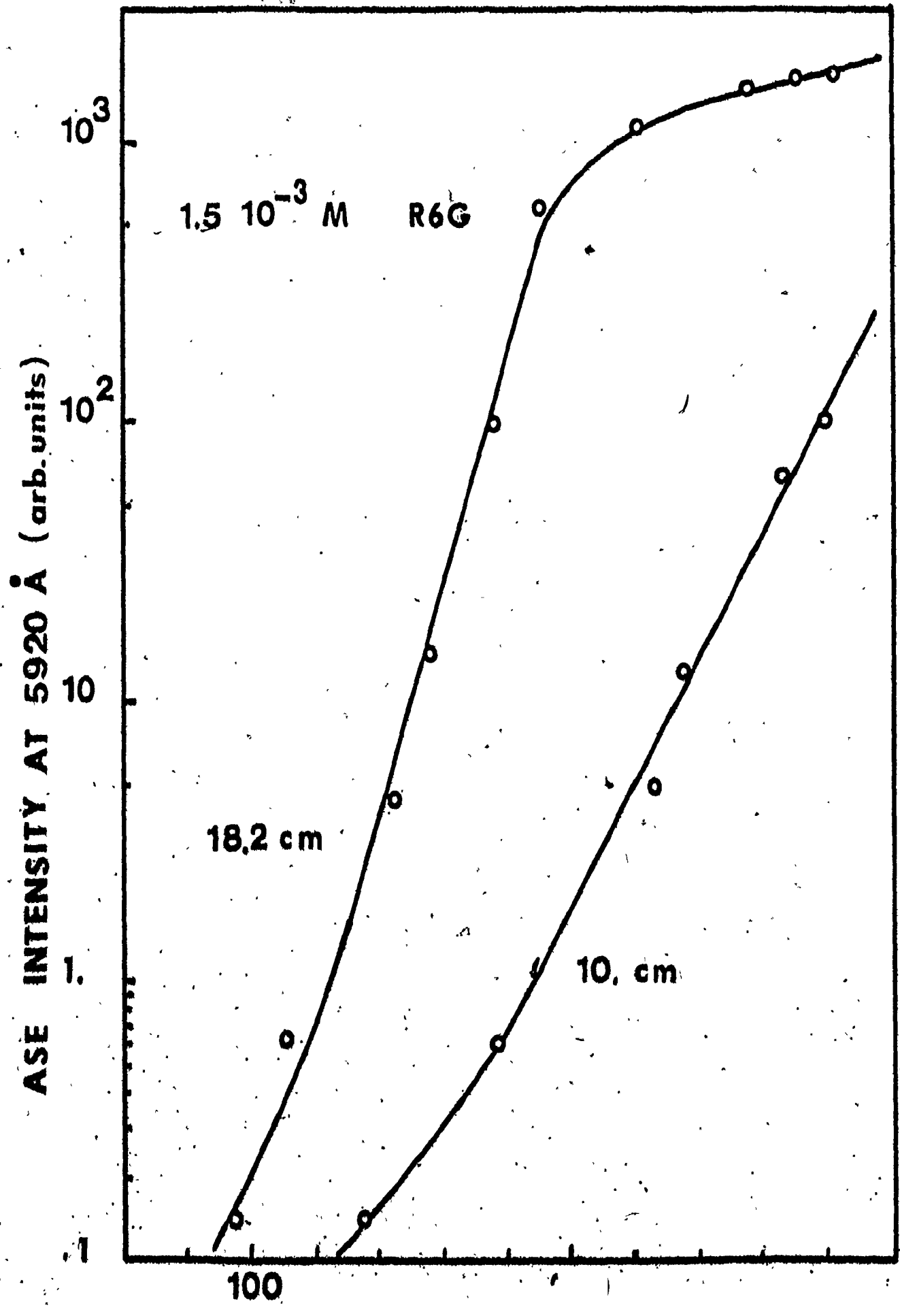
Figure 3-23.   Intensity of the ASE at 5940 Å vs pumping.   The concentration is 2.5 10^{-3} M   rhodamine 6G/ethanol and the cell dimensions are 50 μ x 1 mm x 18.2 cm.
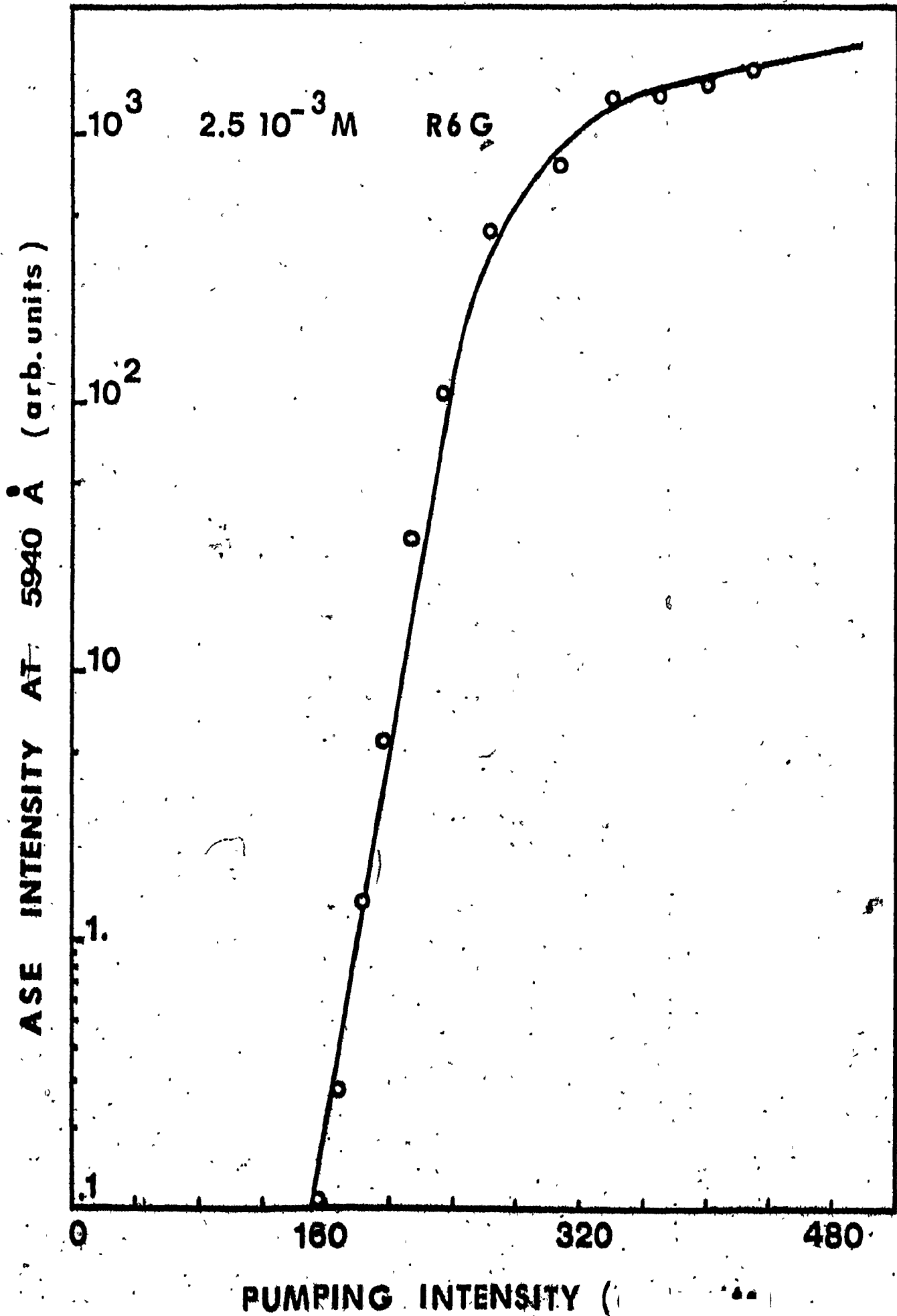
Figure 8-24. Narrowing (FWHM) vs pumping both calculated and experimental. The coupling factor G_x is equal to 0.1. The calculated narrowing has been scaled (1.0×10^6 theoretical pumping corresponds to 125 experimental pumping). The concentration is $2.5 \; 10^{-3}$ M rhodamine 6G/ethanol and the cell dimensions are 50 μ x 1 mm x 18.2 cm.

2.5 10⁻³ M   R6G

FIG. 3-24

PUMPING INTENSITY

1.   2.   3. ×10⁶ (1/sec)

exper.   theory

200   300   (arb.units)

experiment

theory
—— unscaled
--- scaled

$G_x = .1$
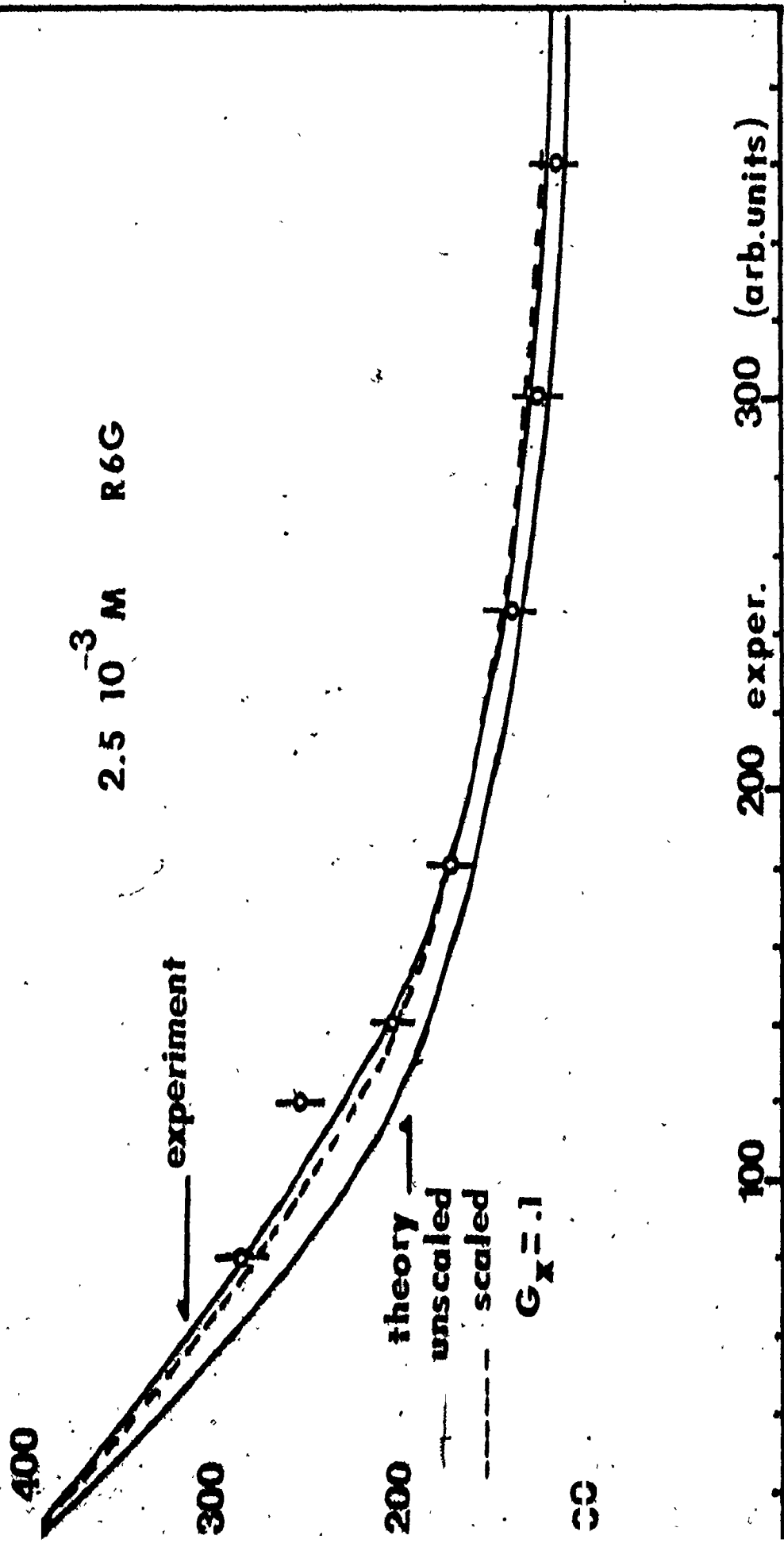
narrowing we got from the theory after the calibration of the pump has
been performed. The matching of the two curves is carried out first in
the low pumping region, which is relatively insensitive to the value of
G_x, the coupling coefficient for the spontaneous emission. Then, the
G_x value is adjusted to "fine-tune" both the matching in the saturated
region and the ASE intensity vs pumping. This plot of the ASE intensity
at the particular wavelength vs pump is shown in Figure 3-25. On this
figure, we also show the matched experimental along with two more theore-
tical curves for $G_x = 0.1$ and $G_x = 0.01$ for demonstration purposes. It
can be seen that the appropriate G_x to be used is $G_x = 0.1$. It should
be noted here that g(x) of equation (3-8), which determines the portion
of the spontaneous emission emitted within cell length dx which is fed
in for amplification in the rest of the cell, and reaches the detector,
is given by the product of G_x and dn, where dn is the (half) solid angle
subtended at one end of the cell by the cross-section at the other end.
For a length of the cell of 18.2 cm a height of 1 mm and a width of 60
micron, dn has a value of 0.77×10^{-6}. The value of g(x) needed for
matching is found to be about 0.23×10^{-7}. This lower value is due
partly to the fact that we use apertures to collect only the central
portion of the light emitted from the 1 mm height cell (in this case
we used a 6 cm aperture 1 meter away from the cell, which reduces g(x)
to 0.39×10^{-7}) and partly to the fact that the coupling is not perfect
and there are losses associated with the cell itself for very narrow
cells, such as scattering in the wall imperfections and non-parallelism
of the two cell glass plates.

Figure 3-28. Measured ASE intensity at 5940 Å vs pumping and calculated
intensities vs scaled pumping (1.0 10^6 theoretical pumping
corresponds to 125 experimental pumping) for two different
values of the coupling parameter, G_x = 0.1, 0.01. The
concentration is 2.5 10^{-3} M and the cell dimensions are
60 μ x 1 mm x 18.2 cm.
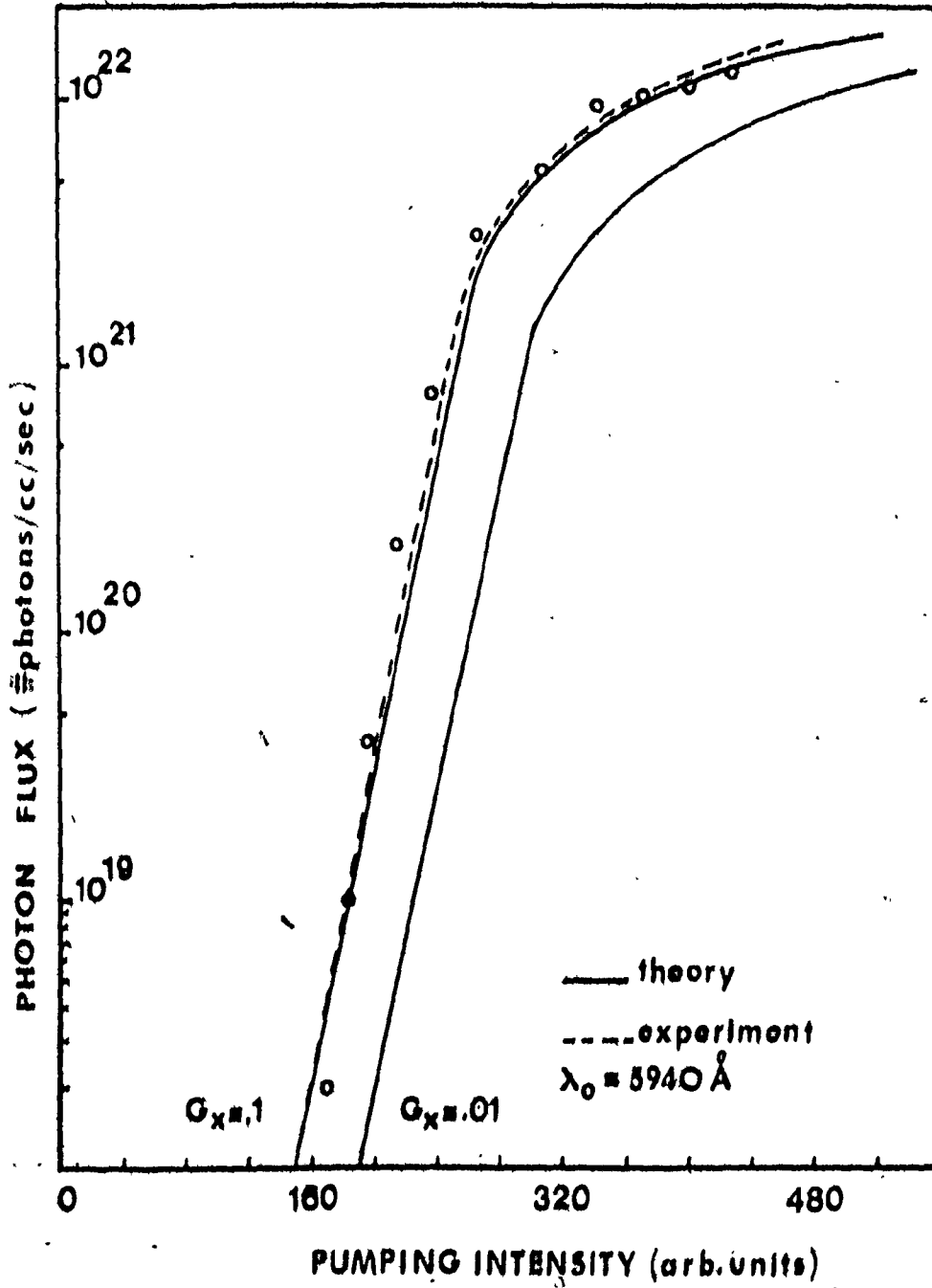
FIG. 3-25

In the preceding section, we demonstrated the matching of theory and experiment for the case of 2.5×10^{-3} M rhodamine 6G. It can be seen that the excellent quality of the matching is independent of the concentration used. It should be noted here though that extreme care is required to take accurate measurement at very high concentrations (and consequently, small cell thickness) because of possible cell wall imperfections or slight bending of the cell. There is one more test we can still subject the matching to, namely concentration scaling. It is, of course, expected that for concentrations below the point where dimers are formed[2] (because dimers will alter the results due to their particular absorption spectra) the gain will scale proportionally to the concentration. In particular, for the same pumping of $P_{th} = 1.0 \times 10^6$, we have calculated for the 1.5×10^{-3} M solution a gain of $g_0^1 = 0.25$ cm^{-1} and for the 2.5×10^{-3} M solution, a gain of $g_0^2 = 0.35$ cm^{-1}. The gain ratio is 1.56 and the concentration ratio is 1.66 and these ratios are within 6% to each other which is reasonably good, taking into account the experimental errors involved and the accuracy of the cross-section used for the theoretical calculations.

So far in this chapter we have presented a model for the ASE which, besides providing an easy way to understand the physical processes involved, can be fitted accurately to experimental observations and used to measure the unsaturated gain. Such gain measurements only require the intensity at a fixed wavelength and the spectral distribution of the intensity be measured as a function of pumping. Our model requires very accurate knowledge of the values of the different cross-sections involved

and, indeed, it can be used to determine values for unknown cross-sections as it was done in our case for the ESSA cross-section. This model is appealing for the accuracy of the predictions. However, more general situations with less well-known parameters require the development of a simpler model which is not system-dependent. Along these lines, we have developed such a simple model for the propagation of the ASE under the assumptions that the gain line is homogeneously broadened and the ASE intensity profile narrows considerably before saturation sets in. In the next section, we present our approximate theory and compare it with our exact model and another similar approximate theory published recently.[40]

3.5.1. An Approximate Analytical Theory of the ASE

In what follows, we first treat the case of the ASE propagating only in one way through the amplifier in order to have some physical insight into the process of ASE and also provide an alternate way of calculating narrowing expressions similar to expressions found independently.[98] Secondly, we extend this treatment of the ASE to cover the two-way propagation. Thirdly, we evaluate the approximate theory by comparing it to the rate equation model developed previously and suggest ways to improve its predictions. This approximate theory is based on the following assumptions.

(i)   The gain medium is transversely homogeneous with respect to pumping (no gain inhomogeneity across the cell).

(ii)   There is a homogeneous Lorentzian gain line.

(iii)   The intensity profile gets narrower than the gain line well before saturation sets in and the gain is reduced.

(1) One Way Propagation Case

The frequency distribution of a collision-broadened emission line, such as the one approximately corresponding to a dye molecule in a solution, has a Lorentzian shape with a spectral width (FWHM) $\Delta\nu$.[97] The normalized line shape function has the form

$$g(\nu) = \frac{1}{\Pi\Delta\nu_h} \frac{1}{1 + \delta^2} \qquad (3\text{-}22)$$

where

$$\delta = \frac{\nu - \nu_0}{\Delta\nu_h} \qquad \text{and} \qquad \Delta\nu_h = \frac{\Delta\nu}{2}.$$

It has also been shown[98] that for homogeneous media, the gain $\gamma(\nu)$ centred at ν_0 is given by

$$\gamma(\nu) = \frac{1}{1 + I(\nu)/I_s(\nu)} \frac{\Delta N^\circ \lambda^2}{8\Pi\, t_{spont}} g(\nu) \qquad (3\text{-}23)$$

where I_s is the saturation intensity

$$I_s(\nu) = \frac{8\Pi h\nu n^2}{\phi\lambda^2 g(\nu - \nu_0)} \qquad (3\text{-}24)$$

with n the refraction index, ϕ the quantum efficiency of the dye system, t_{spont} the spontaneous lifetime of the excited singlet state, and ΔN° the population inversion density at zero intensity. Setting, for the unsaturated gain coefficient,

$$g_0 \equiv \frac{\Delta N^\circ \lambda^2}{8\Pi t_{spont}} \qquad (3\text{-}25)$$

we have:

$$g(\nu) \equiv \gamma(\nu) = \frac{g_0}{[1 + I(\nu)/I_s(\nu)][1 + \delta^2]} \tag{3-26}$$

We can generalize this in the case when distributed frequency radiation is present to get:

$$g(\nu) = \frac{g_0}{(1 + \delta^2)(1 + \frac{1}{I_s(o)} \int \frac{I(\nu')d\nu'}{1 + \delta^2})} \tag{3-27}$$

For the propagation of the radiation intensity, we have the following equation:

$$\frac{dI(\nu,z)}{dz} = g(\nu)I(\nu,z) + \eta g(\nu) \tag{3-28}$$

The first term accounts for the stimulated emission and the second for the spontaneous emission. Let us set

$$q(z) = \frac{1}{I_s(o)} \int \frac{I(\nu',z)}{1 + \delta^2} d\nu' \tag{3-29}$$

and $I + \eta = K$ and integrate equation (3-28) assuming that $q(z)$ is explicitly known as a function of z. Then, we get:

$$\log_e \frac{K_f}{K_i} = \frac{g_0 \, l(z)}{1 + \delta^2} \tag{3-30}$$

when

$$l(z) = \int_0^z \frac{dz}{1 + q(z)} \tag{3-31}$$

For the ASE I_f, the intensity at the end of the cell, is much larger than η, the part of the spontaneous emission which couples in the cell to get amplified. In other words,

$$I_f/n \gg 1 \tag{3-32}$$

and equation (3-30) can be written

$$\log_e \frac{I_f(\nu)}{n} = \frac{g_0 \, l(z)}{1 + \delta^2} \tag{3-33}$$

From this equation, we can calculate the FWHM of the output intensity distribution. At $\nu = \nu_0$, we have $\delta = 0$ and

$$I_f(0) = n\exp(g_0 l(z)) \tag{3-34}$$

When the intensity drops to one-half the maximum, we can write

$$I_f(\nu) = \frac{I_f(o)}{2} = n/2 \, \exp(g_0 l(z)) = \exp(g_0 l(z)/(1 + \delta^2)) \tag{3-35}$$

or

$$g_0 l(z) - \log_e 2 = \frac{g_0 \, l(z)}{1 + \delta^2} \tag{3-36}$$

For the case where $g_0 \, l(z) \gg \log_e 2$, we have

$$\frac{\Delta \nu_L(z)}{\Delta \nu_h} = [\log_e 2/(g_0 \, l(z))]^{1/2} \tag{3-37}$$

This is a similar power law dependence of narrowing on gain as that calculared also by other authors.[98] To proceed further, we must be able to calculate $l(z)$. Now, the major approximation comes into effect. We will assume that the intensity spectrum is narrow relative to $\Delta \nu$, one line shape spectrum width, before strong gain saturation effects take place, while we still have enough gain and the stimulated emission is predominant. The $q(z)$ becomes (because of $\delta \ll 1$)

$$q(z) = \frac{1}{I_s(o)} \int \frac{I(\nu',z)d\nu'}{1 + \delta^2} = \frac{I_t}{I_s(o)} \tag{3-38}$$

where $I_t(z) = \int_\nu I(\nu',z)d\nu'$ is a function of z. Then, the equation (3-28) can be integrated over frequency to give, after some algebraic manipulation:

$$\log_e\left(\frac{I_t(z) + \epsilon}{\epsilon}\right) + I_t(z)/I_s' = g_0'z \tag{3-39}$$

where $\epsilon = \pi n\Delta\nu$, $g_0' = g_0/(1 - \epsilon/I_s(o))$, and $I_s' = I_s(o)(1 - \epsilon/I_s(o))$. The term $q(z)$ in the expression (3-31) is important only near or in the saturation region where the intensity is comparable to the saturation intensity, as can be seen from equation (3-38). In that case, below saturation $q(z) = 0$ and we have from (3-37),

$$\frac{\Delta\nu_L}{\Delta\nu_h} = \left[\frac{\log_e 2}{g_0 L}\right]^{1/2} \qquad \text{Unsaturated region} \tag{3-40}$$

Well into the saturation region, the second term in equation (3-39) is predominant and $I_t(z) = g_0'zI_s' = g_0 zI_s$. Consequently, we calculate for $1(L)$:

$$1(L) \approx \int_0^L \frac{dz}{1 + g_0 z} = \frac{1}{g_0} \log(1 + g_0 L) \tag{3-41}$$

Then, the narrowing is given by

$$\frac{\Delta\nu_L}{\Delta\nu_h} = \left[\frac{\log_e 2}{\log_e(1 + g_0 L)}\right]^{1/2} \qquad \text{saturated region} \tag{3-42}$$

Equation (3-42) shows that in the saturation region, narrowing continues but in a much slower pace.

Next, we extend the above treatment to the two-way propagation case.

(2) Two-Way Propagation Case

In a similar way to the previously treated case, we will have

$$g(\nu) = \frac{g_0}{(1 + \delta^2)(1 + \frac{1}{I_s(0)} \int \frac{I^+(\nu',z) + I^-(\nu',z)}{1 + \delta^2} d\nu')} \tag{3-43}$$

$$\frac{dI^+(\nu,z)}{dz} = g(\nu)[I^+(\nu,z) + n] \tag{3-44}$$

$$\frac{dI^-(\nu,z)}{dz} = -g(\nu)[I^-(\nu,z) + n]$$

Now, we again define

$$q^{\mp}(z) = \frac{1}{I_s(0)} \int \frac{I^{\mp}(\nu',z) d\nu'}{1 + \delta^2} \tag{3-45}$$

Then

$$\frac{dI^+(\nu,z)}{dz} = \frac{g_0(I^+(\nu,z) + n)}{(1 + \delta^2)(1 + q^+(z) + q^-(z))} \tag{3-46}$$

Following the same way as for the one way propagation case we can show that

$$\frac{\Delta\nu(z)}{\Delta\nu_n} = \left[\frac{\log_e 2}{g_0 1(z)}\right]^{1/2} \tag{3-47}$$

where $1(z)$ is now given by

$$1(z) = \int_0^z \frac{dz}{1 + q^+(z) + q^-(z)} \tag{3-48}$$

Under the assumption of $\delta \ll 1$ before saturation which is a reasonable one for high gain media we will have

$$q^{\mp}(z) = \frac{I_t^{\mp}(z)}{I_s(o)} \equiv i^{\mp}(z) \tag{3-49}$$

where $I_s(o)$ is the saturation intensity at line centre. The propagation equations (3-44) can be written

$$\frac{dJ_t^+}{dz} = \frac{g_0'' J_t^+}{I + \frac{J_t^+ + J_t^-}{I_s'}}$$

$$\tag{3-50}$$

$$\frac{dJ_t^-}{dz} = \frac{-g_0' J_t^-}{I + \frac{J_t^+ + J_t^-}{I_s'}}$$

where

$$J_t^{\mp} = I_t^{\mp} + \pi \Delta \nu \eta^{\mp}$$

with

$$g_0' = \frac{g_0}{1 - \frac{2\pi\Delta\nu\eta}{I_{s_0}}} \quad , \quad I_s'' = I_s(1 - \frac{2\pi\Delta\eta}{I_s}) \tag{3-51}$$

and I_s is taken to be at line centre. Because of

$$\frac{d}{dz}(J_t^+ J_t^-) = 0 \quad \text{or} \quad J_t^+ J_t^- = k \tag{3-52}$$

which can be proven directly by using equations (3-50), we can integrate the equations (3-50) in a formal way to get:

$$g_0'z = \log_e\left(\frac{J^+(t)}{J_0^+}\right) + \frac{J^+(z) - J_0^+}{I_s'} - \frac{k}{I_s'}\left(\frac{1}{J^+(z)} - \frac{1}{J_0^+}\right)$$

$$-g_0'z = \log_e\left(\frac{J^-(z)}{J_0^-}\right) + \frac{J^-(z) - J_0^-}{I_s'} - \frac{k}{I_s'}\left(\frac{1}{J^-(z)} - \frac{1}{J_0^-}\right)$$

(3-53)

Adding equations (3-53) together, we have

$$\log_e \frac{J^+(z)}{J_0^+} + \log \frac{J^-(z)}{J_0^-} + \frac{J^+(z) - J_0^+ + J^-(z) - J_0^-}{I_s'}$$

$$= \frac{k}{I_s'}\left(\frac{1}{J^+(z)} - \frac{1}{J_0^+} + \frac{1}{J^-(z)} - \frac{1}{J_0^-}\right)$$

(3-54)

Because of $J^+(z)J^-(z) = J_0^+J_0^- = k$, we have

$$\frac{J^+(z) - J_0^+ + J^-(z) - J_0^-}{I_s'} = \frac{k}{I_s'}\left(\frac{1}{J^+(z)} - \frac{1}{J_0^+} + \frac{1}{J^-(z)} - \frac{1}{J_0^-}\right)$$

(3-55)

and equation (3-54) reduced to

$$\log_e \frac{J^+(z)}{J_0^+} + \log_e \frac{J^-(z)}{J_0^-} = 0$$

(3-56)

For the case where there is no reflector at either end of the amplifier we will have

$$J_0^+ = \pi\Delta\nu\eta \equiv \epsilon \qquad \text{and} \qquad J_L^- = \pi\Delta\nu\eta \equiv \epsilon$$

(3-57)

Then from the first of the equations (3-53) we get, using (3-57) and noting that

$$J^+(z)J^-(z) = J_0^+J_0^- = J_L^+J_L^- \quad ,$$

$$g_0'(z) = \log_e\left(\frac{J^+(z)}{\epsilon}\right) + \frac{\epsilon}{I_s'}\frac{J_L^+}{J'(z)}\left(\frac{J^+(z)}{\epsilon} - 1\right) + \frac{\epsilon}{I_s'}\left(\frac{J^+(z)}{\epsilon} - 1\right) \cdots \qquad (3\text{-}58)$$

We can write (3-58) in terms of $i^+(z)$, since

$$J^+(z) = i^+(z) + \pi\Delta\nu\eta$$

$$g_0' = \frac{g_0}{1 - 2\frac{\pi\Delta\nu\eta}{I_s}} = \frac{g_0}{1 - 2y} \qquad (3\text{-}59)$$

$$I_s' = I_s(1 - 2y)$$

to get finally

$$\frac{g_0 z}{1 - 2y} = \log_e\left(\frac{i^+(z) + y}{y}\right) + \frac{i^+(t)}{1-2y}\left[1 + \frac{y + i^+(L)}{y + i^+(z)}\right] \qquad (3\text{-}60)$$

This equation relates the total intensity at the end of the cell with the intensity at each point z within the cell and it can be used to calculate $i^+(z)$ if $i^+(L)$ is given along with the gain g_0 and the value of the parameter y.

Because of

$$J^+(z)J^-(z) = J^+(L)J^-(L) = J_0^+ J_0^-$$

$$J_0^+ = J_L^- = \epsilon \qquad (3\text{-}61)$$

$$J^-(z) = i^-(z) + \Delta\nu\eta$$

we have

$$\frac{J^-(z)}{I_s} = \frac{J^+(L)J^-(L)}{J^+(z)\,I_s} = \frac{\epsilon}{I_s}\frac{i^+(L) + y}{i^+(z) + y} = y\,\frac{i^+(L) + y}{i^+(L) + y}$$

and

$$\frac{J^-(z)}{I_s} = \frac{I^-(z)}{I_s} + \frac{\pi\Delta\nu\eta}{I_s} = i^-(z) + y.$$

Then equating the two expressions we get

$$i^-(z) = y(i^+(L) - i^+(z))/(i^+(z) + y) \qquad (3\text{-}62)$$

and the expression for $l(z)$ from equation (3-48) will be given by (where we substituted for $i^-(z)$ from equation (3-62))

$$l(z) = \int_0^z \frac{dz}{1 + i^+(z) + \frac{y(i^+(L) - i^+(z))}{y + i^+(z)}} \qquad (3\text{-}63)$$

Equation (3-47), (3-60) and (3-63) are the basic equations which can be solved numerically to calculate the different quantities involved. In other words, for a given set of values of the parameter y and for each value of the gain g_0, we can calculate and plot the corresponding values of $i^+(L)$ using equation (3-60) for $z = L$. Then, for a given value of $i^+(L)$, y and g_0 we can also calculate from equation (3-60) a set of $i^+(z)$ values, to be used in equation (3-63) to calculate $l(z)$ and, consequently, $\Delta\lambda$, the narrowing. A computer program which solves these equations is given in Appendix A.

(iii) Evaluation of the Approximate Theory

In order to evaluate this approximate theory, we will compare it with the results we have described earlier. Figure 3-26 shows the narrowing vs gain for $y = 10^{-6}$, a reasonable value of this parameter for

Figure 3-26. Narrowing vs unsaturated gain from the approximate theory for a particular parameter value ($y = 10^{-6}$) and experimentally measured narrowing vs gain. This gain is calculated from the experimental pumping using the rate equation theory. The concentration is 1.5×10^{-3} M rhodamine 6G/ethanol and the cell dimensions are 70 μ x 1 mm x 18.2 cm.
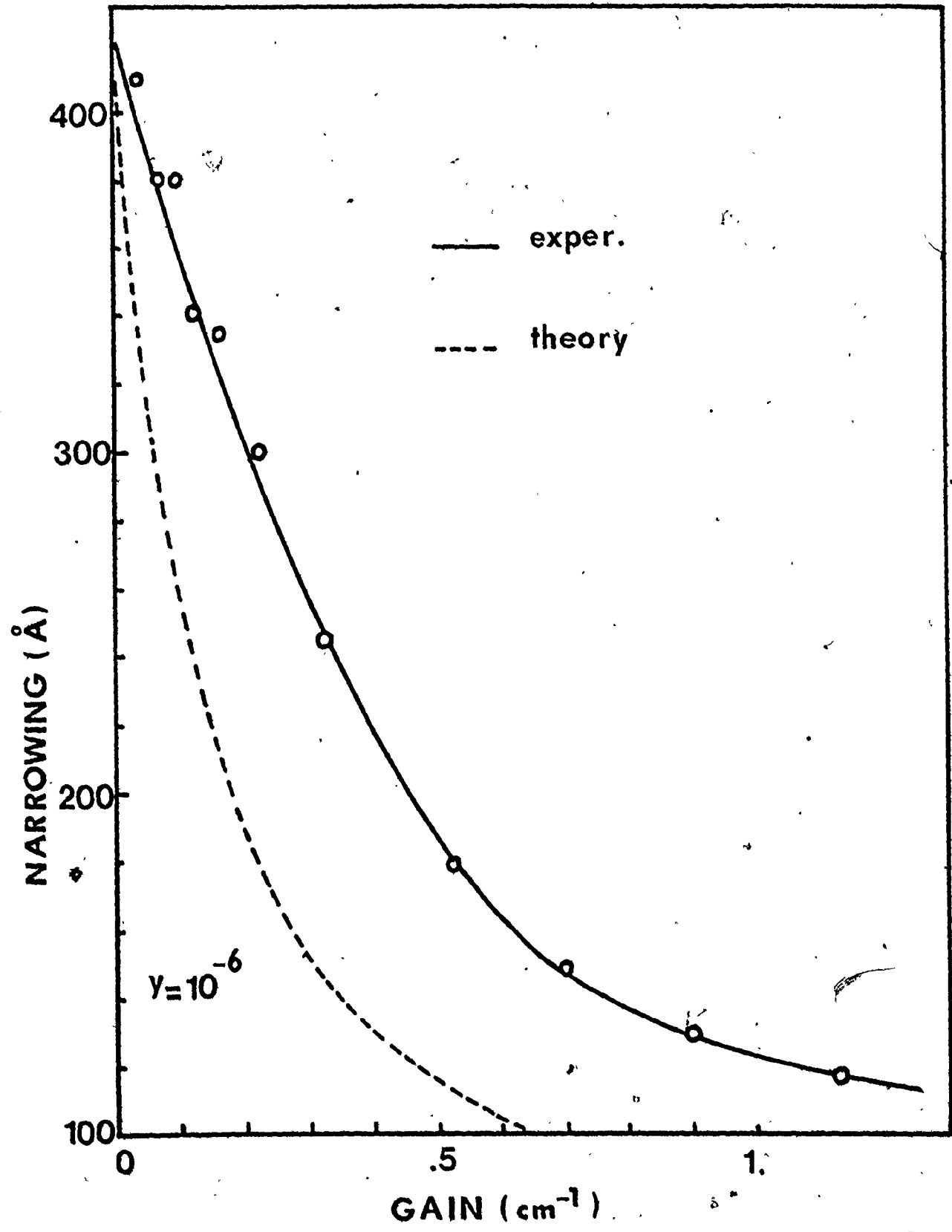
FIG. 3-26

our particular dye cell configuration. On the same graph we show the experimentally measured narrowing $\Delta\lambda$ vs the gain calculated using the rate equation approach theory. The homogeneous linewidth at half maximum in the approximate theory is taken to be 420 Å. We see that the approximate theory gives values for the narrowing well off the values predicted by the more accurate rate-equation theory. We can improve the agreement by treating $\Delta\lambda_{homo}$ as a free parameter. The reasoning behind this approach is that, as we have seen before, most of the shifting of the spectra of the ASE occurs at low pumping and the un-saturated section of the narrowing is nearly independent of the coupling constant of the ASE into the cell; consequently, we can try to match the approximate theory with the experiment at the region below saturation, which is nearly independent of the coupling constant and also is less affected by the intensity spectra shift. Additionally, we can calculate an approximate y value from the dimensions of the particular cell employed and also have a more accurate y value by comparing experimental and theoretical plots of total intensity vs gain. In short, comparison of the intensity curves (theoretical and experimental) below and above saturation provide a reasonably accurate y value to be used and the value of $\Delta\lambda_{homo}$ is treated as a parameter to match the region below saturation of the narrowing vs pumping plots. In this sense, we exploit the saturation region, which is sensitive to the y values to obtain an accurate y value and do the matching in a region which is neither sensitive to the y value nor to the spectra shifting, which cannot be accounted for in the approximate theory. Following this technique, we matched the approximate theory with the experiment in the case of.

1.5×10^{-3} M   rhodamine 6G, whose gain we have already determined from the rate equation theory. Figure 3-27 shows the total experimentally obtained ASE intensity, integrated over wavelength, vs the gain which has been determined by comparison with the rate equation theory. Because we employed a dye cell with a cross-section of 1 mm x 70 μ and a length of 18.2 cm, we have an approximate value for the solid angle subtended by the amplifying medium of 2.1×10^{-6} which, though, has to be reduced to ∿ 10^{-7} if we take into account the fact that we used an aperture of 5 cm 1 meter away from the cell to accept a small fraction of the ASE close to the axis of the cell. We have seen before that the y parameter normalized to the saturation intensity is actually equal to this solid angle. Consequently, we can plot the theoretical intensity vs gain for several y parameter values around $y = 10^{-7}$ and compare the experimental and theoretical plots to determine a more accurate y value, which is then going to be used in the narrowing plot.

Figure 3-28 shows the results of matching the spectral narrowing curves with parameters $\Delta\lambda_{homo} = 600$ Å and $y = 10^{-6}$ determined from the intensity plots in Figure 3-29. We see that an agreement of 20% can be easily achieved over most of the gain region except for very low values. We could probably improve the accuracy further if it was possible experimentally to have more pumping because in that case we could go deeper into the saturation region and then have more evident the dependence of the narrowing on the y parameter. The small discrepancy, which appears in the beginning of the saturation region in Figure 3-29 is due to the shift of the intensity spectra with pumping. This shift will delay the saturation until we reach higher pumping which finally

Figure 3-27. Total intensity, integrated over wavelength, vs gain. This gain is calculated from the experimental pumping using the rate equations theory.
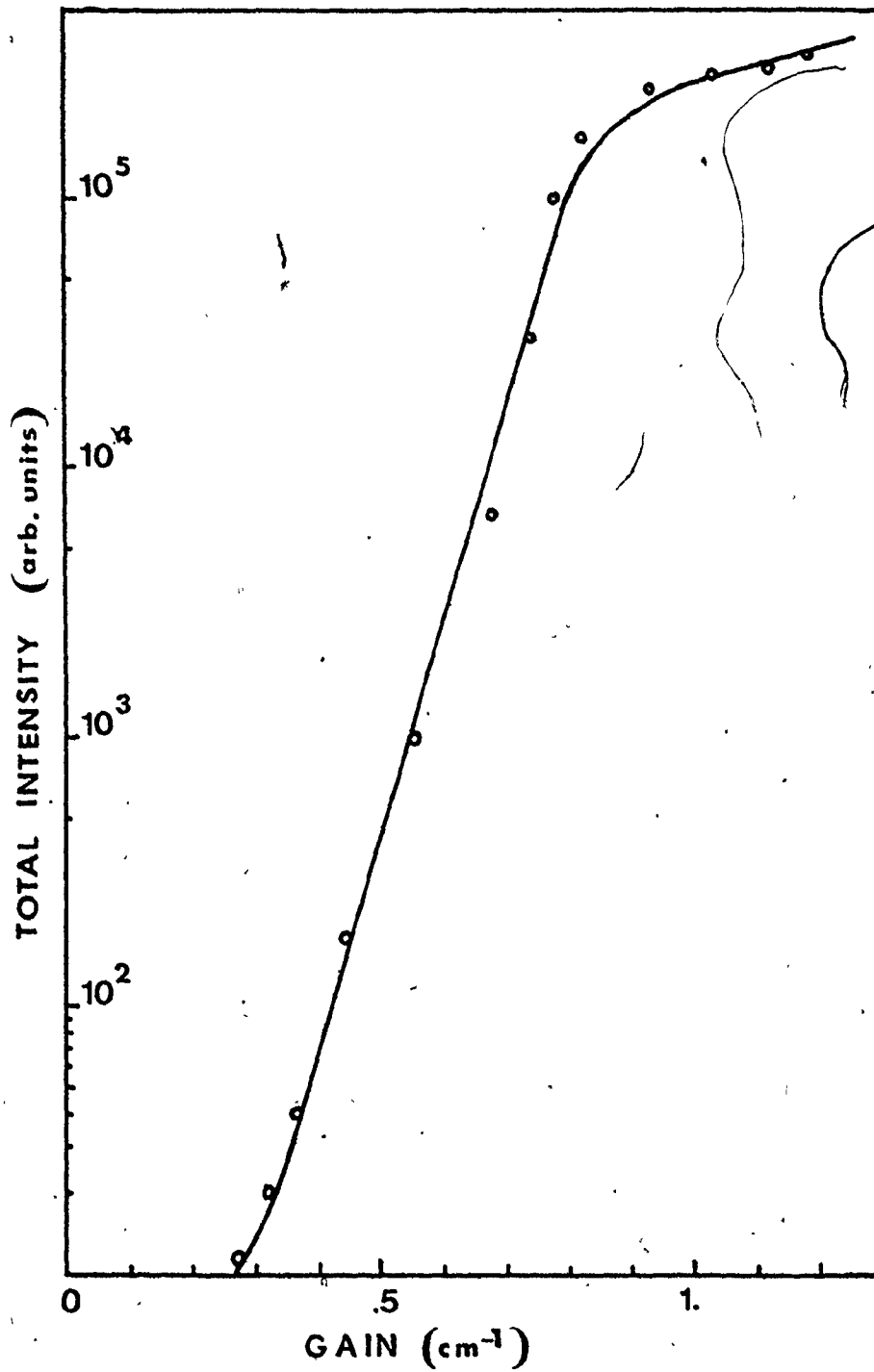
FIG. 3-27

Figure 3-28. Narrowing vs gain. The gain of the experimental plot is calculated from the experimental pumping using the rate equations theory. The concentration is 1.5×10^{-3} M rhodamine 6G/ethanol. The approximate theory plot corresponds to a FWHM of the homogeneous line function of 600 Å.
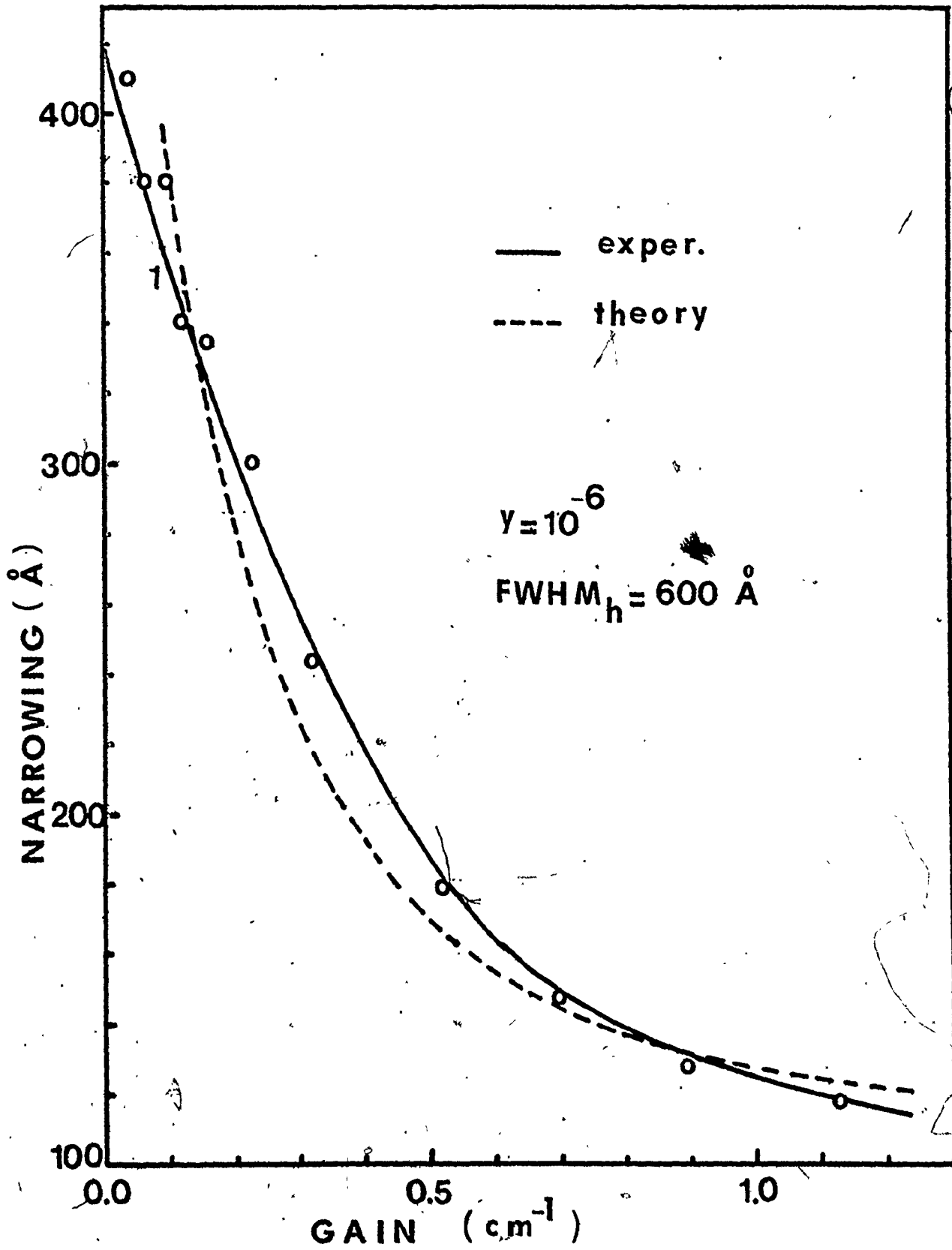
FIG. 3-28

Figure 3-29. Normalized total ASE intensity vs gain for several values
of the ẏ parameter of the approximate theory and experi-
mentally measured intensity vs gain. This gain is calc-
ulated from the experimental pumping using the rate
equation theory. The concentration is 1.5×10^{-3} M .
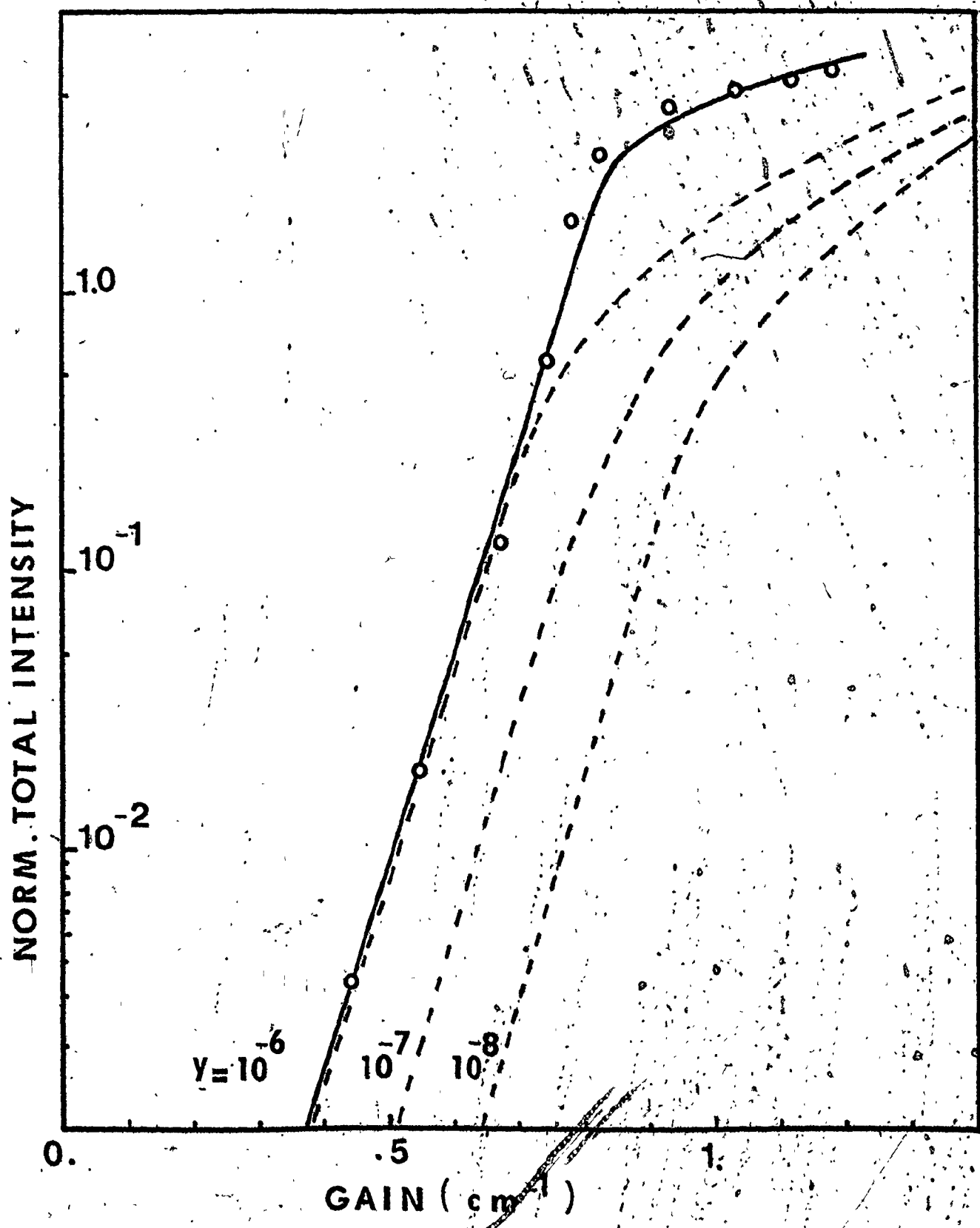
FIG. 3-29

will create such high intensities to saturate the gain, since the shifting of the spectra slows down.

Up to now, we have compared our approximate theory with the rate equation theory and improved its prediction guided by the fact that the gain was already known accurately from the solution of the rate equations. In practice though, it is neither easy nor economical to solve the rate equations for each case and is really useful to be able to find the gain from the direct application of the approximate theory. This, of course, is going to be a two parameter fit approach, since both y and $\Delta\lambda_{homo}$ will be adjusted to have the best fit between experimental and theoretical curves of total intensity vs pump and narrowing vs pump. The necessary steps can be summarized as follows:

(i) plot the experimental total intensity of the ASE vs pumping and calculate an approximate y value for the geometry of the cell. (y will be of the same order of magnitude as the solid angle subtended by the gain column taking account of any possible apertures used in the measurement of the intensity.)

(ii) normalize the intensity to an approximate value of saturation intensity, which can be found from the intersection of the extension of the two linear section of the intensity vs pumping curve (above and below saturation). The point on the intensity curve corresponding to the same pumping as the intersection is approximately equal to the saturation point.

(iii) on the same graph plot the normalized intensity vs pumping from the experiment and a set of intensity vs gain curves for several values

of the y parameter close to the calculated value of y from (i). Scale the x-axis to get the unsaturated section of both sets of plots parallel. This will determine an approximate y value.

(iv)   plot the experimentally obtained narrowing $\Delta\lambda$ vs pumping and determine the limit of narrowing at saturation.

(v)   treat the homogeneous gain linewidth as a free parameter and for the y value obtained in (iii) find the value of $\Delta\lambda_{homo}$ which together with the used y value will determine a best fit plot of $\Delta\lambda$ vs gain.

(vi)   read the gain, for a given narrowing, from the gain axis (x-axis) of the theoretical curve.

In order to clarify the process described above, we will present an example. The experimental data belong to the previously treated case of rhodamine 6G in ethanol of concentration 2.5×10^{-3} M.   Figure 3-30 shows the normalized (see (ii) above) and scaled experimental total intensity of the ASE vs pumping along with a set of theoretical plots of total intensity vs gain for several values of the parameter y. We see that $y = 10^{-7}$ gives a very close fit between experimentally obtained and theoretically calculated intensity curves. From Figure 3-30, we also see that to find the gain which corresponds to the experimental pumping we have to multiply it by the scaling factor 0.004 cm^{-1}. Figure 3-31 shows the experimentally obtained spectral narrowing vs pumping properly scaled and the theoretically obtained best fit for $y = 10^{-7}$ and $\Delta\lambda_{homo} = 650$ Å. On the same plot we also show the unscaled experimental narrowing plot vs gain calculated using the rate equation approach. It can be seen that, with the exception of very low pumping, the gains obtained for the

Figure 3-30. Normalized total ASE intensity vs gain for several y values from the approximate theory and experimentally measured intensity vs pumping for a concentration of 2.5×10^{-3} M and cell dimensions 50 μ x 1 mm x 18.2 cm.
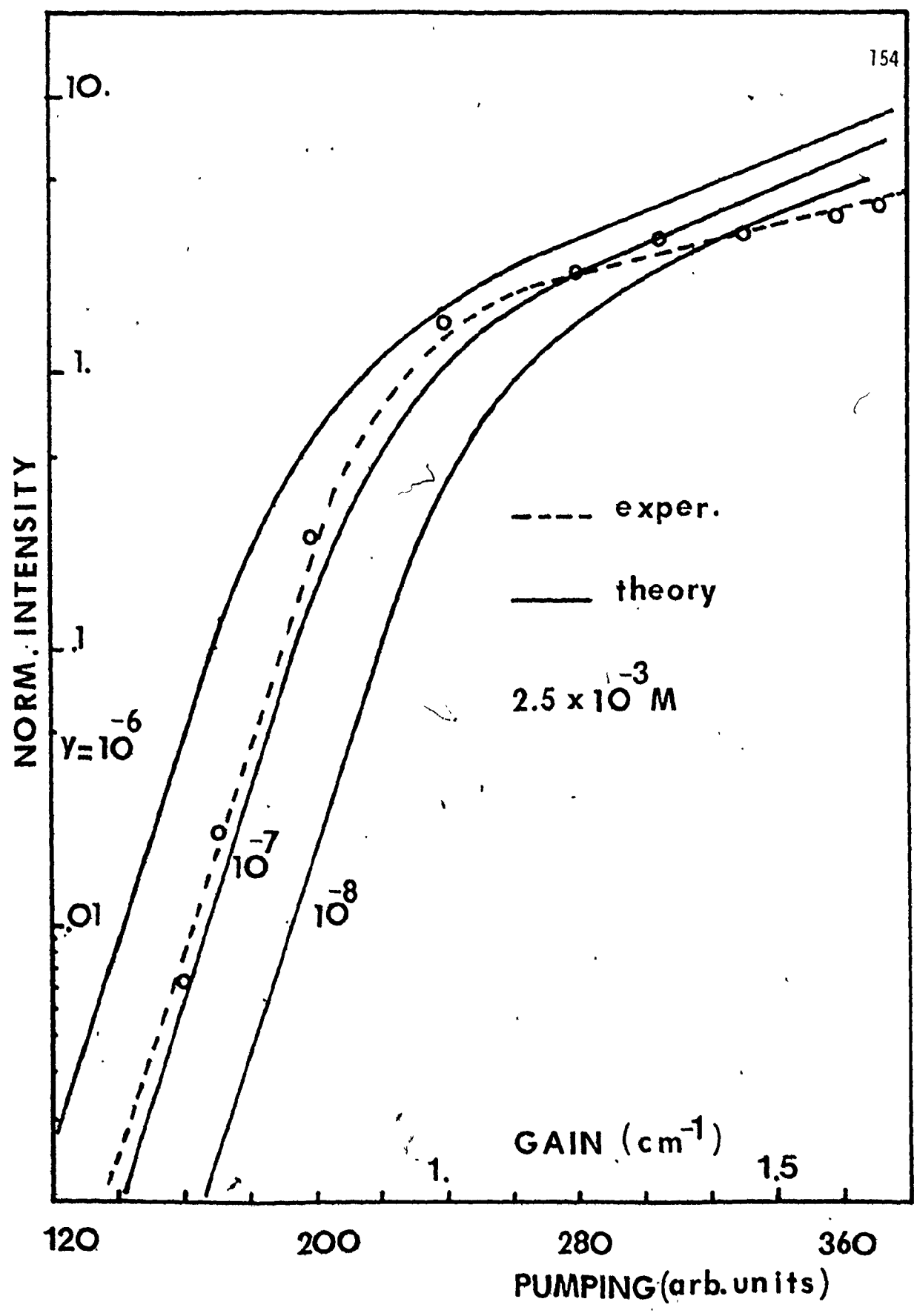
FIG. 3-30

Figure 3-31. Narrowing vs pumping measured experimentally for 2.5 x 10^{-3}
M   rhodamine 6G and narrowing vs gain calculated using
$y = 10^{-7}$ and $\Delta\lambda_{homo} = 650$ Å. The upper x-axis scale corresponds to gain calculated using the rate equations theory.
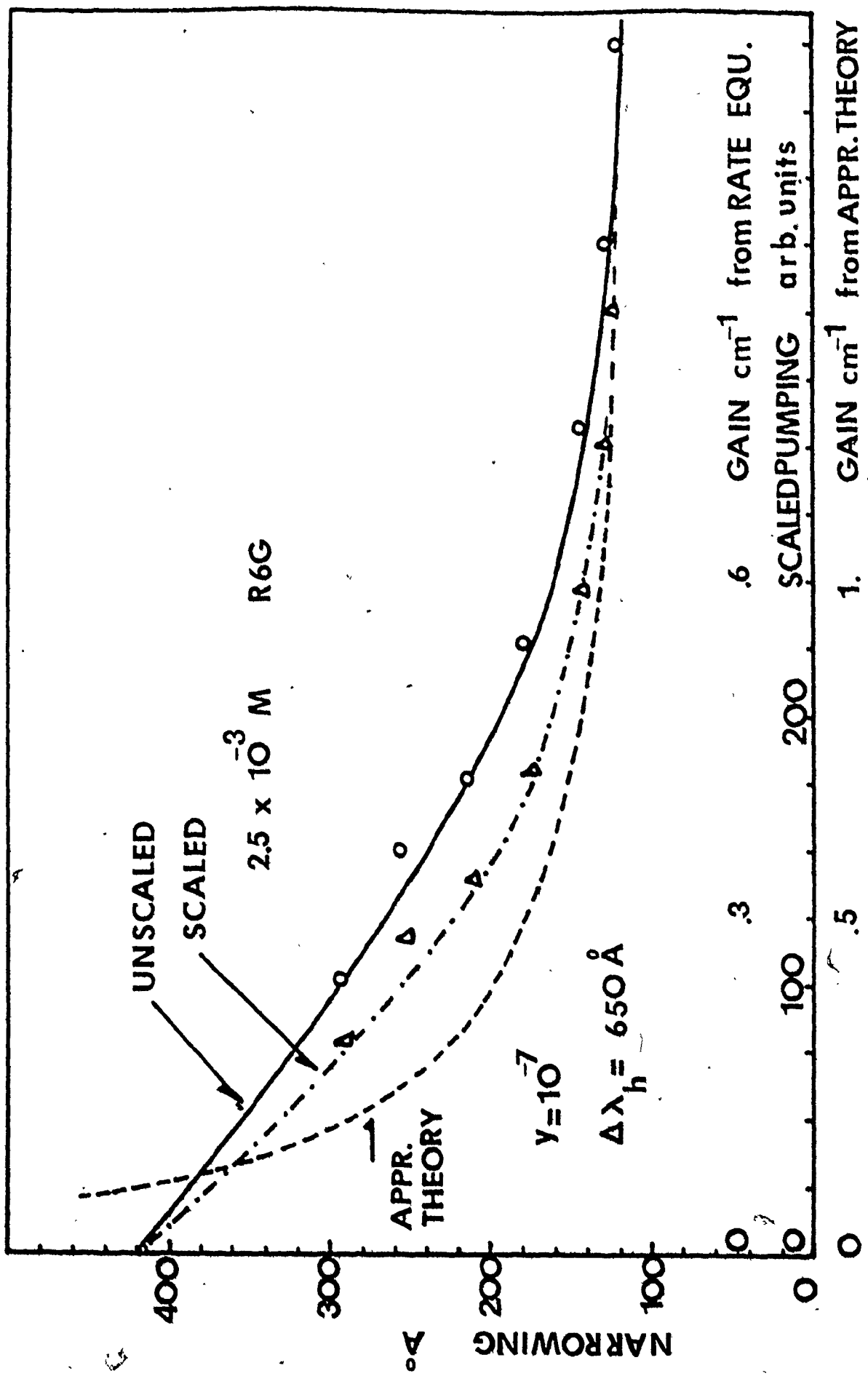
FIG. 3-31

same narrowing from the scaled experimental plot and the one obtained from the more accurate rate equation theory agree within 20% (for example, for a narrowing of 200 $\overset{o}{A}$, we read from the scaled experimental plot, a gain of 0.55 cm^{-1} and from the rate equation through the unscaled plot, a gain of 0.45 cm^{-1}, which agree within 20%). For completeness, next we present a recently published approximate theory on the ASE,[40] which is along the same lines as the one we have developed.

3.5.2 Casperson's Approximate Analytical Theory of the ASE - A Comparison

This theory[40] takes into consideration the two-way propagation of the ASE and the effect of the saturation of the gain. It assumes though no transverse variation of the gain, a Lorentzian gain line for the homogeneous case and an intensity spectrum which is much narrower than the gain linewidth well before saturation settles in. Under these assumptions the complicated intensity propagation equations can be simplified, because now we can deal with total intensities integrated over frequency, to yield the following

$$\frac{dx^+(z)}{dz} = \frac{g_h[x^+(z) + x_o]}{1 + x^+(z) + x^-(z)} \qquad (3\text{-}64)$$

$$\frac{dx^-(z)}{dz} = -\frac{g_h[x^-(z) + x_o]}{1 + x^+(z) + x^-(z)} \qquad (3\text{-}65)$$

where $x^+(z) = s \int_{-\infty}^{+\infty} I^+(y,z)dy$ is the total intensity of the wave travelling in the positive z direction normalized in units of the saturation intensity $I_s (s = 1/I_s)$, g_h is the unsaturated line centre gain coefficient, and x_o is the spontaneous emission input parameter. After some algebraic

manipulations, we end up with the following equations:

$$(1 - 2x_0)\ln(x_t/x_0 + 1) + 2x_t = z_h = g_h L \tag{3-66}$$

$$\frac{\Delta\upsilon}{\Delta\upsilon_h} = [\frac{\ln(x_t/x_0 + 1)}{\ln(x_t/2x_0 + 1)} - 1]^{1/2} \tag{3-67}$$

where x_t is the total intensity emerging from the end of the cell, $\Delta\upsilon$ is the narrowing and L is the length of the cell. Equations (3-66) and (3-67) can be used to determine the gain g_h and the narrowing if x_0 is known. Figure 3-32 shows a plot of the measured $\Delta\lambda$ vs the gain calculated using the rate equation theory. On the same graph we plotted $\Delta\lambda$ vs gain calculated from Casperson's approximate theory, for a reasonable x_0 value for dye lasers.[40] It can be seen that Casperson's predictions are very far off, just as we found for our theory. The spectrum narrows much too fast as far as the gain dependence goes. Again, an obvious way to improve the agreement is to treat the homogeneous linewidth as a free parameter and try to get the best fit of $\Delta\lambda$ vs gain, and intensity vs pump or gain. In doing exactly this, we found that a value of $\Delta\lambda_{homo}$ = 600 Å and a value of the normalized to the saturation coupling parameter $x_0 = 10^{-6}$ will give a reasonable fit. Figure 3-33 shows the fit we can get, assuming $\Delta\lambda_h$ = 600 Å, $x_0 = 10^{-6}$, to the experiment. This fit is reasonably good except at very low pumping (below gains of 0.05 cm^{-1}). Figure 3-34 shows a set of total intensity curves for different x_0 values vs gain from equation (3-66). Also on the same plot, we show the experimental curve of the intensity integrated over wavelength vs gain. We see that $x_0 = 10^{-6}$ gives a reasonably good fit, taking into consideration the approximate nature of the Casperson's theory. From Figure 3-34,

Figure 3-32. Narrowing vs gain calculated from Casperson's theory and narrowing measured experimentally vs gain. This gain has been calculated from the experimental pumping using the rate equations theory. The concentration is 1.5×10^{-3} M rhodamine 6G/ethanol.
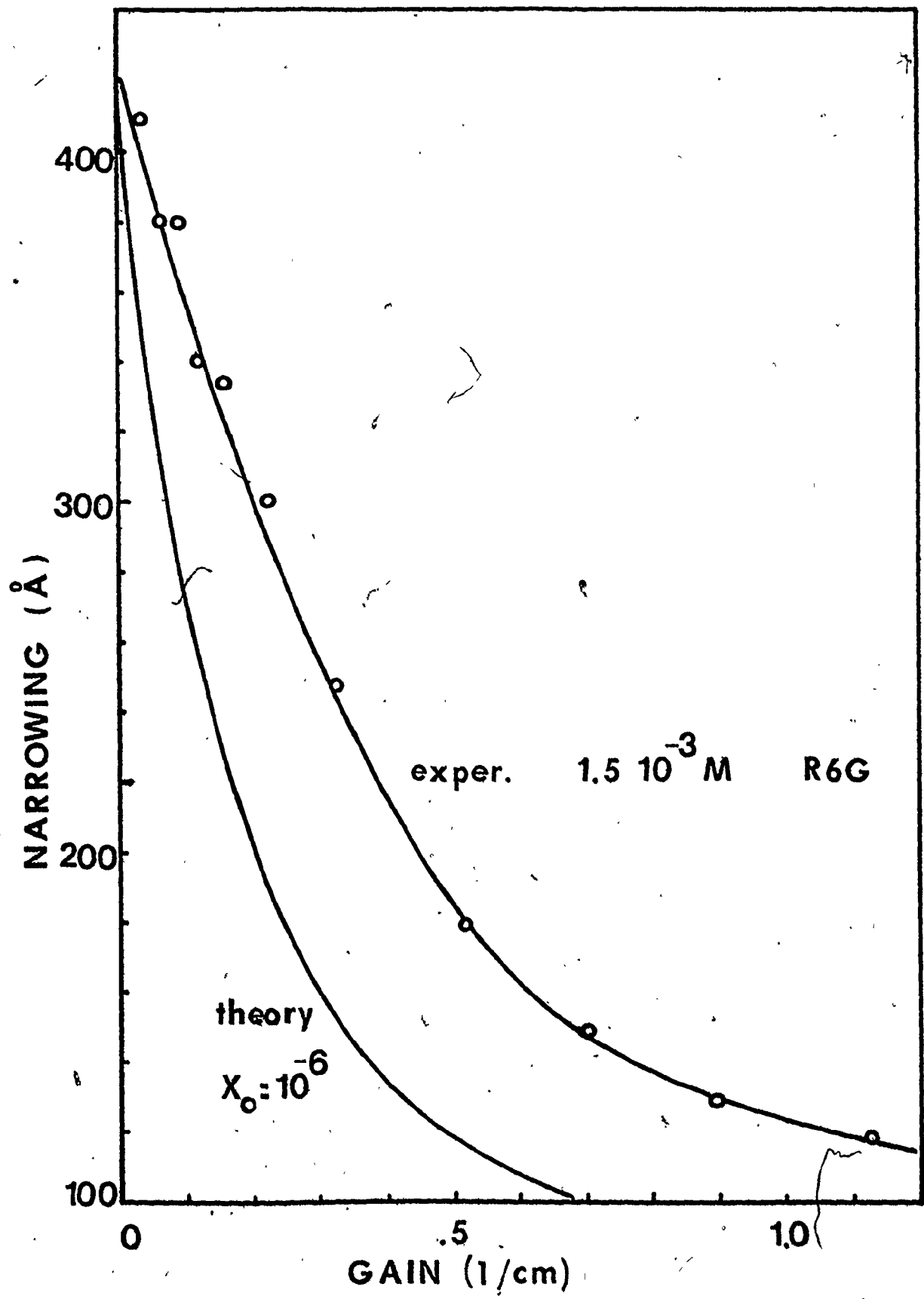
FIG. 3-32

Figure 3-33. Narrowing vs gain calculated from Casperson's theory for $X_0 = 10^{-6}$ and $FWHM_{homo} = 600$ Å and narrowing measured experimentally vs gain calculated from the corresponding pumping by using the rate equations theory. The concentration is 1.5×10^{-3} M rhodamine 6G/ethanol.
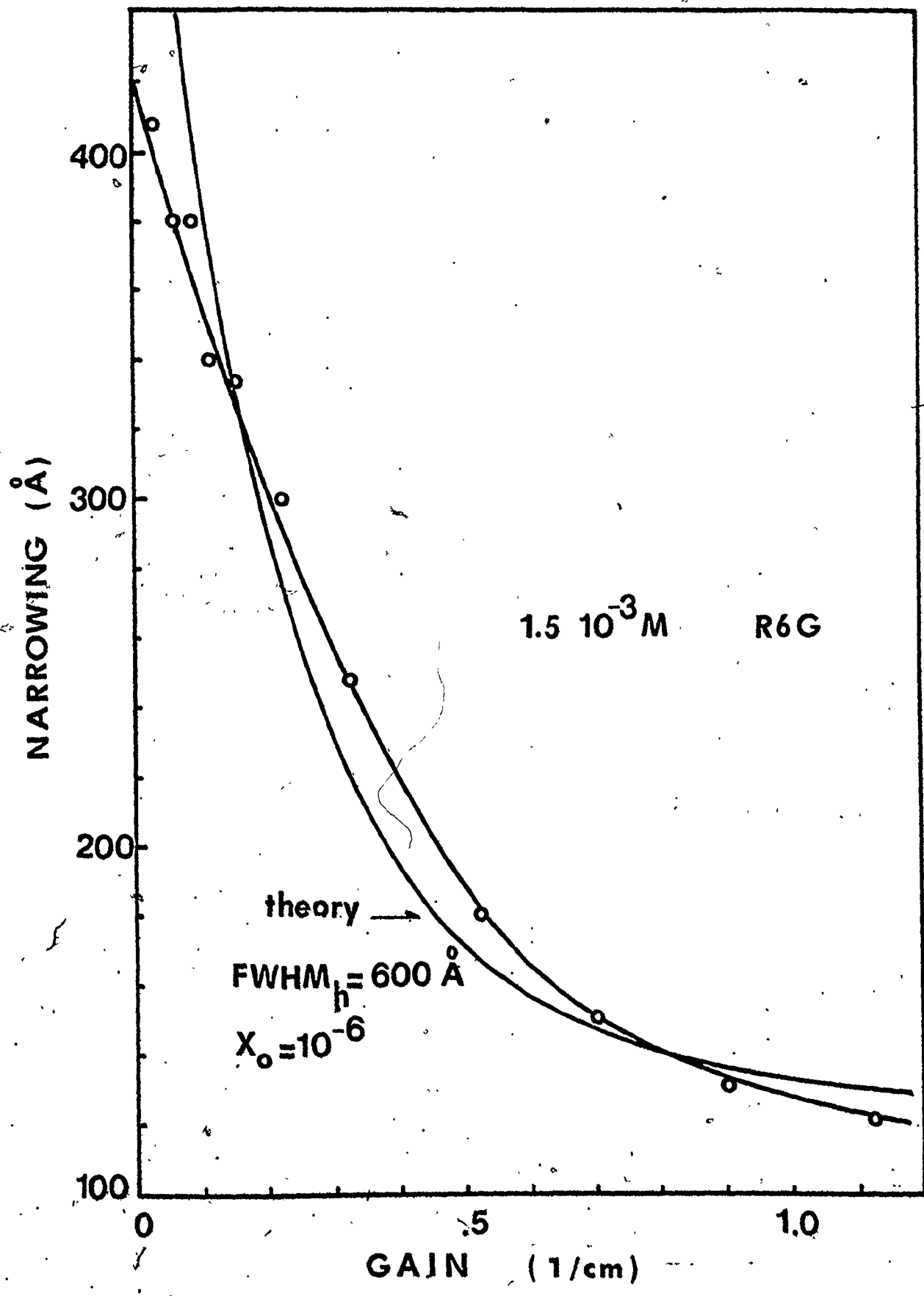
FIG. 3-33

Figure 3-34. Total intensity, integrated over wavelength, vs pumping
intensity for both experiment and approximate theory after
scaling has been performed.

FIG. 3-34

Axis labels:
TOTAL NORM. INTENSITY

10^{-1}

10^{-2}

10^{-3}

theory

exper.

$1.5 \; 10^{-3} M \quad R6G$

$X_0 = 10^{-6}$

$X_0 = 10^{-7}$

0

100

200

PUMPING INTENSITY (arb. units)
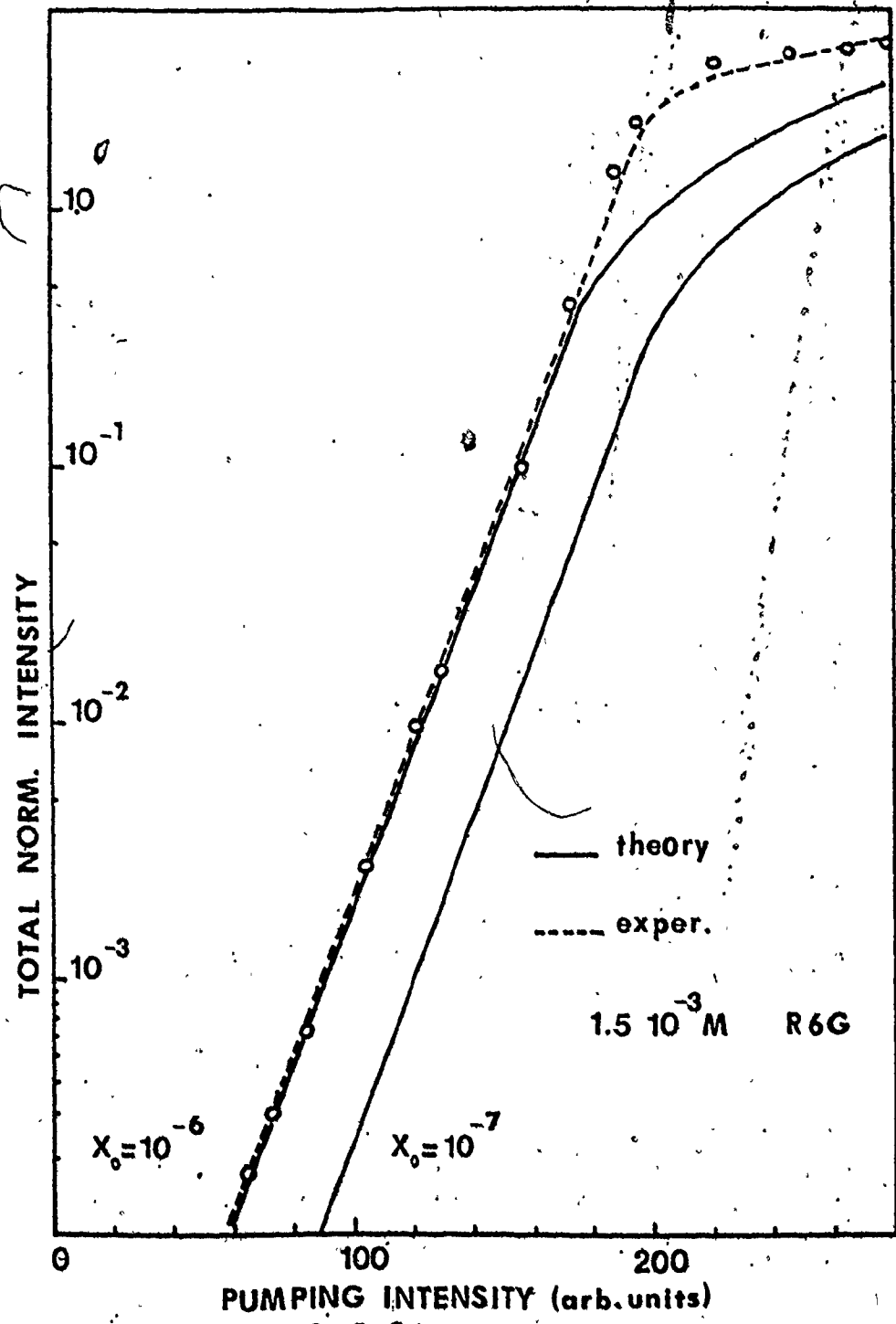
we can see that the calculated intensity saturates faster then the experimentally observed one, because the maximum intensity shift with pumping is not taken into account in the approximate theory. Experimentally, the intensity will keep on increasing and shifting to lower wavelengths until the absorption losses increase to the degree that they cannot be overcome at the low end of the spectrum by the pumping provided. In that case, the extra pumping will produce enough intensity to saturate the gain at wavelengths near the peak intensity.

From the short analysis we presented above, it is clear that Casperson's approximate theory can be used to calculate the gain with reasonable accuracy (in a similar way as in our approximate theory) employing the approximate x_0 value. To improve the predictions of this theory, we have to couple it with a more exact theory such as our rate equation approach.

Casperson's theory can be used to determine gain following a procedure similar to the one described for our approximate theory. Nevertheless, this theory shows some features of the propagation of the ASE, namely, the saturation of the narrowing with no rebroadening for the homogeneous broadened medium and the variation of the gain and intensity along the cell, which are similar to the results we get from our approximate theory presented earlier.

In conclusion, in this section we have presented an approximate semi-analytical method, which can be used to calculate the gain and we have compared the gain calculated by using this method to gain predictions

of the rate equation method. We have also suggested a way to use the approximate method for independent calculation of the gain and we have discussed another similar approximate method of gain calculation and ASE propagation. We have seen that unless care is exercised, the approximate methods can introduce a large error in the gain calculation, but suitably applied, they can give reasonable results for the gain, good to within $\sim$ 20%.

3.6 DISCUSSION AND CONCLUSIONS

In this chapter, we studied the amplification of the spontaneous emission. We developed a model for the ASE based on the rate equation approximation and solved it for the particular case of a dye molecule. This model describes the way the ASE spectrum changes within the cell and makes predictions for the emitted intensity, the narrowing of the ASE and the maximum wavelength shift which can be directly compared with experimental observations. This model also provides us with an accurate way to calculate the unsaturated gain and demonstrates the importance of the excited single state absorption (ESSA) in determining the exact behaviour of the ASE. Actually, using this model we were able to predict the ESSA importance and correct and extend the spectrum of published ESSA cross-section. This important feature of the theory can be used in other cases, where some cross-sections are less well-known, to make useful predictions of these cross-sections by comparison with the experiment.

In particular, within the gain medium, we have noticed the following:

(i)   The spontaneous emission propagating in any of the two directions starts with a broad spectrum, which gets narrower as it propagates within the gain medium and at the same time its peak moves towards shorter wavelength because of the non-uniform gain profile.

(ii)   The number of excited molecules varies within the cell and this variation can be significant in the case of high pumping, where the intensity build up is large enough to lessen the excited molecules number and thus decrease the gain.

(iii)   Propagation in the cell can be divided into three distinct regions, namely a central region where most of the amplification takes place and two symmetrical regions where the intensity could be high enough to saturate the gain. The length of these regions depends on the pumping and an increase of the pumping will shrink the amplification region. We have seen that most of the narrowing takes place within the unsaturated region which leads to the conclusion that extreme pumping will not necessarily produce small spectral widths. Also, increase of concentration, though it will provide more gain for the same pumping, will cause saturation in a shorter distance within the cell and the net narrowing will only improve slightly since most of the propagation again takes place within the saturation region, where the gain is small. The answer to this problem of narrowing is to find a way to limit the intensity of the ASE or use a wavelength selective feedback mechanism (such as a diffraction grating) to limit amplification to a narrow band of the ASE spectrum. In order to limit the photon flux per cm^2, we can use a series of small size cells with neutral density attenuators between them to drop the intensity output of each individual cell below the saturation point. Another

very interesting approach is to use a cell thick with respect to the absorption length of the dye material. In this case, it is possible to have partial propagation of the ASE outside the gain region and consequently, less photon flux inside the pumped region, which implies that higher gains can be achieved by using higher pumping. This is, of course, equivalent to higher narrowing than before, because the narrowing is inversely proportional to the unsaturated gain.

An alternative possible improvement of spectral narrowing is to use a thin cell in conjunction with appropriate saturable absorbers. The absorber will provide a selective strong absorption along the spectral region of interest, which is also intensity dependent and thus it will contribute to the additional narrowing of the peak intensity of the ASE.

With respect to the emitted ASE itself, we should note the following:

(i)   The intensity of the ASE exhibits a special behaviour both spatially and with respect to pumping. The beam, for the case the cell has a uniform absorption cross-section across it, is smooth with a divergence of the order of one-half of a degree. The intensity of the ASE with respect to pumping exhibits the usual behaviour. There are three distinct regions, namely: the very low pumping region below threshold, where there is no significant photon flux in the cell to create an induced emission; the region above threshold but below saturation where the main narrowing takes place and the intensity increase drastically with respect to pumping; the saturation region where the intensity

build-up is large enough to saturate the gain.

(ii)   A main characteristic of the ASE is the lack of mode structure, which is always present in laser oscillator. This lack of modes can be of great importance in absorption spectroscopy in cases where absorption lines lie between successive laser modes and mode hopping prohibits the access to such lines by cavity length tuning.

(iii)   The tuning of the ASE can be done by using a selective loss feedback mechanism[99] or the injection of monochromatic radiation.[100] The use of different concentration of the dye material will provide additional spectrum to tune in and the pumping itself tunes the ASE. Another very interesting tuning method could be the combination of the loss selective mechanism with the injection of monochromatic radiation to produce tunable ASE with wavelengths other than the ones supported by the loss selective element or the injection radiation wavelength. This has been demonstrated for the case of laser oscillators.[100]

Besides the rate equation model, in this section, we have also developed a semi-analytical approximate model which is independent of the characteristics of the particular system. We have seen that using this approximate model, it is possible to calculate the unsaturated gain within 20%. This model is very useful in cases where complete accurate knowledge of the characteristics of the gain medium is not available. This approximate model also gives some insight into the propagation of the ASE and takes account of the saturation on the narrowing and the intensity output.

In conclusion, in this chapter, we have presented a complete

theoretical and experimental investigation of the propagation of the ASE in a gain medium (with constant absorption cross-section across the cell, thin cell case) and shown the main effects of the interaction of light with the molecules for the particular case of dye material. This study was restricted to the time independent phenomena and pumping rates which are appropriate for flashlamp pumped systems. It is then natural to extend the treatment we have done so far to include time dependent phenomena (such as relaxation oscillation[101]). This extension is part of our future research. This study was also restricted to cases with uniform absorption cross-sections across the cell. The extension, though, of the rate equation theory to cover spatial inhomogeneity of gain across the cell is very complicated and will not be presented here. Instead, because of the great experimental interest, we will try to treat the so-called thick cell case (where the cell thickness is larger than the absorption length) in a different way, based on solving Maxwell equations for the field in the cell and looking for spatial modes across the cell, for a particular gain profile. This investigation is reported on in the next chapter.

CHAPTER 4

SPATIAL MODES IN ASE

4.1 INTRODUCTION

In the previous chapter we studied the amplification of the spontaneous emission in a thin cell, where no spatial variations of the parameters across the cell are involved. In most of the experimental situations, though, thick cells (with gain and index of refraction variations across the cell) are used. It seems then natural to extend the treatment of the ASE to cover the thick cell cases, in order to determine when spatial variations become important and to modify our method to measure the gain under these conditions if possible. The solution of this problem is extremely complicated, because it involves both the amplification of the field along the axis and its spatial distribution across the cell. The first attempt to solve this problem is to assume that the processes along and across the cell are separable, which is true under certain conditions mentioned later. In this case we can treat the propagation of the field across the cell using Maxwell's equations with the appropriate boundary conditions and profiles of the parameters involved. Such treatment will provide us with the distribution of the field across the cell, which is going to modify the amplification behaviour along the cell. Before proceeding to solve this problem of field distribution inside the cell, it is appropriate to investigate the processes which give rise to spatial inhomogeneities across the cell.

(i) Gain Profile

At high concentrations of dye material, the pumping light from either a laser or a flashlamp is absorbed in a distance which is generally much less than the width of the dye cell. According to Beer's Law the intensity of the pumping light falls exponentially with the depth inside the cell and because the unsaturated gain is proportional to the pumping, the profile of the gain across the cell is an exponential one. Consequently, the gain varies exponentially across the cell and this will affect the way the ASE propagates along the cell. Also, as we will see in the next section, the gain itself can modify the index of refraction and thus gain inhomogeneity creates index of refraction inhomogeneity as well.

(ii) Index of Refraction Change

There are two processes which will change the index of refraction across the cell, namely the heating of the solution and the existence of gain. The heating of the solution is the result of the thermalization processes within the electronic energy bands, the non-radiative decays and also the absorption of the solvent itself. In our case, the absorption of the solvent (ethanol) is very small and uniform over the cell width for the pumping region of interest and consequently it can be neglected. The spatial profile of the thermalization processes is of course proportional to the profile of the absorption of the pumping light and therefore the index of refraction change has the same profile as the gain across the cell before onset of diffusion. Consequently, because the index of refraction drops with increasing temperature we will have a higher index along the axis of the cell along with an exponential varia-

tion of the index across the cell. This is equivalent to a converging lens and it will push the field propagating along the cell toward the centre of the cell. Then, some of the ASE can propagate outside the gain region. This kind of propagation is only possible when there is a net flow of energy from the gain region inward toward the loss région to offset the losses, which are experienced by that portion of the ASE propagating outside the gain region. Next, we deal with the change of the index of refraction due to the presence of gain.

The relation between gain and index òf refraction can be seen in the following simple way. First, assume a molecule positioned at $\bar{R}$ and an electron bound to the nucleus are at distance $\bar{r}$. Then the interaction Hamiltonian between the electron and an external field is given by

$$H' = -\bar{\mu}\cdot\bar{E}(R,t) \qquad (4.1)$$

where $\bar{\mu} = -e\bar{r}$ is the electric dipole moment.

Then we can define a macroscopic polarization

$$P = N\langle\mu\rangle \qquad (4.2)$$

where N is the number of interacting molecules/cc and $\langle\mu\rangle$ is the ensemble average. The displacement $\bar{D}$ will be given by

$$\bar{D} = \epsilon\bar{E} + \bar{P} \simeq \epsilon\bar{E} + \epsilon_0\chi\bar{E} \qquad (4.3)$$

for the case of small fields $\bar{E}$. Here, ϵ is the dielectric constant and χ is the electric susceptibility. Equation (4.3) can also be written as

$$\bar{D} = \epsilon[1 + \frac{\epsilon_0}{\epsilon}\chi]\bar{E} = \epsilon'(\nu)\bar{E} \qquad (4.4)$$

where

$$\varepsilon'(\nu) = \varepsilon[1 + \frac{\varepsilon_0}{\varepsilon} \chi]$$

In other words, we have associated the interaction of radiation with the molecules to the dielectric constant or the susceptibility of the medium. Next we will see how this change of the susceptibility relates to the gain. Let

$$E(z,t) = E_0 \exp i (\omega t - k'z)$$

be a plane wave propagating in a gain medium along the z axis. Then, the wavevector k' inside the gain medium will be given by

$$k' \equiv \omega(\mu\varepsilon')^{1/2} \approx k(1 + \varepsilon_0 \chi/2\varepsilon) \qquad (4.5)$$

where

$$k = \omega\sqrt{\mu\varepsilon} \quad \text{and} \quad |\chi| \ll 1.$$

Expressing χ with its real and imaginary parts ($\chi = \chi' - i\chi''$) we write equation (4.5) as follows:

$$k' \approx k[1 + \frac{\chi'(\nu)}{2n^2}] - i \frac{k\chi''(\nu)}{2n^2} \qquad (4.6)$$

where $n = (\varepsilon/\varepsilon_0)^{1/2}$ is the index of refraction of the medium far from resonance. Near resonance though,

$$n' = (\varepsilon'/\varepsilon_0)^{1/2} = (\varepsilon(1 + \varepsilon_0\chi/\varepsilon)/\varepsilon_0)^{1/2}$$

or

$$n'^2 = \varepsilon/\varepsilon_0 + \chi = n^2 + \chi' - i\chi'' \qquad (4.7)$$

Then the plane wave can be written as

$$E(z,t) = E_0 \exp i(\omega t - zk(1 + \frac{\chi'(\nu)}{2n^2})) \exp(k\chi''(\nu)z/2n^2) \qquad (4.8)$$

We see that the result of the interaction is to change the phase of the plane wave by $k\chi'(\nu)/2n^2$ and to vary the amplitude by an exponential gain factor of $k\chi''(\nu)/2n^2$. Then the gain for the intensity ($I = EE*$) is given by

$$g(\nu) = k\chi''(\nu)/n^2 \qquad (4.9)$$

This equation relates the gain to the imaginary parts of the suscepti-bility and through the Kronig-Kramers relations (which relate the real and imaginary part of the susceptibility) to the real part also. But from equation (4.7) the real part will contribute directly to the change of the index of refraction. In conclusion we have seen that the pre-sence of gain will increase the index of refraction in the gain region.

It is then clear from what was discussed above that in a thick cell with high concentration, we have a non-uniform gain problem with the addition of a non-uniform index of refraction due to thermalization or non-radiative processes in the lasing material, and the presence of the gain itself. The change of the refractive index will cause a lensing effect and the positive lens (which is formed when the change of index due to temperature increase is larger than the change due to the presence of gain) will redistribute the field away from the walls of the cell, where the gain is maximum. This field will then experience less gain as it propagates further from the walls and the propagation may occur in

modes corresponding to real solutions of the wave equation which are
stable eigenmodes propagating along the cell and confined to a fixed
distribution in space. This type of propagation of the field will mani-
fest itself through the intensity variation in the near field and the
far field.[50] It is also possible that, because part of the field is
propagating outside the gain region, the intensity of the field in the
gain region remains small relative to the saturation intensity for long
propagation lengths. This acts to enhance the spectral narrowing of the
field, because, as we have seen in the previous chapter, most of the
narrowing takes place before saturation. Additional narrowing could
also result from the wavelength dependent diffraction losses, which be-
come significant with high concentrations. It is then important both
from a theoretical point of view and from a practical one to investigate
the propagation of the ASE in a thick cell. Next, we present a review
of the existing literature on ASE propagation in thick cells.

4.2 LITERATURE REVIEW

The refractive index gradient effect in the so-called super-radiant dye amplifier have been observed indirectly by a number of authors, [45][47][79][102][103] both for planer and circular dye cell structures. According to reference (45) a high concentration $(2.9 \ 10^{-3} \ m/l)$ rhodamine 6G ethanol solution is kept in a cell of variable thickness. The slab cell is pumped on one side only. The far field pattern consist of two distinct modes separated by a time averaged angle of $2°$ corresponding, in a crude approximation, to a zig-zag way of light propagation along the cell. Burlamacchi et al. [79][102] reported mode patterns of near and far field for the case of circular dye cell and flashlamp operation and also reported indications of existence of whispering modes, which propagate circulating clockwise and anticlockwise along the wall of the cell. Tikhonov et al., [103] using a planar cell, reported also an angular divergence of the two emitted beams of a few degrees for sufficiently high dye concentration where the absorption length is smaller than the dye cell thickness. Their explanation was also related to the lens-like index of refraction distribution in the cell due to pump heating at those high concentrations. We should note that in a planar cell, which is excited in a perpendicular way the absorption length is directly comparable to the cell thickness to determine the kind of modes we will have. But for a cylindrical dye cell the radiation focuses as it propagates inwards and a proper treatment is needed to determine the effective absorption length and the effect of the cell wall on the oblique incident pumping light. [104]

Beside the experimental observation already mentioned, a theoretical analysis, based on the hydrodynamic approach, which relates the temperature variation (due to non-radiative decay and interband relaxation) to the refractive index variation has been reported by Balucani et al.[49] In this treatment, the refractive index variation for small changes in temperature is given by

$$n(x,t) - n_0 = (\frac{\partial n}{\partial T})_{p_0} \Delta T(x,t) \qquad (4.10)$$

where

$$\Delta T(x,t) = \frac{1}{\rho_0 c_p} \int_{-\infty}^{t} Q^{ext}(x,t')dt'$$

$$(\frac{\partial n}{\partial T})_{p_0} = \frac{n_0^2 - 1}{3n_0} (1 + \frac{n_0^2}{2}) \frac{1}{\rho_0}(\frac{\partial \rho}{\partial T})_{p_0}$$

$$Q^{ext}(x,t) = \alpha I(x,t), \qquad (\frac{\partial n}{\partial T})_{p_0} = -4 \cdot 10^{-4} {}^{\circ}K^{-1} \text{ for ethanal at room temperature}$$

and p_0 is the pressure at thermodynamic equilibrium, ρ_0 the density, C_p the specific heat at constant pressure and $I(x,t)$ the intensity of the pumping light, which is directly proportional to the heat power density. Balucani et al.[49] computed that for a concentration of rhodamine 6G of $1.0 \cdot 10^{-3}$ m/l, an ablation flashtube with a blackbody temperature of about 30,000°K and a pulse of 2.5 µsec, a temperature increase of 0.3°C and an index of refraction change of the order of 5×10^{-4} are produced. We mention these calculations here in order to give a feeling for the changes of temperature and index of refraction involved. Such changes of the index are going to be used in a later section when particular solutions of Maxwell's equation for spatial modes are found. A simpler -

way of analysing the light propagation has been presented by Pratesi and Ronchi,[48] using a geometrical ray-tracing method and assuming a quadratic profile for the spatial variation of the index of refraction and the gain.. From the calculations done by Bulucani et al.,[49] a quadratic approximation for the index of refraction seems quite reasonable for flashlamp pumped planar cells at low enough dye concentration. Pratesi and Ronchi,[48] using the assumption made above and considering only the situation in which the light beam remains almost parallel to the optical axis, in order to use the geometrical optics approximation, have found the ray trajectory equation and the conditions for mode structure for the planar cell geometry. They have found that the refraction index change will determine the position of a certain line, called the caustic, and when the caustic lies outside the cell wall only leaky modes can propagate. On the contrary, when the caustic line lies inside the cell wall propagation at guided modes can occur up to substantially large order. In addition, it is shown that for thick cells some higher order guided modes will require gains, which are readily available in dye amplifiers and they propagate in a real situation. Some experimental results of the far field deviation from the axis of the cell for different cell thickness are also presented and compared with the theory along with time integrated far-field patterns.

These approximate ray trajectory calculations provide a starting point in the mode propagation problem, but in order to apply the theory in realistic situations we will have to develop a more sophistical model, which will include the phase of the propagating wave along the cell and a

more realistic index of refraction and gain distribution across the cell. In the next section, we will present a model for the doubly pumped slab dye cell assuming an index step variation and using a wave equation approach.

4.3 A MODEL FOR THE TRANSVERSE MODES IN THE ASE CELL

The dye cell under consideration is a planar structure which is pumped by two identical flashtubes, one on each side. For sufficiently high concentration the gain region becomes small with respect to the cell thickness. Furthermore, there is a transverse variation of the index of refraction due to the presence of gain itself and the temperature-induced spatial variations. To determine the behaviour of the field in the cell, we have to solve the Maxwell's equations looking for the conditions, which determine the existence of transverse modes in the cell. Under the assumption that both the gain and the index of refraction have a similar distribution, several authors have obtained solutions for specific profiles in the related case of solid state electron-beam-pumped lasers, such as Guassian, $sech^2$ and step functions (reference 50 and references cited) which are approximations to the spatial variations of the gain. The work reported here is an application and extension of this earlier work.

Figure 4-1 shows the particular configuration assumed in the dye amplifier slab cell. A symmetric step gain profile is assumed at both sides of the cell along with a lossy section in the middle due to the absorption of the unpumped region at the wavelength of the emitted ASE. We seek transverse field solutions similar to the one shown in figure 4-1. We assume that the transverse variation of general solutions of the wave equation, propagating along the z direction, have the form

$$A = A_0 \sin px \quad \text{for} \quad 0 \leq x \leq d$$
$$A = A_1 e^{-qx} + A_2 e^{+qx} \quad d < x < d + h$$
$$A = A_3 \sin p'(x-L) \quad d+h \leq x \leq 2d + h$$

(4-11)

Fig. 4-1.   A model for the ASE in a thick planar cell. L is the cell

thickness and d is the width of the index of refraction step.

The dotted line represents a mode of the field across the

cell. The full line is the gain or the loss experienced by

the field across the cell.

$$L = h + 2d$$
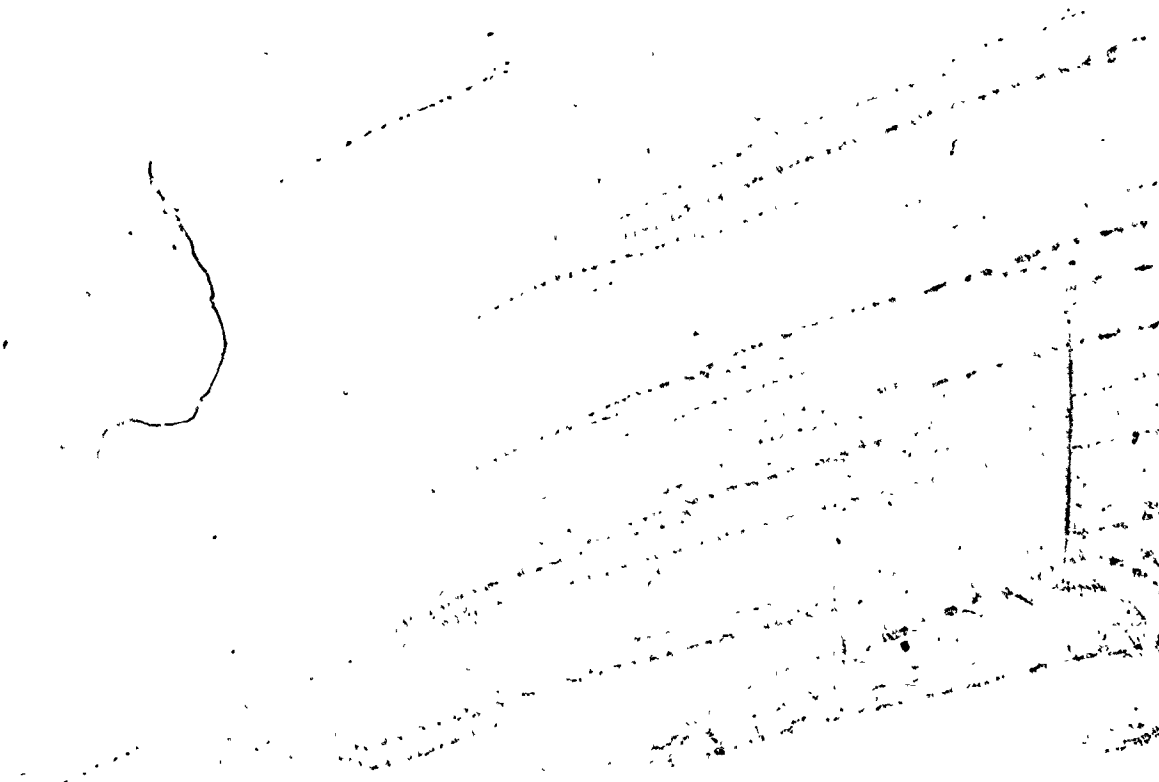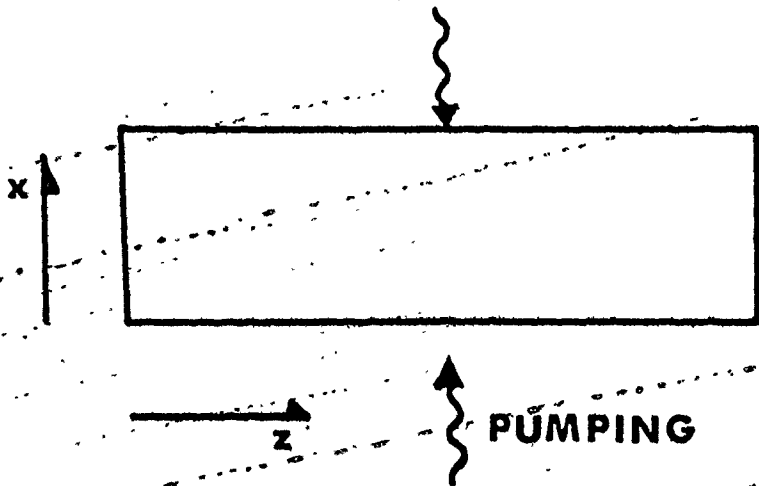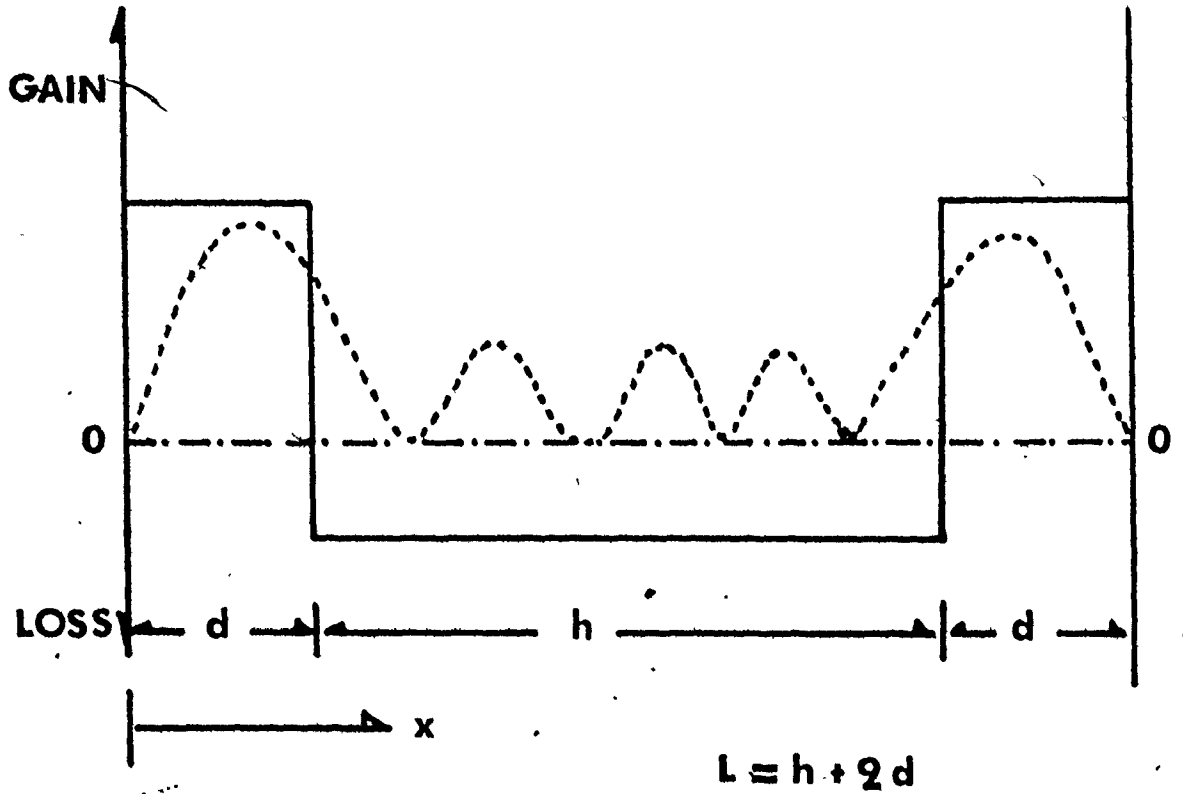
FIG. 4-1

These solutions must satisfy the wave equation (see Appendix B).

$$\frac{\partial^2 A}{\partial x^2} = [k^2 - \frac{\omega^2 \epsilon}{c^2}]A \qquad (4\text{-}12)$$

According to our model we will assume the following index step profile:

$$\epsilon(x) = \begin{cases} \epsilon'_0 + \delta\epsilon'_0 - i(\epsilon''_0 - \epsilon''_g) & \text{for} \quad 0 \leq x \leq d \\[2mm] \epsilon'_0 \qquad\quad - i(\epsilon''_0 + \epsilon''_1) & d < x < d + h \\[2mm] \epsilon'_0 + \delta\epsilon'_0 - i(\epsilon''_0 - \epsilon''_g) & d + h \leq x \leq 2d + h \end{cases} \qquad (4\text{-}13)$$

Here, ϵ'_0 is the real part of the dielectric constant far from resonance, $\delta\epsilon'_0$ is the step change of the real part at the dielectric constant, ϵ''_g, ϵ''_1, ϵ''_0 refer to the effect on the dielectric constant of the gain, the absorption, and the non-resonant losses. In our case, the dye amplifier with no feedback, the non-resonant losses, which can be attributed to absorption of the solvent or mirror distributed losses are negligible. Then, equation (4-13) becomes

$$\epsilon(x) = \begin{cases} \epsilon'_0 + \delta\epsilon'_0 + i\epsilon''_g & \text{for} \quad 0 \leq x \leq d \\[2mm] \epsilon'_0 \qquad\quad - i\epsilon''_1 & d \leq x \leq d + h \\[2mm] \epsilon''_0 + \delta\epsilon'_0 + i\epsilon''_g & d + h \leq x \leq 2d + h \end{cases} \qquad (4\text{-}14)$$

Next we substitute (4-11) and (4-14) into (4-12) to get

$$-p^2 = k^2 - \frac{\omega^2}{c^2}\epsilon'_0 - i\frac{\omega^2}{c^2}\epsilon''_g - \frac{\omega^2}{c^2}\delta\epsilon'_0 \qquad (4\text{-}15)$$

$$q^2 = k^2 - \frac{\omega^2 \epsilon'_0}{c^2} + i\frac{\omega^2}{c^2}\epsilon''_1$$

Define

$$\alpha = \frac{\omega^2}{c^2} \epsilon''_g$$

$$\beta = \frac{\omega^2}{c^2} \epsilon''_1$$

(4-16)

According to (B-19), the intensity gain is given by

$$g = \frac{\omega \epsilon''_g}{cn}$$

Then (4-16) will be given by

$$\alpha = \frac{\omega n}{c}\left(\frac{\omega \epsilon''_g}{cn}\right) = \frac{\omega n}{c} g = \frac{2\pi n g}{\lambda}$$

(4-17)

$$\beta = \frac{\omega n}{c}\left(\frac{\omega \epsilon''_1}{cn}\right) = \frac{\omega n}{c} \alpha_s$$

(4-18)

where g is the gain in cm^{-1} and α_s is the loss in cm^{-1}, n is the real index of refraction far from resonance and c is the velocity of light in vacuum.

Next, we will apply continuity and symmetry conditions to simplify equations (4-15). Provided that the gain and index steps are the same in (o,d) and (d + h, 2d + h) we have p = p' and we need only to deal with the boundary at position d, together with the boundary at L/2.

The boundary conditions and the continuity conditions are given by ((1) is justified experimentally. Also, calculations of the position of the caustic[48] for our case support this assumption)

1)   A = o at x = o,L

11)   A is continuous at x = d,d+h

(4-19)

111) $\frac{dA}{dx}$ is continuous at x = d,d+h

Symmetry conditions are

i) $\quad p = p'$

ii) $\quad A_1 e^{-q(d + h/2)} = A_2 e^{q(d + h/2)}$ $\qquad$ (4-20)

Then at d we have

$$A_1 e^{-qd} + A_2 e^{qd} = A_0 \sin pd \qquad (4-21)$$

and the continuity of logarithmic derivatives gives

$$\frac{-qA_1 e^{-qd} + A_2 e^{qd}}{A_1 e^{-qd} + A_2 e^{qd}} = \frac{A_0 p \cos pd}{A_0 \sin pd} \qquad (4-22)$$

From (4-20, ii) we have $A_2 = A_1 e^{-qL}$, then (4-21) can be written as

$$A_0 \sin pd = A_1 (e^{-qd} + e^{q(d-L)})$$

and (4-22) as

$$\frac{pd}{qd} = \tan(pd) \frac{e^{-q(L-d)} - e^{-qd}}{e^{-q(L-d)} + e^{-qd}} \qquad (4-23)$$

Equation (4-23) together with equations (4-15) determine the solutions.
Here of course p and q are complex numbers. Next, we set

$$pd = (p' + i'')d = u + i\overline{k}u$$

$$qd = (q' + iq'')d = v + isv \qquad (4-24)$$

Then (4-23) may be written as

$$\frac{u + i\overline{k}u}{v + isv} = \tan(u + i\overline{k}u) \frac{e^{(v + isv)(1 - L/d)} - e^{-(v + isv)}}{e^{(v + isv)(1 - L/d)} + e^{-(v + isv)}} \qquad (4-25)$$

Equations (4-15) can be written

$$-p^2 d^2 = (k^2 - \frac{\omega^2 \epsilon_0'}{c^2})d^2 - i\alpha d^2 = \frac{\omega^2 \delta\epsilon_0 d^2}{c^2}$$

$$q^2 d^2 = (k^2 - \frac{\omega^2 \epsilon_0'}{c^2})d^2 + i\beta d^2$$

(4-26)

and taking the square of equations (4-24) we have

$$(pd)^2 = (u^2 - \bar{k}^2 u^2) + 2i\bar{k}^2$$

$$(pq)^2 = (v^2 - s^2 v^2) + 2isv^2$$

(4-27)

Now, we equate real and imaginary parts of (4-26) and (4-27) to get

$$-(u^2 - \bar{k}^2 u^2) = (k^2 - \frac{\omega^2 \epsilon_0'}{c^2})d^2 - \frac{\omega^2 \delta\epsilon_0 d^2}{c^2}$$

$$(v^2 - s^2 v^2) = (k^2 - \frac{\omega^2 \epsilon_0'}{c^2})d^2$$

(4-28)

$$2\bar{k}u^2 = \alpha d^2$$

$$2sv^2 = \beta d^2$$

Then we set

$$\theta \equiv \beta d^2 = \frac{\omega^2}{c^2} \epsilon_1'' d^2 = \frac{\omega n}{c} \alpha_s d^2$$

(because of (B-21))

$$\phi \equiv \frac{\omega^2 \delta\epsilon_0' d^2}{c^2}$$

$$\delta \equiv (k^2 - \frac{\omega^2 \epsilon_0'}{c^2})d^2$$

(4-29)

and replace the equivalent quantities θ, ϕ, δ, in equations (4-28) to get

$$-(u^2 - \bar{k}^2 u^2) = \delta - \phi$$

$$(v^2 - s^2 v^2) = \delta$$

$$2\bar{k}u^2 = \alpha d^2 \qquad\qquad (4\text{-}30)$$

$$2sv^2 = \theta$$

In these relation ϕ is related to the real index step $\delta\epsilon_o$ and θ is related to the loss and both ϕ and θ together with $(1-L/d)$ are to be taken as initial parameters. The solution of the equations (4-25) and (4-30) will give u, v, $\bar{k}$, s and consequently α which is related to the gain necessary to have modes in the system.

In order to be able to use equation (4-25) to calculate u and v we have to separate the real and imaginary parts of the equation. Accordingly, we write for the left hand side of (4-25)

$$\frac{u + i\bar{k}u}{v + isv} = \frac{u}{v}\frac{1 + \bar{k}s}{1 + s^2} + i\,\frac{u}{v}\frac{\bar{k} - s}{1 + s^2} \qquad\qquad (4\text{-}31)$$

for the first term of the right hand side of (4-25) after some algebra

$$\tan(u + i\bar{k}u) = \frac{\sin(u)\cos(u) + i\,\sin\text{-}h(\bar{k}u)\cos h(\bar{k}u)}{\sin h^2(\bar{k}u) + \cos^2(u)} \qquad\qquad (4\text{-}32)$$

and for the second term of the right hand side of (4-25)

$$\frac{e^{qd(1-L/d)} - e^{-qd}}{e^{qd(1-L/d)} + e^{-qd}} = \frac{C_1 C_3 + C_2 C_4}{C_3^2 + C_4^2} + i\,\frac{C_2 C_3 - C_1 C_4}{C_3^2 + C_4^2} \qquad\qquad (4\text{-}33)$$

where

$$A \equiv 1 - L/d$$

$$C_1 = e^{Av} \cos(sAv) - e^{-v} \cos(sv)$$

$$C_2 = e^{Av} \sin(sAv) + e^{-v} \sin(sv)$$

$$C_3 = e^{Av} \cos(sAv) + e^{-v} \cos(sv)$$

$$C_4 = e^{Av} \sin(sAv) - e^{-v} \sin(sv)$$

Then substitute equations (4-31), (4-32), (4-33) into (4-25) and equating real and imaginary parts we have the final equations

$$F_1(u,v,\overline{k},s) \equiv (1 + \overline{k}s)G_4 - (\overline{k} - s)G_2 = 0$$

$$F_2(u,v,\overline{k},s) \equiv u(\overline{k} - s)G_3 - v(1 + s^2)G_4 = 0$$

(4-34)

where

$$A = 1 - L/d$$

$$A_1 = \sin h(\overline{k}u) \cos h(\overline{k}u)$$

$$A_2 = \sin(u) \cos(u)$$

$$D = \sin h^2(\overline{k}u) + \cos^2(u)$$

$$G_1 = G_3 = D[C_3^2 + C_4^2]$$

$$G_2 = A_2[C_1C_3 + C_2C_4] - A_1[C_2C_3 - C_1C_4]$$

$$C_4 = A_2[C_2C_3 - C_1C_4] + A_1[C_1C_3 + C_2C_4]$$

and G_1 have been defined previously. Equations (4-34) and (4-30) are now the new set of basic equations of the problem. Equations (4-30) can be further simplified for use in calculations. If we combine the first and second equations of (4-30) we have

$$u^2(1 - \overline{k}^2) + v^2(1 - s^2) - \phi = 0$$

(4-35)

Rewriting the last equation of (4-30) we have

$$2sv^2 - \theta = 0 \qquad\qquad (4\text{-}36)$$

In conclusion, we have arrived at a set of four equations (4-34), (4-35) and (4-36) with four unknowns, u, v, $\bar{k}$ and s and three initial parameters: A, related to the cell active region, ϕ, related to the index step, and θ, related to the absorption losses in the unpumped region. The solution of these equations will give us the gain necessary to support the transverse modes, through the equation (4-17) after we have calculated α from the third equation of the group (4-30). This gain should be high enough to overcome the losses, which in the case of the amplifier without feedback, are the losses due to radiation leaving the active region by diffraction. Then, we should call this loss the diffraction loss. In the case of the dye oscillator we have to include another loss due to the scattering of light in the mirrors and the coupling of the light through a partially transmitting mirror to the outside of the cavity world. It can be seen though from equation (4-13b) that it is the sum of the losses in the nonpumped region which are important and not the individual contributions. Nevertheless, after we have determined the values for u, v, $\bar{k}$, s we can calculate the field distribution using the equation (4-11), and consequently get the intensity distribution for the near field which for stable modes is the same anywhere in the cell. Then, we can determine the far field intensity distribution using equation (B-33) of Appendix B. Next, we present a computer solution of the basic equations mentioned above along with some results.

4.4 NUMERICAL SOLUTION

It was indicated in the previous section that in order to find the transverse modes we have to solve simultaneous equations (4-34), (4-35) and (4-36). Because of the complexity and nonlinearity of these equations, we still have to solve them numerically to find u, v, $\bar{k}$ and s, the variables which determine the modes and the field. The equations (4-34) include exponential and trigonometric functions of the variables; thus, we will have multiple roots and thus multiple solutions, which are only discriminated by the gain needed to support those solutions. Obviously, the solution with the smallest gain will be amplified the most, and depending on the available gain it can be the only one present. Because of the multiplicity of the solutions, it is then necessary to have some guidelines in finding the lowest gain solutions for given concentration, cell thickness and index step. A close look at the equations (4-11a) and (4-24a) reveals that for u between zero and $\pi/2$ we will have only one peak of the intensity within the gain region and this corresponds to the lowest mode. The next one will have two peaks in the gain region ($\pi/2 < u < \pi$) and so forth. A similar argument holds for the variable v. For smaller values of v the spacing of the field ripples in the region (d, d+L) will be larger, provided that we always keep the $\bar{k}$ value positive in order to have propagation. It is not always possible though to say in advance that the higher order modes will experience higher losses because the combination of the index step, the loss and the cavity thickness may produce a high order mode with a low gain requirement. This makes the search for modes and the comparison with real experimental situa-

tions difficult and time-consuming. Figure 4-2 shows a block diagram of the first programme which is used to find the potential pairs of (u,v) which might be root of the equation. For a certain prechosen spectrum of u and v we calculate the functions $F_1(u,v,s,\overline{k})$ and $F_2(u,v,s,\overline{k})$ and find the combinations of (u,v) for which F_1 or F_2 crosses the zero axis. Then we plot these pairs of u and v for both functions on the same plot. The crossections of these plots will determine possible initial values for the root searching programme whose block diagram appears in Figure 4-3. In this second programme, after we check for convergence, we calculate the gain needed to support the particular mode which is completely determined by the exact values of u, v, $\overline{k}$ and s. Then we plot the near field distribution across the cell and the far field distribution against angular deviation from the cell axis. The listing of these two programmes appears in Appendix B.

Fig. 4-2. A flowchart for the computer programme, which calculates

the approximate roots of the equations $F_1(u,v,\overline{K},s) = 0$

and $F_2(u,v,\overline{K},s) = 0$ described in the text.
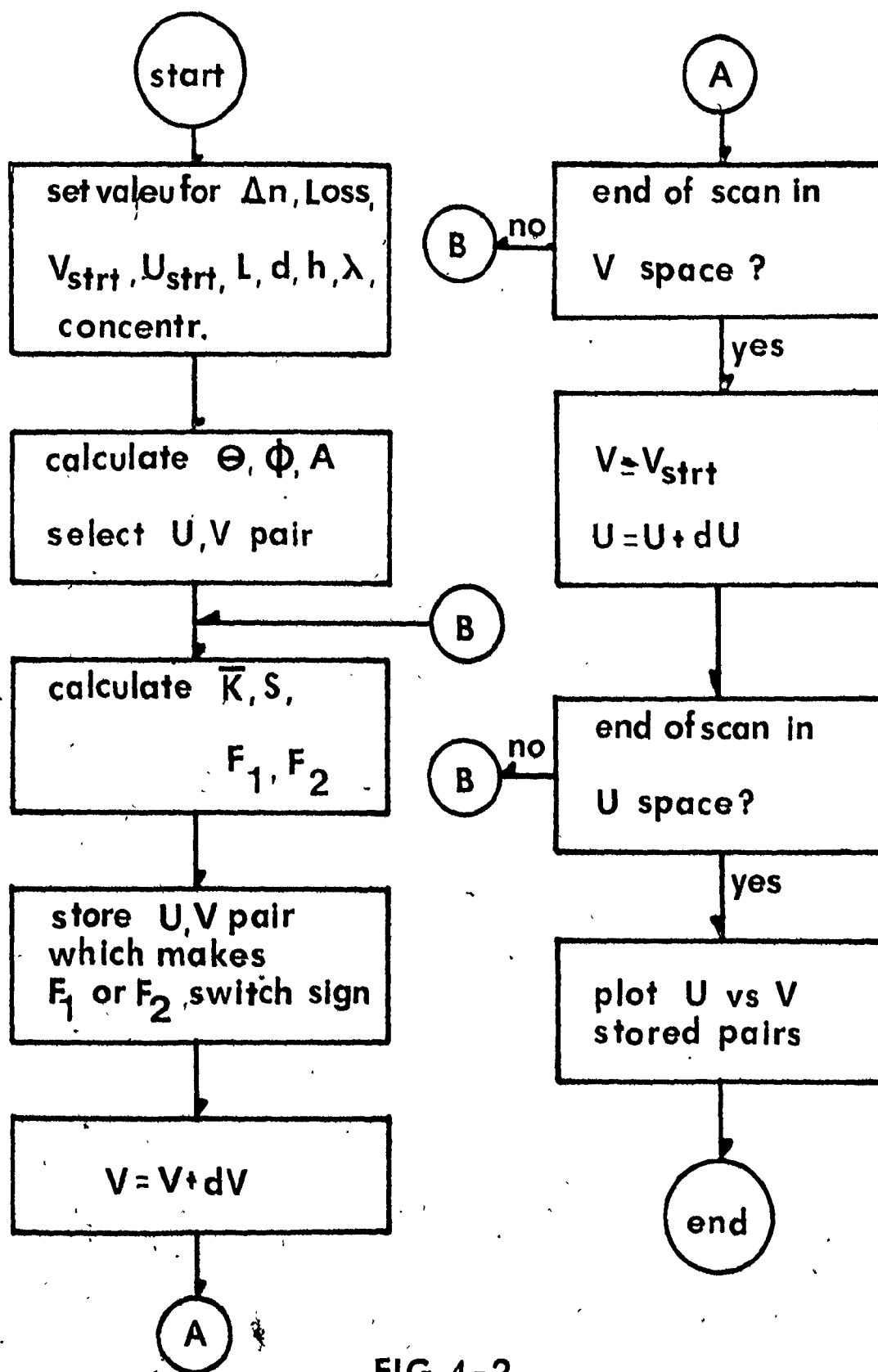
FIG. 4-2

Fig. 4-3. A flowchart for the programme, which calculated the exact roots of the $F_1(u,v,\overline{K},s) = F_2(u,v,\overline{K},s) = 0$ system of equations plots the near and far fields and calculates g_{diff} for each root pair.

```
        ┌─────────┐
        │  start  │
        └─────────┘
             │
             ▼
   ┌───────────────────────┐
   │ set valeu for Δn, Loss,│
   │                       │
   │ L, d, h, λ, concentration│
   └───────────────────────┘
             │
             ▼
   ┌───────────────────────┐
   │ read in approx. roots; │
   │                       │
   │ U, V                  │
   └───────────────────────┘
             │
             ▼
   ┌───────────────────────┐
   │                       │
   │ calculate  Θ, Φ, A    │
   │                       │
   └───────────────────────┘
             │
             ▼
   ┌───────────────────────┐
   │                       │
   │ find roots by iteration,│
   │                       │
   │ calculate and plot    │
   │                       │
   │ near and far fields,  │
   │                       │
   │ calc.  g_diff         │
   └───────────────────────┘
             │
             ▼
        ┌─────────┐
        │   end   │
        └─────────┘
```
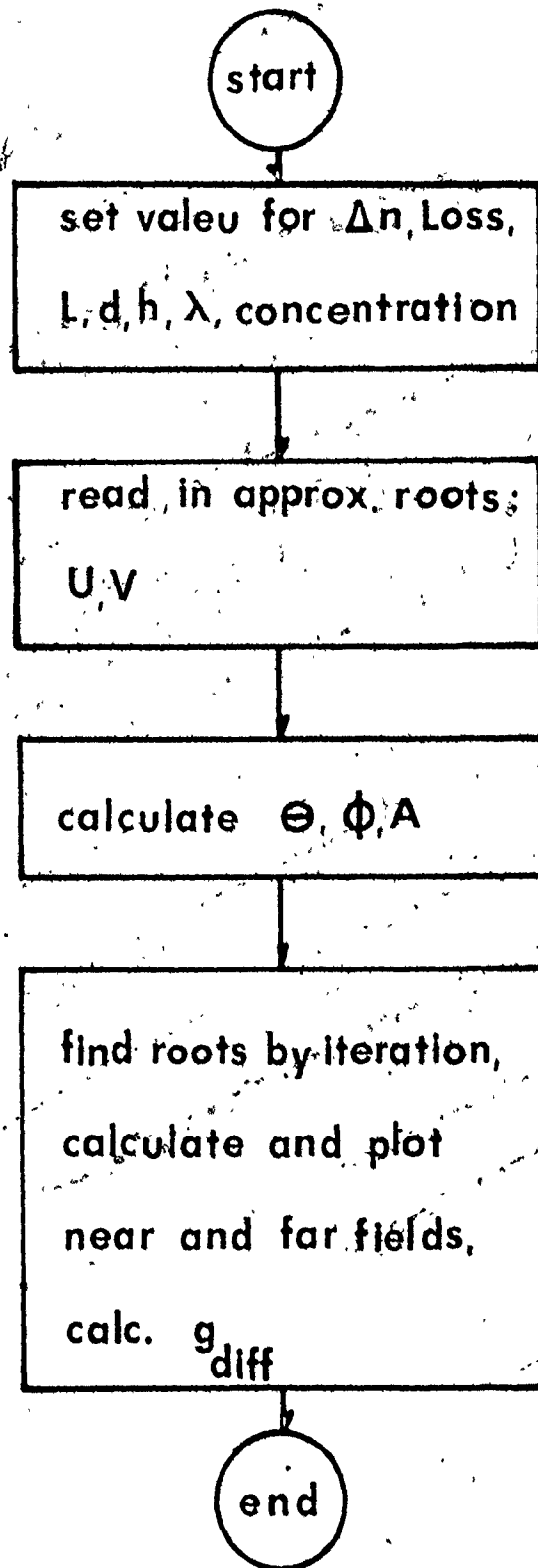
FIG. 4 -3

4.5 THEORETICAL RESULTS

In order to demonstrate the usefulness of the simple model concerning the amplification of the ASE in a thick cell, which was presented in the preceeding section, we present here some results for some particular values of the parameter involved corresponding to actual experimental conditions. In the next section, we will present experimental results and compare them to the theoretical results in order to evaluate the model. Figure 4-4 shows the near field intensity across the cell, for a cell thickness of 300 microns, a rhodamine 6G/ethanol concentration of 2.0×10^{-3} M, and a peak wavelength of the emitted radiation of 5930 Å. The absorption loss of the dye solution in the unpumped region is 0.092 cm^{-1} and the index step Δn is given by $2n\Delta n = -1.0 \times 10^{-4}$, where n is the index of refraction for ethanol (n = 1.359). It can be seen that the field propagates both inside the pumped region d (d is the absorption length at the wavelength of maximum absorption which is 5300 Å for the rhodamine 6G solution) and outside the pumped region. This is because the absorption losses at the peak wavelength are relatively small and the cell thickness of 300 microns is not very large compared to the pumped region length of 42 microns. The effect of the cell thickness on the near field distribution is shown in figure 4-5, where we have kept all the other parameters the same except the cell thickness, which now is 1750 μ. It can be seen that the peak intensity in the unpumped region is smaller than the intensity in the pumped region and also decreases towards the centre of the cell. Similar results are obtained for the case of increased losses experienced by the field for a cell length of 300 microns.

Fig. 4-4. Normalized intensity of the ASE across the cell. The cell
thickness is 300 μm, the index step Δn is given by $2n\Delta n$ =
-10^{-4}, the peak wavelength is 5930 $\overset{\circ}{A}$ and the absorption
loss is 0.092 cm^{-1}. The rhodamine 6G concentration is
2.0×10^{-3} mole/litre.
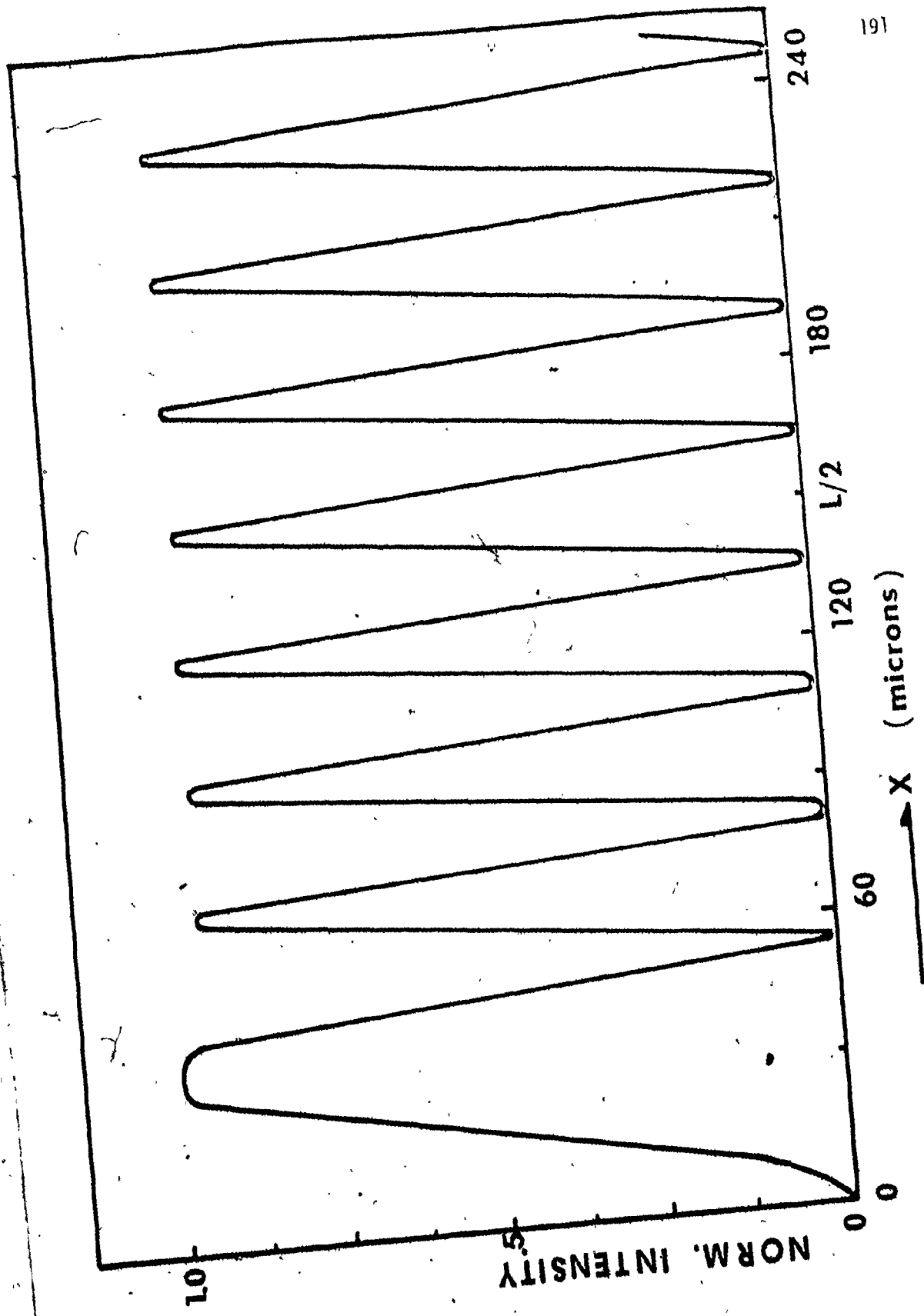
FIG. 4-4
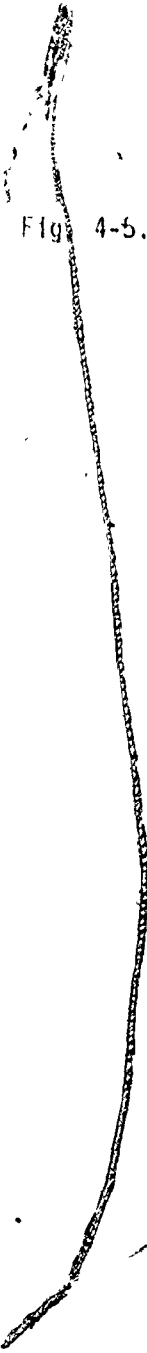
Fig. 4-5. Normalized intensity of the ASE across the cell. The cell thickness is 1750 μm, the width of the index step is 42 μm, the index step Δn is given by $2n\Delta n - -10^{-4}$, the peak wavelength is 5930 Å and the absorption loss is 0.092 cm^{-1}. The rhodamine 6G concentration is 2.0×10^{-3} mole/litre.

L=.175 cm

NORM. INTENSITY

X (microns)   120   240

FIG. 4.-5

192
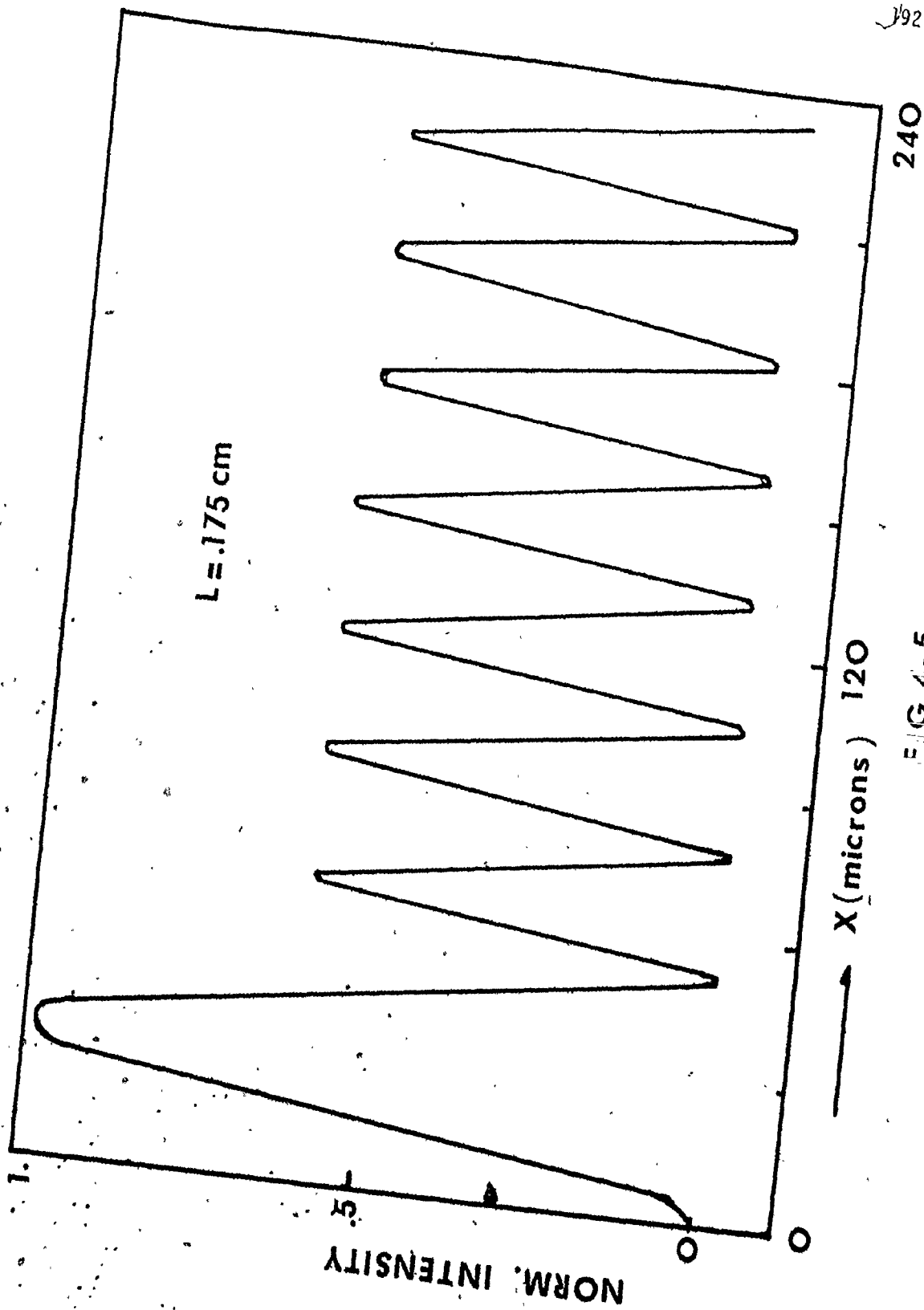
Of course, the combination of high losses and increased cell thickness is going to enhance the propagation of the field within the gain region and eventually confine it to that region completely for this particular index step.

We have seen in section 4-3, equations (4-17) and (4-28), that it is possible to calculate the gain required to overcome the diffraction losses for given index step and losses in the unpumped region for a particular cell thickness. Consequently the solution for a particular case provides us with values for the u, v, $\bar{k}$, s defined in equation (4-24) and values for the gain needed to support the different spatial modes of propagation. The gain is given by the relation

$$g_{diff} = (2\bar{k}u)/(\frac{2\pi n d^2}{\lambda}) \qquad (4-37)$$

which is obtained by combining equations (4-17) and (4-28). This gain is the absolute minimum gain required (and we will call it the diffraction gain, because of the familiar diffraction term appearing in the denominator) and any additional gain is going to be used to amplify the spontaneous emission. For the case shown in figure 4-4, a g_{diff} of 0.2 cm^{-1} is calculated and for the case of figure 4-5 a gain of 0.9 cm^{-1} is needed to establish the spatial mode. This reflects the fact that more energy is lost by the field travelling in a thick cell outside the gain region and this increased energy loss has to be supplied by increased gain in the gain region. In the geometrical ray approximation, the losses are higher in the thick cell because the light has to propagate (in its zig-zag way) for a longer distance within the unpumped loss region.

The far field distribution shown in figure 4-6 corresponds to the near field of figure 4-4. It can be seen that the far field deviates from the cell axis by an angle of 0.6° for this particular case and consists of two symmetrical beams about the cell axis. The far field for the thick cell which corresponds to figure 4-5 is of similar nature with much less rattling around the axis which is due to the very many cycles of the near field inside the unpumped region. The far field angle for the thick cell (1750 μm) is 0.65° indicating the fact that the far field is mainly determined by the index step, which is kept constant for the two cases, since the concentration is kept constant. It is, of course, expected that both near and far fields will depend on the index of refraction step. Figure 4-7 shows the variation of the far field angle (which measures the deviation of the far field from the cell axis) against the change of the index step. For this particular case, the concentration is 1.5×10^{-3} M rhodamine 6G/ethanol, the absorption loss at 5930 Å is 0.04 cm^{-1} and the cell thickness is again 300 μm. It can be seen that the far field angle varies nearly linearly over the region of interest pertinent to our experimental situation (0.4° to 0.65°) which is treated in the next section.

On the same graph we have plotted the far field angle for the cases in which the absorption depth of the pumped radiation is reduced by a factor of 1.15 and 1.33 (corresponding to d = 56 μm, 48 μm, 42 μm). It can be seen that the variation of the far field angle is relatively small over the region of interest to our experimental situation. Then, to a first approximation, this far field angle can be used as a compari-

Fig. 4-6. Far field intensity against the far field angle. The cell
thickness is 300 μm, the width of the index step is 42 μm,
the index step is given by $2n\Delta n = -10^{-4}$. This far field
corresponds to the near field of figure 4-4.

L=.003 cm

NORM. INTENSITY

FAR FIELD ANGLE (degrees)
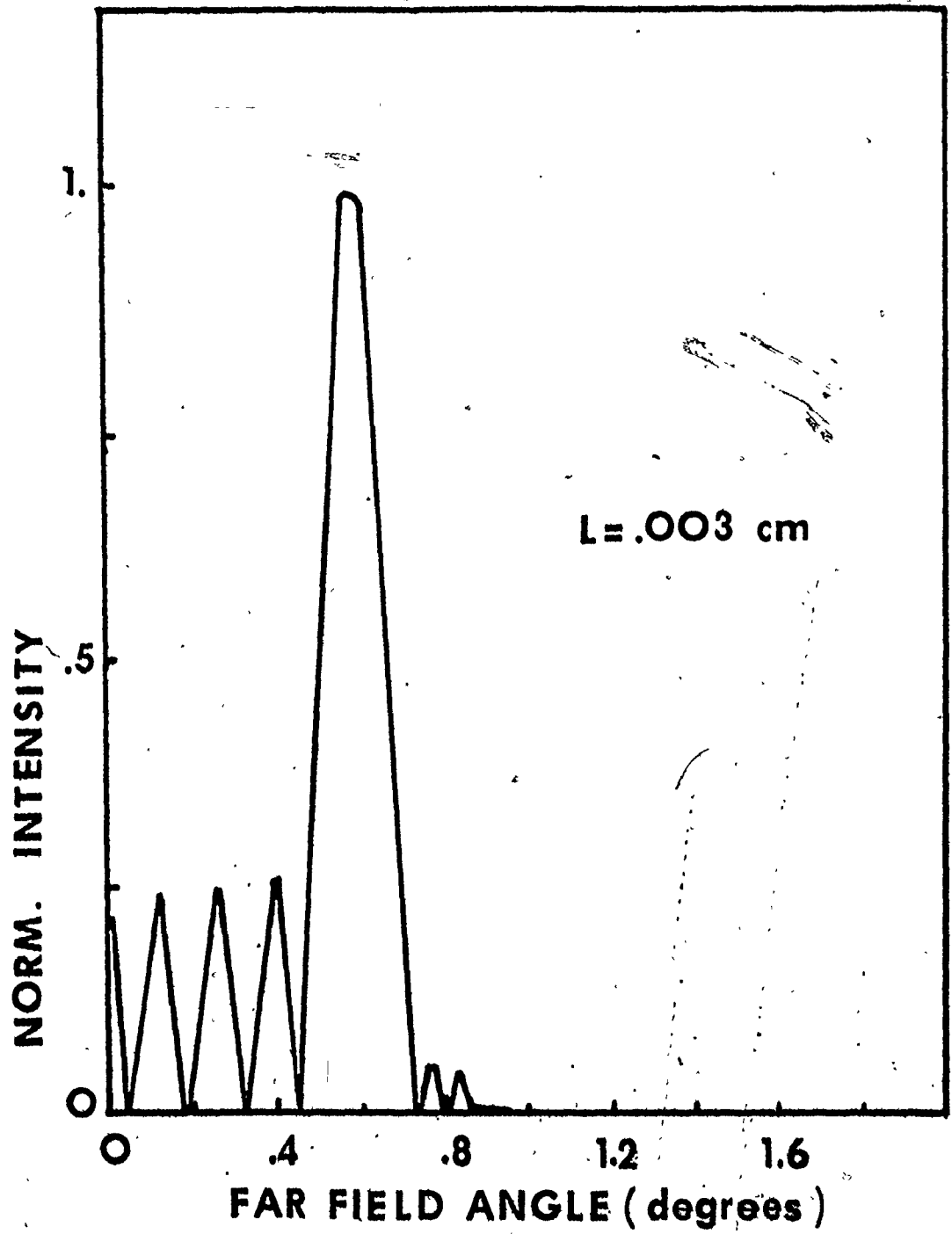
FIG. 4-6

Fig. 4-7. Far field angle against the index of refraction step size for three different values of the width of the index step. The cell thickness is 300 μm, the concentration of rhodamine 6G is 1.5×10^{-3} mole/litre and the absorption loss in the unpumped region is 0.04 cm^{-1} at $\lambda = 5930$ Å.

FIG.4-7

196
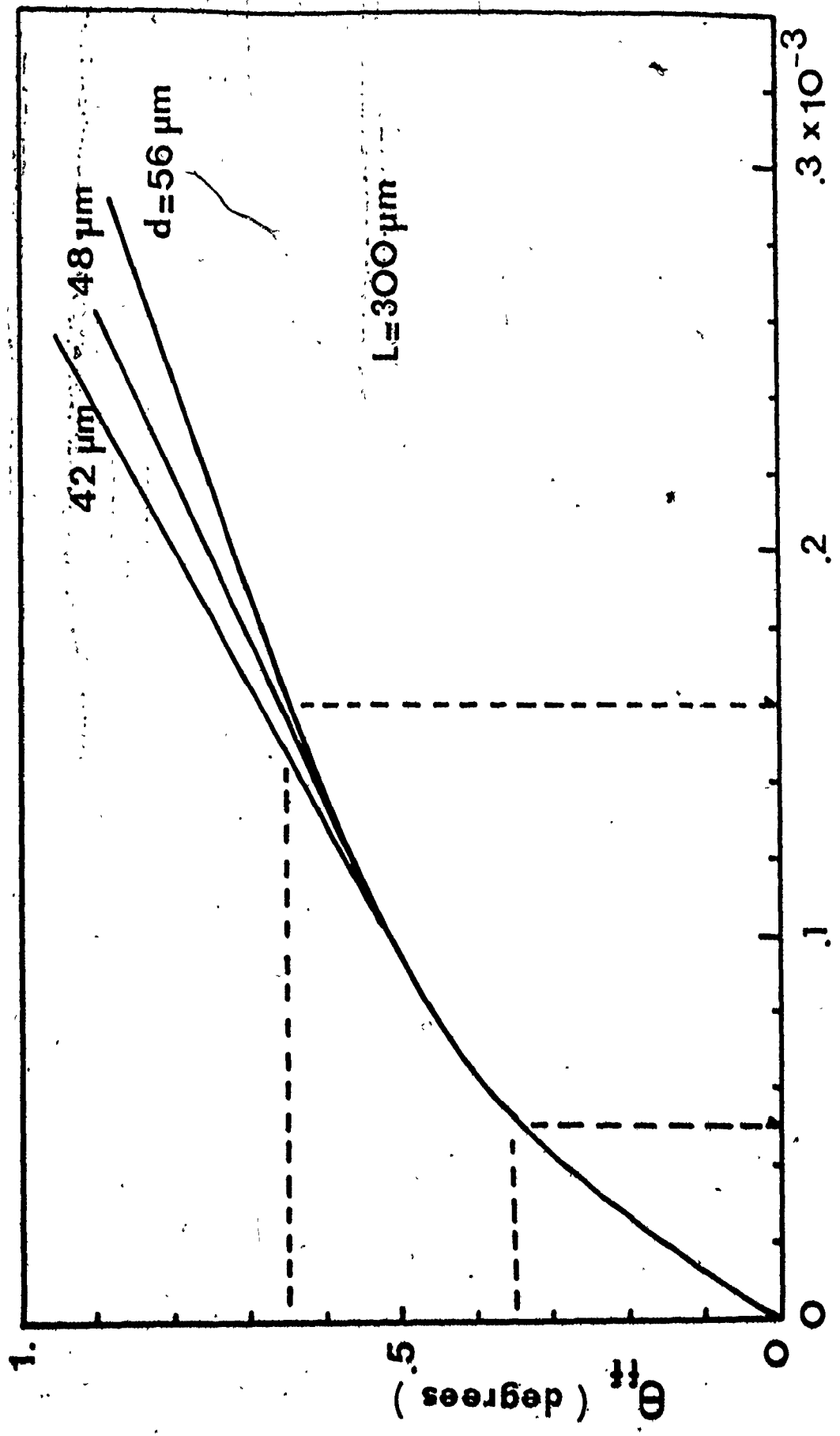
son between theory and experiment, without treating the absorption length as a parameter. A more precise treatment would require a detailed comparison of the experimental and theoretical near field distributions. However, it proved extremely difficult to obtain good near field patterns to do this comparison in order to determine the exact value to be used for the parameter d. Consequently, we will treat the approximate case of fixed d, but we will see that even this approximation gives a very good prediction for the index step range and the temperature variation of the dye material, when excited by a flashlamp pump.

Figure 4-8 shows the variation of the required gain to sustain the spatial modes versus the losses in the unpumped region for a particular index step Δn ($2n\Delta n = -1.0 \times 10^{-4}$) and a concentration of 1.5×10^{-3} M of rhodamine 6G/ethanol in a 300 μm cell width. It can be seen that the gains required are readily available in the case of flashlamp pump dyes as we have seen in the previous chapter. It should be noted here that the far field angle was relatively insensitive to moderate change of the absorption losses in the unpumped region and with a value around $0.53°$. For the 1.5×10^{-3} m/l concentration we have found that the peak wavelength, for gains of the order of 0.8 cm^{-1}, is around 5930 $\overset{o}{A}$, which corresponds to an absorption loss of 0.04 cm^{-1} ($\sigma_{01}^a = 0.352 \times 10^{-9}$ cm^2 from Appendix A) and $g_{diff} = 0.15$ cm^{-1} from figure 4-8. It was emphasized in Chapter Three that in order to get accurate gain measurements by using the narrowing of the output intensity versus pumping, a uniform pumping profile is required across the cell. It is then clear from figure 4-8 that any gain measurement with a non-uniform pumping across the cell will

Fig. 4-8. Diffraction losses against the unpumped region absorption
losses for a cell width of 300 μm, an index step size given
by 2nΔn = -0.1 x 10^{-3} and a width of the index step of
56 μm.

FIG. 4-8

Plot of g_{diff} (1/cm) versus LOSS (1/cm), with parameters $L = 300\,\mu m$, $d = 56\,\mu m$, $2n\,\Delta n = .1 \times 10^{-3}$
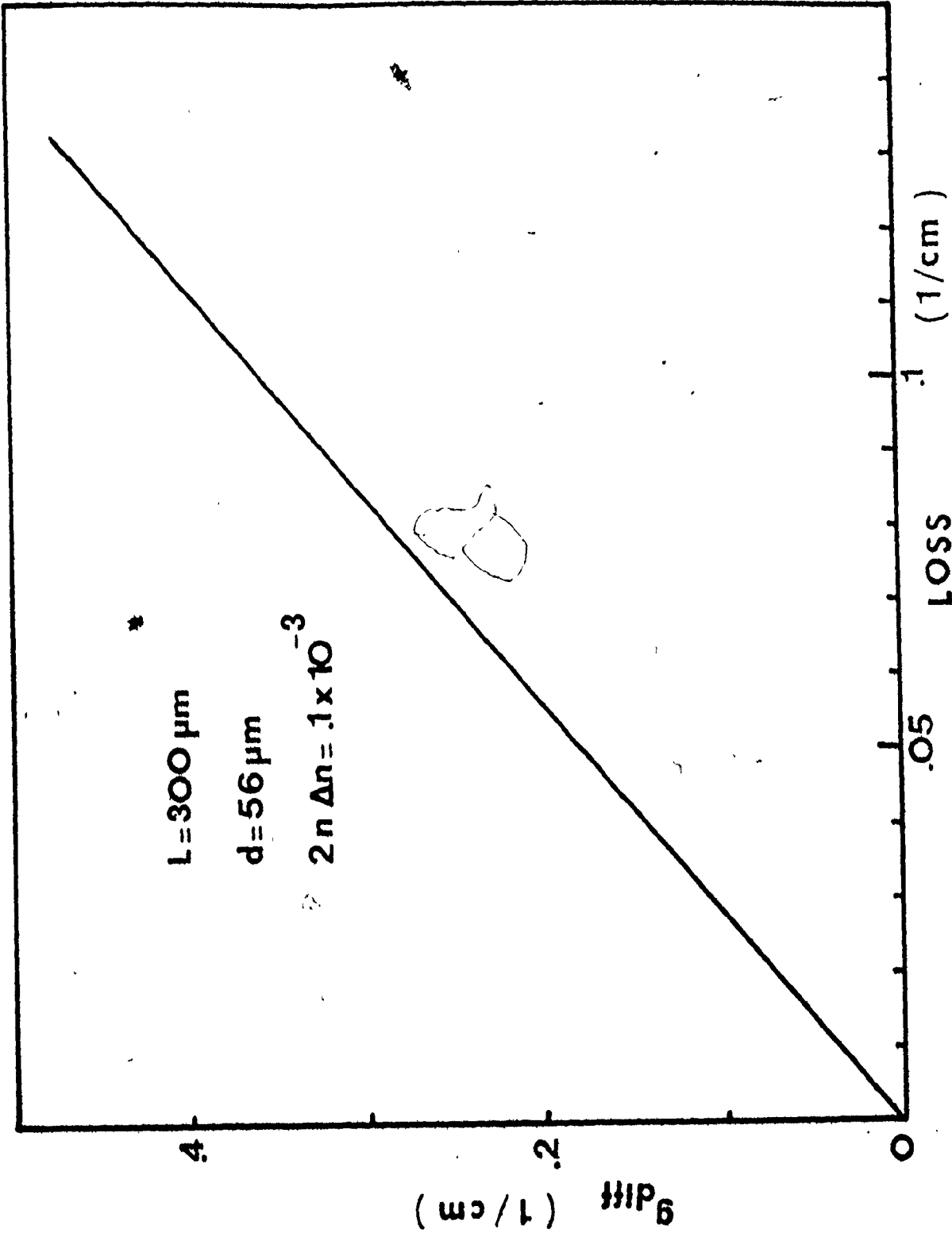
introduce considerable error (It is the product of loss times the cell
thickness, which is of importance in determining the required g_{diff}
and here we changed the product by changing the loss, which is equivalent
to keeping the loss constant for a particular concentration and changing
the cell thickness). In the next section we will present our experimental
data related to narrowing in a thick cell, the effect of concentration on
narrowing and also far field angle data in conjunction with calculations
(based on the theory presented with respect to the spatial modes) and
determine values for the index step and consequently the temperature rise
of the pumped region of a thick cell.

4.6 EXPERIMENTAL RESULTS

It was mentioned before that accurate measurement of the available gain requires a uniform pumping cross-section. Frequently, however, dye cells are used which are thick with respect to the absorption length. It is natural then to try and investigate the behaviour of the dye amplifier under practical thick cell conditions. Some of the results obtained are presented here along with useful comparisons with the results calculated from the model of the spatial mode distribution, which we developed earlier.

Figure 4-9 shows the narrowing of the output intensity versus pumping for a cell of 300 µm thickness and two different concentrations. On the same graph we also present the narrowing versus pumping for a cell with uniform absorption across the cell for comparison. It can be seen that for low pumping the thin cell exhibits more narrowing than the thick cell, because there are no diffraction losses and all the gain is used for narrowing. For higher pumping, though, the intensity of the ASE is so high that it saturates the available gain and the narrowing decreases very slowly with pumping. On the contrary, in the thick cell further narrowing can be obtained at high pumping because now some of the ASE propagates outside the gain region keeping the intensity in the gain region lower than before. This means that there is less saturation of the gain for the same pumping than before and consequently more narrowing can be achieved. This is evident in Figure 4-9 for pumpings of 300 and above. Increasing the concentration to 4.0×10^{-3} mole/l in the thick cell will cause the gain region to decrease and the diffraction losses to increase resulting in smaller spectral narrowing for pumping below 300 and more narrowing for high pumping above 300 as we can see in Figure 4-9 (because the intensity of the ASE is still well below the saturation point).

Fig. 4-9. Spectral narrowing of the ASE (FWHM) against pumping for two cell widths of 70 μm and 300 μm and two different concentrations of 1.5 x 10^{-3} mole/litre and 4.0 x 10^{-3} mole/litre.

PUMPING (arb.units)
FIG. 4-9

$\Delta \lambda$ (Å)

201
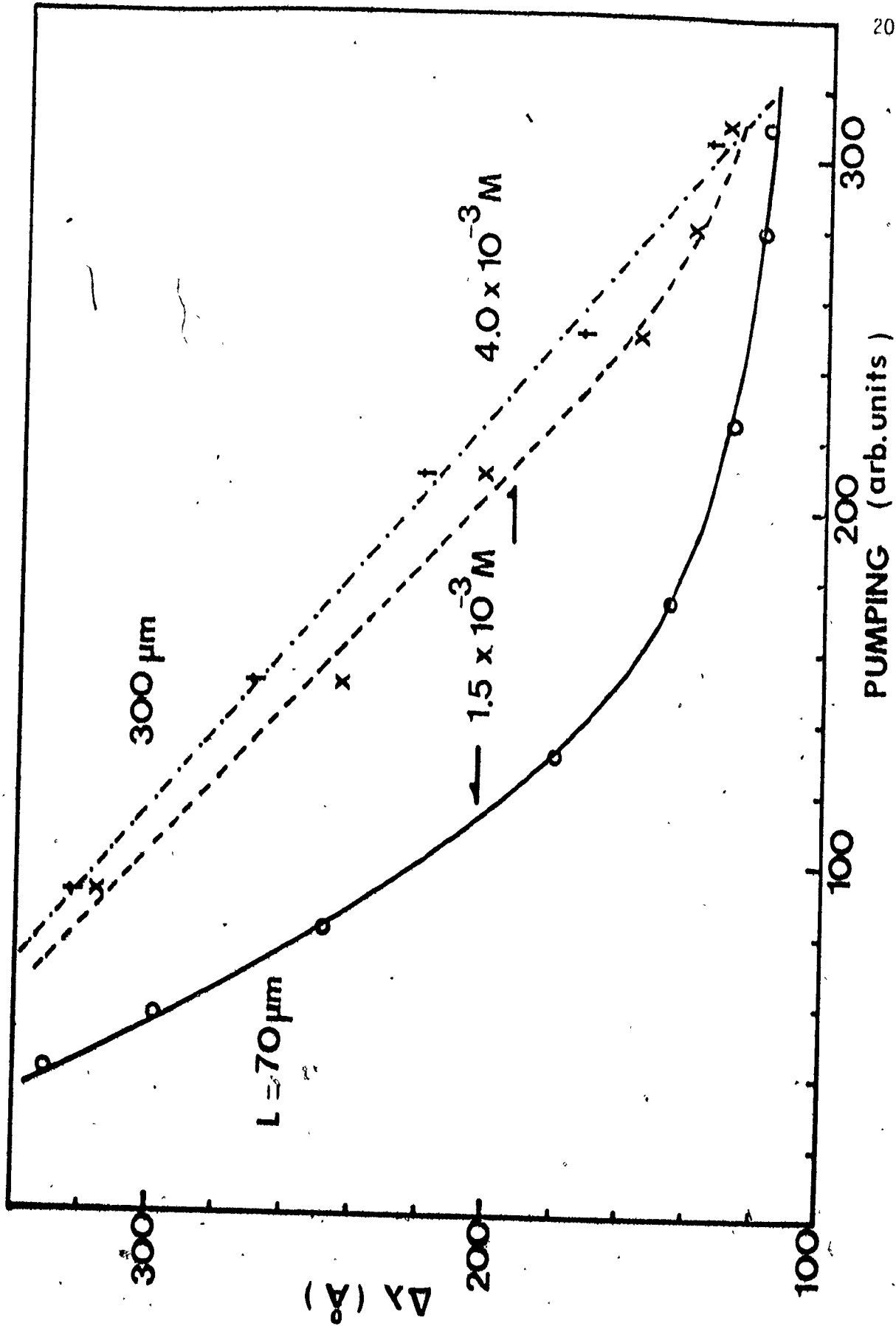
For low and medium pumping the narrowing is smaller than the one corresponding to 1.5×10^{-3} mole/l, because the diffraction loss change is larger than the increase of the gain due to the concentration change; but for high enough pumping more narrowing can be achieved than before, because of high gains available and low intensities in the gain region. In other words, the introduction of losses (either absorption in the unpumped region or diffraction losses) keep the intensity of the ASE in the gain region low with respect to the saturation intensity and consequently high gains can be achieved with high pumping and thus more narrowing than before. It should be noted here that there is, of course, an upper limit in the concentration to be used which is determined by either the roughness of the cell surface (which becomes crucial when it is of the same order as the absorption length) or the formation of dimers from the dye molecules. These dimers can have absorption bands in the emission band of the monomers and their formation also lessens the number of the available molecules.[2] It is then clear that for a particular cell thickness and pumping there is a specific concentration which will give the narrowest spectral output intensity. This is shown in figure 4-10 for a cell of 300 microns and a pumping which corresponds to the saturation region for the 70 μm cell and 1.5×10^{-3} mole/l (I_p ≈ 210 in figure 4-9). It can be seen that a limit in narrowing of 175 Å can be achieved with a concentration of approximately 3×10^{-3} mole/l. This limit is still higher than the one we can achieve with the same pumping and a thin cell, which is about 130 Å. This result is consistent with the argument with respect to narrowing in thick cells presented above, because the pumping used is not high enough to supply sufficient gain, and higher

Fig. 4-10. Spectral narrowing of the ASE (FWHM) against concentration of rhodamine 6G for a particular pumping $I_p = 210$ of figure 4-9. The cell width is 300 μm and the length is 18.2 cm.

$I_p = 210$
$L = 300 \mu m$

ΔY (Å)

300

200

100

0.2   CONCENTRATION   1.0   (mole/l)

5.0 x 10⁻³

FIG.4-10

203
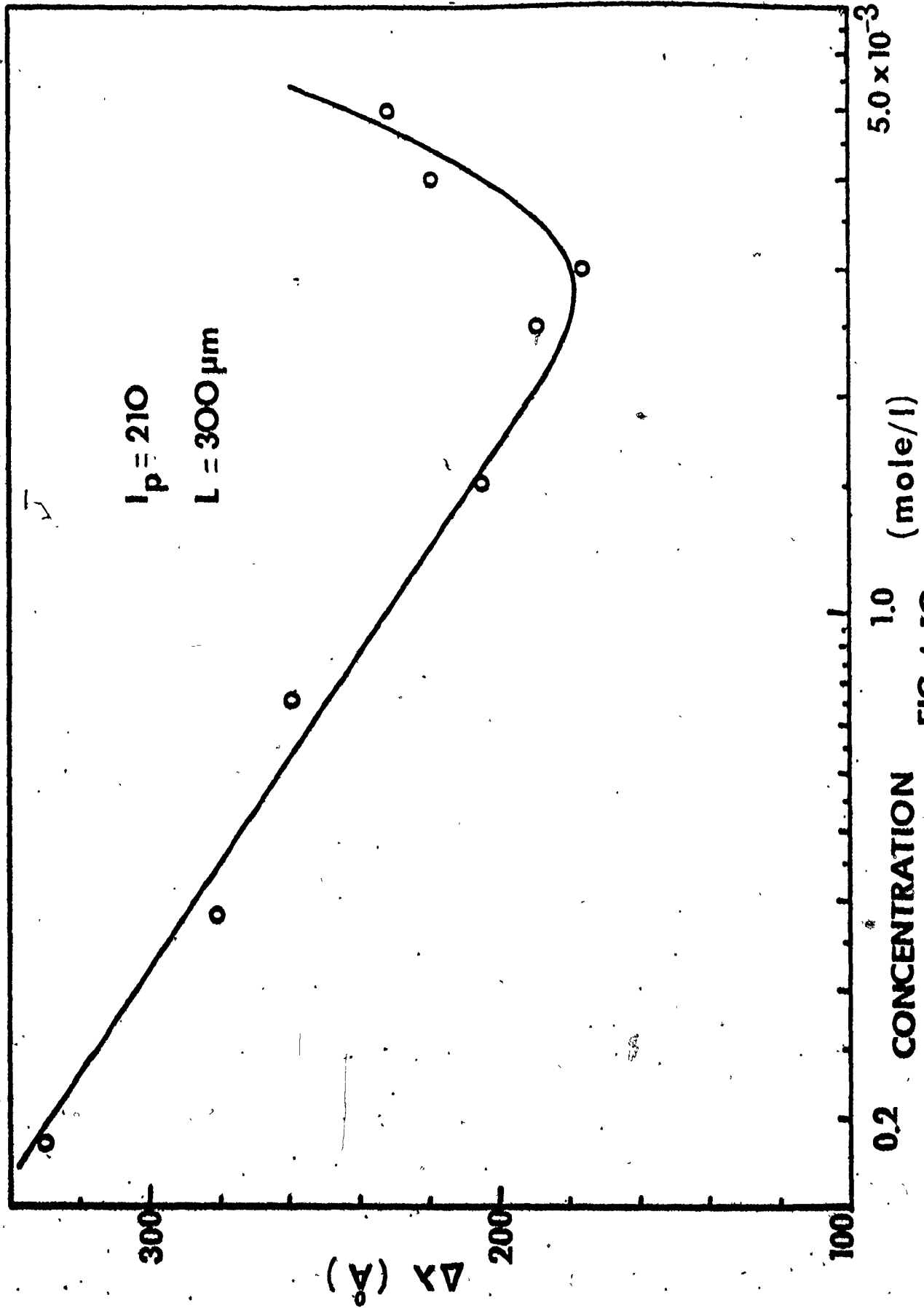
pumping will certainly give a narrowing below 130 Å.

Figure 4-11 shows the variation of the peak wavelength of the ASE versus concentration for the same conditions of pumping (I_p = 210) and cell thickness (300 microns) as in figure 4-10. It can be seen that a .wavelength tuning of over 250 Å can be easily achieved and though the spectral width itself is not very small a wavelength dependent loss (such as a diffraction grating) can greatly increase the narrowing.

Figure 4-12 shows the effect of cell thickness on narrowing of the ASE over the available pumping range for a fixed concentration of 1.5×10^{-3} mole/l of rhodamine 6G in ethanol. It can be seen that the spectral narrowing of the ASE decreases with respect to the cell thickness increase for low or medium pumping. Again, increase in pumping will certainly produce more spectral narrowing of the ASE for the thick cells. It should be noted here that as we have concluded from figure 4-8 a thicker cell will require a higher g_{diff} to sustain the propagation of spatial modes in the cell and thus less gain is left to amplify the spontaneous emission. Alternatively, in the geometrical ray-approximation of travelling of the ASE, the zig-zag travelling light will encounter less gain medium to contribute to its narrowing. Consequently, we have less narrowing as the thickness increases for pumpings below or near the saturation region of the thin cell case.

As was mentioned before, the distribution of the far field is directly related to the near field distribution, which in turn depends on the index step produced mainly by the heating due to the non-radiative transitions for a particular concentration and cell thickness. It is then natural to investigate the behaviour of the far field with respect

Fig. 4-11. Peak wavelength of the ASE against the concentration of
rhodamine 6G/ethanol for a particular pumping $I_p = 210$
of figure 4-9. The cell width is 300 μm and the cell
length is 18.2 cm.
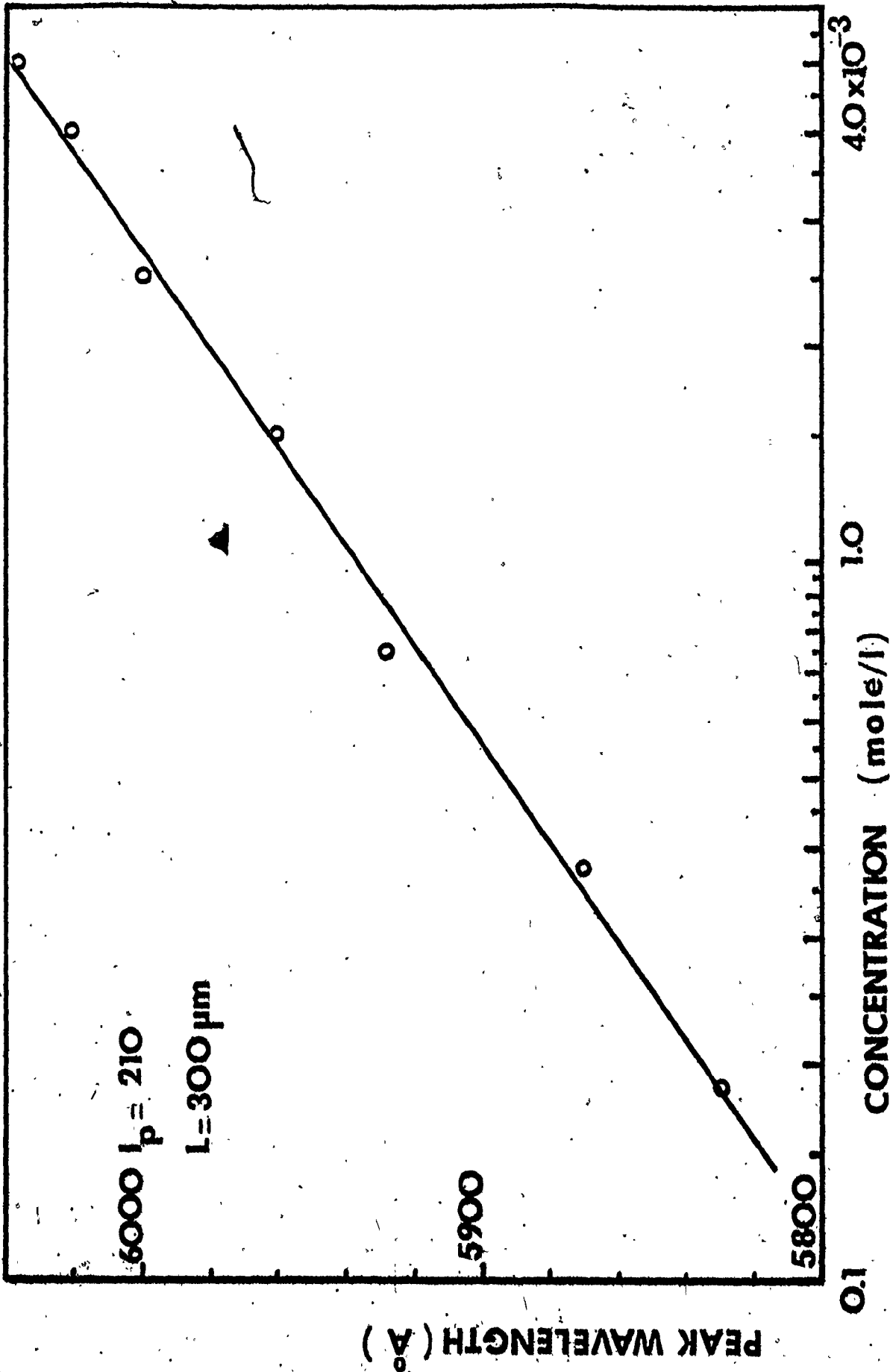
FIG. 4-11

Fig. 4-12. Spectral narrowing of the ASE (FWHM) against pumping for three different cell widths. The concentration of rhodamine 6G is 1.5×10^{-3} mole/litre. The cell length is 18.2 cm.
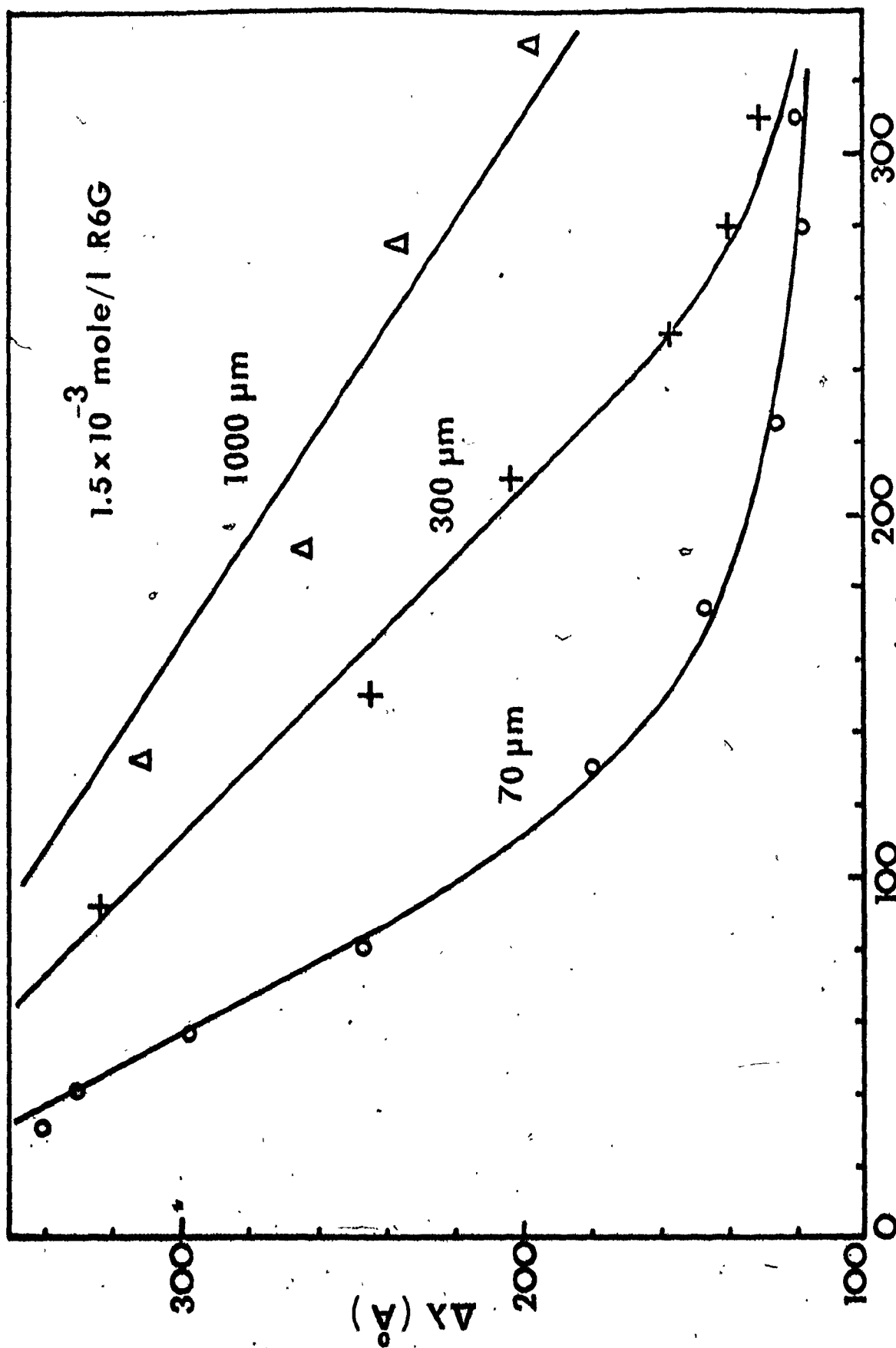
FIG.4-12

to concentration and index step. Our aim is to establish primarily a way to measure this index step and also estimate the gain from the observed narrowing. Figure 4-13 shows the measured far field angles versus pumping for several concentrations and for a particular cell thickness of 300 μm. It can be seen that for very low concentration the far field angle and its change are relatively small reflecting the fact that the temperature increase is smaller because the heating is spread over a larger volume. For relatively high concentration and high pumping the far field angle varies rapidly up to values as high as 1°. It is possible to match the experimentally measured far field angle in a particular case to the far field calculated by our theory to determine the index step value. Once we know Δn for a particular case we can use this as a calibration, which allows us to find Δn for any concentration and pumping. The accuracy of this calibration can be tested by comparing far field angles predicted in this way with those measured experimentally. Next we use the technique described above to determine the index step and test the accuracy of the predictions of the theory.

Figure 4-14 shows the far field angle against the scaled pumping for a particular concentration (1.5×10^{-3} m/l) measured experimentally and the far field angle against the index step calculated according to our model for a cell of 300 micron thickness, the same concentration, a peak wavelength of $\lambda_0 = 5930$ Å and an absorption loss of 0.04 cm^{-1} (corresponding to the wavelength λ_0). It can be seen that the far field angle in the experiment changes from 0.35° to a maximum of 0.66° and matching this change to the predicted one gives an index step range of

Fig. 4-13. Far field angle against pumping for several concentrations. The cell width is 300 μm and the amplifying medium is rhodamine 6G.

R6G

$t = 300\ \mu m$

4×10^{-3} mole/l

3.

1.5

.75

.375

θ_{ff} (degrees)
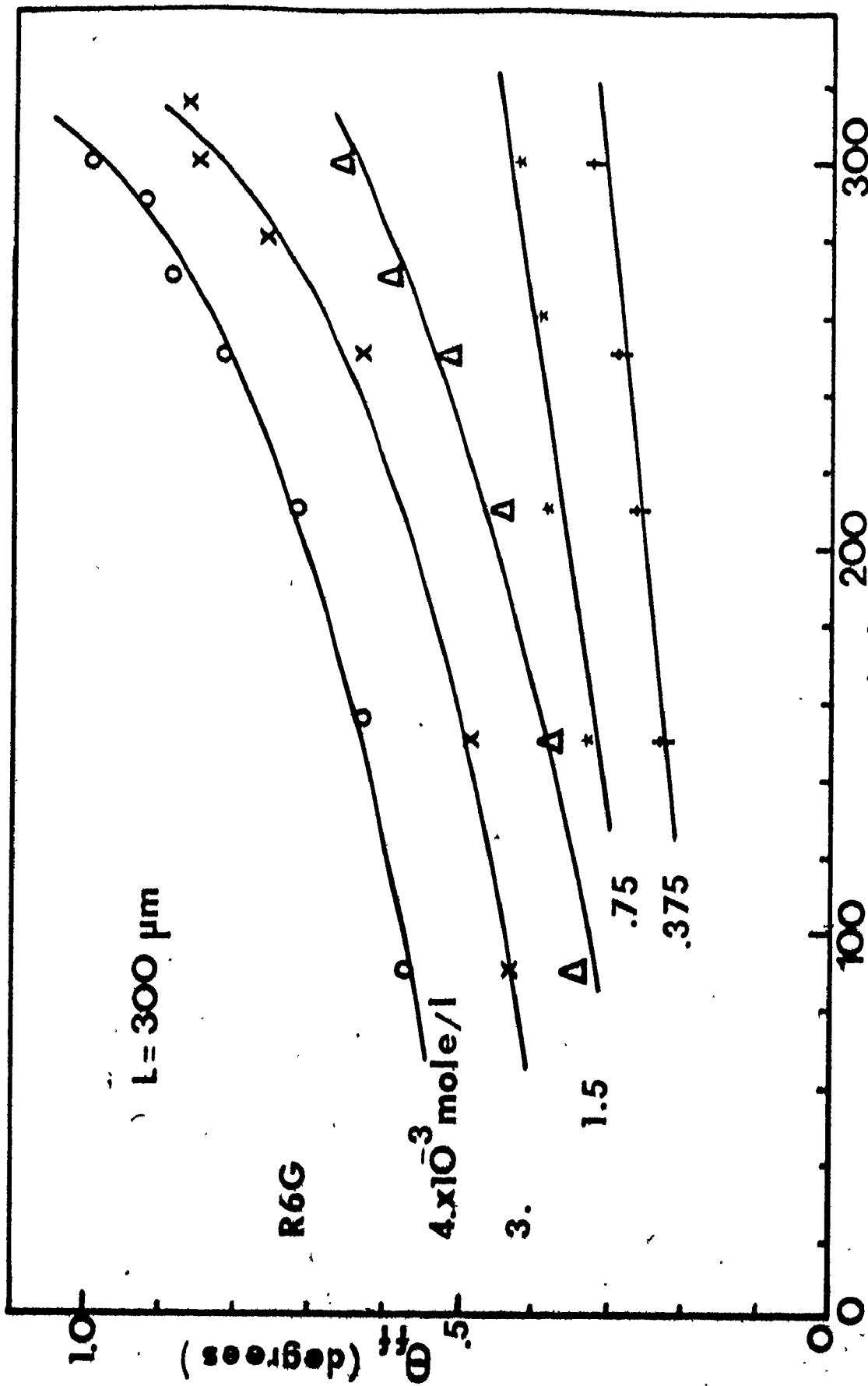
PUMPING (arb. units)
FIG. 4-13

Fig. 4-14.   Far field angle against index step size for three different
             widths of the index step (56 μm, 48 μm, 42 μm). On the same
             graph we have plotted the far field angle measured against
             pumping to get a best fit with the theory and thus callibrate
             the pumping against the index step size caused by the heating
             of the pumping.
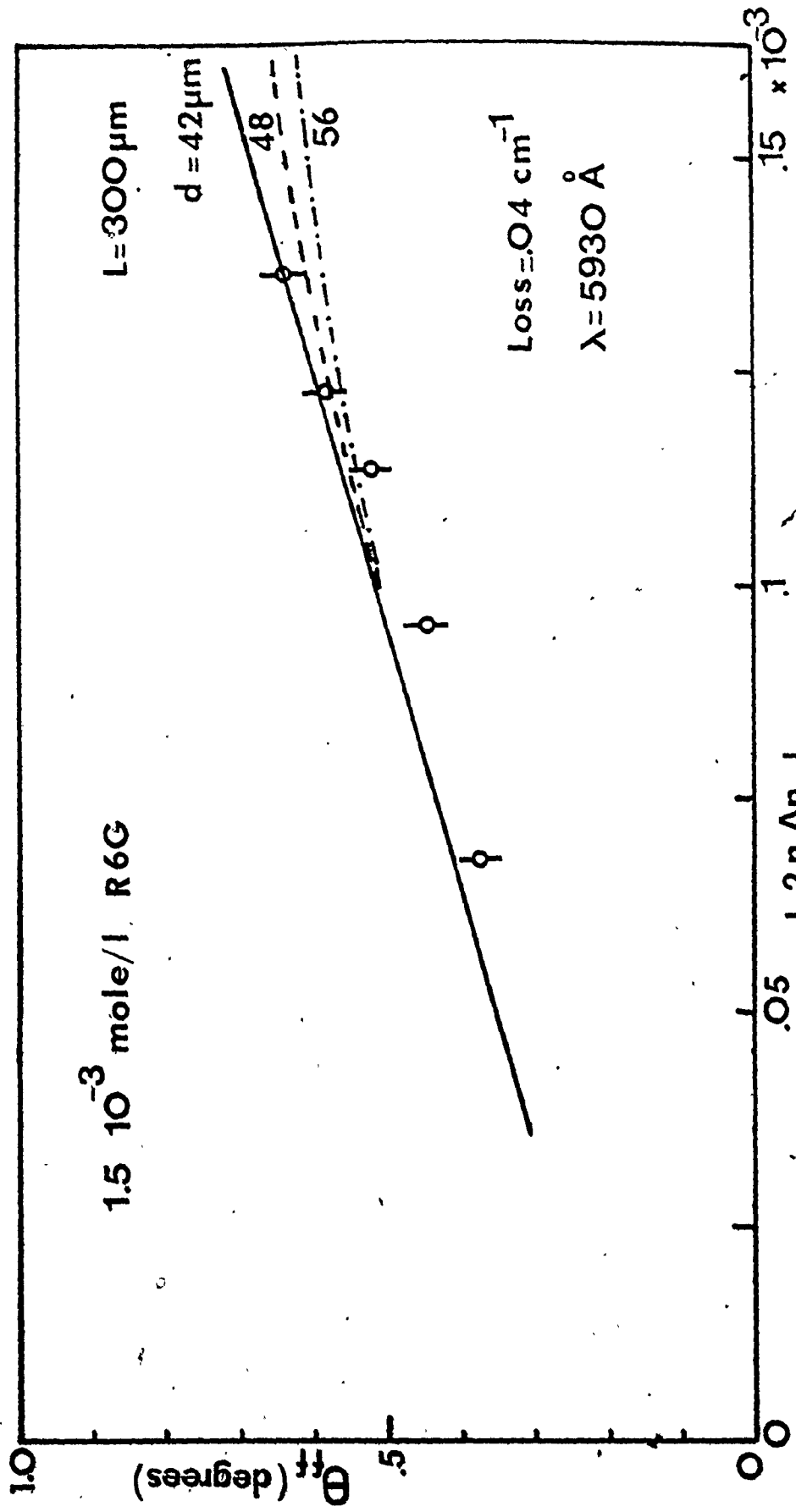
FIG. 4-14

$0.05 \times 10^{-3} \leq |2n\Delta n| \leq 0.141 \times 10^{-3}$ (where n is the index of refraction at room temperature, taken to be equal to 1.359). Slight adjustment of the parameter d will certainly change the range somewhat but in the first approximation, in the medium or low pumping regions, we will have a small change as we can see from the plots for index step widths of 56 μm, 48 μm and 42 μm in figure 4-14. Nevertheless, the knowledge of the index step magnitude gives us the temperature increase. According to the last of the equations (4-10) we have for the ethanol at room temperature:

$$\frac{\Delta n}{\Delta T} = -4.0 \times 10^{-4}\,^{\circ}K^{-1}$$

Then for the observed index step range of

$$1.8 \times 10^{-5} \leq |\Delta n| \leq 5.2 \times 10^{-5}$$

we have a temperature increase range of

$$0.05^{\circ} \leq \Delta T \leq 0.13^{\circ}K$$

It is possible to compare this value of ΔT with the predicted value of Balucani and Tognetti.[49] Using their results, and scaling appropriately for a cell thickness of 300 microns, a concentration of 1.5×10^{-3} mole/l and a pumping pulse risetime of 1.5 μsec we get a temperature increase near the cell walls of $\sim 0.18^{\circ}$. This value is somewhat higher than the one we have calculated because they use a flashlamp blackbody spectrum extending from 3000 Å to 5700 Å when they calculate the temperature increase. However, in our experimental situation we use Wratten filters to block the UV radiation from reaching the dye solution. Consequently, they have some additional pumping from the UV part of the spectrum and

therefore more heating as well. Additionally, Balucani and Tognetti[49] have not accounted for the losses of the reflectors, which project the light from the flashlamp onto the dye cell.

Next, we use the index step we have already determined to test the accuracy of the calibration mentioned before. Accordingly, for concentrations of 3.0×10^{-3} m/l and 4.0×10^{-3} mole/l (which have peak wavelengths of 5940 Å and 5980 Å, absorption losses of 0.57 cm^{-1} and 0.52 cm^{-1}, correspondingly) and for the highest pumping available, we have index steps of $2n\Delta n = -0.282 \times 10^{-3}$ and -0.376×10^{-3}, respectively. These index step values have been scaled appropriately to take account of the effect of the concentration on the index step width. From our theory we have calculated far field angles values of 0.86° and 1.08° for the two concentrations. Experimentally we have measured far field angle values of 0.83° and 1.0° for the two concentrations, which agree within 8% with the predicted values from the theory. This strongly supports the accuracy of the measured index step.

It was mentioned before that our model for the propagation of the ASE in thick cells can predict the least gain (equation (4-37)) required to establish the propagation of the lowest loss mode in the system. Figure 4-15 is a plot of this gain, g_{diff}, against $2n\Delta n$, where Δn is the index of refraction step and n is the index itself. A cell thickness of 300 μm, a concentration of 1.5×10^{-3} mole/l is used with a loss of 0.04 cm^{-1} at 5930 Å. It can be seen that the g_{diff} varies quite rapidly with the index step change and for the index step corresponding to our highest pumping available g_{diff} is approximately equal to 0.4 cm^{-1}. The accuracy

Fig. 4-15. Diffraction losses against the index of refraction step size

for a cell length of 300 μm, a width of the index step of

56 μm, a concentration of rhodamine 6G of 1.5×10^{-3} mole/litre

and an unpumped region absorption loss of 0.04 cm^{-1} at 5930 Å.

Figure parameters:

$L = 300\,\mu m$

$d = 56\,\mu m$

$Loss = .04\ cm^{-1}$

$\lambda = 5930\ \overset{\circ}{A}$

$1.5\ 10^{-3}$ mole/l R6G

Y-axis: g_{diff} (cm^{-1})
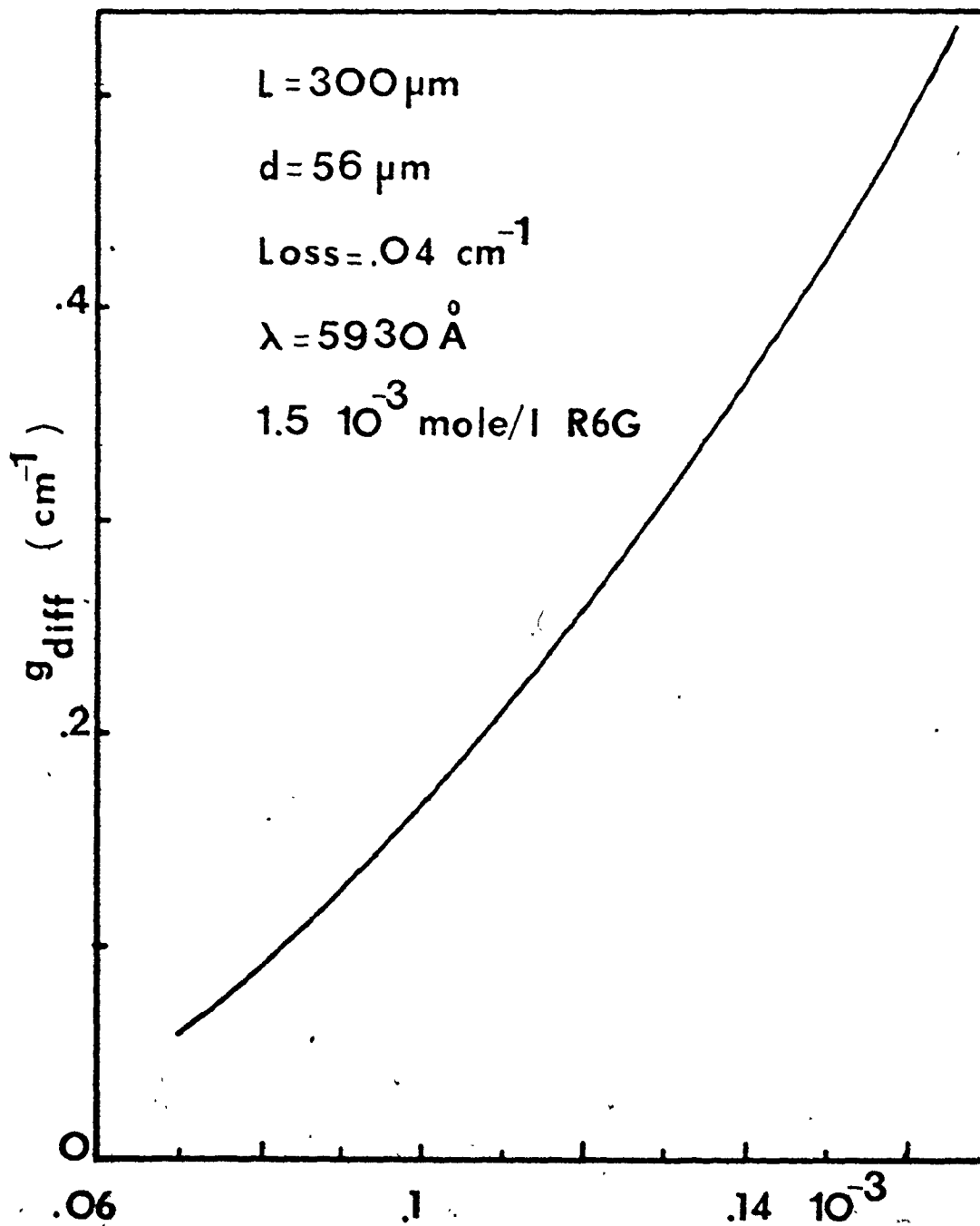
X-axis: $|\ 2n\,\Delta n\ |$

FIG 4-15

of the prediction can be tested experimertally. In order to do this we measure the ASE intensity against pumping, for a particular wavelength, for a thin cell (with no spatial variation of the index across the cell) and a thick cell for the same concentration. The separation of the two plots is a measure of the additional pumping needed to overcome the diffraction losses and it can be directly compared to g_{diff}, when a calibrated pump in available. The results obtained are shown in figure 4-16 along with the calibration of the pump (from Chapter Three we have found that $I_p = 180$ corresponds to an unsaturated gain of $g_0 = 0.76$ cm^{-1}). It can be seen that near the highest available pumping the two plots are separated by pumping difference which corresponds to a gain difference of 0.5 cm^{-1}, while the g_{diff} calculated is 0.4 cm^{-1}. In conclusion, our g_{diff} values give a reasonably good indication of the amount of losses involved in the thick cell and these losses are within 20% of the measured ones for the particular case investigated.

Fig. 4-16. Intensity of the ASE at a particular wavelength against

pumping for the same concentration of 1.5×10^{-3} mole/litre

of rhodamine 6G and two different cell widths of 70 μm and

300 μm. On the pumping scale we indicate the callibration

of the pumping with respect to the unsaturated gain for the

case of the rhodamine 6G of the same concentration obtained

in Chapter Three.
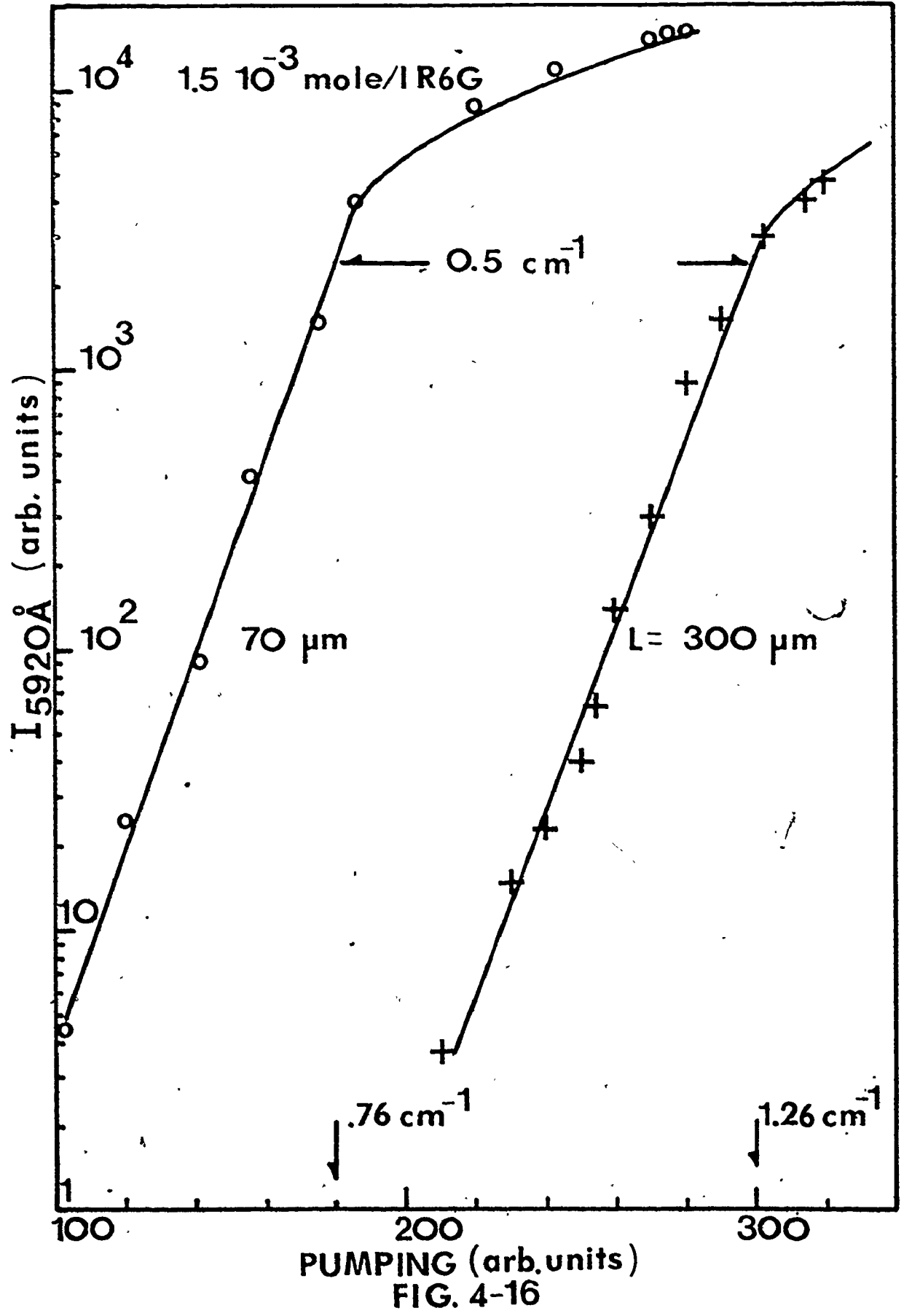
FIG. 4-16

4.7 DISCUSSION AND CONCLUSIONS

In this chapter we have investigated the propagation of the amplified spontaneous emission in a thick cell, whose width is greater than the absorption length of the amplifying medium. We have developed a model for the propagation of the ASE, which provided for the establishment of spatial modes of the field across the cell. This model predicted quite accurately the far field angle, the index step associated with the temperature increase due to the non-radiative transitions and the necessary gain needed to support such a field distribution. According to this model, the index step established at both sides of the planar cell will push some of the field outside the gain region. The exact distribution of the field depends in a complex way on the index step, its width, the losses in the unpumped region and the cell thickness. For example, high absorption losses force the field to stay mostly inside the gain region and thick cells require more gain to support the mode distribution because the field sees the loss in the unpumped region for longer distances than before. In thick cells there is a constant flow of energy from the gain region to the unpumped region and the propagation of the field partly outside the gain region affects the narrowing of the ASE. In a thin cell, with no spatial variations of the gain across it, the intensity of the ASE builds up relatively fast and saturates the gain thereby restricting the narrowing achieved. In a thick cell, part of the intensity leaks outside the gain region and this decreases the ASE intensity and thus keeps the gain unsaturated for higher pumping. As we have seen in Chapter Three, the narrowing

depends on the available gain and since in thick cells we can have much higher pumping without causing saturation we will ultimately have much more narrowing of the ASE. This is clearly demonstrated in Figure 4-9, where the narrowing of the ASE is compared for three different cell widths.

We also have investigated the effect of the concentration on narrowing for a particular cell width and pumping. We have found that for fixed pumping, there is a specific concentration, which will give the smallest narrowing of the ASE and this narrowing will be less than the one obtained in the thin cell if the pumping is not high enough. In other words, concentration, cell thickness and pumping will have to be obtimized to give a particular value of spectral narrowing in the ASE. We should mention here that there is another parameter which can be varied, namely the unpumped region absorption losses. Because of the great variety of dyes available, absorbing in regions extending from the UV to the IR region, it is possible to mix with the amplifying dye medium another combination of dyes having an absorption at the peak wavelength of the ASE. In this case both the magnitude of the absorption and its wavelength dependence will affect the propagation of the ASE and its narrowing.

The effect of the index of refraction change on the field manifests itself most unambiguously in the far field distribution and the deviation of the far field from the cell axis. We have seen that our theory predicts quite accurately the far field angle, which for flashlamp dye amplifiers can be as high as one degree. It should be noted

here that the far field we measured is to some degree integrated over time and the index step corresponds to the adiabatic heating of the dye since the duration of the pumping pulse (3 μsec) is much too short to allow any significant diffusion to take place.

A comparison of the far field angles predicted by the model with the ones measured experimentally allows the determination of the index step and consequently the temperature change, which produced it. We found that the index step due to temperature is much larger than the one due to the gain and we are thus completely justified in omitting the contribution of the latter. The temperature increase measured in this way (0.13°C) compares well with the value obtained by extrapolation from values predicted from thermal calculations reported earlier. Finally, we were able to predict from our model the shift of the intensity of the ASE versus pumping toward higher pumping when a thick cell is used instead of a thin one both with the same concentration. Additionally, we have predicted and verified experimentally the far field angle for several other concentrations from the already measured index step. We should note here that the ability to predict the far field angle and the index step is of great practical importance in the case we want to use the system as an amplifier and have an efficient coupling of the signal to be amplified into the cell.

CHAPTER 5

DISCUSSION AND CONCLUSIONS

Because we have already presented a detailed discussion in each
individual chapter, we will limit ourselves to a brief presentation of
the main achievements of this work and also discuss possible extensions
of this work to other fruitful areas of research.

In Chapter Two we dealt with the study of the ablation-type
flashlamp and the main results are as follows:

(i)   it has been shown that high-current short-pulse flashlamps can be
        characterized in a very useful way by studying their behaviour as
        a function of the specific input energy to the plasma of the
        flashtube;

(ii)   it has been shown that the radiation of these ablation-type flash-
        lamps resembles the blackbody radiation at the temperature of the
        plasma over a considerable range of input energies;

(iii)   we have extended an already existing model, which relates the
        flashlamp plasma resistivity to the discharge current, to find
        a more accurate relation between resistivity and plasma tempera-
        ture or specific input energy rate;

(iv)   we have developed a useful design criterion for determining the
        physical dimensions of the ablation-type flashlamps;

(v)   we have found the effect of the filling gas pressure on the pulse
        risetime and output intensity and also the advantage to be gained

in terms of light pulse risetime by delivering energy to the
flashlamp plasma at as high an overvoltage as possible; and,

(vi)   finally, we demonstrated experimentally that ablation-type flash-
lamps can be used to pump efficiently dye amplifiers in the
visible region.

Of course, the study of the flashlamp is far from complete and
possible areas of research could include the extension of the risetime
to lower limits than before, the repeatabilyty of the pulse output (which
is related to the initial development of the discharge), the design of
appropriate circuits to take care of the change of the flashlamp resis-
tance and inductance with time, the scaling of the flashlamps to higher
total output power, the effect of the wall of the tube on the spectrum
of the emitted light and finally the spatial confinement of the plasma,
which could produce blackbody radiation without ablation.

In Chapter Three we dealt with the amplification of the spontaneous
emission in a dye material both theoretically and experimentally. A model
for the ASE based on the rate equation approximation has been developed
for the case of dye cells with no spatial variation of the gain across
the cell. This model describes the way the ASE spectrum changes within
the dye cell and makes predictions for the emitted intensity, the narrowing
of the ASE and its peak wavelength shift with pumping. This model also
provides us with an accurate way to calculate the unsaturated gain and
demonstrates the importance of the excited single state absorption (ESSA)
in determining the exact behaviour of the ASE. The predictions of the
model have been tested experimentally and a very good agreement was found.

In particular, it was found that:

(i)   the spontaneous emission propagating in any of the two directions within the dye cell starts with a broad spectrum, which gets narrower as it propagates and its peak wavelength shifts because of the non-uniform gain profile;

(ii)   for high pumping it is possible to have a considerable variation of the excited state population along the cell which leads to considerable decrease of the gain. Accordingly, the intensity of the ASE and its narrowing are affected by this gain reduction. Most of the narrowing is done within the unsaturated region in the cell and narrowing in the saturation region continues but at a much slower pace;

(iii)   the intensity of the ASE at the end of the cell exhibits the usual behaviour with respect to pumping. There are three distinct regions present (below threshold, above threshold and saturation region);

(iv)   the spectral narrowing and the intensity of the ASE with respect to pumping can be used to find the unsaturated gain and its spectrum for a particular dye material with known parameters and cross-sections of the processes involved;

(v)   the excited singlet state absorption is very important in determining the profile of the ASE and the gain in the system. Additionally, our model can be used to predict the ESSA cross-section for other dye systems with less known parameters;

(vi)   it is possible to develop a semi-analytical approximate model,

which is independent of the characteristics of the particular ϐ
dye system, to be used in the approximate calculation of the un-
saturated gain. This approximate model assumes a Lorentzian
gain profile for a homogeneously broadened system and takes into
account the saturation effect of the gain. The predictions of
this approximate method are in fairly good agreement with the
experimentally observed values of gain and narrowing (which were
evaluated using the rate equation model) under certain conditions.

With respect to the extension of this work, future research could
certainly include the dynamic behaviour of the ASE, the laser excitation
of the dye material to achieve much higher pumping in a shorter time to
study relaxation phenomena, the introduction of wavelength tuning feed-
back elements in the system and finally the amplification of an input
signal of a given spectrum.

In Chapter Four we investigated the propagation of the ASE in a
thick cell, which exhibits spatial variation of the gain and the index of
refraction across the cell. We developed a model for the field structure
across the cell, which predicts the near and far field distribution and
the temperature variation of the dye solution because of the non-radiation
processes present in the dye molecule. Additionally, we investigated the
effect of the cell thickness and the diffraction losses on the narrowing
of the spectrum of the emitted ASE.

In particular, it was found that:

(i)   in a thick cell part of the ASE propagates outside the gain re-
        gion, because of the positive lens effect due to the local heating

of the medium. This kind of propagation introduces a certain
amount of diffraction losses (which have to be overcome before
any amplification of the spontaneous emission take place) and
also can keep the intensity of the ASE in the gain region low
with respect to the saturation intensity, which affects the pos-
sible spectral narrowing;

(ii)   the field across the cell can exhibit stable spatial modes, which
will be present in the near field, and which produce a far field
away from the axis of the cell;

(iii)   a far field angle of up to 1° can be easily produced by index
variation across the cell in an ablation flashlamp pumped dye
amplifier;

(iv)   a considerable diffraction loss is present which is especially
pronounced in the case of high pumping, high loss of the unpumped
region and high cell thickness;

(v)   the narrowing of the spectrum of the ASE can be improved by the
use of thick cells and high pumping, because the introduced losses
will keep the intensity at the gain region low with respect to
the saturation intensity. The increase of the concentration
will improve the spectral narrowing also up to the point where
cell surface flatness and formation of dimer dyes become important;

(vi)   the far field angle variation with pumping can be used to predict
the change of the index of refraction due to temperature increase.
In turn this index of refraction change can be used to make use-
ful predictions for far field angles of other cell thicknesses

and concentrations and provide estimates of the diffraction losses involved in the amplification of the spontaneous emission in a thick cell.

As far as the extension of this work is concerned, future research could include the detailed experimental investigation of the near field, which will help to further evaluate the model, a study of the coupling of a signal of specific spatial mode structure into the thick cell amplifier, the employment of high laser pumping to achieve lower limit of narrowing, the use of controllable absorbing losses to study their effect on the spectral narrowing, the use of selective loss tuning elements, the use of non-resonant feedback to enhance the spectral narrowing and finally the development of more realistic models with respect to the shape of the index of refraction profile.

In conclusion, in this work we have studied the ablation flashlamp characteristics and the amplification of the spontaneous emission both in thin cells (without any spatial variation of the gain and of the index of refraction across the cell) and thick cells. In all three areas we have developed appropriate theoretical models (which describe the behaviour of the systems involved) and verified experimentally most of the predictions of these models. This work, besides being useful in understanding the flashlamp dye amplifiers, is of great practical importance in developing dye amplifier systems appropriate to particular applications.

Rhodamine 6G Cross-Sections

WVLGTH	S0(ABS)	S1(EMISS)	T1(ABS)	S1(ABS)
CM	CM.CM	1/CM	CM.CM	CM.CM
.5600E-04	.3858E-17	.1797E+06	.3000E-16	.7020E-16
.5610E-04	.3808E-17	.1797E+06	.3150E-16	.8240E-16
.5620E-04	.3745E-17	.1779E+06	.3330E-16	.8533E-16
.5630E-04	.3646E-17	.1746E+06	.3547E-16	.8800E-16
.5640E-04	.3513E-17	.1694E+06	.3807E-16	.9000E-16
.5650E-04	.3324E-17	.1649E+06	.4067E-16	.9147E-16
.5660E-04	.3044E-17	.1596E+06	.4333E-16	.9213E-16
.5670E-04	.2634E-17	.1545E+06	.4590E-16	.9227E-16
.5680E-04	.2195E-17	.1490E+06	.4850E-16	.9187E-16
.5690E-04	.1790E-17	.1434E+06	.5107E-16	.9107E-16
.5700E-04	.1498E-17	.1377E+06	.5363E-16	.8973E-16
.5710E-04	.1258E-17	.1319E+06	.5603E-16	.8787E-16
.5720E-04	.1055E-17	.1265E+06	.5813E-16	.8560E-16
.5730E-04	.8356E-18	.1212E+06	.6000E-16	.8320E-16
.5740E-04	.7398E-18	.1159E+06	.6160E-16	.8088E-16
.5750E-04	.6199E-18	.1111E+06	.6307E+16	.7840E-16
.5760E-04	.5203E-18	.1066E+06	.6420E-16	.7600E-16
.5770E-04	.4372E-18	.1024E+06	.6520E-16	.7360E-16
.5780E-04	.3679E-18	.9863E+05	.6593E-16	.7120E-16
.5790E-04	.3107E-18	.9513E+05	.6653E-16	.6893E-16
.5800E-04	.2631E-18	.9147E+05	.6700E-16	.6693E-16
.5810E-04	.2240E-18	.8953E+05	.6740E-16	.6493E-16
.5820E-04	.1911E-18	.8563E+05	.6777E-16	.6280E-16
.5830E-04	.1631E-18	.8283E+05	.6807E-16	.6080E-16
.5840E-04	.1395E-18	.8027E+05	.6830E-16	.5893E-16
.5850E-04	.1193E-18	.7767E+05	.6850E-16	.5733E-16

.5960E-04	.1026E-18	.7533E+05	.6870E-16	.5570E-16
.5870E-04	.8856E-19	.7300E+05	.6897E-16	.5427E-16
.5880E-04	.7640E-19	.7100E+05	.6900E-16	.5283E-16
.5890E-04	.6505E-19	.6903E+05	.6910E-16	.5147E-16
.5900E-04	.5756E-19	.6720E+05	.6917E-16	.5013E-16
.5910E-04	.5055E-19	.6547E+05	.6920E-16	.4885E-16
.5920E-04	.4480E-19	.6377E+05	.6920E-16	.4747E-16
.5930E-04	.3956E-19	.6203E+05	.6917E-16	.4600E-16
.5940E-04	.3535E-19	.6040E+05	.6913E-16	.4459E-16
.5950E-04	.3181E-19	.5907E+05	.6907E-16	.4365E-16
.5960E-04	.2863E-19	.5795E+05	.6900E-16	.4285E-16
.5970E-04	.2620E-19	.5692E+05	.6890E-16	.4240E-16
.5980E-04	.2391E-19	.5592E+05	.6880E-16	.4177E-16
.5990E-04	.2214E-19	.5470E+05	.6870E-16	.4093E-16
.6000E-04	.2022E-19	.5337E+05	.6857E-16	.3987E-16
.6010E-04	.1875E-19	.5197E+05	.6840E-16	.3880E-16
.6020E-04	.1727E-19	.5073E+05	.6820E-16	.3787E-16
.6030E-04	.1609E-19	.4953E+05	.6800E-16	.3707E-16
.6040E-04	.1498E-19	.4827E+05	.6777E-16	.3613E-16
.6050E-04	.1387E-19	.4697E+05	.6750E-16	.3507E-16
.6060E-04	.1299E-19	.4560E+05	.6720E-16	.3400E-16
.6070E-04	.1225E-19	.4420E+05	.6697E-16	.3293E-16
.6080E-04	.1159E-19	.4310E+05	.6667E-16	.3195E-16
.6090E-04	.1086E-19	.4207E+05	.6637E-16	.3067E-16
.6100E-04	.1011E-19	.4093E+05	.6597E-16	.2933E-16
.6110E-04	.9667E-20	.3967E+05	.6560E-16	.2792E-16
.6120E-04	.9227E-20	.3833E+05	.6520E-16	.2640E-16
.6130E-04	.8857E-20	.3700E+05	.6480E-16	.2467E-16
.6140E-04	.8487E-20	.3573E+05	.6440E-16	.2293E-16
.6150E-04	.8190E-20	.3453E+05	.6400E-16	.2107E-16
.6160E-04	.7970E-20	.3343E+05	.6360E-16	.1933E-16
.6170E-04	.7750E-20	.3230E+05	.6313E-16	.1747E-16
.6180E-04	.7530E-20	.3100E+05	.6250E-16	.1573E-16

.6190E-04	.7307E-20	.2990E+05	.6207E-15	.1400E-16
.6200E-04	.7120E-20	.2857E+05	.6153E-15	.1240E-16
.6210E-04	.6970E-20	.2737E+05	.6107E-15	.1093E-16
.6220E-04	.6823E-20	.2620E+05	.6060E-15	.9467E-17
.6230E-04	.6713E-20	.2513E+05	.6020E-15	.8080E-17
.6240E-04	.6603E-20	.2410E+05	.5980E-15	.6747E-17
.6250E-04	.6530E-20	.2310E+05	.5940E-15	.5547E-17
.6260E-04	.6383E-20	.2203E+05	.5900E-15	.4533E-17
.6270E-04	.6200E-20	.2103E+05	.5860E-16	.3467E-17
.6280E-04	.5980E-20	.1997E+05	.5820E-16	.2533E-17
.6290E-04	.5757E-20	.1910E+05	.5780E-16	.1600E-17
.6300E-04	.5533E-20	.1827E+05	.5740E-15	.7999E-18
.6310E-04	.5310E-20	.1750E+05	.5700E-15	.2666E-18
.6320E-04	.5090E-20	.1673E+05	.5660E-15	0.
.6330E-04	.4870E-20	.1590E+05	.5620E-16	0.
.6340E-04	.4650E-20	.1500E+05	.5580E-15	0.
.6350E-04	.4467E-20	.1423E+05	.5540E-16	0.
.6360E-04	.4320E-20	.1370E+05	.5500E-15	0.
.6370E-04	.4210E-20	.1333E+05	.5460E-15	0.
.6380E-04	.4100E-20	.1283E+05	.5420E-16	0.
.6390E-04	.3987E-20	.1227E+05	.5380E-16	0.
.6400E-04	.3873E-20	.1167E+05	.5340E-16	0.
.6410E-04	.3758E-20	.1122E+05	.5300E-16	0.

```
      PROGRAM TST (INPUT,OUTPUT,TAPE5=INPUT,TAPE6=OUTPUT)
C
C     COMPUTER PROGRAM LISTING OF THE   A S S  .
C
C     THIS PROGRAM SOLVES TGE
C     THIS PROGRAM SOLVES THE COUPLED
C     RATE EQUATIONS FOR THE A.S.E.
C
      COMMON N,NN
      REAL  NMOL,N0,N1,NT,KST,II
      REAL MAXL
      REAL MAXLG
      DIMENSION STGII(1000)
      DIMENSION TTLI(82)
      DIMENSION AINT(82)
      DIMENSION II(82),SE(82)
      DIMENSION W(82),ASS(82),E(82),AT(82),S1(82)
      DIMENSION SPII(82),STII(82),SRAST(82),GMW(400),SEST1(82)
      DIMENSION STN1(2000)
      DIMENSION CSTR(16400)
      DIMENSION GMW1(200),GMW2(200)
      DIMENSION GDIF(92)
      DIMENSION DIFER(82)
      READ 1357,P,LMTJJ,GX,R,TBHIT,TRL,CONC,OF
1357  FORMAT(E10.3,I10,4F10.3,E10.3,F10.8)
      PRINT2468,P,LMTJJ,GX,R,TBHIT,TRL,CONC,OF
2468  FORMAT(1X    ,*P=*,E10.3,*  LMTJJ=*,I10,*  GX=*,F10.3,*  R=*,
     1 F10.3,*  TBHIT=*,F10.3,*  TRL=*,F10.3,*  CONC=*,E10.3,*  OF=*,
     2 F10.8,///)
C--------- READ DATA-----
C          ASS------ABS. CROSS SECTION 0-1...
C          SE(L)----EMISS. CROSS SECTION 1-0...
C          ST(L)----TRIPLET ABSORPTION CROSS SECTION.....
C ------  STARTING WAVELENGTH IN CM ----------
      STRM=5600.E-8
C------ WAVELENGTH SPACING  -----
      DL=10.0E-8
      NN=0
      READ 10,NN
10    FORMAT (I2)
C      WAVELENGTH IN CM
C        ABSORPTION      SPECTRUM
C      EMISSION SPECTRUM
C      TRIPLET SPECTRUM
C      S1  IS THE EXCITED STATE ABSORPTION
      READ11,(W(I),ASS(I),E(I),AT(I),S1(I),I=1,NN)
11    FORMAT(5F10.5)
      DO 14 I=1,NN
      W(I)=W(I)*1.0E-8
      ASS(I)=ASS(I)*1.0E-19
      E(I)=E(I)*1.0E+5
      S1(I)=S1(I)*1.0E-16 *0.8
      AT(I)=AT(I)*1.0E-17
14    CONTINUE
C
      GO TO 91929
```

```
C
CCC          THIS ROUTINE SHIFTS THE EMISSION SPECTRUM TO LONGER WAVELENGTHS.
C            BY KKLMT*10 ANGSTROM
      KKF=NN
      KKS=NN-1
      KKLMT=2
      DO 19999  KK=1,KKLMT
      KOKLM=NN-1
      DO 18888 KCK=1,KOKLM
      E(KKF)=E(KKS)
      KKF=KKF-1
      KKS=KKS-1
18888 CONTINUE
      KKF=NN
      KKS=NN-1
19999 CONTINUE
C
C
C     GO TO 91929
C          THIS ROUTINE SHIFTS THE ABSCR.    SPECTRUM TO LONGER WAVELENGTHS.
C            BY KKLMT*10 ANGSTROM
      KKF=NN
      KKS=NN-1
      KKLMT=1
      DO 29999  KK=1,KKLMT
      KOKLM=NN-1
      DO 28888 KCK=1,KOKLM
      ASS(KKF)=ASS(KKS)
      KKF=KKF-1
      KKS=KKS-1
28888 CONTINUE
      KKF=NN
      KKS=NN-1
29999 CONTINUE
      GO TO 91929
C          THIS ROUTINE SHIFTS S1 TO THE LONG WAVELENGTH
C            BY KKLMT*10 ANGSTROM.
      KKF=NN
NO PATH TO THIS STATEMENT
      KKS=NN-1
NO PATH TO THIS STATEMENT
      KKLMT=4
NO PATH TO THIS STATEMENT
      DO 39999  KK=1,KKLMT
NO PATH TO THIS STATEMENT
NO PATH TO THE ENTIRE RANGE OF DO
      KOKLM=NN-1
      DO 38888 KCK=1,KOKLM
      S1(KKF)=S1(KKS)
      KKF=KKF-1
      KKS=KKS-1
38888 CONTINUE
      KKF=NN
      KKS=NN-1
39999 CONTINUE
C
```

```
 81929 CONTINUE
C
C
C              ------------
C              SMOOTH THE INPUT DATA .
C              ------------
       IER=13
       CALL SG13(W,ASS,ASS,NN,IER)
       CALL SG13(W,E,E,NN,IER)
       CALL SG13(W,AT,AT,NN,IER)
       CALL SG13(W,S1,S1,NN,IER)
       IF(IER.NE.0)  STOP
C
C              ------------
C----          PRINT AND PLOT THE INPUT DATA ------
C       GO TO 25000
        PRINT 14999
14999 FORMAT(1H1,//////)
        PRINT 149
149    FORMAT(*      WVLGTH       S0(AES)       S1(EMISS)*
      1*     T1(ABS)      S1(ABS)*,//)
        PRINT 1498
1498   FORMAT(*      CM         CM.CM        1/CM*,
      1  *      CM.CM        CM.CM       *,//)
        DO 25 I=1,NN
        PRINT 15,W(I),ASS(I),E(I),AT(I)   ,S1(I)
15     FORMAT(1H0,5E13.4)
25     CONTINUE
25000 CONTINUE
        PRINT 14999
C---    TEST ------TEST------
        GO TO 114
C---    TEST ------TEST------
        DO 840 I=31,NN
NO PATH TO THIS STATEMENT
NO PATH TC THE ENTIRE RANGE CF DO
        CALL PLOTPT(W(I),ASS(I),21)
840    CONTINUE
        CALL OUTPLT
        DO 841 I=31,NN
        CALL PLOTPT(W(I),E(I),25)
841    CONTINUE
        CALL OUTPLT
        DO 842 I=31,NN
        CALL PLOTPT(W(I),AT(I),40)
842    CONTINUE
        CALL OUTPLT
        DO 843 I=31,NN
        CALL PLOTPT(W(I),S1(I),39)
843    CONTINUE
        CALL OUTPLT
C       INITIAL VALUES OF NMCL, N0,N1,NT,TS,KST,PUMP O
C          CONCENTRATIONS IN  (CM)**3
114    CONTINUE
C       STCP
C-----   PLAIN CELL   50 MICRON X 18.2 CM
C         TBHIT IS THE CELL HIGHT  TBL IS THE CELL LENGTH
C         DX IS THE MICROCELL . JLIM IS THE NUMBER OF MICROCELLS.
        JLIM=100
```

```
PROGRAM TST          73/74    TS TRACE                      FTN 4.6+460

         CX=TCE/FLOAT(JLIM)                                          /
C--------       CONCENTRATION ----------
C          CONCENTRATION IN MOL/LITER
         AVOG=6.0225E+23
         NMOL=CONC*AVOG*1.0E-3
C--------       MOLECULES PER/CC   -------
C       --------------------
         TT=2.5E-7
C-----   MW=33 CORESPONTS TO 5920 A  -----
         MW=29
C          CF    IS THE TRIPLET STATE QUENCHER
C          P     IS THE PUMPING
C          LMTJJ    IS THE NUMBER OF PROPAGATIONS
C          ETA IS THE COUPLING PARAMETER FOR THE SPONTANEOUS EMISSION.
C          GX    IS A CORRECTING COUPLING FACTOR
C          CONVERGENCE LIMIT FOR THE COUPLING EQUATIONS
         AALMT=1.0E-8
C          THIS LIMIT MAY NOT BE ENOUGH FOR HIGH PUMPING
C          (P=6.5E+7 GIVES N1(X+1)/N1(X) =1.9 PERCENT
         TT=TT*CF
         TS=5.5E-9
         KST=3.4E+6
         A1BO=KST*TT
         HTTA=1.35
         C=2.99AE+10
         G6=0.0
         SPONT=0.0
         HMW=0.0
         PSUB1=0.0
         PSUB2=0.0
         PSUB3=0.0
         CNTR1=0.0
C------ CSTR (52*JLIM) IS THE STORAGE AREA OF II(L) FOR ALL X......
C------       ZERO THE CSTR(L)
         NNN=NN*JLIM
         DO 1999  LL=1,NNN
         CSTR(LL)=0.0
1999     CONTINUE
C--------
C-------
C--- ROUGH CALCULATION OF N1 AT 0 TO CX INTERVAL---------
         TKT=1.0/TS +KST
         TKTT=1.0+KST*TT
         N1=NMOL*P/(TKT+TKTT*P)
         PRINT 35444
35444    FORMAT(1X,*N1,NO,NT,NMOL,    AT 0-CX,,,I=0*,///)
         PRINT 354,N1,NMOL
354      FORMAT(1H0,*N1(I=0)=  *,E16.10,*   NMOL=*,E16.10,///)
         NT=KST*TT*N1
         NO=NMOL-N1-NT
         PRINT 3544,NT,NO
3544     FORMAT(1X,*NT=*,E16.10,*   NO=*,E16.10,///)
C-------
C-------- CALCULATE  SE(I) SP.EMISSION CROSSECTION -------
         DO 70 I= 1,NN
         SE(I)=(  SE(I)*W(I)**4  )/(4*3.14159*TS*C*HTTA**2 )
         IF(W(I).GE.5.5E-5) GO TO 73901
```

```
        GO TO 70
7C801   IF(W(I).GT.6.1E-5) GO TO 70
C       CALL PLOTPT(W(I),SC(I),25)
70      CONTINUE
C       CALL SCALE(5.3E-5,6.1E-5,0.5E-16,1.7E-16)
C       CALL OUTPLT
C       PRINT 170
IF RESULTS IN A TRANSFER TO THE NEXT LINE
170     FORMAT(1H0,* SPONT. EMISSION CROSSECTION  VS WAVELENGTH *)
C---    TEST -------TEST------
        DO 1000 JV=1,LMTJJ
CC----------------------     BOOTH WAYS PROPAGATION LOOP-----
        K1=1
        K2=1
C------    ZERO THE STORAGE AREA -------------
        DO 703 I=1,NN
        SPII(I)=0.0
        STII(I)=0.0
        SPAST(I)=0.0
        II(I)=0.0
        SPST1(I)=0.0
703     CONTINUE
C------
C---------- CALCULATION OF INTENSITY ,N1,N0,NT. FOR EVERY SECTION DX----
        CNTR1=0.0
        STORE=1.0
        X=0.0
        DO 500 J=1,JLIM
        DO 818 L=1,NN
        SPST1(L)=CSTP(K1)
        K1=K1+1
818     CONTINUE
        STT=0.0
        X=X+DX
C       --------------------
101     CONTINUE
C       ETA CORESPONTS TO THE SOLID ANGLE SUSPENDED BY THE CELL END
        ETA=P*T4HIT/3.7/(TPL**2)
        FACT=N1*GX/TS *ETA
        DO 100 L=1,NN
        H=N1*SE(L)-N0)*ASS(L)-NT*AT(L)    -S1(L)*N1
        PEXP=EXP(H*DX)
        ST1=SPAST(L)*PEXP
        SP1=FACT*E(L)*(PEXP-1.0)/H
C       PRINT 1122,SP1,ST1
        II(L)=ST1+SP1
        SII=SII+II(L)
100     CONTINUE
C       --------------------
C-----  SELF CONSISTENCY LOOP-------
        AA=ABS(SII-STORE)/STORE
        IF(AA.LE.IALMT )GO TO 200
        CNTR1=CNTR1+1.
        IF(CNTR1.GE.33. ) GO TO 555
        STORE=SII
C       PRINT 1122,CNTR1,SII,N1,N0,NT,AA,X,PSUB1,PSUB2
1122    FORMAT(1X,4E13.7)
```

```
          SII=C.J
C------- ADJUST N1 VALUE ------
          CO 1331 K7=1,NN
1331      II(K7)=II(K7)+SPST1(K7)
          CALL SUB1(S1,II,PSUB3)
          CALL SUB1(SE,II,RSL31)
          CALL SUB2(ASS,II,PSUB2)
          N1=AMOL*(P+RSUB2)/(PSUB1+TKT+TKTT*(P+PSUB2)+PSUB3)
          NT=A1RO*N1
          NO=AMOL-N1-NT
          GC TO 101
C------------
200       CONTINUE
          CNTR1=CNTR1+1.
789       CONTINUE
C-------   STORE SII (L) IN SPAST(L) TO BE USED NEXT STEP
          CC 777 L=1,NN
          SPAST(L)=II(L)
777       CONTINUE
C-------
C----STORE SPAST(L) IN CSTP(L,X)
          CO 828 L=1,NN
          CSTP(K2)=SPAST(L)
          K2=K2+1
828       CONTINUE
C---------
          STSII(J)=SII
          STN1(J)=N1
          STORE=SII
          SII=0.0
          CNTR1=0.0
          IF(JJ.NE.LMTJJ) GO TO 5007
+99       CONTINUE
C------------
C--- PLOT I VS L FOR CERTAIN X....
          MAXL=0.0
C         IF(J.NE.JLIM) GO TO 5007
          CALL SKTCH(II,H,J,X,NN,MAXL,LMTJJ,JJ,AMOL,ASS)
C--- PLOT G VS L FOR CERTAIN X....
          CALL     GAIN(N1,NO,NT,SE,ASS,AT,NN,X,H,J,JDIF,MAXLG,E1)
5007      CONTINUE
C--------
500       CONTINUE
          IF(JJ.NE.LMTJJ) GO TO 51525
C-----    CHANGE PHOTON DENSITY TO INTENSITY (PHOTONS/CM**3/SEC)
C------------     DL=10 ANGSTROM ------
C----- PLOT LOG10 OF INTENSITY VS X---------
          XX=CX
          CO 1043 I=1,JLIM,2
          ALGI=ALOG10(STSII(I)*1.0E-4)
          CALL PLOTPT( XX,ALGI,4)
          XX=XX+CX *2.
1043      CONTINUE
          CALL OUTPLT
          PRINT 201
201       FORMAT(1H0,* LOG10 OF TOTAL INTENSITY (NO. OF PHOTONS/CM..2/SEC
         1 )   VS   X *)
```

```
C---------
 1525 CONTINUE
C----------- PRINT N1(X)/NMOL ---------
      IF(JJ.GT.LMTJJ) GO TO 29000
      XX=DX
      DO 7654 I=1,JLIM,2
      STN1(I)=STN1(I)/NMOL*100.0
      CALL PLOTPT(XX,STN1(I),4)
C     PRINT 105,STN1(I)
      XX=XX+DX*2.
 7654 CONTINUE
C     CALL SCALE(0.0,20.0,0.8,2.0)
      CALL PLTPLT
      PRINT 7655,P,TRL
 7655 FORMAT(1H0,*N1(X)/NMOL    X 100   VS   X      *,* PUMP= *,F15.5,
     1 * CELL LGTH=*,F10.2,*  CM*)
      WPEAK=(MAXLG-STRN)/CL
      WPEAK=WPEAK+1.1
C     LPEAK=IFIX(WPEAK)
C        UNSATURATED VALUES
      USN1=NMOL*C/(TKT+TKTT*P)
      USNT=K*T*TT*USN1
      USNLE=NMOL-USN1-USNT
C     ----------------------
C        PLOT UNSATURATED GAIN
      DO 2030 LPEAK=1,NN
      USG=USN1*RS(LPEAK)+USNC*ASS(LPEAK)  -USNT*AT(LPEAK)
     1    -USN1*S(LPEAK)
      IF(USG) 2030,2032,2032
 2032 CALL PLOTPT(W(LPEAK),USG,27)
 2030 CONTINUE
C     CALL SCALE(5.E3-5,6.4E-5,0.0,1.0)
      CALL PLTPLT
      PRINT 2033
 2033 FORMAT(1X,* UNSATURATED  GAIN  VS
     1   W LGTH *)
C     ----------------------
29000 CONTINUE
11111 CONTINUE
      IF(JJ.LT.LMTJJ) GO TO 1000
      CALL SWTCH(JLIM,OSTP)
      N1=NMOL*C/(TKT+TKTT*P)
 1000 CONTINUE
      STOP
C------ NO CONVERGENCE-------
 555  PRINT 556
      PRINT 205,X,STORE,N1,NC,NI,CNTR1
 556  FORMAT(1X,* NO CONVERGENCE -----*)
 205  FORMAT(1H0,6E15.4)
      STOP
C--------
      END
```

```
      SUBROUTINE SUB1(SE,II,RSUB1)
C     ----- INTEGRATION OF SE (L)*II(L)*DL
      COMMON W  ,NN
      REAL II
      DIMENSION SE(82),II(82),SEII(82),CSEII(82),   Z1(82),W(82)
      IER1=0
      DO 60 I=1,NN
      SEII(I)=SE(I)*II(I)
60    CONTINUE
      CALL DGT3(W,SEII,DSEII,82,IER1)
      IF(IER1  .EQ. 0) GO TO 66
      PRINT 67
67    FORMAT(1X,*IER1 NOT ZERO AT SUB1*)
      STOP
66    CONTINUE
      CALL QHFG(W,SEII,DSEII,Z1,82)
      RSUB1=Z1(NN)
      RETURN
      END
```

.OCKS--

    1230 //

·---

        DGT3   OUTCI.   OUTPUT#   QHFG   STOP.

· LABELS--

    .60   ID.   OP   .66   328   .67   F   50B

MAP--

R·		SUBROUTINE		DSEII	R	215B		A
R	215B			IER1	II	462B		
R A	0B		82	NN	I	122B	//	
-R		EXTERNAL.		OUTPUT#			EXTERNAL.	
R A	0B	SUBROUTINE	82	RSUB1	R A	7B		
-R		EXTERNAL.		SEII	R	73B		A
R	0B	//	82	SUB1		42B	ENTRY	
				Z1	R	34B		A

PROGRAM-UNIT LENGTH   19 SYMBOLS

:M STORAGE USED   .088 SECONDS

JPROUTINE SUB2   73/74   TS TRACE   FTN 4.6+.60

```
      SUBROUTINE SUB2(ASS,II,RSUB2)
C  -----+ INTEGRATION OF ASS(L)*I(L)*CL
      COMMON W  ,NN
      REAL II
      DIMENSION     ASS(82),II(82), ASSII(82), DER2(82),Z2(82),W(82)
      IER2=0
      DO 60 I=1,NN
      ASSII(I)=ASS(I)*II(I)
60    CONTINUE
C------- TAKE DERIVATIVE OF   ASSII(I)
      CALL DGT3(W,ASSII,DER2,82,IER2)
      IF(IER2 .EQ. 0) GO TO 66
      PRINT 67
67    FORMAT(1X,*IER2 NOT ZERO AT SUB2*)
      STOP
66    CONTINUE
      CALL OHFG(W,ASSII,DER2,Z2,82)
      RSUB2=Z2(82)
      RETURN
      END
```

LOCKS--

   1230 //

.J--

          DGT3   OUTCI.   OUTPUT#   OHFG   STOP.

T LABELS--

  .60   IO   C8   .66   320   .67   F   508

MAP--

```
    R A        C8             82        ASSII    R       3408        SUBROUTINE
    R          2160           82        DGT3     R       4628
    R  A       2150                     IER2     I       4629
    R  A       03             82        NN       I       1228  //
I.  -      EXTERNAL.                    OUTPUT#  -  R         18     EXTERNAL.
    -      SUBROUTINE                   RSUB2    R  A       18
    -      EXTERNAL.                    SUB2     -  R       426 ENTRY
    R        60  //           82        Z2       R         738
```

ROGRAM-UNIT LENGTH   19 SYMBOLS

M STORAGE USED   .047 SECONDS

236

```
      SUBROUTINE SKTCH(II,W,J,X,NN,MAXL,LMTJJ,JJ,NMOL,ASS)
C---- PLOTS INTENSITY VS LAMDA  ---------------
      REAL NMOL
      REAL II
      REAL MAXII,MAXL
      DIMENSION ASS(82)
      DIMENSION II(82),W(82)
      IF(JJ.NE.LMTJJ) GO TO 7
      IF(J.EQ. 1) GO TO 66
      IF(J.EQ.25) GO TO 66
      IF(J.EQ.50) GO TO 66
      IF(J.EQ.75) GO TO 66
      IF(J.EQ.100) GO TO 66
      GO TO 7
66    CONTINUE
C     -------------------------
C
C         THIS ROUTINE TAKES IN TO ACCOUNT THE UNPUMPED DYE REGION.
C     -------------------------
C         UNPUMPED DYE CELL LENGTH IN CM  .......
      ULGTH=2.0
      DO 1917 IABS=1,NN
      II(IABS)=II(IABS)  /  EXP(ASS(IABS) * NMOL*ULGTH)
1917  CONTINUE
C     -----------
C     -----------
C         TOTAL INTENSITY (INTEGRATED OVER ALL WAVELENGTHS)
      SUMI=0.0
      DO 80 LL=1,NN
      SUMI=SUMI+II(LL)
80    CONTINUE
      SUMI=SUMI*1.0E-8
      PRINT 81,SUMI
81    FORMAT(1X,*TOTAL INTENSITY =  *,1E16.4,* PHOTONS/CM/CM/SEC*,//)
C     -----------
C--- FIND WAVELENGTH OF MAX. INTENSITY --------
      MAXII=II(1)
      MAXL=W(1)
      DO 70 L=2,NN
      IF(MAXII.LT.II(L)) GO TO 71
      GO TO 70
71    MAXII=II(L)
      MAXL=W(L)
70    CONTINUE
      MAXII=MAXII*1.0E-8
      PRINT 29,MAXII,MAXL
29    FORMAT(1X,*MAX. INTENSITY( NO. OF PHOTONS / CM..2 /SEC)=*,
     1 1E16.4,*   WVLNGTH OF MAX INTENS.=*,E16.4)
C-----------
7     CONTINUE
C     -------------------------
C         SMOOTH THE INTENSITY PLOT
      IER=12
      CALL SC13(W,II,II,NN,IER)
      IF(IER.NE.0)STOP
C     -------------------------
      DO 9 K=1,NN
C         NORMALISE THE INTENSITY          DIVIDE BY MAXII
```

```
SUBROUTINE SKTCH      73/74    TS TRACE                    FTN 4.6+460      7

      C--------     CL = 10 ANGSTROMS------
                AII=II(K)*1.0E-9           /MAXII
      C         ----------------------
                CALL PLOTPT(W(K),AII,4)
      3         CONTINUE
      C         CALL SCALE(5.7E-5,6.3E-5,0.),1.0)
                CALL OUTPLT
                PRINT 19,X,MAXII
      19        FORMAT(1H0,* X =*,F 6.2,* INTENS. (NO. OF PHOTONS/CM2*,
               1*/SEC VS WAVELENGTH*,* MAXII=*,E15.3)
      7         CONTINUE
                RETURN
                END
```

```
.5--

            EXP         OUTCI.      OUTPLT      OUTPUT#     PLOTPT      SG13        STOP.
```

```
F LABELS--

    .6                  1310                    1716                    .9    ID              08
    .29     F           2120        .66         335                    .70   0       1209
    .80     ID            08        .41    F    2038                    .1917 ID              08
```

```
MAP--

          R         3039                        ASS       R A           08                  A
          R II                9.E.F.            IABS      R I R         301B                 A
          I I   A   2778                        II        R I A          08
          I I       00                          JJ        R I A          00
          I I       2750                        L         I I A         3020
          I I   R A 2764                        L+IJJ     I R A          08
    I     I I   R A  2740                        MAXL      I R A          08
    I     R   A       08                         NN        I R A          08
    I+        =                EXTERNAL.          OUTPLT    R           SUBROUTINE
    UT#       =P               EXTERNAL.          PLOTPT    R           SUBROUTINE
    N         =                SUBROUTINE         SKTCH                 174B ENTRY
    N     R             EXTERNAL.                 SUMI      R A         2738
          R         3008                         W         R A          08                  A0
          R   A      08
```

```
PROGRAM-UNIT LENGTH         58 SYMBOLS
CM STORAGE USED             .258 SECONDS
```

```
      SUBROUTINE GAIN(N1,NO,NT,SE,ASS,AT,NN,X,W,I,GDIF ,MAXLG,S1)
C         THIS ROUTINE PLOTS THE GAIN VS WVLNGTH
      REAL N1,NO,NT
      REAL MAXLG
      DIMENSION SE(82),ASS(82),AT(82),X(82) ,GDIF(82),S1(82)
      IF(I.EQ.100)GO TO 6
      GO TO 7
6     CONTINUE
      MAXLG=W(1)
      GMAX=0.
      DO 8 J=1,NN
      G=N1*SE(J)-NO*ASS(J)-NT*AT(J)      -N1*S1(J)
      IF(G.GE.GMAX) GO TO 90
      GO TO 100
90    GMAX=G
      MAXLG=W(J)
100   CONTINUE
      IF (G) 8,13,13
13    CONTINUE
      CALL PLOTPT(W(J),G,4)
8     CONTINUE
C     CALL SCALE(5.6E-5,6.4E-5,0.0,1.0)
      CALL OUTPLT
      MAXLG=MAXLG*1.0E+8
      PRINT10, X,GMAX,MAXLG,N1
10    FORMAT( 1X, *   X=*,F8.2,* CM*,  *  GMAX=*,F10.4,* AT *,
     1 F10.2,*   ANGSTROMS*,*    N1=*,E16.5)
      MAXLG=MAXLG/1.0E+8
7     CONTINUE
      RETURN
      END
```

OUTCI.   OUTPLT   OUTPUT#   PLOTPT

T LABELS--

| .6 | 12B | .7 | 102B | .8 0 | 510 |
| .13 | 53B | .9C | 42B | .100 | 508 |

MAP--

R A	C B	82	AT	R A	0B	82
R R A A	142B		GAIN	R A	103B ENTRY	
R I P A	0B	82	GMAX	R I I I A	140B	
P P A A A	C B		J		141B	
P P A A	G B		NN	I I A	0B	
P R A	G B		NO	R A	3B	
R R	SUBROUTINE		OUTCI.		EXTERNAL.	
T R R A	SUBROUTINE		OUTPUT#		EXTERNAL.	
T P A	0 B	82	SE.	R A	0B	82
R A	G B		W	R A	0B	82

```
      SUBROUTINE SWTCH(JLIM,CSTR)
      DIMENSION CSTR(16400),SPEC(82),K(82)
      NN=82
      JMID=JLIM/2
      LGTH=NN*JLIM
C-----     PRINT CSTR BEFORE SWITCHING
C          PRINT 181,CSTR
181   FORMAT(1X,10E12.5)
C------
      K=0
      KK=0
      DO 80 J=1,JMID
      L=LGTH-J*NN
      DO 70 I=1,NN
      L=L+1
      SPEC(I)=CSTR(L)
70    CONTINUE
      L=LGTH-J*NN
      DO 75 I=1,NN
      L=L+1
      K=K+1
      CSTR(L)=CSTR(K)
75    CONTINUE
      DO 76 I=1,NN
      KK=KK+1
      CSTR(KK)=SPEC(I)
76    CONTINUE
80    CONTINUE
C----  PRINT CSTR AFTER SWITCHING
C          PRINT 290
290   FORMAT(1X, *SWITCHED ARRAY STARTS HERE*)
C          PRINT 181,CSTR
      RETURN
      END
```

.T LABELS--

.70	IO	CR	.75	IO	IR	.76	IO	DR
.181	F	1000	.290	F	1038			

MAP

R	A	CR	16400		I	JLIM	I	A	1115
I	I	1120			I		I		108
I	I	3630			K		I		1138
I	*	1160			L		I		1140
I	I	1150			NN		I		3620
R		1168	82		SWTCH		I		740 ENTRY
R	4	2400	82						

```
      PROGRAM TST (INPUT,OUTPUT,TAPE5=INPUT,TAPE6=OUTPUT)
C     -------------------------------------------------
C     -------------------------------------------------
C     NUMERICAL SOLUTION OF THE APPROX.A S E THEORY.
C     -------------------------------------------------
C     -------------------------------------------------
      EXTERNAL FCT
      REAL IL,IZ,L,IZZ,LHOMO
      REAL LEFF
      DIMENSION  DERZ(200),ZZ(200)
      DIMENSION CL(100),IZ(200),F(200),CL(50),STPIL(50)   ,STPG0(50)
      DIMENSION DERF(200),DEN(200),STRZ(200)
      COMMON G0,IL,PSI,Z
C        CELL LGTH IN CM
      L=18.2
      STEP=100.
      ISTEP=IFIX(STEP)
      PSI=1.0E-7
      LMTJ=76
      LHOMO=600.
      DO 1 JHOMO=1,8
      IL=1.0E-8
      DO 10 J=1,LMTJ
      CL(J)=ALOG(1.+IL/PSI)+2.*IL
      G0=CL(J)/L
      DZ=L/STEP
      Z=DZ
C     ----------------------------------------
C     ------ CALCULATE I(Z)  ,Z=0  TO L
      DO 20 M=1,ISTEP
      EPS=1.E-5
      IEND=100
      IER=10
      ZINIT=1.0E-13
      CALL RTNI(IZZ,FF,DFRFF,FCT,ZINIT,EPS,IEND,IER)
      IF(IER.NE.0) GO TO 99
      IZ(M)=IZZ
      F(M)=FF
      DERF(M)=DERFF
      STRZ(M)=Z
      PRINT 200,Z,IZZ
200   FORMAT(1X,*  Z=*,E10.2,*   I(Z)=*,E15.3)
      CALL PLOTPT(Z,IZZ,29)
      Z=Z+DZ
20    CONTINUE
C
C
      CALL OUTPLT
C
      PRINT 76
76    FORMAT(1X,*          LIGHT INTENSITY  V S        POSITION*,//)
C     ----------------------------------------
C     CALCULATE THE INTEGRAL  LEFF.
      DO 70 K=1,ISTEP
      DEN(K)=1.+IZ(K)+PSI*(IL-IZ(K))/(PSI+IZ(K))
      DEN(K)=1.0/DEN(K)
70    CONTINUE
C     ----------------------------------------
      IER3=100
      CALL OGT3(STRZ,DEN,DERZ,ISTEP,IER3)
```

```
PROGRAM TST          73/74    TS TRACE                          FTN 4.6+460

      IF(IEP3.NE.2)  GO TO 998
      CALL OFEG(STEZ,DEN,CFR2,72,ISTEP)
      LEFF=72(ISTEP)
C                     CALCULATE NARROWING DL
      DL(J)=LHOMO*SQRT((ALOG(2.)/G0/LEFF))
      STRIL(J)=IL
      STRG0(J)=G0
      IL=IL* SQRT(SQRT(10.0))
10    CONTINUE
C                     PRINT RESULTS
      PRINT 110,L,STEP,PSI,LHOMO
110   FORMAT(1H1,*  L=*,F10.2,*    STEP=*,F10.2,*    PSI=*,E15.2,
     1    *    LHOMO=*, F10.2,///////)
      PRINT 130, (STRIL(JJ),STRG0(JJ),DL(JJ),JJ=1,LMTJ)
130   FORMAT(1X, *IL=*,F15.7,* G0=*,F10.2,*  1/CM*,*    DL=*,F10.2,
     1    * ANGSTROMS*,//)
C     ----------------------
C                     PRINT DL VS G0
C     ----------------------
      DO 700 JJ=1,LMTJ
700   CALL PLOTPT(STRG0(JJ),DL(J),27)
C     CALL SCALE(0.0,2.0,100.,400.)
      CALL OUTPLT
      PRINT 701,LHOMO,PSI
701   FORMAT(1X, *    NARROWING IN ANGSTROMS   VS   GAIN IN 1/CM*,
     1    * LHOMO=*,F6.2,*   PSI=*,E15.2,//)
      LHOMO=LHOMO+50.0
1     CONTINUE
C     ----------------------
      GO TO 333
99    PRINT 999,IER
999   FORMAT(1X,I10)
      GO TO 333
998   PRINT 999,IEP3
333   CONTINUE
      STOP
      END

LOOKS--

   49  //

INTC--

   78  INPUT#              54B   OUTPUT#              38   TAPE5#
 1348  TST

;--

      ALOG     DCT3     FCT     FINRP2.  OUTCI.  OUTCR.  OUTPLT   DL
      OFEG     FINI     SQRT    STOP.
```

```
      C
              ------------------------
              SUPROUTINE  FCT(IZ7,FF,DERFF)
              PEAL IZ7,IL
              CCMMCN GO,IL,PSI,7-
              FF=      ALCG(1.+I77/PSI)+ I77*(1.C + (PSI+IL)/(PSI+IZZ))-GO*7
              CERF=1.C/(PSI+IZZ) +1.0+(PSI+IL)*PSI/(PSI+I7Z)**2
              CERFF=CERF
      C       PRINT 12,IZ7,FF,DERF
      12      FORMAT(1X,3E15.5)
              RETURN
              END
```

LCCKS--
     4B //

S--

          ALCG

T LABELS--

 .12   F   41B

 MAP--

	P		C.E.F.		CERF		B		46B	
	R	A	CR		FCT				35B	ENTRY
	R	A	CR //		GC		R	A	0B //	
	P		1B //		I2Z		R		0B //	
	R		2B //		Z		R		3B //	

PROGRAM-UNIT LENGTH   11 SYMBOLS
CM STORAGE USED   .073 SECONDS.

APPENDIX B

1. Solution of Maxwell's Equation

Maxwell's equations to be solved for the dye amplifiers are in the MKS system of units:

$$\nabla \times \overline{H} = \overline{j} + \frac{\partial \overline{D}}{\partial t} \qquad (B1)$$

$$\nabla \times \overline{E} = -\frac{\partial \overline{B}}{\partial t} \qquad (B2)$$

$$\nabla \cdot \overline{D} = 0 \text{ (no charge)} \qquad (B3)$$

$$\nabla \cdot \overline{B} = 0 \qquad (B4)$$

also for a polarization linear with the field

$$\overline{D} = \epsilon_0 \overline{E} + \overline{P} = \epsilon_0 \overline{E} + \epsilon_0 \chi \overline{E} = \epsilon_0 \epsilon \overline{E} \qquad (B5)$$

$$\epsilon = \qquad (1 + \chi)$$

and

$$\overline{B} = \mu_0 \overline{H} \qquad (B6)$$

From (B2)

$$\nabla \times \nabla \times \overline{E} = -\nabla \times \frac{\partial \overline{B}}{\partial t} = -\frac{\partial}{\partial t} (\nabla \times \overline{B}) \qquad (B7)$$

or

$$\nabla(\nabla \cdot \overline{E}) - \nabla^2 \overline{E} = -\mu_0 \frac{\partial}{\partial t} (\nabla \times \overline{H}) = -\mu_0 \frac{\partial}{\partial t}[\sigma \overline{E} + \epsilon_0 \frac{\partial}{\partial t} (\epsilon \overline{E})] \qquad (B7)$$

Because of $\nabla \cdot \overline{D} = \nabla \cdot (\epsilon_0 \epsilon \overline{E}) = \epsilon_0 \nabla \cdot (\epsilon \overline{E}) = 0$, we have

$$\epsilon \nabla \cdot \overline{E} + \overline{E} \cdot \nabla \epsilon = 0$$

or

$$\nabla \cdot \overline{E} = -\overline{E} \cdot \frac{\nabla \epsilon}{\epsilon} = -\overline{E} \cdot \nabla \log \epsilon \qquad (B8)$$

Using (B8) we can write (B7) as follows

$$\nabla(-\overline{E} \cdot \nabla \log \epsilon) - \nabla^2 \overline{E} = -\mu_0 \frac{\partial}{\partial t}[\sigma \overline{E} + \epsilon_0 \frac{\partial}{\partial t}(\epsilon \overline{E})]$$

·or·

$$\mu_0 \sigma \frac{\partial \overline{E}}{\partial t} + \frac{1}{c^2} \frac{\partial^2}{\partial t^2}(\epsilon \overline{E}) - \nabla^2 \overline{E} - \nabla(\overline{E} \cdot \nabla \log \epsilon) = 0 \qquad (B9)$$

The last term in (B9) is negligible for the small index changes encountered in this work even when E is not perpendicular to $\nabla \log \epsilon$. Also, for a lossless dielectric $\sigma = 0$. Then, (B9) can be written as

$$\nabla^2 \overline{E} - \frac{1}{c^2} [\frac{\partial^2 \epsilon}{\partial t^2} \overline{E} + 2 \frac{\partial \epsilon}{\partial t} \frac{\partial \overline{E}}{\partial t} + \epsilon \frac{\partial^2 \overline{E}}{\partial t^2}] = 0 \qquad (B10)$$

The derivatives of ϵ are taken to be small compared to the derivatives of $\overline{E}$. Then (B10) becomes for a constant ϵ with respect to time in the pumped and unpumped region of the cell.

$$\nabla^2 \overline{E} - \frac{\epsilon}{c^2} \frac{\partial^2 \overline{E}}{\partial t^2} = 0 \qquad (B11)$$

Subsequently, it will be necessary to ensure that the boundary conditions on the field are satisfied at the surface separating the pumped and unpumped regions where the dielectric constant is discontinuous. Additionally, we will assume no variation of the gain along the y axis, perpendicular to the plain defined by the direction of the propagation z.

and the direction of pumping x, which is true for the case of cell height less than the width of the parallel pumping light. Moreover, for a dye amplifier there is no mode structure along the cell and consequently we expect no transverse and longitudinal mode interference, which is the case for oscillators with comparable gain region thickness and cavity lengths. In other words, we can decouple the variation of the field along the cell and across the cell. Then for a propagating plane wave along z

$$E(x,t,z) = A(x,t)e^{i(kz + \omega t)} \tag{B12}$$

where $A(x,t)$ is a slowly varying complex function. Then (B11) can be written as

$$\frac{\partial^2 A}{\partial x^2} - k^2 A - \frac{\epsilon}{c}\frac{\partial^2 A}{\partial t^2} - \frac{2i\epsilon\omega}{c^2}\frac{\partial A}{\partial t} + \frac{A\epsilon\omega^2}{c^2} = 0 \tag{B13}$$

Because $\frac{\epsilon}{c}\frac{\partial^2 A}{\partial t^2}$ is very small with respect to the other terms, since $A(x,t)$ is a slowly varying function, we get from (B13)

$$\frac{\partial A}{\partial t} = \frac{-c^2}{2i\epsilon\omega}[\frac{\partial^2 A}{\partial x^2} + k^2 A - \frac{\omega^2\epsilon}{c^2} A] \tag{B14}$$

For stable eigenmodes $\partial A/\partial t = 0$ and (B14) becomes

$$\frac{\partial^2 A(x,t)}{\partial x^2} = [k^2 - \frac{\omega^2\epsilon}{c^2}]A(x,t) \tag{B15}$$

This is the basic equation to be solved. In order to solve this equation we need to assume a general form for the solution pertaining to the problem along with the appropriate boundary conditions.

2. Relation of parameters to gain and loss

From (B-11) we have

$$\nabla^2 \bar{E} - \frac{\varepsilon}{c^2} \frac{\partial^2 \bar{E}}{\partial t^2} = 0 \qquad\qquad (B\text{-}16)$$

with

$$\varepsilon = \varepsilon_0' + i\varepsilon_0'', \qquad \sqrt{\varepsilon} = \eta + i\kappa$$

where ε is the dielectric constant and η the real index of refraction far from any resonance.

Then, squaring the third of the above relations, we get

$$\varepsilon = \varepsilon_0' + i\varepsilon_0'' = (\eta^2 - \kappa^2) + i2\eta\kappa$$

or

$$\varepsilon_0' = \eta^2 - \kappa^2$$
$$\varepsilon_0'' = 2\eta\kappa \qquad\qquad (B\text{-}17)$$

Next, assume a solution to the wave equation of the form $E = E_0 e^{i(\omega t - kz)}$ (plane wave) and substitute this solution in (B-16) to get for k the relation

$$k = \frac{\omega}{c} \sqrt{\varepsilon} = \frac{\omega}{c}(\eta + i\kappa).$$

Then the plane wave is

$$E = E_0 \exp i \left(\omega t - \frac{\omega\eta}{c} z\right) \exp\left(\frac{\omega\kappa}{c} z\right) \qquad\qquad (B\text{-}18)$$

There is thus gain and the amplitude increases when $\kappa > 0$. The intensity ($I = EE^*$) gain is given by

$$g = \frac{2\omega\kappa}{c} = \frac{2\omega}{c} \frac{\varepsilon_0''}{2\eta} = \frac{\omega\varepsilon_0''}{c\eta} \qquad\qquad (B\text{-}19)$$

Then we can define the parameters.

$$\alpha = \frac{\omega^2}{c^2} \epsilon_g'' = \frac{\omega\eta}{c}\left(\frac{\omega}{c\eta} \epsilon_g''\right) = \frac{\omega\eta}{c} g \qquad (B-20)$$

$$\beta = \frac{\omega^2}{c^2} \epsilon_\ell'' = \frac{\omega\eta}{c}\left(\frac{\omega}{c\eta} \epsilon_\ell''\right) = \frac{\omega\eta}{c} \alpha_s \qquad (B-21)$$

where g is the gain in cm^{-1} and α_s is the loss in cm^{-1}.

3. Near and far-field relations

In this section we will try to find the appropriate equations, which relate the far field pattern to the near field distribution. First, we will show that there is a Fourier Transform relation between the near and far field distributions. From figure B-1 we have that

$$r_0 = [x^2 + z^2]^{1/2} \tag{B-22}$$

$$r = [(x - n)^2 + z^2]^{1/2} = [r_0^2 + n^2 - 2nx]^{1/2}$$

because $r_0 \gg x, n$ we can write

$$r \approx r_0 (1 - \frac{nx}{r_0^2}) \tag{B-23}$$

Let $E(n)$ be the near field and $E(x)$ the far field. Then from the Huygens formulation of diffraction we have

$$E(x) = \int_A \frac{1}{r} E(n) e^{ik \cdot r} dn \tag{B-24}$$

where the integral is taken over the aperture A. Substituting for r from the relation (B-23) we get

$$E(x) \approx \frac{e^{ikr_0}}{r_0} \int_A E(n) e^{(iknx/r_0)} dn \tag{B-25}$$

which shows that, to within a multiplication factor, the far field $E(x)$ is given by the Fourier transform of the near field $E(n)$.

In our case, we will have for the near field according to equation (4-11)
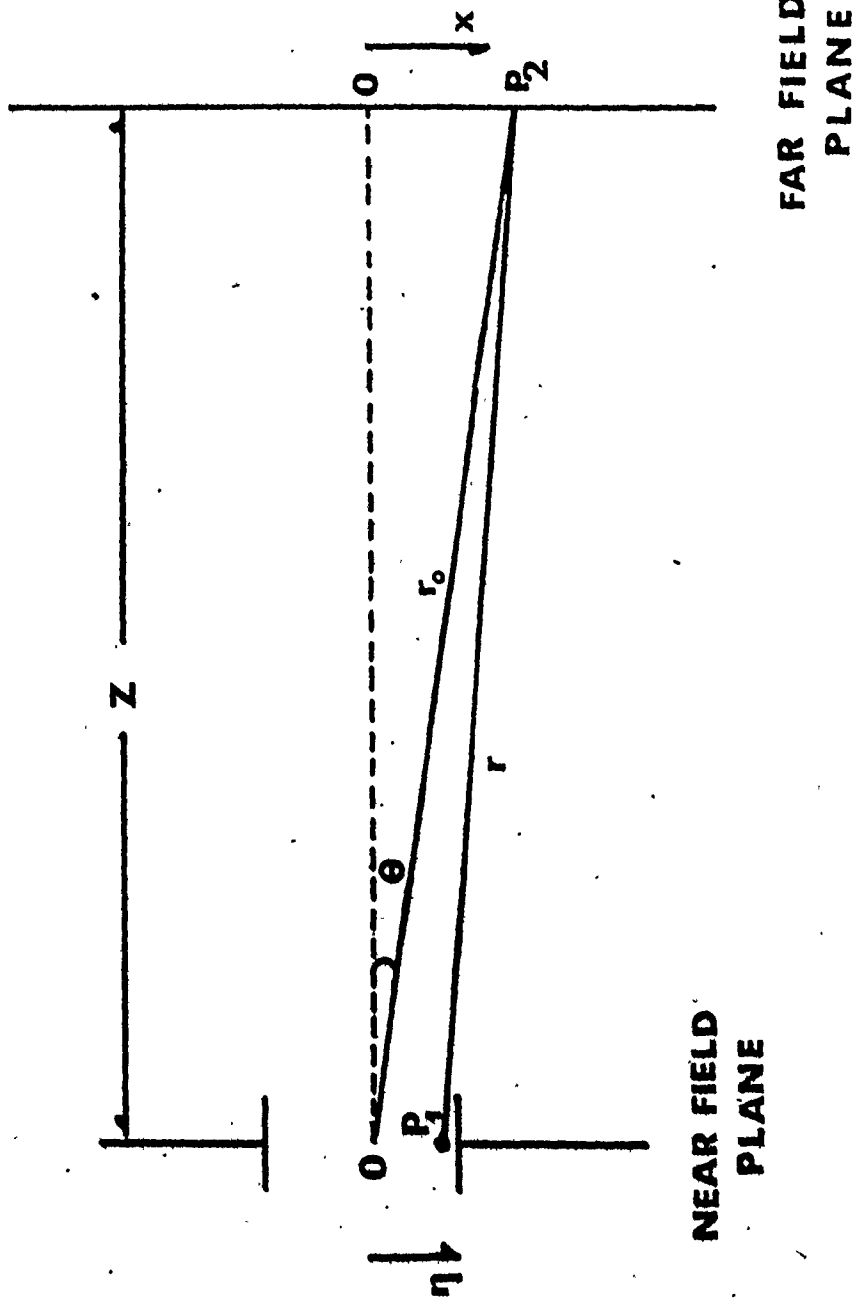
FIG.B-1. Near- and far-field model

$$A = A_0 \sin px \qquad \text{for } (o,d)$$

$$A = A_1 e^{-qx} + A_2 e^{qx} \qquad (d,d+h) \qquad \text{(B-26)}$$

$$A = A_3 \sin p(x-L) \qquad (d+h,2d+h)$$

Then, the far field will be, if we switch variables between η and x and set $B = \exp(i\kappa r_0)/r_0$,

$$E(\eta) = B \int_A A(x) e^{i(k\eta x/r_0)} dx \qquad \text{(B-27)}$$

where k is the wavevector in free space ($k = 2\pi/\lambda$). Using symmetry relations and boundary conditions we can relate the coefficients A_1, A_2 and A_3 of (B-26) to A_0, which can be chosen arbitrarily in the case we are not interested in absolute intensity measurements. Accordingly, we can easily show that

$$A_1 = \frac{A_0 \sin(pd)}{e^{-qd} + e^{q(d-L)}}$$

$$A_2 = \frac{A_0 \sin(pd)}{e^{-qd} + e^{q(d-L)}} e^{-qL} \qquad \text{(B-28)}$$

$$A_3 = -A_0(e^{-q(L-d)} + e^{-qd})/(e^{-qd} + e^{q(d-L)})$$

Then the total far field intensity will be the sum of the contributions of the individual near fields taken over the region of their validity.

(1)   For the region (o,d) we have

$$E(\eta)_1 = B \int_A A(x) e^{i(k\eta x/r_0)} dx = A_0 B \int_0^d \sin(px) e^{i(k\eta x/r_0)} dx$$

But

$$\int \sin(px)e^{ax}dx = \frac{e^{ax}}{a^2 + p^2}[a \sin(px) - p \cos(px)]$$

Then after some algebra we find

$$E(n)_1 = \frac{A_0 B}{(ik_n/r_0)^2 + p^2}[e^{(ik_n d/r_0)}(\frac{ik_n}{r_0}\sin(pd) - p\cos(pd)) + p] \quad (B-29)$$

(ii)   For the region (d,d+h) we have

$$E(n)_2 = \frac{e^{ikr_0}}{r_0}\int_d^{d+h} A_1[e^{-qx} + e^{q(x-L)}] e^{(ik_n x/r_0)}dx$$

This is a standard exponential integral and after the normal integration we get

$$E(n)_2 = A_1 \frac{e^{ikr_0}}{r_0}[[\frac{e^{\zeta(d+h)}}{\zeta} + e^{-qL}\frac{e^{\delta(d+h)}}{\delta}] - [\frac{e^{\zeta d}}{\zeta} + e^{-qL}\frac{e^{\delta d}}{\delta}]] \quad (B-30)$$

where A_1 is given by (B-28a) and ζ and δ by

$$\zeta \equiv -q + \frac{ik_n}{r_0}$$

$$\delta \equiv q + \frac{ik_n}{r_0}$$

(iii)   For the region (d+h,L), in a similar way to the one used for the region (o,d), we get

$$E(n)_3 = [BA_3 e^{(ik_n L/r_0)}]\cdot[e^{-(ik_n d/r_0)}[\frac{ik_n}{r_0}\sin(pd) + p\cos(pd)] - p] \quad (B-31)$$

where A_3 is given by (B-28c).

Then the far field is given by

$$E(\eta) = E(\eta)_1 + E(\eta)_2 + E(\eta)_3 \qquad (B-32)$$

and the intensity distribution will be

$$I(\eta) = E(\eta)E^*(\eta) \qquad (B-33)$$

The intensity can be plotted versus the angle θ, which is calculated from the relation

$$\theta = \tan^{-1}(\eta/z) \qquad (B-34)$$

where z has been taken large enough in order that the Huygens formulation is valid. Equations (B-29) to (B-34) are directly used in the computer program to calculate the far-field after we have found $u, v, \overline{K}, s$, which satisfy the transverse mode equations (4-34), (4-35) and (4-36).

4. Estimation of the contribution of the gain to the refractive index

From the Kronig-Kramers relation we have for the real and imaginary parts of the dielectric constant

$$\varepsilon'(\nu) - 1 = \frac{1}{\pi} \int_{-\infty}^{+\infty} \frac{\varepsilon''(\nu')}{\nu - \nu'} d\nu' \qquad (B-35)$$

Also, from equation (4-13a) we have

$$\varepsilon(\nu) = \varepsilon'(\nu) + \delta\varepsilon'(\nu) + i[\varepsilon''(\nu) - \delta\varepsilon''(\nu)] \qquad (B-36)$$

Then (B-35) can be written as

$$\varepsilon'(\nu) + \delta\varepsilon'(\nu) - 1 = \frac{1}{\pi} \int_{-\infty}^{+\infty} \frac{\varepsilon''(\nu')}{\nu - \nu'} d\nu' - \frac{1}{\pi} \int_{-\infty}^{+\infty} \frac{\delta\varepsilon''(\nu')d\nu'}{\nu - \nu'} \qquad (B-37)$$

Far from resonance $\varepsilon(\nu) = \varepsilon'(\nu) + i\varepsilon''(\nu)$ and equation (B-35) is valid. Then (B-37) can be written as

$$\delta\varepsilon'(\nu) = -\frac{1}{\pi} \int_{-\infty}^{+\infty} \frac{\delta\varepsilon''(\nu')d\nu'}{\nu - \nu'} \qquad (B-38)$$

Also far from resonance $\varepsilon(\nu) = \varepsilon'(\nu) + i\varepsilon''(\nu)$ and $n = n_0 + i\kappa$ with $\varepsilon'(\nu) = n_0^2 - \kappa^2 \approx n_0^2$. Then,

$$\delta\varepsilon' = 2n_0\delta n_0 \qquad (B-39)$$

From the gain parameter calculations we have found that (equation (B-19))

$$\varepsilon''(\nu) = \frac{\lambda}{2\pi} n_0 g(\nu) \qquad (B-40)$$

where g is the gain in cm^{-1}.

Substituting for $\delta\epsilon'(\nu)$ and $\delta\epsilon''(\nu)$ in equation (B-38) from (B-39) and (B-40) we have

$$\delta n_0 = \frac{-\lambda}{4\pi^2} \int_{-\infty}^{+\infty} \frac{g(\nu')}{\nu - \nu'} d\nu' \qquad (B-41)$$

If we assume that the gain line can be represented by a Lorentzian

$$g(\nu) = g_0 \frac{\Delta\nu^2}{(\nu_0 - \nu)^2 + \Delta\nu^2} \qquad (B-42)$$

Then we can write (B-41) in the form

$$\delta n_0 = \frac{-\lambda g_0 \Delta\nu^2}{4\pi^2} \int_{-\infty}^{+\infty} \frac{d\nu'}{[(\nu_0-\nu)^2 + \Delta\nu^2](\nu-\nu')} = \frac{+\lambda g_0 \Delta\nu^2}{4\pi^2} \int_{-\infty}^{+\infty} \frac{dx}{(x^2+\Delta\nu^2)(-x+\nu_0-\nu')}$$

which after the integration gives

$$\delta n_0 = \frac{-g_0\lambda\Delta\nu^2}{4\pi^2} \frac{\pi(\nu_0 - \nu')}{2\Delta\nu[\Delta\nu^2 + (\nu_0 - \nu')^2]} \qquad (B-43)$$

This function has a maximum when $\nu_0 - \nu' = \Delta\nu$. Then

$$|\delta n_0|_{max} = \frac{g_0\lambda}{18\pi} \qquad (B-44)$$

Assuming some reasonable values for g_0 and λ such as $\lambda = 0.6$ μ and $g_0 = 1.0$ cm^{-1}, we have

$$|\delta n_0|_{max} = 10^{-6} \cdot \qquad (B-45)$$

Evidently, the gain-induced index is small and it may mean that the index step induced by the heating is more important. We have already seen in section 4-1 that Balucani et al.[49] have computed, for the case

of a 2.5 μsec pulse, a blackbody-like flashtube at 30,000°K temperature and a concentration of 1.0×10^{-3} m/l of rhodamine 6G/ethanol) a temperature increase of 0.3°C and an index or refraction change of the order of 5×10^{-4}. We have chosen these experimental conditions as such because they resemble our own.

In conclusion it seems that the change of the index of refraction due to temperature is much more important than the change due to gain for the dye laser systems.

```
      PROGRAM TST (INPUT,OUTPUT,TAPE5=INPUT,TAPE6=OUTPUT)
C     ------------------------------------
C         THIS PROGRAM CALCULATES THE CONTOURS OF F1 AND F2.
C         IT PLOTS  U  VS  V  WHERE F1,OF F2 CHANGES SIGN.
C         THE CROSS-SECTION OF THE TWO PLOTS GIVE APPROX.
C         (U,V) ROOTS TO BE USED IN THE NEXT PROGRAM.
C     ------------------------------------
      REAL LGTH,K,LOSS
      REAL NCN1,NCN2
      DIMENSION STF1(900),STF2(900),STV(900)
      C= 3.0E+10
      PI=3.141592654
      HTTA=1.359
C         INDEX STEP
      DHTTA=  -0.05 E-3/2.0/HTTA
C..       STEP OF  INDEX  INCREMENT
      DHSTP=0.0
C         START OF SCAN FOR V
      VSTRT=0.02
      STEP=0.01
      DO 1111 JK=1,3
      VMAX= VSTRT+STEP
C         CONCENTRETION IN UNITS OF  10 TO -4.
      CONC=15.
C         INDEX STEP WIDTH.
      CD=1.0/12.0/CONC
      VZERO=VSTRT
C------- ABSORPTION LOSS IN CM TO -1    .........
C         WAVELENGTH
      W=5940.
      W=W*1.0E-8
      LOSS=.057
C----          DEQ=2*HTTA*DHTTA=
C-------   THE WINDTH IS IN CM ----------
C         LGTH IN CM
C         CELL WICTH.
      LGTH=0.0300
      A=1.-LGTH/CD
      OMEGA=2.*PI*C/W
      H=LGTH-2.*CD
      E1=HTTA**2
      DEQ=2.0*HTTA*DHTTA
      THETA=2.0*PI*HTTA*(CD**2)*LOSS/W
      PHI=(OMEGA**2)*DEQ*(CD**2)/C**2
      PRINT 110,PHI,THETA,CONC,LOSS
110   FORMAT(1H0,*PHI=*,1E16.8,*THETA=*,1E16.8,*CONC=  *,1E16.8,*  LOSS
     1=  *,1E16.8)
C-------- CALCULATE K(U,V) AND PRINTED  -------------
      JLIM=200
      U=0.1
      CU=0.1
      CV=0.5E-4
      VLIM=DV*FLOAT(JLIM)+VSTRT
      DO 188 L=1,40
      FCN1=0.0
      FCN2=0.0
      NCN1=0.0
```

```
          ACN2=0.0
          CNT1=1.
          CNT2=1.
          V=VZERO
          DO 77 J=1,JLIM
1543      CONTINUE
          K=       (1.-PHI/U**2+(V/U)**2  -(THETA/2./V/U)**2)
          IF(K) 88,88,6
6         K=SQRT(K)
          S=THETA/(2.0*V**2)
          C1= EXP(A*V) *COS(S*A*V)   -EXP(-V) *COS(S*V)
          C2=EXP(A*V)*SIN(S*A*V)   +EXP(-V)*SIN(S*V)
          C3=EXP(A*V)*COS(S*A*V)   + EXP(-V)*COS(S*V)
          C4=EXP(A*V) *SIN( S*A*V)   -EXP(-V)* SIN(S*V)
          C=(SINH(K*L))**2+(COS(U))**2
          A1=SINH(K*L)*COSH(K*U)
          A2=SIN(U)*COS(U)
          G1=D*(C3**2+C4**2)
          G2=A2*(C1*C3+C2*C4)   - A1*(C2*C3-C1*C4)
          G3=G1
          G4=+A2*(C2*C3-C1*C4)   +A1*(C1*C3+C2*C4)
          F1=U*(1.0+K*S)*G1-  V*(1.0+S**2)*C2
          F2=U*(K-S)*G3-V*(1.+S**2)*C4
          GO TO 1928
C      --------- TEST PLOT  F1,F2  -----
          PRINT 1213,U,V,F1,F2
NO PATH TO THIS STATEMENT
1213  FORMAT(5X,4E16.5)
          CALL PLOTPT(V,F1,4)
NO PATH TO THIS STATEMENT
          CALL PLOTPT(V,F2,3)
NO PATH TO THIS STATEMENT
          GO TO 7971
NO PATH TO THIS STATEMENT
1928  CONTINUE
C      --------- TEST PLOT  F1,F2  -----
C--------------------- CHANGE OF SIGN CHECK ------------------
          IF(CNT1.EQ.1.) GO TO 350
          IF(F1) 450,450,460
450       IF( ACN1 .EQ.1.) GO TO 500
          GO TO 707
460       IF(PCN1.EQ.1.) GO TO 500
          ACN1=0.0
          PCN1=1.0
          GO TO 700
707       ACN1=1.0
          PCN1=0.0
700       CONTINUE
C-----    SELECTIVE PLOTING ----
C         IF(V.LE.0.077)GO TO 9700
          IF(V.GE.VMAX )GO TO 9700
          CALL PLOTPT(V,U,4)
9700  CONTINUE
C         PRINT 701,V,U
701       FORMAT(1X ,2E16.1)
          GO TO 500
350   CNT1=0.0
```

```
          IF(F1) 360,360,370
   360    NCN1=1.
          GO TO 380
   370    PCN1=1.0
   380    CONTINUE
   500    CONTINUE
          IF(CNT2.EQ.1.0) GO TO 1350
          IF(F2) 1450,1450,1460
  1450    IF(NCN2.EM.1.0) GO TO 5000
          GO TO 1707
  1460    IF(FCN2.EQ.1.0) GO TO 5000
          NCN2=0.0
          FCN2=1.0
          GO TO 1700
  1707    NCN2=1.0
          PCN2=0.0
  1700    CONTINUE
C-----    SELECTIVE PLOTING ----
C         IF(V.LE.0.077)GO TO 8700
          IF(V.GE.VMAX )GO TO 8700
C------------------
          CALL PLOTPT(V,U,3)
  8700    CONTINUE
C         PRINT 702,V,U
   702    FORMAT(1X  ,50X,2E16.8)
          GO TO 5000
  1350    CNT2=0.0
          IF(F2) 1360,1360,1370
  1360    NCN2=1.0
          GO TO 1380
  1370    PCN2=1.0
  1380    CONTINUE
  5000    CONTINUE
C---------------------- CHANGE CF SIGN CHECK ----------------ND-----
C         ----------
  7971    CONTINUE
C         ----------
          V=V+CV
   77     CONTINUE
  7777    CONTINUE
          U=U+CU
          VZERC=VSTRT)
   188    CONTINUE
          CALL OUTPLT
          PRINT 8778,CONC,LOSS,DEO,LGTH
  8778    FORMAT(1H0,*CONC=*,1E16.8,*    LOSS=  *1E16.4,*   DEC= *,1E16.8,
         1 *  LGTH=  *,1E16.8)
          GO TO 7769
C  ------- FIND VZERO TO MAKE K POSITIVE ------
   88     CONTINUE
C         PRINT 89
   99     FORMAT(1H0,*  NEGATIVE K  --------*)
          CNTR7=0.0
  7337    STRK=1.0-PHI/U**2+(V/U)**2    -(THETA/2.0/U/V)**2
          IF(STRK) 7447,7447,7557
  7447    V=V+CV/5.0
C         CNTR7=CNTR7+1.0
```

```
PROGRAM TST        73/74    TS TRACE                      FTN 4.6+460

            IF(V.GE.VLIM) GO TO 75310
            GC TC 7337
      7557  CONTINUE
            CNTR7=0.0
      C     VZERO=V
            STRK=SQRT(STRK)
      C     PRINT  2468, VZERO,STRK
      2468  FORMAT(1X ,2E16.4)
            GO TO 1543
      75310 CNTR7=0.0
      C     PRINT 97531,U
      97531 FORMAT(1X, *U=*,1E16.6)
            GO TO 7777
      C  -------- FIND VZERO TO MAKE K POSITIVE --------
      7769  CONTINUE
            CHTTA=CHITA+DHSTP
            VMAX=VMAX+STEP
            VSTRT=VSTRT+STEP
      1111  CONTINUE
            STOP
            END
```

INTS--

```
    38    INPUT#              543    OUTPUT#              79   TAPE5#
  1340    TST
```

S--

```
      CCS        CCSH       EXP        FTNSP2.   QUICI.    OUTPUT    PLOTPT    CI
      SINH       SCRT       STOP.
```

T LABELS--

```
.6          276B        .77     0    676B          .88          717B
.110    F   1015B       .148    0    707B          .250         577B
.373        6108        .340         613B          .453         543B
.500        613B        .730         567B          .701    F    103AB
.707    .   667B        .1111   0    767C          .1213   F    136EB
.1360       663B        .1270         667B         .1390        471B
.1460       673B        .1543         263B         .1703        646B
.1924       534B        .2468   F    1053B         .5000        672B
.7447   c   734B        .7557        744B          .7769        757B
.7972       673B        .8700        654B          .8778   F    103EB
.7531C      757C        .37531  F    105EB
```

MAP--

```
    2       1234B                        A1      R    6526B
    8       6527B                        C       R    1237B
    8       6533B                        CNT1    R    5520B
    4       4656B                        CCAC    R    6504B
```

```
      PROGRAM TST (INPUT,OUTPUT,TAPE2=INPUT,TAPE4=OUTPUT)
      ---------------------------------------------------
C         THIS PROGRAM CALCULAT_ , THE ROOTS (U,V) OF F1(U,V)=,
C         F2(U,W)=L (W) PLOTS 1 4- AND FAR FIELD.
      ---------------------------------------------------
      COMMON K,UL,LGTH,PHI,THETA,S,AF
      COMPLEX AU,A1,A2,A3,P,W,G,B1,B2,T1,T2,FLD1,FLD2,FLD3,FLD,XI
      COMPLEX DELTA,SFLD
      COMPLEX T7,T8,T9
      REAL LGTH,K,LOSS
      REAL K1,K2,K12
      DIMENSION F12(100)
      DIMENSION F1(100),F2(100)
      DIMENSION WA(100),X(2)
      DIMENSION  SFLD(300),STPH(300) ,SY(300)
      EXTERNAL F
      C= 3..E+10
C----- LENGTH IN CM
      PI=3.1415920
C------- CONCENTRATION IN 10 TO -.MUL/LITRE
      CONC=15.
C-----     ABSORPTION LOSS IN CM TO -1    ---------
      LOSS=0.04
      HTTA=1.559
C         INDEX STEP
      DHTTA=  -0.05 _-5 /2./HTTA
C         INDEX STEP WIDTH
C      THIS D IS THE 1/2 POINT  AT MAX. ABSORPTION.
      DD=1.5/12.0/CONC
C         CELL WIDTH
      LGTH=0.500
      A=1.-LGTH/DD
C---- WAVELENGTH IN ANGSTROM
      W=900.
      W=W*1.0E-8
      OMEGA=2.*PI*C/W
C-----  H    IS THE UNPUMP-D ~E,IUI------
      H=LGTH-..400
C--- LOSS IN CM  TO -1          LOSS=AS
C--- DIELECTRIC CONSTANT -----
C-------- E=1+IMAG(A)-DEL -----
      E1=HTTA**2
C----  DEL=2*HTTA*DHTTA   =- --------------
C         .......... MAX. GAIN ABOVE WHICH DO NOT PRINT ......
      GMAX=4.0
C------    CALCULATE THE INITIAL PARAMETERS  PHI, THETA -----
      THETA=2.0*PI*HTTA*(DD**2)*LOSS/W
      DEL=2.0*HTTA*DHTTA
      PHI=(OMEGA**2)*DEL*(DD**2)/C**2
      PRINT 110,PHI,THETA,CONC,LOSS
110   FORMAT(1H0,*PHI=*,1E15.3,*THETA=*,1E16.8,*CONC=  *,1E15.3,*  LOSS
     1=  *,1E16.8)
C------- CALCULATE ROOTS OF F1,F2.........
C--------     U=X(1),V=X(2)--------
      READ 7700,JCARD
7700  FORMAT(I2)
      DO 99999 JCARD=1,JCARD
```

```
       READ 5077,X
5077   FORMAT(1F10.)
       PRINT 5775,X
5775   FORMAT(1X,*   ... STARTING VALUE = *,2F20.1,///)
       RA=ANG...
       ...
       ...
       N=...
C----     X(1)=U  ,,,,X(2)=V         ---------
       ITMAX=100
       IC=111
C
C      ---------------------------------
C      INSE  LIBRARY ROUTINE (ZSYSTM) TO DETERMINE THE ROOTS
C      OF A SYSTEM OF N SIMULTAN. NON-LINEAR EQUATIONS F(Y)=0.
C      ---------------------------------
       CALL ZSYSTM(F,EPS,NSIG,N,X,ITMAX,WA,PARAM,IER)
C
       PRINT 501,ITMAX,X(1),X(2),IER,N,AF
501    FORMAT(1H0,*ITMAX=*,I5,*   V=*,F8.2,*   V=*,F10.4,
      1*  I=*,I5,*  N=*,F4.2,*  SEX*,F4.2,*  FUNCTION=*, 13..,/)
       PRINT 9110,C..
9110   FORMAT(1H0,*VALUE=*,2E15.5)
       IF (IER.GU.0) GO TO 9001
C------    CALCULATE GAIN IN U(I,I)-1   ------
       GAIN=*(X(1)**2) *2PI/(PI /))**2
       PRINT 1321,GAIN,LOTM,...,GAIN
1321   FORMAT(1H0,*GAIN= *,E15. ,* DB *,F11.50,*  LATHE *,F11.12.*
      1   *  LOSS(1/CM)= *,E15., ,  GAIN(1/CM)= *,....*/)
C------    CALCULATE GAIN IN U(I )-1   ------
       IF( GAIN.GT. AAX) GO TO  501)
       CALL PLTG=(X(1),X(2),N,AN,PI,QC,CONC,...)
       U=X(1)
       V=X(2)
C------ FAR FIELD CALCULATIONS ---------
C------ (U,I),(V,J+M),(GM,L)  DEFINITIONS
C----     ROT FAR DISTANS ---- IN CM ----
       XU=....
       R=CMPLX((1/ U,S*U/ )
       Y=CPLX((1/U0,S*/ U)
       A0=CMPLX(1.,0.0,0)
       A1=A0*U*I*(F*.0)/  (..XP(-.*AC)+..P(.*(CU-C.5T.)))
       AV=A.U  S1/N
       S1=C..LX(U.,U.WV*.0)
       R=C.XP(*1)/AU
       ..=C..PLX(U.,U.WV/U)
C------ YENITA COORDINAT ---
       JYM=..
       Y=J.U
       JY=...T-5
       TI=CUIN(P*U)
       T =PCOS(P*U)
       ASP=AI*( C.XP(-. *(LGTH-U))+C.K3(-.*U ))/Z..SIN(P*U )
       DU  ...=1,JY1
       FU1= (..,.)/ ((.*Y)**+P**2) * (... +((2*Y*P))*(  .*(VP...P )* )
       XI=...U PLX(U.,U. *Y/U)
       DELTA=..CMPLX(U.,U.WV*Y/U)
```

```
        T7=A1*B
        T8=CEXP(XI*(DO+H))/XI   +CEXP(-O*LGTH +DELTA*(DO+H))/DELTA
        T9=CEXP(XI*DO)/XI+ CEXP(-O*LGTH+ DELTA*DO)/DELTA
        FLD2=T7*(T8-T9)
        FLD3= U*A3*CEXP(O2*LGTH*Y)/ ((O2*Y)**2+ P**2)*
     1   (CEXP(-O2*Y*DO)   *(  O2*Y*T1+  T2)  -P)
        FLD=FLD1+FLD2+FLD3
        SFLD(JY)=FLD
C------ STORE ANGLE IN DEGREES --------
        SY(JY)=  ATAN(Y/RO)*180.0/PI
        Y=Y+DY
1944    CONTINUE
C------ PLOT FAR FIELD INTENSITY AND PHASE -----
        DO 1949 JY=1,JYM
        FLDIN= REAL( SFLD(JY))**2    + AIMAG( SFLD(JY))**2
        FLDPH=ATAN(AIMAG(SFLD(JY))/REAL(SFLD(JY)))
        STPH(JY)=FLDPH
        CALL PLOTPT( SY(JY),FLDIN,4)
1949    CONTINUE
        CALL OUTPLT
        PRINT 1421,CONC,DO,LGTH,LOSS,GAIN
        GO TO 13579
        DO 1950 JY=1,JYM
NO PATH TO THIS STATEMENT
NO PATH TO THE ENTIRE RANGE OF DO
        CALL PLOTPT( SY(JY),STPH(JY),3)
1950    CONTINUE
        CALL OUTPLT
        PRINT 1421,CONC,DO,LGTH,LOSS,GAIN
13579   CONTINUE
C------ FAR FIELD CALCULATIONS ---- END----
99999   CONTINUE
        STOP
        END
```

BLOCKS--

     78 //

IINTS--

    38   INPUT#   548   OUTPUT#   38   TAPE5#
   1348   TST

.3--

        ATAN   CCOS   CEXP   CSIN   F   ZSYSTM   FTNFP1. INPCI.   O'
        OUTPLT   PLOTPT   PLTOR   STOP.   ZTO18

```
      FUNCTION F(X,KK,PARAM)
C-------- FUNCTION  F---------
      COMMON K,DO,LGTH,PHI,THETA,S,AF
      REAL K,LGTH
      DIMENSION X(2)
      PARAM=0.0
      U=X(1)
      V=X(2)
      A=1.-LGTH/DO
      K=      (1.-PHI/DO**2+(V/DO)**2  -(THETA/2./V/))**.)
      IF(K) 88,99,5
    5 K=SQRT(K)
      S=THETA/(2.0*V**2)
      C1= EXP(A*V) *COS(S*A*V)  +EXP(-V) *COS(S*V)
      C2=EXP(A*V)*SIN(S*A*V)  +EXP(-V) *SIN(S*V)
      C3=EXP(A*V)*COS(S*A*V)  + EXP(-V)*COS(S*V)
      C4=EXP(A*V) *SIN( S*A*V)  -EXP(-V)* SIN(S*V)
      U=(SINH(K*U))**2+(COS(U))**2
      A1=SINH(K*U)*COSH(K*U)
      A2=SIN(U)*COS(U)
      G1=U*(C3**2+C4**2)
      G2=A2*(C1*C3+C2*C4)   - A1*(C2*C3-C1*C4)
      G3=G1
      G4=+A2*(C2*C3-C1*C4)  +A1*(C1*C3+C2*C4)
      GO TO (5,10) KK
    5 CONTINUE
      F =U*(1.0+K*S)*G1-  V*(1.0+S**2)*G2
      AF=F
C     PRINT 444,U,V,F ,K,S
  444 FORMAT(1H0,5E16.10)
      RETURN
   10 CONTINUE
      F =U*(K-S)*G3-V*(1.+S**2)*G4
      AF=F
C     PRINT 555,U,V,F,K,S
  555 FORMAT(1H0,30X,5E16.10)
  222 FORMAT(1H0,10E12.5)
      GO TO 77
   18 PRINT  19,X
   19 FORMAT(10X,* NEGATIVE K    *,2F10.5///)
C     STOP
   77 CONTINUE
      RETURN
      END
```

LOCKS--

     18 77

          COS   COSH   EXP   GOTOER.   OUTCI.   OUTPUTW   SIN   SI
          SQRT

```
        SUBROUTINE PLTGR(U,V,K,S,LGTH,DD,CONC,DEU)
        COMPLEX CA2,CA1,CA_,P,Q,C_EN,CNUM,CND
        REAL K,LGTH
        DIMENSION AMPL(3UU),PHASE(3UU)
        DIMENSION AREAL(HUU),AIMAG(HUU)
        DIMENSION STOPA(3UU),STOPF(3UU)
C---- CALCULATE AMPLITUDE AND PHASE OF    A=A1.SIN(P.X) ----
        NN=5U
        P=CMPLX(U/DD,K*U/DD)
        Q=CMPLX(V/DD,S*V/DD)
        CA_=CMPLX(1.,u.)
        CDEN=CEXP(-Q*DD)    +   CEXP(1*(DD-LGTH))
        CNUM=CAU*CSIN(P*DD)
        CND=CNUM/CDEN
        DX=DD/FLOAT(NN)
        NN1=NN-1
        X=DX
        DO 570 J=1,NN1
        CA1=CAU*CSIN(P*X)
        AMPL(J)=      (REAL(CA1)**2+AIMAG(CA1)**2)
        PHASE(J)=ATAN(AIMAG(CA1)/REAL(CA1))
        STORA(J)=AMPL(J)
        STORF(J)=PHASE(J)
C-----------------------------------------
C       PRINT 7676,X,AMPL(J),PHASE(J)
7676    FORMAT(1HU,3E15.5)
C-----------------------------------------
        X=X+DX
570     CONTINUE
        X=DX
        DO 580 J=1,NN1
        CALL PLOTPT(X,AMPL(J),4)
        X=X+DX
580     CONTINUE
        CALL OUTPLT
        PRINT 581,U,V,K,S
        X=DX
        DO 590   J=1,NN1
        CALL PLOTPT(X,PHASE(J),3)
        X=X+DX
590     CONTINUE
        CALL OUTPLT
        PRINT 581,U,V,K,S
581     FORMAT(1HU,*U=  *,1E15.7,*   V=   *,1E15.7,*  K=  .*,1E15.7,
       1 *   S=   *,1E15.7,*A=Au.SIN(P.X)*)
C--- CALCULATE AMPLITUDE AND PHASE OF   A=A1*EXP(-1*X)+A2*EXP(Q*X)
        X=DD
        L=NN1
        NN2=IFIX((LGTH-2.*DD)/DX)
C----    PLOT APPOX. 173 OF LGTH ...........
C        NN2=NN2/3
C------------------
        DO 597 J=1,NN2
        CA2=CND*(CEXP(-1*X)   +   CEXP(Q*(X-LGTH)))
        AMPL(J)=      (REAL(CA2)**2+AIMAG(CA2)**2)
        PHASE(J)=    ATAN(AIMAG(CA2)/REAL(CA2))
        L=L+1
```

```
         STORA(L)=AMPL(J)
         STORF(L)=PHASE(J)
C        PRINT 7576,X,AMPL(J),PHASE(J)
C--------------------------------------------
         X=X+DX
 597     CONTINUE
         X=OU
         DO    J, J=1,NN2
         CALL PLOTPT(X,AMPL(J),4)
         X=X+DX
 591     CONTINUE
         CALL OUTPLT
         X=OU
         PRINT 593,U,V,K,S
         GO TO 12345
         DO 592 J=1,NN2
NO PATH TO THIS STATEMENT
NO PATH TO THE ENTIRE RANGE OF DO
         CALL PLOTPT(X,PHASE(J),S)
         X=X+DX
 592     CONTINUE
         CALL OUTPLT
         PRINT 9110,DEO
 9110    FORMAT(1H0,"DEO=",1E15.5)
         PRINT 593,U,V,K,S
 593     FORMAT(1H0,"   U=   ",1E15.7,"    V=  ",1E15.7,"   K=    ",1E15.7,
        1"   S=  ",1E15.7,"  A=A1.EXP(-Q.X)+A2.EXP(QX)")
 12345   CONTINUE
         X=DX
         JN=NN1+NN2
         DO 592 J=1,JN
         CALL PLOTPT(X,STORA(J),4)
         X=X+DX
 592     CONTINUE
         CALL OUTPLT
         PRINT 593 ,U,V,K,S,CONC,LGTH,DEO
         X=OX
         GO TO 13579
         DO 594 J=1,JN
NO PATH TO THIS STATEMENT
NO PATH TO THE ENTIRE RANGE OF DO
         CALL PLOTPT(X,STORF(J),S)
         X=X+DX
 594     CONTINUE
         CALL OUTPLT
         PRINT 593 ,U,V,K,S,CONC,LGTH,DEO
 593     FORMAT(1H0,"U=",1E10.5," V=",1E10.5," K=",1E10.5," S=",1E10.5,
        1" CONC=",1E10.5," LGTH=",1E10.5," DEO=",1E15.5)
 13579   CONTINUE
         RETURN
         END
```

REFERENCES

1. P.P. Sorokin and J.R. Lankard, IBM J. Res. Develop. 10, 162 (1966).

2. F.P. Schäfer ed., Dye Lasers, Topics in Applied Physics, Vol. 1, Springer-Verlag, New York, 1973.

3. Kuhn, H., Fortschritte der Chemie Organischer Naturstaffe, Vol. 16, pg. 169-205 (1958).

4. Parker, C.A., Photoluminescence of Solutions. pg. 428, Elsevier, Amsterdam (1968).

5. Birks, J.B., Photophysics of Aromatic Molecules, pg. 142, Wiley-Interscience, London (1970).

6. Huth, B.G., Farmer, G.I., Kagan, M.R., J. Appl. Phys., Vol. 40, No. 13 (1969).

7. Drexhage, K.H., Laser Focus 9(3), 35 (1973a).

8. Markiewicz, J.P. and Emmett, J.L., IEEE J. Quantum Electr., QE-2, No. 11 (1966).

9. Perlman, D.E., Rev. Sci. Instr. 37, 340 (1966).

10. Perlman, D.E., Rev. Sci. Instr. 38, 68 (1967).

11. Oliver, J.R. and Barnes, F.S., IEEE J. Quantum Electr. QE-5, 232 (1969).

12. Holzrichter, J.F. and Emmett, J.L., Appl. Opt. 8, 1459 (1969).

13. Oliver, J.R. and Barnes, F.S., Proc. IEEE 59, 638 (1971).

14. Holzrichter, J.F. and Schawlow, A.L., Annals N.Y. Academy of Sciences 168, 703 (1970).

15. Güther, K., Opt. Spectrosc. 34, 620 (1973).

16. Mavroyannakis, E., IEEE Transac. on Electron Dev., ED-18, No. 2 (1971).

17. Gusinow, M.A., J. Appl. Physics, Vol. 46, No. 11 (1975).

18. Gusinow, M.A., Optics Comm., Vol. 15, No. 2 (1975).

19. Goncz, J.H., and Newell, P.B., J. Opt. Soc. of America, Vol. 56, No. 1 (1966).

20. Bunkenburg, J., Rev. Scient. Instr., Vol. 43, No. 3 (1972).

21. Lindquist, L., Rev. Scient. Instr., Vol. 35, No. 8 (1964).

22. Edwards, J.G., Appl. Optics, Vol. 6, No. 5 (1967).

23. Goncz, J.H., J. Appl. Phys., Vol. 36, No. 3 (1965).

24. Demenik, I.V., Mnuskin, V.E., Skvortsov, B.V., and Fedorov, V.B., Soviet Physics-Technical Physics, Vol. 13, No. 6 (1968).

25. Bakeev, A.A. and Rovinskii, R.E., Teplofizika Vysokikh Temperatur, Vol. 8, No. 1, 207 (1970).

26. Biberman, L.M. and Norman, G.E., Soviet Physics Uspekhi, Vol. 10, No. 1 (1967).

27. Spitzer, L. Jr., Physics of Fully Ionized Gases, Interscience Publ. Inc., second ed. (1962).

28. Levikov, S.I. Optica-Mechanicheskaia promyshlennost (Soviet Journal of Optical Technology), Vol. 36, pg. 570, July-August (1969).

29. Maeda, M. and Miyazoe, Y. Japanese J. of Appl. Physics, Vol. 11, No. 5 (1972).

30. Ewanizky, T.F. and Wright, R.H., Jr., Appl. Opt., Vol. 12, No. 1 (1973).

31. Ferrar, C.M., Rev. Scient. Instr., Vol. 40, No. 11 (1969).

32. Gusinow, M.A., J. Appl. Phys., Vol. 44, No. 10 (1973).

33. Gusinow, M.A., Efficiency of Flashlamp Excited Lasers, Sandia Lab. Research Report, SLA-73-9005 (1973).

34. Gusinow, M.A., _The Electrical Characteristics of High Current Gas Filled Flashlamps_, Sandia Lab. Research Report, SLA-73-0352 (1973).

35. Goldstein, R. and Mastrup, F.N., IEEE J. Quantum Electr., Vol. QE-3, No. 11 (1967).

36. Baker, H.J. and King, T.A., J. Phys. E., Vol. 8, No. 3 (1975).

37. Efthymiopoulos, T., and Garside, B.K., J. Appl. Opt., Vol. 16, No. 1 (1977).

38. Huth, B.G., Appl. Phys. Lett., Vol. 16, No. 4 (1970).

39. Shank, C.V., Dienes, A., Silfvast, W.T., Appl. Phys. Letters, Vol. 17, No. 7 (1970).

40. Casperson, L.W., J. Appl. Phys., Vol. 48, No. 1 (1977).

41. Yariv, A. and Leite, R.C.C., J. Appl. Phys., 34, 3410 (1963).

42. Casperson, L.W. and Yariv, A., IEEE J. Quant. Elect., QE-8, 80 (1972).

43. Maeda, H. and Yariv, A., Phys. Lett., 43A, 383 (1973).

44. Yariv, A., _Quantum Electronics_ , 2nd edition, Chapter 12, New York, John Wiley (1975).

45. Burlamacchi, P., Pratesi, R. and Vanni, U., Optics Commun., Vol. 9, No. 1 (1973).

46. Burlamacchi, P., Pratesi, R., and Ronchi, L., Appl. Optics, Vol. 14, No. 1 (1974).

47. Loiko, M.M., Bar, Zs., Kozma, L., Racz, B. and Ketskemety, I., Optics Commun., Vol. 15, No. 2 (1975).

48. Pratesi, R. and Ronchi, L., Optica Acta, Vol. 23, No. 11 (1976).

49. Balucani, U. and Tognetti, V., Optica Acta, Vol. 23, No. 11 (1976).

50. Garside, B.K., Shewchun, J. and Kawasaki, B.S., J. Appl. Phys., Vol. 43, No. 10 (1972).

51. Gusinow, M.A., IEEE J. Quant. Electr., Vol. QE-11, No. 12 (1975).

52. Gusinow, M.A., Optics Commun., Vol. 15, No.2 (1975).

53. Emmett, J.L. and Schawlow, A.L., Appl. Phys. Lett., Vol. 2, No. 11 (1963).

54. Beynon, J., Conduction of Electricity Through Gases, London,
    G.G. Harrap & Co., 1972 (pp. 28).

55. Rovinskii, R.E., Zh. Tekh. Fiz., 33, No. 4, 489 (1963).

56. Maeda, M., Uchino, O., Doi, E., Katanabe, K. and Miyazoe, Y.,
    IEEE J. Quant. Elect., Vol. QE-13, No. 2 (1977).

57. Olsen, S.O., J. of Physics E: Scient. Instr., Vol. 5, No. (1972).

58. Cormack, G.D., Miller, A.D. and Tan, K.O., Rev. Scient. Instr.,
    Vol. 43, No. 1 (1972).

59. I.L.C., Technical Bulletin No. 5, Design of Short Pulse Flashlamp
    Systems for Dye Lasers and Flash Photolysis. 164 Commercial St.,
    Sunnyvale, California 94086, U.S.A.

60. Dishington, R.H., Hook, W.R. and Hilberg, R.P., Appl. Optics,
    Vol. 13, No. 10 (1974).

61. EG & G Xenon Flashtubes. EG & G Electro-optics Div., 35 Salem
    Street, Salem, Mass 01970, U.S.A.

62. Hook, W.R., Dishington, R.H. and Hilberg, R., IEEE Trans. Electron
    Devices, ED-19,308 (1972).

63. Xenon Corp., High Energy Linear Flashtubes, 39 Commercial Street,
    Medford, Mass. 02155, U.S.A.

64. Xenon Flashtubes, applications bulletin, Verre et quartz, 254
    Avenue Aristide-Briand, 93320 Pavillons-Sous-Bois, Paris, France.

65. Mroczkowski, J.A. and Milburn, R.H., Rev. Sci. Instrum., Vol. 48,
    No. 12 (1977).

66. Furomoto, H.W. and Ceccon, H.L., Appl. Optics, Vol. 8, No. 8 (1969).

67. Mack, M.E., Appl. Optics, Vol. 13, No. 1 (1974).

68. Morrow, T. and Price, H.T.W., Optics Commun., Vol. 10, No. 2 (1974).

69. Okada, T., Fujiwara, K., Maeda, M. and Miyazoe, Y., Appl. Phys., Vol. 15, No. 2 (1978).

70. Pivovonsky, M. and Nagel, M.R., Tables of Blackbody Radiation Functions, The MacMillan Company, New York, 1961.

71. Snavely, B.B., Continuous wave dye lasers in Dye Lasers, Schäfer, F.P., ed., Springer-Verlag, New York, 1973, Chapter 2.

72. Sargent, III, M., Scully, M.O. and Lamb, Jr., W.E., in Laser Physics, Addison-Wesley, 1974, Ch. 14.

73. Allen, L. and Eberly, J.H., in Optical Resonance and Two-Level Atoms, J. Wiley, 1975, Ch. 7.

74. Mack, M.E., Appl. Phys. Lett., Vol. 15, No. 6 (1969).

75. Chin, S.L. and Bedard, G., Opt. Commun., Vol. 4, No. 2 (1971).

76. Lin, C., Gustafson, T.K. and Dienes, A., Opt. Commun., Vol. 8 (1973).

77. Marowsky, G., J. Appl. Phys., Vol. 45, No. 6 (1974).

78. Mumola, P.B., J. Appl. Phys., Vol. 43, No. 2 (1972).

79. Burlamacchi, P. and Pratesi, R., Appl. Phys. Lett., Vol. 22, No. 7 (1973).

80. Shank, C.V., Dienes, A., and Silfvast, W.T., Appl. Phys. Lett., Vol. 17, No. 7 (1970).

81. Maeda, H. and Yariv, A., Phys. Lett., Vol. 43A, No. 4 (1973).

82. Ganiel, U., Hardy, A., Neumann, G. and Treves, D., IEEE J. Quant. Elect., Vol. QE-11, No. 11 (1975).

83. Menegozzi, L.M. and Lamb, Jr., W.E., Phys. Rev. A, Vol. 17, No. 2 (1978).

84. Topp, M.R., Rentzepis, P.M. and Jones, R.P., Chem. Phys. Lett., Vol. 9, No. 1 (1971).

85. Lin, C. and Dienes, A., Opt. Commun., Vol. 9, No. 1 (1973).

86. Bradley, D.J., Hutchinson, M.H.R., Koetser, H., Morrow, T., New, G.H.C. and Petty, M.S., Proc. R. Soc. Lond. A., 328, 97-121 (1972).

87. Webb, J.P., McColgin, W.C., Peterson, O.G., Stockman, D.L. and Eberly, J.G., J. Chem. Phys., Vol. 53, pp. 4221-4229 (1970).

88. Marling, J.B., Gregg, D.W. and Wood, L., Appl. Phys. Lett., Vol. 17, No. 12, (1970).

89. Shahar, E. and Treves, D., IEEE J. Quant. Electr., Vol. QE-13, No. 12 (1977).

90. Snavely, B.B., Proc. IEEE, Vol. 57, No. 8 (1969).

91. Teschke, O., Dienes, A. and Winnery, J.R., IEEE J. Quant. Electr., Vol. QE-12, No. 7 (1976).

92. Yamashita, M. and Kashiwagi, H., IEEE J. Quant. Electr., Vol. QE-12, No. 2 (1976).

93. Pappalardo, R., Samelson, H. and Lempicki, A., Appl. Phys. Lett., Vol. 16, No. 7 (1970).

94. Borisevich, N.A., Gruzinskii, V.V. and Davydov, S.V., Sov. J. Quant. Electron., Vol. 4, No. 8 (1975).

95. Wang, H.H.L. and Taji, C.H., IEEE J. Qu. Electr., QE-13, No. 3 (1977).

96. Mroczkowski, J.A. and Milburn, R.H., Rev. Sci. Instrum., Vol. 48, No. 12 (1977).

97. Loudon, R., The quantum theory of light, pp. 84-90, Clarendon Press, Oxford, 1973.

98. Yariv, A., Quantum Electronics, pp. 286-288, second ed., J. Wiley, New York, 1975.

99. Burlamacchi, P. and Pratesi, R., Appl. Phys. Lett., Vol. 28, No. 3 (1976).

100. Erickson, L.E. and Szabo, A., Appl. Phys. Lett., Vol. 18, No. 10 (1971).

101. Lin, C., IEEE J. Quant. Electr., Vol. QE-11, No. 8 (1975).

102. Burlamacchi, P., Pratesi, R. and Ronchi, L., Opto-electronics, Vol. 6 (1974).

103. Tikhonov, E., Bertolotti, M., and Scudieri, F., Appl. Phys., Vol. 11 (1976).

104. Blit, S., and Ganiel, U., Optical and Quant. Electr., Vol. 7 (1975).